RADIOWAVE PROPAGATION MEASUREMENTS AND PREDICTION IN BUSHFIRES

Thesis submitted by

Kgakgamatso Marvel MPHALE MSc (University of Botswana)

in May 2008

for the Degree of Doctor of Philosophy

in the School of Mathematical and Physical Sciences

James Cook University

STATEMENT OF ACCESS TO THESIS

I, the undersigned, author of this work, understand that James Cook University will make this thesis available for use within the University Library and, via the Australian Digital Theses network, for use elsewhere.

I understand that as unpublished work, a thesis has a significant amount of protection under the Copy Right and;

I do not wish to place any further restriction on access to this work

_____ 19-May-2008

Kgakgamatso Mphale Date

STATEMENT OF SOURCES

DECLARATION

I declare that this thesis is my own work and has not been submitted in any form for another degree or diploma at any university other institution of tertiary education. Information derived from the published or unpublished work of other has been acknowledged in the text and a list of references is given.

_____ 19-May-2008

Kgakgamatso Mphale Date

STATEMENT OF CONTRIBUTION OF OTHERS

Financial contributions toward this PhD thesis were from;

- University of Botswana Staff Development Office,
- Emergency Management Australia Funding Under Project 2001/6001, and
- James Cook University.

There were some general contributions towards this PhD thesis in form of:

- Access to use of Network Analyser equipment from James Cook University's Electrical and Electronic Engineering Department (Chapter 6).

- Access to take sugar cane fire radio wave propagation measurements at Burdekin Agricultural College in Clare (Chapter 5).

- Access to take radio wave propagation measurements in a controlled grass fire at plot B from James cook University fire officers (Chapter 4)

There was a continual normal supervision and guidance from Prof. Malcolm Lewis Heron and Dr Peter Ridd throughout this PhD thesis.

ACKNOWLEDGEMENTS

I thank my supervisors Prof. Malcolm. Heron and Dr. Peter Ridd for the guidance they have given me throughout this work. Many thanks to Prof. Mal Heron for his never-ending patience and guidance with enthusiasm he provided to the end of this work. My sincere thanks to friends Drs Jonathan Bathgate and Audi Susilo for the encouragement they gave me during the research project.

I sincerely extent my gratitude to the University of Botswana Staff Development Office and Emergency Management Australia (EMA) for the funding they provided for the research. Also, my sincere thanks go to members of the Physics and Electrical and Electronic Engineering Departments of the James Cook University for providing necessary equipment for the research, especially help provided by Drs Graham Woods and Mohan Jacobs and Mr. Ray Casey.

ABSTRACT

Australian vegetation is fire-prone. Every year, wet and dry sclerophyll forests of Western Australia, southeastern Australia and grassland ecosystems of the northern part of the continent are subject to high intensity fires. The sclerophyll vegetation contains up to 2.71 % of the element potassium. The element exists in plants' organic matrix: attached to the oxygen-containing and carboxyl functional groups; in aqueous form such as potassium (K^+) ions surrounded by water; and as discrete particles in dried plant parts. Theoretically, temperature in the conflagrations can be as high as 2000ºC. During the high intensity bushfires, potassium atoms and salts are released from the plant structure as it crumbles into the combustion zone where the species are ionized. Up to 20 % of the potassium present in plants is ionized in a bushfire environment.

During suppression of the threat, high frequency (HF) - ultra high frequency (UHF) radio communications systems are in constant use by suppression crews in firegrounds. Despite their use, HF and very high frequency (VHF) radio communications are reported to be failing in extreme bushfire conditions. The reports of radio communication failure tend to be anecdotal and therefore warrant an investigation. This study aims at carrying out field and laboratory radio wave attenuation and phase shift measurements at HF to X-band frequencies in moderate intensity fires. Very high intensity bushfires often spread very fast and change direction rapidly therefore it is unsafe to set up equipment for measuring attenuation and phase shift in the fires. Consequently, numerical experiments were used to study radio wave propagation in very high intensity fires.

Propagation measurement data at radio wave (HF-VHF) frequencies through fire are scarce and that which is available lacks precision. It is also the purpose of the study to produce attenuation and phase measurement data at these frequencies. The field and laboratory measurements were carried out using a Radio Wave Interferometer (RWI) and Vector Network Analyzer (VNA - HP 8277C). RWI uses the same principles as Microwave interferometer (MWI) except that RWI works at radio frequencies. Electron density and momentum transfer collision frequency in moderate intensity bushfire plumes were estimated from the attenuation and phase shift measurements.

Laboratory and field measurements using a VNA - HP 8277C and RWI respectively in moderate intensity fires (700-1000 K) have revealed that electron density in the plume could range from 10^{14}-10^{16} m^{-3}. Theoretical calculations based on local thermal equilibrium in grassfires flames with temperatures up to 1200 K suggest that electron density could be up to 10^{17} m^{-3} if up to 20 % of the inherent potassium atoms are ionized.

There are at least two possible mechanisms that could lead to a significant signal strength reduction (attenuation) in bushfire environments. They are signal refraction due to thermal bubble and ionization-induced signal absorption in the plume. Electrons, which result from thermal ionization of potassium in the fire, transfer energy from the incident radio wave to the fire plume through collision with inherent neutral particles. The transfer of energy can significantly attenuate and induce a phase shift on radio wave signals. Experimental work carried out in the project suggest that radio wave attenuation is significantly higher at UHF and X-Band frequencies than at HF. Field radio wave propagation measurements at 1.50 m above the seat of a moderate intensity grassfire revealed that 30 MHz signals can be attenuated by up to 0.03 dB/m while 151.3 MHz signals were attenuated by up to 0.05 dB/m. An intense cane fire attenuated 151.3 MHz signals by 0.05 dB/m. The attenuation effect was observed to increase when X-band (10.0 -12.5 GHz) signals were considered. Attenuation coefficients up to 4.45 dB/m were measured.

Phase shift induced on the signals was also observed to increase with the increase in frequency band (low for HF and high for X-band). A 30 MHz signal suffered a 3.08º phase shift in the moderate intensity grassfire whereas in the X-band frequencies, a phase shift of up to 29.31º was observed in a fire of about the same intensity.

Numerical experiments have shown that signal loss due to refraction is frequency dependent in very hot regions of bushfire plumes. X-band waves are more affected than VHF waves. Numerical experiments predicted maximum attenuation coefficients of 0.11 dBm^{-1} for 150 MHz and 0.31 dBm^{-1} for 3 GHz radio waves when they propagate about a meter above fuel-flame interface of a 90 MWm^{-1} bushfire with fuel potassium content of 0.50 %. Theoretical studies also revealed that; for potassium content of about 0.20 %, a collimated beam of radio signals (10 cm wide) propagating at grazing angles to the fuel-flame interface of a very high intensity bushfire (1600 K) could suffer attenuation coefficients of about 1.45 dBm^{-1}. This effect is calculated to decrease with the increase in height above the combustion zone. For very high intensity bushfires in fuels with high potassium content (e.g., up to 3.00 %), attenuation by refraction is likely to be

the most significant form of radio wave energy loss for collimated beams propagating at grazing angles to the fuel-flame interface.

The Line-Of-Sight (LOS) radio wave propagation measurements in moderate intensity vegetation fires (700-1000 K) have shown that signal attenuation is plume temperature and frequency dependent. Transmission through hottest region of the fire (combustion zone) suffers significant signal strength loss whereas low attenuation has been observed at cooler regions of the plume. This could be explained by the fact that "collisional plasma effect" on radio waves is more pronounced at combustion zone than at the thermal plume region of the fire as the effect is temperature dependent.

Bcontinent with a potential combustion zone temperature of 2000ºC. These bushfires have a potential to adversely affect LOS radio wave communications when transmission is through the hottest part of the fire. It must be noted that radio wave communication blackout could even occur at temperatures as low as 1300 K provided that the fire is sufficiently ionized.

TABLE OF CONTENTS

LIST OF TABLES

LIST OF FIGURES

CHAPTER 1

Introduction

1.1. High intensity bushfires in Australia

Australian climate and vegetation can support very high intensity bushfires. In most cases, high intensity bushfires occur during dry seasons (Price *et al.* 2003; Williams *et al.* 1999 and Andersen *et al.* 2005). Australian dry-seasons are characterized by high ambient temperatures, which can desiccate vegetation to a tinder dry state. *Eucalyptus* species are endemic to most parts of Australia. Leaves of *eucalyptus* are laden with highly flammable resins, which make Australian *eucalyptus* forests the most hazardous when they have accumulated high fuel loads under the prevalence of dry and gusty wind conditions. The coincidence of hot and dry climate with bad fire weather (high gusty winds, high atmospheric instability and low relative humidity) have in the past lead to disastrous bushfires e.g. the Ash Wednesday (1983) and Black Friday (1939) (Sullivan, 2004). Regrettably, ignition source for most disastrous bushfires in Australia is anthropogenic in nature. Human activity initiated bushfires account for 62.2% of fires that burnt across Australia (Rawson *et al.* 1982).

1.1.1. Fire-prone vegetation

Due to low annual rainfall, frequent droughts and fire-prone vegetation, Mediterranean regions and tropical savannas of Australia are subjected to recurring bushfires of varying intensities (Britton, 1982; Williams *et al.* 1999 and Collett, 2000). Eucalyptus and corymbia species dominate in these forested regions, making them the most flammable sclerophyll forests in the world (Williams *et al.* 2003; Underwood *et al.* 1981; Collett, 2000 and Catchpole, 2000). It is of note that the recurrence of bushfires predominates in the wet and dry sclerophyll forests of Western Australia and southeastern Australia during summer and the grassland ecosystems of the northern parts of the continent during austral winter (Morrison, 2002 and Williams *et al.* 2001). In Western, South and southeastern Australia, summers are generally hot and dry with hot winds blowing from the desert interior (Underwood *et al.* 1981). Under these dehydrating conditions, eucalyptus species such as Jarrah (*Eucalyptus marginata*) and Karri (*Eucalyptus diversicolor*) in Western Australia, shed large quantities of litter that accumulate rapidly on forest floors

(Underwood *et al.* 1981). The eucalyptus leaves are laden with highly flammable oil, making eucalyptus forest highly susceptible to bushfires. Similar climatic conditions are also prevalent in northern Australia in winter, hot dehydrating winds sweep across the grassy savanna creating a highly fire prone environment. The approach of a cold front in southeastern Australia draws the dry north westerlies into the region creating conducive conditions for bushfires which have catastrophic effect on natural vegetation (e.g. in Chafer *et al.* 2004 and Morrison, 2002) and property as it is shown in Figures 1.1 and 1.2.

1.1.2. Antecedent climatic and prevalent synoptic weather conditions during high intensity catastrophic bushfires

1.1.2.1. ENSO related rain deficiency

Australian rainfall is seasonal. The seasonality in rainfall pattern is an influence of tropical and midlatitudinal weather systems. During summer, an intense thermal heating warms up ocean waters in the Australian-Pacific Ocean region bringing about widespread convective and cyclonic activity to tropical northern and eastern Australia. Cold fronts are a dominant force in southern Australia's winter rainfall. The passage of the frontal system causes the advection of moist air that can bring about abundant rainfall and thunderstorm activity in the region. However, the rainfall producing mechanisms are complicated by the onset of El Nino-Southern Oscillation (ENSO) events. ENSO is a large-scale quasi-periodic anomalous ocean-atmosphere coupled climate phenomenon that disrupts global climate patterns every 3 - 4 years on average (Power *et al.* 1999). The climate anomaly is known to affect the climate of northern and eastern Australia by making them rain-deficient but its effect is not pronounced in Western Australia (Sullivan, 2004 and Nicholls, 1997).

The ocean component of the ENSO has two episodes: the warming (El Nino) and cooling (La Nina) events of the tropical central and eastern Pacific Ocean. La Nina event brings about wide spread convective activity all over Australia especially to southern or eastern Australia. The converse is true for an El Nino event. During El Nino episodes, major wind circulation that influences the climate of the pacific region (i.e. Walker circulation) is shifted eastwards due to the displacement of warm ocean water to central Pacific (Allan *et al.* 1996 and Peixoto *et al.* 1992). The eastward shift of the Walker circulation signifies that the low-pressure system has been displaced from its normal position, an effect that results in disastrous hot and dry spells in

Figure 1.1. *High intensity bushfire consuming understorey vegetation and ground fuel-litter and logs.* (Photo: CSIRO, BBM)

Figure 1.2. *Pub destroyed during the Canberra 2003 bushfires* (Photo: Belinda Mepham)

northern and eastern Australia. The 1982-83 El Nino episodes have lead to the most disastrous climate variations around the world. Australia, southeast Africa and Borneo were plunged into the worst drought ever (Fauchereau *et al.* 2003 and Chu *et al.* 2002). Catastrophic bushfires that destroyed millions of hectares of precious ecosystems in Australia and Hawaii during this period are linked to the climate anomaly (Kitzberger, 2002 and Chu *et al.* 2002).

During 1982-83 El Nino episodes, a strong subsidence prevailed over eastern Australia with above normal air temperatures and dehydration effects on vegetation (Arblaster *et al.* 2002). Prolonged severe drought prevailed in the region as there was below average rainfall (Meyer *et al.* 2001). Evaporation and evapotranspiration were exacerbated by the dry conditions. With tinder dry vegetation, low relative humidity and above normal temperature conditions, catastrophic bushfires burned in Victoria during the Ash Wednesday killing 71 people and causing extensive damage to property.

1.1.2.2. Heat waves

Netherlands Royal Meteorological Institute (NRMI) defines heat waves as periods of more than five consecutive days with a maximum temperature of at least 25ºC and three of those with a maximum temperature of at least 30ºC (Hajat *et al.* 2002). The heat waves create conducive conditions for catastrophic bushfires in Australia, e.g. 1939 ACT bushfires (Luke *et al.* 1978). The high temperature events are trigged by various weather anomalies. In Mediterranean southern Europe (e.g. in Greece); a region tormented by frequent bushfires, heat waves are caused by a simultaneous northward displacement of the main axis of Subtropical Jet Stream (SJS) at 200-hpa levels and a Hadley Cell. A large subsidence develops beneath of the SJS axis. The subsidence results in the advection of warm air, which increases ambient temperatures to above average (Giles *et al.* 1990).

In Australia, heat waves are caused by meridional shift in the frontal system (Kuhnel *et al.* 2000). Besides the meridional shift, blockage the frontal system by an intense anticyclone in the Great Australian Bight may also cause heat waves (Underwood *et al.* 1981). During Austral summer, an intense high-pressure system lies across southern Australia. The system breaks down with time, into a series of intense anticyclones, with a simultaneous development of a low-pressure system over the west coast of Western Australia. The series of intense anticyclones thereafter moves eastward with a frequency of 7 - 10 days with a cold front preceding each anticyclone. However,

if an anticyclone becomes stagnant, usually over the Bight, the advection of cold moist air to the landmass stops and persistent dry and hot northwesterly air from the desert interior predominate raising the ambient air temperature to above normal.

Generally, major bushfires that occurred in Australia were fueled by the existence, for several days, of above normal ambient temperatures. For an example, a heat wave which affected most of the southern states of Australia in late November of 1982 created conditions conducive to catastrophic bushfires which killed at least 5 people in Sydney in early December of the same year (Kuhnel *et al.* 2000). During the Ash Wednesday, several places in Victoria recorded abnormally high temperatures for more than 6 consecutive days. Melbourne recorded a maximum of 43.2ºC (Sullivan, 2004). Many more such instances exist.

1.1.2.3. Synoptic weather conditions and bushfire danger index

Synoptic weather conditions of high atmospheric instability, high gusty winds and low relative humidity create very bad fire weather when they co-exist with antecedent climate of extreme heat and El Nino events (Liu *et al.* 2004). This concurrent condition often leads to catastrophic high intensity bushfires (Sullivan, 2004). A measure of the potential for intense bushfires to develop is expressed in terms of Forest Fire Danger Index (FFDI). The index is given by Noble *et al.*1980 as:

$$FFDI = 1.275 Df^{0.987} \left\{ e^{[0.0338T - 0.0345RH + 0.0234U]} \right\} \qquad \text{(Equation 1.1)}$$

Where: T = air temperature,
U = wind speed in open at 10m height,
RH = Relative humidity.

Df in Equation 1.1 is the drought factor also given by Noble *et al.* 1980 as:

$$Df = \frac{\left[0.191(I + 104)(Nr + 1)^{1.5}\right]}{\left[3.52(Nr + 1)^{1.5} + (R - 1)\right]} \qquad \text{(Equation 1.2)}$$

Where: I = Keetchy Byram Drought Index,

Nr = Number of days since the last rain,

R = Precipitation received.

The drought index is a reflection of the amount of dry fuel available for the spread of high intensity bushfires. During an El Nino episode, the Keetchy Byram drought index and drought factor are often both high. Relative humidity is also low. The occurrence of a heat wave can worsen the situation by raising air temperatures abnormally high and the influx of hot dry northwesterly winds may increase the rate of spread of bushfires. Sydney fires of 1994, in which 4 people perished, were characterized by more than 5 days of extreme fire danger with FFDI of more than 50. The maximum FFDI reached during the conflagration was 96 on the 8th of January. The grassfire that burned in Mangoplah in 1952 was characterized by a very high value of Grassland Fire Danger Index (GFDI). On the 25th January 1952 in Mangoplah, GFDI was 115. This was brought about by extreme conditions of 100 % grass curing, ambient temperatures at 41^{o}C and gale force north westerly winds at a speed of 48 km/h (Sullivan, 2004).

1.2. Radio communication failure during high intensity bushfires

Radio communication in close proximity to high intensity bushfires has been a safety concern to firefighters. Several cases of failure to maintain HF-VHF radio communication through and in close proximity to a high intensity bushfire have been reported, for example, the Lara 1969 (Williams *et al.* 1970) and Dwellingup 1961 (Foster, 1976) bushfire disasters. An explanation of how this could happen is still a problem for radio scientists to solve. In this work we are considering signal attenuation produced by absorption in the partially ionised plasma and by ray path interference. The impact on communications will depend on specific modulation being used, and is not considered here

Bushfire plumes consist of a slightly ionized gas. That is, there exist a small number of charged particles (electrons and ions) and a large number of uncharged particles (neutrals) in fire plumes. Due to their mass, electrons in the flame are highly mobile while ions and neutrals are approximately stationary relative to the electrons. The particles interact with each other through collision. In a slightly ionized gas, electron-neutral collision is the dominant mode of particle interaction as there are fewer electrons compared to neutrals and also because of the electron's high mobility.

Fire plumes are conductive due to the presence of the free electrons. When the bushfire flame is illuminated with a weak electromagnetic wave, the electrons are accelerated by the electric field of the incident electromagnetic waves. Thus electrons acquire energy from the incident wave. The absorbed energy is transferred to the neutrals in the plume through collision. If we assume that collisions between electrons and neutrals are elastic, then electrons are scattered isotropically such that the average velocity after collision is zero. Most of the electron-absorbed energy is dissipated as heat. In this way energy is transferred from the electromagnetic wave to the neutral gas. The dissipation of the energy leads to incident radio wave's electric field attenuating with distance into the flame. Clearly, radio wave absorption depends on the amount of ionization (electron density) and the frequency of collision between electrons and the neutral particles. The greater is the neutral particle density, the higher is the probability of collision with the electrons and the greater the amount of absorption in the bushfire plume. Electron density and electron-neutral collision frequency are subject to neutral gas temperature, density and nature of plume particles.

Temperatures in bushfires can be very high as the oxidation reaction is exothermic. The vegetation combustion liberates a wide range of products of which CO, H_2O, and CO_2 are some of its main products. Depending on fire intensity and behavior, a series of organic and inorganic particulates are also produced. Free radicals exist in very high intensity bushfires. Some of these radical species act as catalysts in flame reactions. Hydrogen (H*) and methyl (CH*) radicals, if present, become reactants in chemi-ionization processes that produce electrons. In chemi-ionization, exothermic heat produced in the flame and heat produced during dissociation of flame species supplement the energy required for ionization of flame species. However, flame temperatures limit the contribution of chemi-ionization to bushfire plume ionization. The contribution may be significant in very high intensity bushfires. The presence of inorganic particulates, e.g. Alkali and Alkaline Earth Metals (AAEM) species in the flame produces enhanced ionization that limits the catalytic-effect of the contribution due to chemi-ionization even at high temperatures.

AAEM atoms have low ionization energy. Potassium and sodium have ionization energies 4.34 and 5.14 eV respectively. If it is assumed that bushfire flame is in local thermal equilibrium and velocity distribution function is Maxwellian, at normal bushfire temperatures (~1300 K), a partial pressure of one-millionth atmospheres of potassium atoms can produce an electron density of

about 10^{17} m^{-3}. This ionization density is enough to cause appreciable absorption of up to 11.43 dB/m on radio waves.

Radio wave absorption may be the most important way by which radio wave energy is lost to a bushfire provided there is a significant amount of alkalis present in the plume. Another significant way by which radio wave signals may be altered is by wave refraction in fire plumes with steep temperature gradients.

Radio wave refraction can be caused by gradients in pressure, temperature and ionization in the propagation medium. Propagation velocity of a radio wave in a medium of such gradients changes with the physical properties, i.e., wave velocity is increased when the wave traverses from a cool to a hot region of a medium. The increase in speed bends wave fronts away from the hot to cool regions of the medium. The overall effect is a change in the direction of propagation of the wave. A similar effect is observed in a medium with ionization gradients. Radio wave signals are bent away from a highly ionized to a less ionized region of the medium. Deviation of radio waves from their path causes focusing/de-focusing of signal intensity at a targeted receiver.

1.3. Motivation and aims

There are reports of radio communication failure during high intensity bushfires. These reports are anecdotal; therefore a scientific investigation into the matter is necessary. This work is a contribution to understanding the dynamics of radio communication signal loss through a very high intensity bushfire plume and in its close proximity. The thesis also aims at carrying out a scientific investigation focusing primarily on radio wave absorption and refraction in a bushfire plume. On absorption, the thesis aims at:

- Performing a numerical experiment that predicts Radio Wave (R-Wave) absorption and phase shift in moderate to high-intensity bushfires. Using a suitable fire plume model, propagation of radio waves in vegetation fires could be predicted. Numerical simulation is a cost-effective means of determining whether bushfires can significantly attenuate radio waves. It is a crucial part of this research as it guides us as to what; (a) magnitudes of attenuation are to be expected in field measurements, and (b) equipment is to be deployed in order to obtain attenuation data with reasonable accuracy. Propagation characteristics of R-Waves in bushfires are to some extent influenced by potassium

content in vegetation. There is potassium content of up to 3.4 % in plants (Radojevic, 2003). However, Australian vegetation may contain up to 2.71 % potassium by dry weight (Smith, 1974). The alkalis are released, from the structural bondage during combustion of plant matter, into the fire plume (Dayton *et al.* 2000, Olsson *et al.* 1997 and Davidsson *et al.* 2002). Temperatures in very high intensity bushfire flame are high enough to cause significant thermal decomposition of the potassium salts and subsequent thermal ionization of the alkali atoms. A significant percentage (up to 20 %) of potassium atoms may be ionized as they have low ionization energy (Vodacek *et al.* 2002). Assuming thermal equilibrium and Maxwellian distribution function of particles' velocity, electron density due to the potassium and momentum transfer collision frequency can be determined. The electron density and momentum transfer collision frequency can then be used to predict radio wave absorption and phase change in very high intensity bushfires.

- Measuring R-wave absorption and phase shift at HF, VHF and X-band frequencies in moderate intensity fires. R-Wave propagation data in bushfire environments at HF to VHF is scarce. Some propagation measurements at other frequency bands such as the UHF and SHF (Williams *et al.* 1970), 23-40 GHz (SHF) (Hata *et al.* 1983), and 37-250 GHz (EHF) (Gibbins *et al.* 1987) have been reported though some of it lacks precision. At VHF, there are no measurements reported. The VHF frequency is relevant to bushfire suppression as some Australian fire brigades still use the frequency band for communication during fire suppression. Field and laboratory measurement of LOS radio wave propagation in vegetation fires is the only direct way to find out whether bushfires can significantly affect radio wave communications. For safety reasons, the measurements cannot be carried out in very high intensity fires.

- Williams *et al.* 1970 and Hata *et al.* 1983 respectively attributed the SHF R-Wave signal loss to refraction and ionization in flames. The researchers acknowledged that an increase in fire intensity could significantly affect signal strength due to increased ionization and refraction effects. However, an explanation of how these effects can happen in the bushfire plume has not been addressed. The thesis proposes a mechanism on how the two processes could occur in a bushfire plume.

On refraction, the thesis does not address the measurement of deviation of VHF R-Wave signals in bushfire environment. However, Williams *et al.* 1970 and Palmer, 1981 have measured deviations of SHF radio rays in bushfire plumes. In the thesis, it is intended to:

- Construct a 2D - ray tracing scheme and a biconcave thermal lens model to trace radio rays 0.5 mm transversally apart through moderate and high intensity bushfire plumes. Attenuation and deviation of R-Waves due to bushfire plume would then be estimated by comparing the number of rays leaving a transmitter to the number arriving at a target point. The numerical determination of R-wave energy defocusing in the fire plume is also important in answering the question of whether bushfires can cause radio communication failure

- Use the constructed 2D-ray tracing scheme to model and explain the deviation data obtained from multinational *mass fire* experiments; Operation Euroka (Williams *et al.* 1970) and Project Flambeau (Palmer *et al.* 1981). The mass fires were of moderate intensity.

1.4. Layout of the thesis

Chapter 2 of the thesis examines the proposition that the omnipresent alkalis are main source of ionization in bushfires. High temperatures (up to 2000ºC) involved in bushfires volatilize alkalis from combusting vegetation into the fire plume where up to 20 % of the molecules are thermally ionized. Potassium is the most important alkali in this proposition because of its low excitation energy (4.34 eV) and it is also the most abundant alkali in most plants. Low excitation energy of potassium makes it an easy element to ionize in high temperature environments.

Radio wave propagation predictions in grassfire flames of varying heat intensities and dimensions are made in Chapter 3. The predictions made in the chapter are based on the proposition that alkalis, more especially potassium atoms, are the main source of ionization in the bushfire plume (Chapter 2). Local Thermodynamic Equilibrium (LTE) and Maxwellian velocity distribution of particles velocity are assumed in the prediction. With these assumptions, electron number density and concentrations of other species in the flames are estimated. Chapter 3 also discusses the theory of radio wave propagation through a weakly ionized medium such as the bushfire flame.

As a *first approximation*, a slab model of grassfire flame of varying dielectric permittivity is proposed in the chapter. Numerical experiment results obtained from the chapter are later compared with the attenuation measurements carried out in chapters that follow.

Field measurements of signal attenuation and phase shift were carried out in moderate intensity controlled grass (black spear grass) and cane fires using a Radio Wave Interferometer (RWI). The measurements are reported in Chapters 4 and 5 respectively. The RWI was designed and built at the University for this purpose. The design of the RWI is discussed in the Chapter 4. RWI uses the same principles as a Microwave Interferometer (MWI) except that it has been designed to operate at lower frequencies. Phase shift and absorption measurements in forest litter flames at microwave frequencies were carried out in a laboratory experiment using a Vector Network Analyzer (VNA) in Chapter 6.

On refraction, a theoretical study of the effect of the thermal bubble on radio waves propagation was carried out by ray tracing methods in Chapter 7. The intensity and maximum temperature of a simulated very high intensity bushfire used in the numerical experiment were 90 MWm^{-1} and up to 1400ºC respectively. The chapter considers radio wave focusing/de-focusing due to plume density and temperature gradients. Plume constituents concentrations are a very important factor in radio wave refraction, more especially that of water vapor and electrons as they contribute quite significantly to the plume radio refractivity. The issue is explored in the chapter by varying plume water vapor and potassium concentration. Chapter 8 concludes the thesis by discussing major findings of experiments carried out in this work.

Electromagnetic wave theory, which is fundamental to this work, is not new. It can be found in radio propagation papers and electrodynamics textbooks. This includes the influence of electric field on charges in a slightly ionized medium. The dominant mode of ionization in wildfires has been thought to be chemi-ionization (chemical reaction, dissociation and then ionization). The literature acknowledges thermal ionization as another ionization mechanism that cannot be ignored in forest fires. This thesis suggests that the latter mode of ionization may dominate over chemi-ionization especially when there are alkalis present in the flame. Radio wave propagation measurements in grassfires and cane fire together with the design of Radio Wave Interferometer (RWI) provide new results and conclusions about the importance of potassium content in the fuel. The technique of determining propagation constants of radio waves through a material using a network analyzer is not new, however its application in determining the electron density in forest

fuel flames is novel. The discussion and calculations of refraction of radio waves by a combination of density gradients and ionization in Chapter 7 is new work.

The middle chapters in the thesis were developed and written as stand alone papers. Because of this there may be some repetition in the introduction and theory sections of these chapters. Their sequential arrangement develops the theme of the thesis. Currently, nine (9) papers have been published from the thesis in refereed journals. Two (2) papers have been resubmitted and one is under review by Meteorology and Atmospheric Physics journal. These papers are:

1. Mphale K.M., and M.L. Heron, 2007. Plant alkali content and radio wave communication efficiency in high intensity savanna wildfires. *Journal of Atmospheric and Solar-Terrestrial Physics* **69** (4 - 5), 471- 484.

2. Mphale K.M., and M.L. Heron, 2007. Wildfire plume electrical conductivity *Tellus B* **59** (4), 766 – 772.

3. Mphale K.M., and M.L. Heron, 2007. Microwave measurement of electron density and collision frequency of a pine fire. *Journal of Physics D: Applied Physics*, **40** (9), 2818 – 2825.

4. Mphale K.M., and M.L. Heron, 2007. Ray tracing radio waves in wildfire environments. *Progress in Electromagnetics Research* (*PIER*) **67**, 153 – 172.

5. Mphale K.M., M.L. Heron, and T. Verma, 2007. Effect of wildfire-induced thermal bubble on radio communication. *Progress in Electromagnetics Research* (*PIER*) **68**, 197 – 228.

6. Mphale K.M., and M.L. Heron, 2007. Absorption and transmission power coeffiecients for millimeter waves in a weakly ionized vegetation fire. *Int. J. Infrared Millimeter Waves* **28** (10), 865 - 879.

7. Mphale K.M., D. Letsholathebe, and M.L. Heron, 2007. Effective complex permittivity of a weakly ionized vegetation litter fire at microwave frequencies. *Journal of Physics D: Applied Physics*, **40** (21), 6651 - 6656.

8. Mphale K.M., and M.L. Heron, 2008. Non-intrusive measurement of ionization in a vegetation fire plasma . *European Physical Journal: Applied Physics* **41**, 157 - 164.

9. Mphale K.M., and M.L. Heron, 2007. Interferometric measurement of ionization in a grassfire. *Meteorology and Atmospheric Physics* (under review).

10. Mphale K.M., and M.L. Heron and G. Kurusa, 2007. On large subsidence, wildfires and changes in atmospheric boundary layer electromagnetic properties. *Terrestrial, Atmospheric and Oceanic Sciences* (re-submitted)

11. Mphale K.M., and M.L. Heron, 2007. The influence of plant inorganic ash content on wildfire plume electronic conductivity. *Journal of Electrostatics* (re-submitted)

12. Heron M.L. and K. Mphale, 2004. Radio wave Attenuation in Bushfires, Tropical Cyclone, and Other Severe atmospheric Conditions - Final Report on EMA Project 60/2001, James Cook University.

13. Mphale K.M., M. Jacob, and M.L. Heron, 2007. Prediction and measurement of electron density and collision frequency in weakly ionized pine fire. *Int. J. Infrared Millimeter Waves* **28** (3), 251 - 262.

CHAPTER 2

Mechanism of alkalis emissions from vegetation during very high intensity bushfires

2.1. Introduction

The main objective of this chapter is to review the literature on alkali content in Australian fire-prone vegetation and alkali emission from the vegetation during flaming. Bushfire flames are a weakly ionized gas. The thesis examines the proposition that the omnipresent alkalis are main source of ionization in bushfires. Owing to the high temperatures (875-2000ºC) involved in very high intensity bushfires, alkalis are volatilized from combusting vegetation into the fire plume where up to 20 % of the molecules are thermally ionized. Emphasis is put on element potassium because of its low excitation energy (4.34 eV) and it is also the most abundant alkali in most plants. Low excitation energy of potassium makes it an easy element to ionize in high temperature environments such as bushfires.

Electron density in bushfire flames can be as high as 10^{17} m^{-3}. This can significantly affect radio wave communication by reducing signal strength and changing its phase. The effect of ionization in bushfire environment on radio wave propagation is documented (e.g., Foster, 1976) and will be discussed in chapters that follow.

Potassium and other alkalis are present in significant amounts in Australian vegetation. Foliage from Australian eucalyptus species contains up to; 2.71 %K, 1.77 %Ca, 0.33 %Na and 0.55 %Mg on dry weight basis. In vegetation, alkalis exist in different physical forms. They can exist; ionically or organically attached to the organic structure of the plants, as discrete particles in voids of the organic matrix and in solution form such as in transport vessels (e.g. xylem). The concentration of alkalis is higher in live than in dead foliage. Very high fire-line intensity bushfires (7.7 - 100 MWm^{-1}) consume both nutrient rich live foliage and forest floor litter (see Figures 2.1 and 2.2). Alkalis are liberated from plant's organic matrix and drawn by convective currents into the bushfire plume.

Figure 2.1. *A very high intensity bushfire-crown fire* (Photo: CSIRO BBM)

Figure 2.2. *Devastated vegetation after a very intense bushfire* (Photo: W.R. Wallace)

This chapter is arranged in the following manner. Section 2.2 gives an account of the occurrence of very high intensity bushfires in fire-prone regions of Australia and prevalent weather conditions during these fires. Alkali content in the fire–prone vegetation is briefly discussed in Section 2.3. Physical forms of existence of alkalis in plants are discussed in the Section 2.4. Section 2.5 discusses the mechanism of the alkali emission from plants during the combustion.

Qualitative analysis of alkali-based emissions from the combustion of vegetative material is reviewed in Section 2.6 for temperatures up to 1400°C. Alkali salt species at this temperature are thermally unstable. They decomposed to give alkali atoms. An account of observations of excited potassium atoms is given in Section 2.7. Up to 20 % of alkalis in plant matter are ionized during bushfires (Vodacek *et al.* 2002). The Chapter is concluded in Section 2.8 with the major points of interest in the thesis enunciated and summarized.

2.2. Very high intensity bushfires in regions of Australia

Very high intensity bushfires are defined as those having fire-line intensity greater than 7700 kWm^{-1} (Grant *et al.*1997). High fuel loads, and the prevalence of extreme bushfire weather, sustain the fires. Unstable atmospheric conditions, high ambient temperatures, hot gusty windy conditions and antecedent dry conditions characterize extreme bushfire weather. Southeastern and southern Western Australia forests are under a constant threat of these catastrophic fires during summer as weather conditions are conducive for their occurrence. Very high intensity bushfires are not common in north Australia's tropical savannas as fuel loads are rarely enough to support the fires. However during late dry season, very high intensity bushfires occur occasionally (Williams *et al.* 2001).

The intensity of the highest bushfires in the tropical savannas is generally less than a third of those occurring in temperate southeastern Australia. Peak intensity of bushfires occurring in southeastern Australia is more than 60 MWm^{-1} whereas in tropical northern Australia peak fire intensity is up to 20 MWm^{-1} (Williams *et al.* 2001).

2.2.1. Very high intensity bushfires in southwest Western Australia

Jarrah (*Eucalyptus marginata*) and Karri (*Eucalyptus diversicolor*) dominate overstorey vegetation of southwestern Western Australia forests. Marri (*Corymbia calophylla*) occasionally mix with the *E. marginata* and *E. diversicolor* stands in the overstorey stratum. Cycad (*Macrozamia riedlei*), *Banksia* spp., Brakenfern (*Pteridium aquilium*) and *Bossiacea laidlawina* are common in the middle layer of the *E. diversicolor* and *E. marginata* ecosystems (O'Connell *et al.* 1996). Karri Hazel (*Trymalium spathutum*) and *Xanthorrhea* spp. shrubs populate the ground layer of the both the ecosystems (Underwood *et al.* 1981).

As seasons change, eucalyptus foliage desiccates as it is subjected to varying moisture and temperature stress. The foliage eventually falls to the ground and accumulates on forest floors as litter. The litter is composed of dead leaves, twigs, branches, floral parts and shed tree bark. Southwest Western Australia *E. diversicolor* and *E. marginata* communities shed about one-quarter (1/4) of their leaves every year. In *E. marginata* forests leaves make up about 70% of the litter (Burrows, 2001). Understorey shrubs, tree crowns and litterfall are a fuel for VHIBs (see Figures 2.1 and 2.2).

In the eucalyptus forests of southwest Western Australia litter accumulates rapidly and the accumulation on forest floors is observed to reach its maximum during summer (O'Connell *et al*. 1996). The litter fall accumulates at rate described by a modified Olson (1963) model. O'Connell *et al* give the modified model as:

$$L_t = L_{ss}\left(1 - e^{-kt}\right) + L_0 e^{-kt} \qquad \text{(Equation 2.1)}$$

Where: L_t = current forest floor mass,

$L_{0,}$ = initial forest floor mass,

k = decomposition constant,

L_{ss} = mass of the forest floor at equilibrium conditions.

The build up of litter is at different rate for *Eucalyptus diversicolor* and *Eucalyptus marginata* communities. According to O'Connell *et al*., L_{ss} for *Eucalyptus diversicolor* forest floor is approximately 40 tha^{-1}. Litter accumulation (L_t) could reach 23-30 tha^{-1} over 8 years.

Accumulation is much slower in *Eucalyptus marginata* communities. The L_{ss} for *Eucalyptus marginata* forest floors is estimated to be in the range 10 - 18 tha^{-1}. Underwood *et al.* 1981 estimate that *E. marginata* and *E. diversicolor* forests accumulate 1-3.5 and 2.5-11 tha^{-1} of litter every year respectively.

Southwest Western Australia experiences a Mediterranean climate, thus dry summers and cool wet winters predominate. Conditions exist in summer when the region experiences heat waves and strong dry windy conditions. This happens when trains of intense high-pressure cells that normally propagate from west to east are blocked in the Great Australian Bight (Underwood *et al.* 1981). This may coincide with an appearance of a cyclone in the northwest coast of the continent. The effect of the whole system is the advection of hot dry air into the region from the country's interior (Sullivan, 2004). The influx of hot dry air causes dehydration and heat stress conditions in the eucalyptus species. This ultimately leads to very high intensity bushfires when the fuels are ignited.

The Dwellingup bushfire disaster of 1961 is a result of extreme bushfire weather. During the bushfire disaster, relative humidity dropped to a minimum of 14 % and ambient temperature rose to a maximum of 41.1°C (Sullivan, 2004). Strong gusty winds with an average speed up to 37 kmh^{-1} fanned bushfires to a fire line intensity in excess of 15 MWm^{-1} (Fernandes *et al.* 2003).

2.2.2. Very high intensity bushfires in northern Australia Savannas

Darwin Stringy Bark (*Eucalyptus tetrontonda*), Grey Bloodwood (*Eucalyptus porrecta*) and Darwin Woollybutt (*Eucalyptus miniata*) are the dominant eucalyptus species in woodlands and forests of northern Australia tropical savannas. Annual Sorghum (*Sorghum intrans*) and Spear grass (*Hetropogon triticeus*) dominate the grassy understorey in these ecosystems (Setterfield, 2002 and Cook, 1994). Other deciduous shrubs such as *acacia* spp. share the understorey stratum with the sorghum spieces. Overstoreys of open woodlands consist of Broad-leaved Paper Bark (*Melaleuca viridiflora*) and *Pandams spiralis* as predominant species and *Paspalum* spp. and *Digitrea* spp. are prominent in their understorey.

Senescent grass is the main combustion material on savanna woodland and forest floors (Willams R.J. *et al.* 2003). The model for accumulation of both grass and tree leaf litter on forest floors is similar to that described by Olson (1963). Cook (2003) gives the litter accumulation model as:

$$L_t = \frac{L_a}{k}\left(1 - e^{-kt}\right) \qquad \text{(Equation 2.2)}$$

Where: L_t = accumulated fuel load,

L_a = average annual litter production,

k = litter decomposition rate respectively.

The ratio L_a / k gives the steady state fuel load (L_{ss}). Sorghum grass accumulates litter at the rate up to 3 $tha^{-1}yr^{-1}$ while eucalyptus species accumulates at the rate up to 4.4 $tha^{-1}yr^{-1}$ (Williams R.J. *et al*, 2003). The steady state fuel load (L_{ss}) for sorghum grass is 10 tha^{-1} and this can be achieved in 3 years (Williams *et al.* 2002).

Australian tropical savannas have two distinct fire seasons that differ in both intensity and patchiness. They are; the early dry, and the late dry fire seasons (Williams *et al*. 2003). The early dry season usually starts from June. Grass is a dominant fuel for fires that burn in this season; it comprises about 75 % of the floor litter (Williams *et al*. 2003). In the early dry season the grass is moist from monsoon rains, which retreat in early May. High moisture content in the fuel dampens the ferocity of the fires, which therefore are usually of low intensity. Average intensity of bushfires in the season is about 2200 kWm^{-1}

Atmospheric humidity decreases as the dry season progress. A decrease in humidity ultimately leads to an increase in fuel load due to leaf fall from desiccating vegetation. Late dry fire season starts around September. Twigs and tree leaves constitute most about 57 % of the litterfall. Fuel loads may be up to 10 tha^{-1}(Williams *et al.* 1999). The high fuel loads combined with conditions conducive to extreme fire weather results in intense conflagrations with average intensities of 7.7 MWm^{-1} (William *et al.* 2002).

Bushfire weather in northern Australia is characterized by two fire indices. The indices are the Forest Fire Danger Index (FFDI) and Grassland Fire Danger Index (GFDI) (Gill *et al.* 1996). The indices are an indication of the possibility of bushfire occurrences. They range from 0 to 100, where 50 represents extreme fire weather. The maximum FFDI and GFDI for the tropical savannas occur during the late dry season. An average of FFDI recorded over 11 years period in Jabiru in the tropical northern Australia was between 60 and 65 (Gill *et al.* 1996). At the peak of

the late dry fire season daily maximum temperatures may rise to an average value of 36°C with daily wind patterns changing continuously (Gill *et al*.). This signifies extreme bushfire weather, which is conducive to high intensity bushfires.

A very high intensity bushfire burned in Kakadu National Park at Kapalga Research Station in the late dry season, September 1994. The intensity of the fire was approximately 20 MWm^{-1}. The fuel load for the vegetation was 8 tha^{-1} and rate of spread was 1.2ms^{-1}. The scorch height was observed to be 22 m (William *et al.* 1999).

2.2.3. Very high intensity bushfires in southeastern Australia forests

The eucalyptus species of southeastern Australia are known to be the most fire-prone vegetation in the world (Collett, 2000). Fire frequency in these sclerophyll forests ranges between 4 to 400 years (Braithwaite, 1994). Very high intensity bushfires burn in these ecosystems with average intensities more than 60 MWm^{-1} (Williams *et al*. 2002). Eucalyptus forests in Victoria shed a large amount of litter, with Mountain Ash (*Eucalyptus regnan*s) forests accumulating 9.40 $tha^{-1}yr^{-1}$ (Attiwill *et al*. 1996). Forest floors of Little Snowman (*Eucalyptus pauciflora*), Blackbutt (*Eucalyptus pilularis*) and Alpine Ash (*Eucalyptus delegatensi*s) may also be a potential bushfire threat as they can accumulate 37.2 to 34.2 tha^{-1} respectively (Turner *et al.* 1976).

*Eucalyptus regnan*s are mainly found in montane areas south of the Great Dividing Range in Victoria. Some stands are also found in Wilson's Promontory. *E. regnans* is one of the tallest eucalyptus trees and can reach a height of 100 m. It can grow mixed with *Eucalyptus cypellocarpa* as in Powelltown, Victoria (Collett, 2000). In this area, common understorey are silver wattle (Acacia *dealbata*), Mountain Hickory Wattle (*Accacia obliquinervia)*, Victorian Christmas-bush (*Prostanthera lasianthos*), Forest wire-grass (*Tetrarrhena juncea*) and Oats grass (*Avena fatua*), just to name a few. *Eucalyptus regnan*s communities in Wallaby creek, *Pomaderris aspera* and *Olearia argophylla* are common understorey plants (Ashton *et al.*1999).

Blackbutt (*Eucalyptus pilularis*) grows on the eastern coast of Australia, from New South Wales to Queensland (Turner *et al.* 2002). *E. pilularis* often grows as pure stands, however in drier areas; it can co-exist with Spotted Gum (*Corymbia maculata)* and Barked Apple (*Angophora costata*). In area around Sydney, it grows with Blue Gum tree (*Eucalyptus saligna)*.

Southern Tasmania's wet sclerophyll forests are dominated by *Eucalyptus obliqua*, *E. regnans* and *Eucalyptus obliqua*. They are known as mixed forest due to the fact that they have dense understorey of Myrtle (*Nothofagus cunninghamii*). East Tasmania is vegetated with dry sclerophyll eucalyptus species such as *E. nitida*, *E. viminalis*, *E. seiberi* and *E. globulus.*

Litterfall amount of about 22 tha^{-1} has been reported in *E. regnans* (Collett, 2000). The litter accumulation in pure stands of *E. regnan*s can be modeled by equation (2.2), with litter accumulated over time taking the form (Mackey *et al.* 2002);

$$L_t = 24.75\left(1 - e^{-kt}\right) \qquad \text{(Equation 2.3)}$$

Where: t = age of stand up to 250 years,

L_t = amount of litter on the forest floor.

Litterfall in eastern Tasmania's *Eucalyptus seiberi* is modeled by equation (2.1) with X_0 being 1.92 (Neyland *et al.*1994):

$$X_t = X_{ss}\left(1 - e^{-kt}\right) + 1.92e^{-kt} \qquad \text{(Equation 2.4)}$$

The variables have the same meaning as in equation (2.1).

The climate in southeastern Australia is quasi-Mediterranean and is temperate in southern Tasmania. During summer, ambient temperatures are between 30-40°C (Collett, 2000). The combination of the high temperatures and high fuel loads with the periodic hot gusty northerly winds render the region an extreme fire hazard. In southern Tasmania, very strong northwesterly winds, temperatures of above 39°C and low humidity of 11 % have brought devastating bushfires to the region after drought.

Devastating fires have raged through the southeastern Australia eucalyptus ecosystems. Some of them are the memorable Ash Wednesday of 1983 and the Hobart fire of 1967. These fires burned in an environment dominated by the worst bushfire weather conditions.

2.2.4. Very high intensity bushfires in southern Australia heath and shrub lands

Heaths are treeless vegetation, which grow in nutrient deficient soils. Australian heaths span a wide range of climatic environments, from the wet monsoon climate of tropical northern Australia to wet winter Mediterranean climate of southwestern Australia (Keith *et al*. 2002). In New South Wales, heaths occur along the eastern coast seaboard under the warm temperate climate. Banksia, Hakea, Acacia, Leptospermum and Xanthorrehea species dominate these heaths.

Mallee shrublands cover central New South Wales, northwest Victoria, southern South Australia and southern Western Australia. These ecosystems are dominated by overstorey of eucalyptus species such as Grey Mallee (*E. socialis*), Narrow-Leaved Red Mallee (*E. foecunda*) and Dumosa Mallee (*E. dumosa*). The height of overstorey mallees may be up to 10 m. Hammocks of Porcupine grass (*Triodia irritans*), Wattle (*Acaccia Wilhelmina*), Scrub Cypress pine (*Callitris verrucosa*) and Broom bush (*Melaleuca uncinata*) form the understorey for the shrublands. The fuels are not homogeneous but erratically distributed.

Fuel load in heaths reach equilibrium loads of less 15 tha^{-1} after 10 to 20 years. The equilibrium fuel load is 30 tha^{-1} in the dry east coast heath. This is very low compared to that of wet sclerophyll forests such as the *E. diversicolor* and *E. regnans* (Sullivan, 2004). Keith *et al*. (2002) describes fuel loads in heathlands (L_t) as:

$$L_t = \alpha\left(1 - e^{-kt}\right) \qquad \text{(Equation 2.5)}$$

Where: α = maximum amount of litter,

t = time since the last fire.

The litter in the shrublands piles around individual plants and varies between 5-15 tha^{-1}. On average the fuel loads are 15 tha^{-1}. For East coast heathland the fuel load takes the form (Keith *et al*. 2002);

$$L_t = 30\left(1 - e^{-kt}\right) \qquad \text{(Equation 2.6)}$$

Where maximum amount of fuel (α) is 30 tha^{-1}.

Fuels in heath and shrublands are highly flammable. Leaves of some shrubs and grasses contain flammable resins and waxes. For example Oil mallee (*Eucalyptus oleosa*) contains 3 - 4% essential oils that are flammable. Porcupine grass (*Triodia irritans*) is highly flammable also, as its detritus forms a well-aerated fuel bed.

The climate of the southern Australia ranges from Mediterranean in southern Western Australia to temperate in New South Wales. Extreme fire weather in the shrub lands occurs when a tropical depression is shifted southward. Winds associated with a tropical low cause a sudden change in wind direction making it gusty. If during summer, ambient temperatures rise more than 30°C, it exacerbates the fire weather to extreme. The combination of the high temperatures and high fuel loads with the hot gusty northerly winds render the region an extreme fire hazard.

In mallee heath lands, very high intensity bushfires fires up to 35 MWm-1 have been observed (Keith *et al.* 2002). Wind speeds of about 30 $kmhr^{-1}$ and bushfire spread of rate 2.08 ms^{-1} were reported (Keith *et al.*, 2002).

2.3. Alkali content in Australian fire-prone vegetation

2.3.1. Chemical compositions of plant matter

The organic structure of plants is mainly composed of three interconnected biopolymers: cellulose; hemicellullose and lignin. The composition of the biopolymers in plants is in the approximate ratio of 2:1:1 (Krishna *et al.*1985 and Hu *et al.*1999). These polymeric compounds account for over 90 % of the plant's dry weight (Ward, 2001). The rest of the constituents are fillers (Simoneit, 2002). Fillers are a mixture of several low molecular weight organic compounds (extractives), water and inorganic elements.

Cellulose is the most important of the constituents as it forms the skeletal structure of plants. Its content varies, however it is generally in the range of 40-50 % of the organic structure (Brown *et al.* 2000). Its thermal degradation behavior resembles that of wood (Levan, 1989) and due to this, cellulose is often used as a representative of vegetation in combustion reactions (e.g. in Nussbaumer, 2003; Stott, 2000 and Zhou *et al.* 2000). Structurally, cellulose is a linear, highly stable, chemically resistant homopolysaccharide made up of a repeated 7000-12000 glucose (D-glucopyranose) monomer (Simoneit, 2002). The glucose units are "glued" together by β-

glycosidic bonds. The β-glycosidic bond makes cellulose very stable thereby giving a plant its structural strength. Cellulose monomers organize to create micro-fibers and ultimately bind into larger parallel fibers by forming inter and intra-molecular bonds with each other.

The matrix that lies between the cellulose fibers is made up of a mixture of polymers. Hemicellulose is a major component of the mixture (Grønli *et al.* 2000). Hemicellulose is a name given to all non-cellulosic polysaccharides and other substances such as uronic acids and their derivatives. It is a highly branched hetero-polysaccharide. It contains about 100–200 different monomers (Simoneit, 2002). The monomeric units of the molecule are mainly 5-carbon sugars (e.g. L-arabinose and D-xylose) and 6-carbon sugars (e.g. D-glucose and D-mannose). It is also possible to have L-rhamnose, D-glucoronic acid, 4-O-methyl-D-glucoronic acid in the polysaccharides. Because of its high branching, hemicellulose is less rigid and easy to hydrolyse to its constituent sugars.

The lignin component of wood is quite different chemically from cellulose and hemicellulose. It is not a carbohydrate but a phenolic compound. This phenolic compound consists of polymeric, aromatic materials characterized by the presence of secondary phenyl propane units (coumaryl, coniferyl and sinapyl alcohols) with methoxyl, phenolic hydroxyl and carboxyl functional groups (Salisbury *et al.*1991). Because of its strength, lignin provides compression resistance in cellulose structures. Lignin is highly insoluble because of its high molecular weight. The insolubility of lignin makes it a suitable material for xylem wall lining. Apart from serving as a fiber binder that gives strength and rigidity, lignin also protects wood from pathogens.

The extractables are fats, resins, sugars, oils, starches, alkaloids and tannins that can be extracted from plants by polar or non-polar solvents such as water. The function of the extractives is that they serve as intermediates in plant metabolism and are also internal energy reserves. There are responsible for the plant's characteristic color and flammability and odours of various plants species.

Water makes up to 60 % of plant's fresh weight (Lobert *et al.*, 1993). It occurs in three phases; the hygroscopic (adsorbed) water, capillary (free) water and water vapor (Grønli *et al*., 2000). Adsorbed water exists attached to the hydroxyl functional groups by hydrogen bonds in plant's organic matrix while free and gaseous water exist within vascular bundles, cell walls and voids. Water in plants facilitates the transportation of dissolved nutrients to metabolism and enzyme

activity sites. It is one of the main contributing substances to plant photosynthesis.

The inorganic matter component varies from 0.1 to 10 % in vegetation (Radojevic, 2003). Alkalis, chlorine and sulphur are part of the inorganic matter (ash) in the plant matter. Plants require large quantities of these elements for a healthy growth. Consequently, the inorganics exist in substantial amount in cell fluids in vacuoles (Obernberger *et al.* 1996; Whiting *et al.* 2004 and Maser *et al.* 2002). Significant quantities of the macronutrients are found in foliage and bark, but predominately in growing tissues of plants.

2.3.2. Alkalis content in plants

The origin of alkalis in plants could be traced back to the earth's crust where the elements exist as a structural part of naturally occurring minerals. The natural abundance of the element potassium in the earth's crust is 2.6 % (Tarburk and Lutgens, 2002). It occurs mainly as potassium orthoclase feldspar and muscovite micas. Calcium and magnesium account for 3.6 % and 2.1 % of the weight of the earth crust respectively. Calcium occurs naturally as calcite, gypsum and aragonite while magnesium as dolomite and serpentine.

2.3.2.1 Availability of alkalis elements to plants

About 2.0 % of potassium that is in the soil is available for plant use in four different forms (Schulte *et al*. 2002). These forms are; soluble, exchangeable, fixed and structural potassium. Soluble potassium is that which is dissolved in soil water (soil solution). This form is most readily available for plant use and is absorbed by plant roots as potassium ions (K^+) (Schulte *et al*. 2002). The exchangeable form acts as a reservoir for the soluble form. Since plants require a lot of potassium, the soluble form may sometimes get depleted. It is then that potassium ions are drawn from the exchangeable potassium pool. In the fixed potassium pool, the potassium is trapped between expanding clay minerals such as illite (Øgaard *et al.* 2001) and is available to plants slowly over a long time. The structural form has the highest amount of potassium in the feldspar and micas (Øgaard *et al.* 2001). The minerals take hundreds of years to disintegrate into a significant amount of potassium that could be used by plants (Pal *et al*.2002). For example, in soils where quartz and kaolin constitute most of the mineralogy, soluble and exchangeable are the main form of potassium available for plant consumption. Generally, fixed and structural potassium forms are not readily available for plant use.

Potassium in the exchangeable form exists as cations attached to organic matter or clay surfaces. These surfaces, often referred to as soil colloids, are negatively charged and they attract the aqueous potassium cations from the soil. The soil colloids hold the potassium cations temporarily and as the bonds between the colloids and potassium ions are weak, colloids readily exchange potassium ions for other positively charged ions such as hydrogen, calcium or magnesium. Plants are efficient in the use of nutrients.This is shown by the fact that when there is an excess of potassium ions which are not in immediate use by plants, they are released back into in the soil to the exchangeable potassium pool (see Korb *et al*. 2002).

Plants absorb magnesium as divalent ions Mg^{2+} in the soil solution from soil colloids. Like potassium ions, magnesium ions are mobile. If equal concentration of positively charged nutrients ions are present at the exchange surface, Mg^{2+} ion will displace K^{+} ions from colloids.

Calcium exist as divalent ions (Ca^{2+}) in the soil. Carbonic acid formed from carbon dioxide dissolved in soil water reacts with calcite to produce the divalent ions, which attach themselves to the negatively charged clay and organic matter colloids. Ca^{2+} ions are less mobile than K^{+}, however diffusion and membrane potential help to transport the calcium ion into the plant. Unlike potassium ions, calcium ions use xylem tubes to reach the leaves, as they are phloem immobile (Duesing, 1985).

In vegetation, alkalis are dispersed through the organic matrix in different physical and chemical forms. Some are organically or ionically bound but most are in aqueous form (Westberg *et al*., 2003). The forms in which they exist, are in accordance with their functions in the host plant tissue. For example, potassium in a guard cell of a leaf is in aqueous form to facilitate rapid export and import of K^{+} ions into the cells during stomatal closing and opening respectively.

2.3.2.2 Functions of alkali and alkaline earth elements in plants

Potassium is the most abundant monovalent cation in higher plants (Maser *et al.*, 2002). The element plays a vital role in daily functional activities of plants, primarily in plant nitrogen and carbohydrate metabolism (Hannant *et al*.1982). Potassium promotes the growth of meristematic tissue and it activates more than 60 enzymes responsible for plant growth. Potassium has a special role of regulating the water use by plants as it controls the stomatal opening and closing.

Complete stomatal closing also serves as a barrier to pathogens from entering the plant. In situations where there is insufficient water for plant use in the topsoil, potassium helps in root elongation to deeper soil layers and activates root regeneration to maximize available moisture consumption. Potassium strengthens the natural resistance of plants to diseases such as leaf blight and stalk rot in corn.

Calcium has an important task of maintaining the cell permeability and integrity. In this respect, it regulates the absorption of nutrients across the plasma cell membranes and neutralizes organic acid in plant cells. In a plant cell, calcium acts as a facilitator in cell division and elongation an in nitrogen metabolism and carbohydrates translocation (Bennett, 1996). It also serves as a detoxifying agent by attracting toxic compounds and also it maintains anion-cation balance in the vacuoles. In plant cells, calcium with magnesium form salts of pectic acid, which makes up the middle lamella that binds adjacent plant cells. Thus, calcium is an important part of the physical structure of plants as it maintains the strength of stalks and stems of plants.

Magnesium is main inorganic component of the chlorophyll molecule. The element serves as a cofactor in the production of most enzymes responsible for the formation of carbohydrates, sugars and fats. It is an activator of *Adenosine TriPhosphase*(ATP)-*Adenosine DiPhosphase*(ADP) metabolism reactions. It facilitates the formation of *DeoxyriboNucleic Acid* (DNA) and messenger *RiboNucleic Acid*(mRNA).

2.3.3. Alkali and alkaline earth elements content in Australian fire-prone vegetation.

Potassium content in vegetation biomass is estimated to be in the range of 0.51-3.4 % (Radojevic, 2003). Studies carried by Attiwill, 1981; Stewards *et al.* 1981 and Turnner, 1981 have revealed that some Australian eucalyptus and pine species contain much lower potassium in their biomass than estimated by Radojevic. Attiwill and Turnner studied two eucalyptus species; *Eucalyptus obliqua* and *Eucalyptus grandis* in southeastern Australia. According to the study by Attiwill and Turnner, *Eucalyptus obliqua* and *Eucalyptus grandis*'s biomass contains about 0.08 % potassium. Stewards *et al.* have worked out the percentage of potassium in oven dry weight of *Pinus radiata*'s biomass and found it to be 0.23 %. Despite this low potassium content in Australian eucalyptus biomass, potassium content in living foliage falls within the Radojevic's estimate.

Eucalyptus species are classified into monocalyptus, symphyomyrtus and corymbia subgenera. Examples of these subgenera are *Eucalyptus regnans, Eucalyptus grandis, and Corymbia calophylla* respectively. Analysis of foliar nutrient content in the subgenera has shown that, in an "average" Australian eucalyptus forest, symphyomyrtus species contain 0.7 %K, 0.26 %Mg and 1.00 %Ca. Corymbia species contain 0.61 %K, 0.26 %Mg and 0.48 %Ca and monocalyptus species have 0.46 %K, 0.31 %Mg and 0.48 %Ca (Judd *et al.* 1996). A comprehensive table compiled by Feller 1980 has shown that the ranges of nutrients in Australian eucalyptus foliage are: 0.12-1.25 %K; 0.16-0.55 %Mg; 0.18-1.22 %Ca and 0.04-0.33 %Na.

Jones *et al.* 2001 conducted a study to estimate the amount of calcium content in an average plant matter. Jones *et al.* estimated the amount of calcium in plants to be in the range of 0.22-1.04%, however the calcium content could be up to 3.52 % in certain plant species (Duesing, 1985). Comparatively, Australian eucalyptus calcium content in living tissues is within range as Feller, 1980 calculated it to be 0.03-3.21 % on dry weight basis. The maximum calcium content analyzed from the stem bark while the minimum value from the stem wood.

2.3.3.1. Alkali and alkaline earth element content in eucalyptus forests of southwest Western Australia

Eucalyptus marginata, *Eucalyptus diversicolor* and *Corymbia calophylla* belong to monocalyptus, symphyomyrtus and corymbia subgenera respectively. Symphyomyrtus subgenus is known to be nutrient loving and thrives very in fertile soils (Judd *et al.* 1996). In this respect, symphyomyrtus species are likely to contain more nutrients in the foliage than monocalyptus and corymbia species. Judd *et al.* have also compiled a table showing the range of foliar nutrient content in eucalyptus subgenera in southwest Western Australia. According to Judd *et al.*1996, *Eucalyptus marginata* foliage contain 0.29-0.59 %K, 0.34-0.49 %Mg and 0.30 - 0.64 %Ca. *Eucalyptus diversicolor* contain 0.61- 1.28 %K, 0.22 - 0.31 %Mg and 0.82 - 1.68 %Ca. while the *Eucalyptus calophylla* contain 0.89 %K, 0.65 - 0.76 %Ca and 0.33 - 0.36 %Mg.

An analysis of litter accumulated over 9 years on *Eucalyptus diversicolor* forest floors for macronutrient content by O'Connell *et al.* gave 0.08 %K, 0.24 %Mg, and 1.20 %Ca. For *Eucalyptus marginata,* O'Connell *et al.* analyzed the content to be 0.09 %K, 0.17 %Mg, and 0.76 %Ca. When these litter fall nutrient contents are compared with those of living foliage, it is found that there is a significant decrease in the nutrient element at the time of fall.

A common understorey shrub in *Eucalyptus marginata* forests of southwest Western Australia is *Macrozamia riedle.* Grove *et al.* 1980 have analysed the nutrient content in the living foliage of a growing *Macrozamia riedle* shrubs. Previously, the shrub understorey had been devastated by a bushfire. Grove *et al.* noted that over the years (up to 7 years), the concentration of the nutrients increased except for potassium. For a 1year old and 7 years old shrub, Grove *et al.* analyzed the shrub to contain: 0.92 %K, 0.35 %Ca, 0.15 %Mg, 0.03 %Na, 0.22 %Cl and 0.09 %S; and 0.78 %K, 0.55 %Ca, 0.15 %Mg, 0.10 %Na 0.37 %Cl and 0.12 %S respectively. Another understorey plant; *Xanthorrea preissii* can contain up to 2.01 % potassium on dry weight basis (Lamont *et al.* 2004).

2.3.3.2. Alkali content in eucalyptus forests of southeastern Australia

*Eucalyptus regnan*s and *Eucalyptus obliqua* belong to the monocalyptus subgenus. Symphyomyrtus species in Victoria are *Eucalyptus nitens* in mountain forests and *Eucalyptus globus* and *Eucalyptus viminalis* in Foothills forest (Attiwill *et al.*1996). As expected, the foliar macronutrients content variables depending on the soil contamination. Macronutrients content in eucalyptus subgenera in Victoria is however lower than that of southwestern Western Australia. Kasel, 1991 studied the mean foliar concentration of macronutrients in the monocalyptus and symphyomyrtus eucalyptus subgenera endemic to Victoria. According to Kasel, 1991 for randomly sampled leaves, foliar nutrient content in monocalyptus species is: 0.43 %K, 0.43 %Ca and 0.24 %Mg. Symphyomyrtus species contain 0.49 %K, 0.65 %Ca and 0.16 %Mg. Judd *et al.* 1996 have assessed foliar macronutrient content in forests dominated by *Eucalyptus obliqua* in Victoria. According to Judd *et al.*, the range of macronutrient content in *Eucalyptus obliqua* forests is; 0.32 - 0.45 %K, 0.39 - 0.66 %Ca and 0.24 - 0.39 % Mg.

In forests where *Eucalyptus regnan*s and *Eucalyptus obliqua* are predominant, forest floors accumulate at the rate of 9.4t ha^{-1} per year. The litter contains 0.15 %K, 0.12 %Mg and 0.52 %Ca (Attiwill *et al*. 1996). Low macronutrient content is expected in typical eucalyptus litter accumulated over 50 years and will contain about 0.08 %K, 0.98%Mg and 0.37 %Ca (as in Attiwill *et al*. 1996).

In another study of a mixed eucalyptus forest ecosystem in the eastern Victoria by Turner and Lambert 1996, much lower macronutrients exist in understorey vegetation and litter. In the understorey vegetation, the nutrient content was found to be 0.05 %K, 0.11 %Mg and 0.47 %Ca

while in the litter fall, the content was found to be 0.04 %K, 0.07 %Mg and 0.55 %Ca.

2.3.3.3. Alkalis content in pine species of southeastern Australia

Potassium is highly mobile. When a plant component becomes dormant, potassium translocates to other parts of the plant that are active. According to Hinnant *et al*. 1982, potassium can also to migrate from older dormant tissue through phloem tubes into the soil. This is evident when comparing the potassium content in living and dead *Pinus radiata* plant components. Stewart *et al.* have estimated the percentage of potassium in living and dead foliage of *Pinus radiata* on average to be 0.71 % and 0.10 % respectively. On living and dead branch wood Steward *et al.* estimated 0.43 % and 0.1 %K respectively. Another study by Turvey *et al*. 1994 shows similar potassium content in *Pinus radiata* with a mean value of 0.78 % and 0.11 % living and dead foliage.

Australian pine species generally have less than 1.02 % calcium content. Studies carried out by Steward *et al.* 1981; Turner, 1981; and Attiwill, 1980 show low percentage of calcium in *Pinus radiata* plants. Lambert, 1981 has estimated calcium in the living foliage to be 0.24 % respectively in *Pinus radiata* respectively. Steward *et al.* have estimated that calcium content in live branch wood; dead branch wood, live foliage and dead foliage is 0.35 %, 0.41 %, 0.21 % and 0.96 % respectively. This is explained by the fact that calcium is phloem immobile; it cannot be translocated back to the soil by transport vessels, like potassium. It accumulates in a plant component until the component becomes dormant and thus when it can be returned to ground when the dormant component falls to the ground.

The percentage of magnesium in the living foliage of Australian *Pinus radiata* has been found to range from about 0.05 - 0.17 % (Stewart *et al*. 1981 and Lambert, 1981). As magnesium is not phloem immobile, magnesium can migrate back to the soil when the plant becomes dormant. Thus dead plant components contain less magnesium than live ones. The study by Steward *et al.* 1981 supports this, as they measured 15.52 $kgha^{-1}$, 6.05$kgha^{-1}$, 19.03 $kgha^{-1}$ and 1.03 $kgha^{-1}$ for living branchwood, dead branchwood, living foliage and dead foliage respectively.

2.3.3.4. Alkali element content in understorey vegetation of Australian tropical savannas.

Cook (1994) studied macronutrient concentration in grass understorey vegetation in Northern Australia savannas. In the study, Cook concluded that on average, savanna grasses have the following nutrient concentration: 0.22 %K; 0.16 %Ca; 0.10 %Mg and 0.033 %S. Earlier, Cook (1991) analysed the macronutrient in sorghum species only. Cook (1991) observed that in 2 months old *Sorghum intrans*, the macronutrient content are in the range of: 1.07 %K; 0.09 %S; 0.41 %Ca; 0.19 %Mg and 0.12 %Na. In sorghum (*Sorghum stipoideum*) of the same age Cook observed the following macronutrient content: 1.50 %K; 0.20 %S; 0.62 %Ca and 0.64 %Mg while Na was not determined. The nutrient content decreased as the sorghum species matured. The nutrients content of both *Sorghum intrans* and *Sorghum stipoideum* decreased to an average of: 0.63 %K; 0.07 %S; 0.32 %Ca and 0.14 %Mg.

Fensham *et al.* (1995) studied the nutrient content in the savanna of northern Australia. In the study, live foliage of some understorey vegetation such as Green Plum (*Buchanania obovata*) and Cocky apple (*Planchonia careya*) were in the range: 0.56 %K, 0.86 %Ca, 0.74 %Mg and 0.80 %K, 0.50 %Ca and 0.46 %Mg respectively. Overstorey vegetation of the savanna; *Eucalyptus tretrodonta*, *Eucalyptus miniata* and Broad – leaved Carbeen (*Eucalyptus confertiflora*) contained: 0.21 %K, 0.20 %Ca, 0.26 %Mg; 0.23 %K, 0.19 %Ca, 0.21 %Mg and 0.77 %K, 0.61 %Ca, 0.35 %Mg respectively.

Forest floors in woodlands and forests of northern Australia tropical savanna also accumulate litter at the rate that can be described as well by Olson's model. According to Williams *et al*. 2003, senescent grass is the main combustion material on tropical savanna woodland and forest floors. It accumulates litter at the annual rate of $3tha^{-1}$. Eucalyptus species accumulate litter at the rate up to 4.4 tha^{-1} per year (Williams *et al.* 2003). Litter in mature sorghum species may have nutrient content as follows: 0.13 %K; 0.04 %S; 0.35 %Ca and 0.06 %Mg. Leaf fall may contain this nutrient content: 0.23 %K; 0.06 %S; 0.94 %Ca and 0.31 %Mg.

Other tropical savanna grasses such as buffel grass (*Cenchrus ciliaris*) and Siratro (*Macroptilium atropurpureum*) can have potassium and calcium content ranging from 0.64 – 1.82 % and 0.66 – 0.85 % respectively (Mannetje *et al*. 1983). Fleming (1973) analysed *Paspalum notatum* to contain 1.82 % K and 0.44 % Ca. The concentration of potassium in grasses is seasonally

dependent. It has been observed to be high during spring and low during winter for kleingrass *(Panicium coloratum*), little bluestem (*Schichrium scoparium*) and brownseed paspalum (*Paspalum plicatulum*) (Hinnant *et al.* 1982). This is due to the fact that climatic changes affect plant metabolism rate and hence plants' mineral content is altered. According to the study by Hinnant *et al.*, potassium content in the stem material for the kleingrass, little bluestem and brownseed paspalum grasses reached a maximum of 2.81 %, 1.63 % and 2.39 % respectively during spring.

In a study to determine the mineral content in tropical grasses; perennial ryegrass (*Lolium perenne*), Cocksfoot (*Dactylis glomerata*) and Tall fescue (*Festuca arundina*), Thomas *et al.* (1952) observed that perennial ryegrass contains; 0.46 %Ca, 2.01 %K and 0.21 %Mg, Cocksfoot contains; 0.42 %Ca, 2.3 %K and 0.22 %Mg and Tall fescue contains; 0.30 %Ca, 2.07 %K and 0.26 %Mg.

2.4. Mode of existence of alkali and alkaline-earth elements in plants

Alkalis in vegetation exist in aqueous form, for example as metals ions such K^+, Ca^{2+}, and Mg^{2+} are surrounded by water. These aqueous ions exist in: (a) xylem and phloem tubes where they are taken to various growing tissues; (b) organic matrix voids; and plant cell sap or fluids in vacuole (Jensen *et al.* 2000). Most of the alkali elements that exist in plants are in this form (Westberg *et al*. 2003). According to studies by Dayton *et al.* 1999 and Knudsen *et al*. 2004a, over 90 % of potassium in plants is water-soluble. The soluble alkali ions exist as companion of anions such as chloride and sulphate, e.g. potassium atoms have been found by x-ray photography to exist close to chlorine atoms in straw (Bjorkman *et al.* 1997 and Jensen *et al.* 2000). This suggests that in chlorine rich plants, most of the inherent potassium exists as a chloride. This has also been verified by Olsson *et al.* 1997 and Jensen *et al*. who observed that during pyrolysis of plant matter, a significant amount of potassium is emitted as potassium chloride. However, in chlorine deficient plants, complex organic *malate* (2^-) ions are companions of potassium in cell vacuoles (Knudsen *et al*. 2004b).

Oxygen-containing and carboxyl carbohydrates functional groups in the plant's organic matrix such as lactone, phenoxide and carbonyl can attach alkalis elements as cations to form complexes (Jensen *et al.* 2000 and Westberg *et al.* 2003). Potassium is known to form a weak ionic bond with these functional groups (Knudsen *et al*. 2005). In plant cells, magnesium and calcium bind

two the *polygalacturonic* acid molecules together in the formation of pectin polymer, a minor constituent of plant structure (Mohr *et al.*1994). The ability to bind the acids is due to fact that the elements are divalent and are able to form an ionic bond with carboxyl functional group in each *polygalacturonic* acid. Magnesium potassium and calcium form complex chelates with ATP and ADP where they act as metal activators for enzymes (Salisbury *et al*. 1991).

Apart from potassium, calcium and magnesium are metabolized to form organic compounds in the plants organic matrix. Magnesium is an important element in the manufacture of chlorophyll. It combines with *protoporphyrin IX* to form *Mg-protoporphyrin monomethylester*, which ultimately leads to the formation of chlorophyll after a series of reactions (Mohr *et al.*1994).

Another way alkalis could exist in plants matter is as discrete salt particles (Knudsen *et al*. 2004 and Jensen *et al*. 2000). During the dehydration of vegetal matter, sap dissolved alkalis in xylem and phloem tubes and those in organic matrix voids precipitate as solid crystals (e.g. potassium carbonate and chloride crystals) when water evaporates. Another form of salts as discrete particles is when oxalic acid, which can be in substantial amounts in some plants, reacts with calcium to form insoluble calcium oxalate, which precipitates in cell vacuoles (see Salisbury *et al.*1991). *Phytic* acid or phytin(a form in which plant phosphate is stored cells) forms insoluble white *phytate* crystals when it reacts with magnesium or calcium in cell vacuoles (Mohr et *al.*1994). Figure 2.3 below shows all these modes of existence in a herbaceous plant stem.

2.5. Mechanism of alkali release during bushfires

Depending on meteorological conditions, bushfires can burn erratically, spreading very fast on eucalyptus forest floors and crowns. Nutrient-rich vegetation, fallen leaves, twigs, bark, grass, low-lying and crown vegetation provide fuel for the free spreading combustion (see Figure 1.1). The combustion of plant material produces a wide range of chemical compounds depending on various factors such as weather conditions, chemical composition of fuel, amount of vegetative fuel and availability of oxygen for combustion.

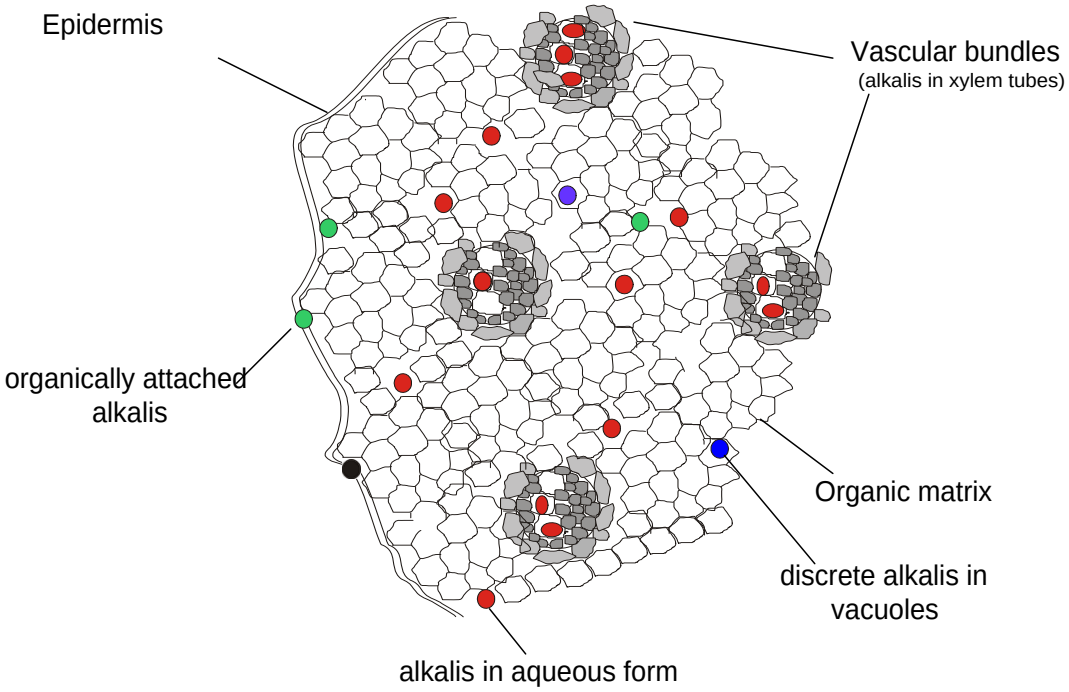

Figure 2.3. *Mode of alkali existence in a herbaceous plant tissue*

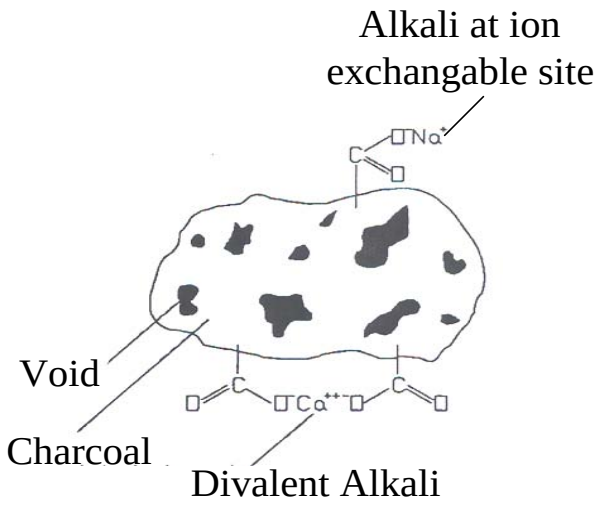

Figure 2.4. *Alkali attached to a functional group on the surface of a charcoal.*

2.5.1. Chemistry of Bushfires

Despite the complexity of the products, it is known that the main products of bushfires are carbon dioxide (CO_2) and water vapor (H_20). They are often referred to as the products of complete combustion (PCC), for if bushfires were highly efficient, water vapor and carbon dioxide would be the only products. This can be seen from a reaction equation of an average composition of vegetation, $CH_{1.44}O_{0.66}$ with atmospheric air below (Nussbaumer, 2003):

$$CH_{1.44}O_{0.66} + 1.03\beta(O_2 + 3.76\ N_2) \longrightarrow \text{intermediates(C, CO, } H_2, CO_2, C_mH_n, \text{ etc.})$$
$$\longrightarrow CO_2 + 0.72\ H_2O + (\beta\text{-}1)O_2 + 3.87\beta N_2 \quad \text{(Equation 2.7)}$$

Where β is the excess air ratio. The ratio determines the nature of products from bushfires. If β is unity, a bushfire will be efficient. Unfortunately, bushfires are nowhere near efficient. Smoke plumes often seen rising from burning vegetative fuels suggest that a variety of other particles are produced as well. In a real situation, PCCs account for up to 90 % of the products given out during burning. The other products which are a function of combustion regime, have been sampled and identified by: Kuhlbusch *et al.*1996; McMahon, 1983; Yokelson *et al.* 1996 and many other researchers as; carbon monoxide (CO), nitrogen oxides (NOx), sulphur oxides (SOx), formaldehyde (CH_2O), graphite carbon (C), methane (CH_4), ethylene, methyl (CH_3) and other nonmethanehydrocarbons (NMHC) as well as other particulate matter. These are called products of incomplete combustion (PICC) or by-products of vegetative burning, for the reason that they are produced along side PCCs under an inefficient regime.

2.5.2. Phases of plant combustion.

There are two distinct phases of vegetation combustion. They are: (a) thermal degradation of solid plant material in an oxygen limited environment to give volatiles (combustible and noncombustible) and charcoal and (b) exothermic oxidation reaction of the combustible volatiles and charcoal (Liu *et al.*1998). The first phase involves *devolatilization* and *pyrolysis* of the fuel while the second is flaming and/or char combustion phase. The thermal degradation phase is temperature sensitive. For example, when a plant is heated for a long time at a low temperature, noncombustible volatiles are prominent and this leads to glowing instead of flaming combustion (see Levan, 1989).

2.5.2.1. Alkali emissions during devolatilization of vegetative fuel

During combustion of vegetation, a significant amount of alkali atoms and salts are volatilized. Examples of alkali salts volatilized are chlorides, carbonates, hydroxides and sulphates. The emissions are dependent on combustion temperature and the size of combusting fuel particle (Davidsson *et al.* 2002). Flaming combustion is distinctive for having a significant amount of alkali emission. Small amounts of alkalis are emitted in other phases of combustion. Figures 2.5(a)-(c) give a comprehensive illustration of how alkalis are emitted from a herbaceous plant stem during bushfires.

As radiant heat from an advancing bushfire front reaches the stem its surface temperature rises. This creates a heat gradient between the inner core and the stem surface. Consequently, heat is then conducted through the stem's organic matrix creating a drying front. In the drying front, most of the conducted energy heats and evaporates gaseous and capillary water from voids and cell walls in to the surrounding environment outside the stem as shown in Figure 2.5(a). Some of the free water in the stem diffuses further into the inner core by the pressure gradient force (Hagge *et al.* 2002). Evaporation of water from the organic structure has an effect of precipitating dissolve alkalis into discrete salts in the voids, xylem and phloem tubes (Westberg *et al.* 2003). The dehydration process occurs when the temperatures within the stem structure are less than 170°C. At this stage, an insignificant amount of alkalis are emitted from the matrix with outgassing water vapor.

An increase in the stem surface temperature above 200°C provides more energy to drive the drying front further into the fuel matrix. The drying front is then followed by a pyrolyzing front. In this front, the temperatures are between 200 and 300°C or even higher. The dehydrated vegetal matter thermally degrades with the production of CO, CO_2, hygroscopic H_2O and incombustible inorganics such as formic and acetic acids. Charcoal forms a crusting layer over the pyrolyzing zone, which grows in size with the increase in temperature. The three regions are shown in Figure 2.5(b). Charcoal traps alkalis in voids in the char matrix near to the surface. At temperatures between 200 and 300°C, organically associated alkalis are thermally dissociated from attachment sites because of weak attachment bonds and they diffuse to the surface where they react with the functional groups such as: carboxyl and carbonyl at the charcoal surface (Knudsen *et al.* 2005). Graphite in the charcoal also forms intercalates with alkali metal atoms as they diffuse through the char matrix from their attachment sites. Possible intercalates formed with graphite are C_8K

and $KC_{24}K$.

Cracks and fissure that often appear on the charcoal may let a small amount of alkalis to escape with volatiles at temperature below 300°C. This leads to very little measurable alkali emission (see Olsson *et al.* 1997 and Davidsson *et al.* 2002).

.

At temperatures between 300 and 450°C, combustible volatiles (H_2, CH_4, CO, CO_2), and more charcoal are produced from the pyrolysis of lignin. This further traps alkalis inside the char matrix. Emission of the volatile gases from the char matrix is accompanied by some alkalis and nutrients such as chlorine in the form of hydrogen chloride because of its low boiling point. The heat energy from the drying front is not enough to break free the weakly bonded alkalis (organically bonded alkalis) therefore insignificant alkali salts are emitted at this stage (Olsson *et al.*, 1997 and Davidsson *et al.*, 2002).

2.5.2.2. Alkali emission during flaming and char combustion phase

Significant alkali emission occurs during flaming (Vodacek *et al.* 2002 and Dayton *et al.* 1997). Heat from exothermic reactions at temperatures >500°C results in the rapid decomposition of cellulose and lignin, the major components of plant matter, into anhydroglucose and lots of volatiles and highly reactive hydrogen radical are released into the flame (McMahon, 1983). The heat decomposes charcoal into secondary products such as CO_2, CO and H_2O (White *et al.* 2001). This exposes attached alkali atoms and discrete salts in the charcoal matrix. The exposed alkalis are then drawn into the flame by convective up draughts. Convection may also force air to flow through the combusting char and with the availability of hydrogen radical from thermal cracking of volatiles, oxygen-associated alkalis in char reacts with the radical to produce atoms according to the following reaction mechanism (Okuno *et al.* 2005):

$$CMAT\text{-}A\ (s) + H\ (g) = CMAT\text{-}H(s) + A\ (g) \qquad \text{(Equation 2.8)}$$

Where: *CMAT-A* = alkali atom attached to char matrix,

A = alkali atom,

H = hydrogen radical.

As the alkalis attached to the oxygen-containing and carboxyl functional groups, leave the attachment sites as atoms, some of them may react with other flame anions such as chloride and hydroxyl ions to form salts depending on the combustion environment. A significant amount of alkalis are released from vegetation through this mechanism. However the salts are released into high temperature regions of the flame (combustion zone) to be decomposed further, back into atoms. Alkali chloride salts e.g. potassium chloride (KCl) are the most stable. However under very intense heat the salts are decomposed into their respective atoms that are subsequently ionized to give electrons and metal ions. The metal ions are then drawn out of the hot region of the flame to recombine at cooler regions with cations like chloride or sulphates. A significant amount of alkalis have been detected in this phase (Vodacek *et al.* 2002).

2.6. Qualitative analysis of the alkali release during vegetation combustion.

Chemical equilibrium calculations were carried to find the species of alkali and their phase during the combustion of plant matter such as straw and Salix (Jensen *et al.* 2000 and Ljung *et al.* 1997). Ljung *et al*. ran a chemical equilibrium program CHEMSAGE 3.0 to obtain a distribution of alkalis during the combustion of Salix. According to the calculations potassium may exist as potassium carbonate (K_2CO_3), potassium sulphate (K_2SO_4) and KCl in Salix.

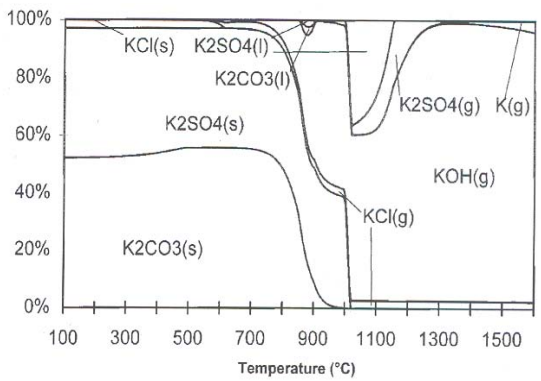

Figure 2.6(a). *Distribution of potassium during the combustion of Salix* (After Ljung *et al.* 1997)

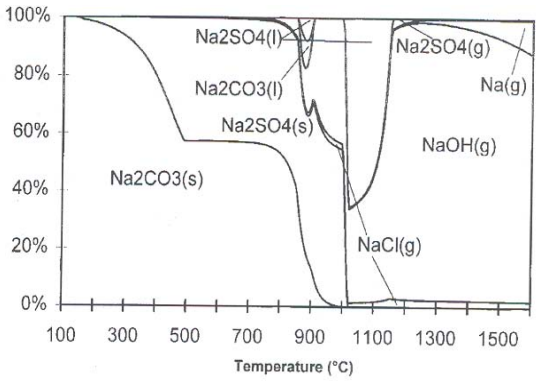

Figure 2.6(b). *Distribution of sodium during combusting of Salix* (After Ljung *et al.* 1997)

The alkali species continue to exist in solid form until temperature reaches 700°C. As the Salix is heated to temperatures above 700°C gaseous KCl and potassium hydroxide (KOH) are produced.

At about 950°C, K_2SO_4(s) is vaporized to the gaseous form. At temperature more than 1300°C some of the potassium in the Salix exists as potassium atoms. It could be due to thermal decomposition of the potassium salts.

Sodium follows a similar trend as potassium. Most of sodium exists as sodium carbonate. Gaseous Sodium chloride is formed at temperature more than 700°C. Around 800°C gaseous sodium hydroxide (NaOH) is formed. Around 1100°C gaseous sodium sulphate (Na_2SO_4) is formed. A significant amount of sodium atoms are present at 1200°C. The distribution of the alkali species is shown in the Figure 2.6(a)-(b).

Jensen *et al.*, 2000 also used the Chemical equilibrium program MINTSQ to work out speciation of potassium in combustion of Straw. According to the equilibrium calculation, potassium, which exists in condensed state as KCl and K_2CO_3, are vaporized to gaseous KCl, KCl_2 and K atoms at a temperature above 700°C. As temperature increases the concentration of K atoms increases while that of KCl (g) levels off. The increase in Concentration of K atoms could be the thermal decomposition of potassium salts such as KOH (g). Figure 2.7 below shows the distribution of potassium during combustion of straw.

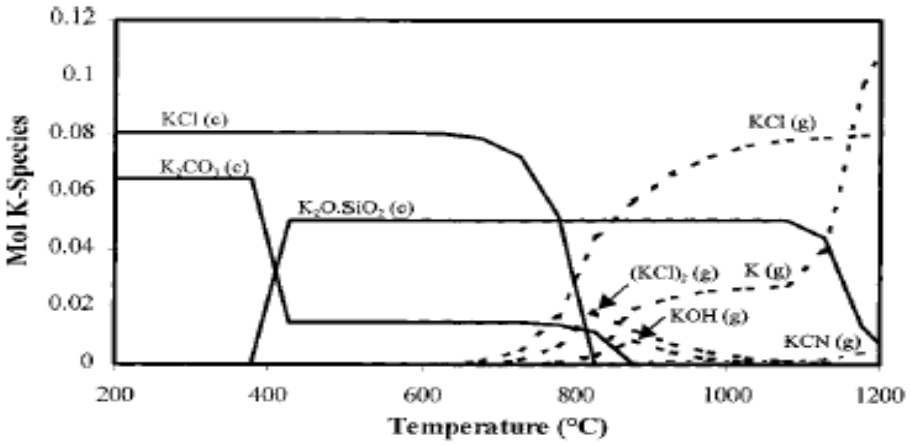

Figure 2.7. *Distribution of potassium species during the combustion of straw*
(After Jensen *et al.* 2000)

2.7. Observation of alkali release during bushfires

Latham, 1998 and Vodacek *et al.* 2002 have observed the emission of potassium from bushfires. Latham used an *Ocean Optics Model S2000* spectrophotometer in conjunction with a *Schmidt-Cassgrain* telescope to obtain emission spectra from a crown fire 50 m away. The spectra were of green to near infrared wavelengths, from 500 to 1000 nm. In the 500 -1000 nm spectrum, two prominent peaks were observed; one at 766.5 and the other at 769.9 nm as shown in Figure 2.9 (*Bushfire graph*). These correspond to K line emissions for resonance transitions; $^2P_{3/2}$ - $^2S_{1/2}$ and $^2P_{1/2}$ - $^2S_{1/2}$. The two peaks correlate with those present in the spectrum produced by introducing potassium chloride solution into a Bunsen burner flame (see Figure 2.8).

Vodacek *et al.* also obtained the green to near-infrared spectrum for a bushfire (control burn) flame. The 766.5 and 769.9 nm peaks were also prominent. The spectrum is shown in Figure 2.9 (*Bushfire graph*). Though not shown in Figure 2.9, the sodium doublet was also present at 589.3 nm. The radiance of the peak was very much weaker than that due to potassium. The reason for the low radiance is that sodium concentration is low compared to that of potassium. Its concentration in plants is a quarter or less that of potassium (Feller, 1980). Another reason for low radiance is that sodium has a higher ionization energy of 5.14 eV.

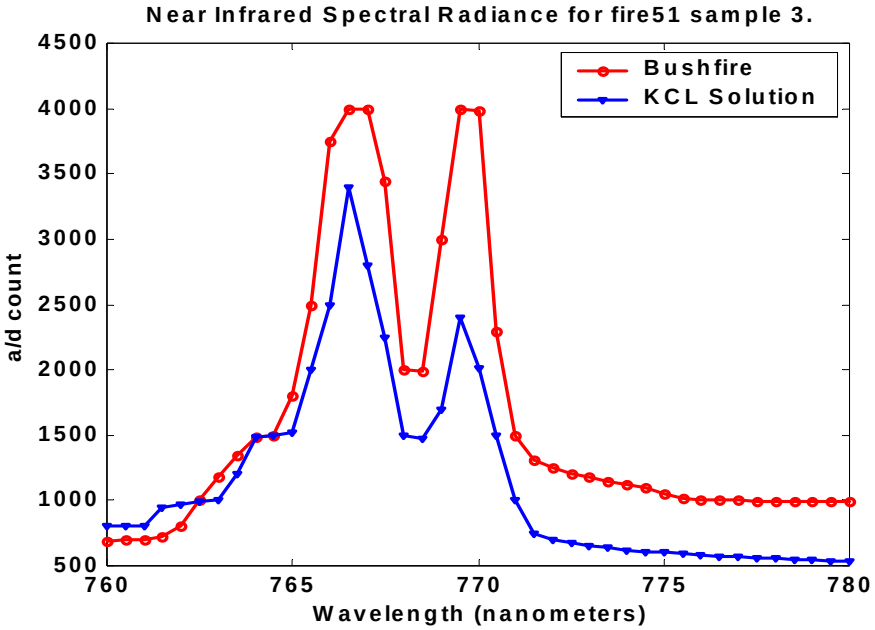

Figure 2.8. *The spectra produced from a bushfire and KCl solution correlate (*after Latham 1998*)*

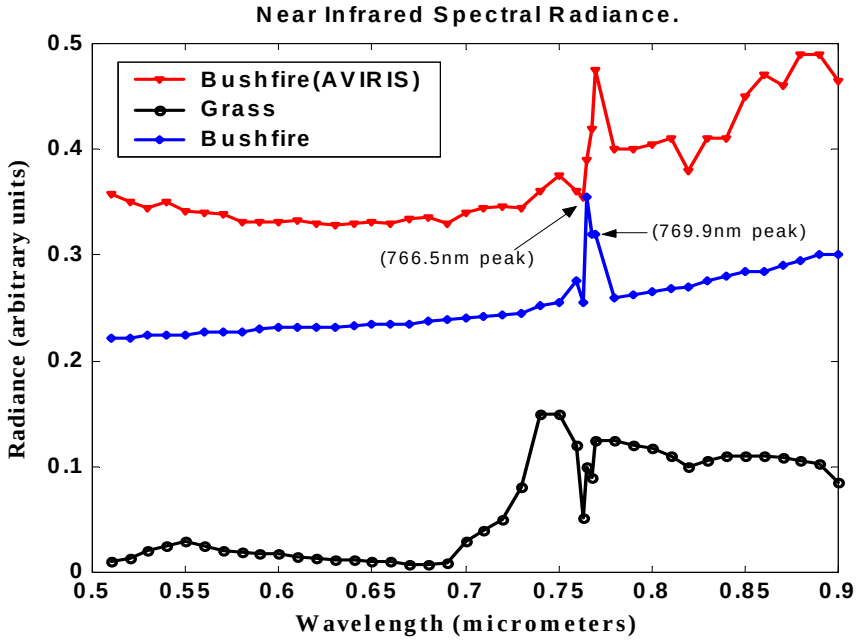

Figure 2.9. *Green to near infrared spectra produced from a bushfire and grass (*after Vodacek *et al.* 2002*)*

2.8. Radio wave propagation in fire

Microwaves propagation tests in very hot flames suggest significant signal attenuation. Most of the tests were carried out at X-Band frequencies, e.g., in Belcher *et al.* 1950 and Koretzky *et al.* 1998. Propagation measurements at other frequency bands consist of those carried out: at UHF and SHF (Williams *et al.* 1970); at SHF (Hata *et al.* 1983); and at 37-250 GHz (Gibbins *et al.* 1987). However, there are very few or no documented propagation measurements at HF and VHF radio wave bands.

A study carried out by Koretzky *et al.* 1998 considered X-band microwave transmission through plasma torches. The temperatures of torch flames were on average 1760 K. Koretzky *et al.* observed that the microwaves were significantly attenuated by the flames. Very high attenuation of more than 25 dB was measured over a propagation path of 2.4 cm. This could be explained by the fact that the torch flames were highly collisonal and high electron density of the order of 10^{19} m^{-3} strongly attenuation microwave signal through collisonal damping. In another experiment at X-band frequency, Belcher *et al.* 1950 measured a specific attenuation of 1 $dBcm^{-1}$ when they propagated 10 GHz microwave signal through a 1.5 cm diameter alkali sprayed coal gas-air

flame. The attenuation coefficient was increased to 2.1 $dBcm^{-1}$ when propagation frequency was decreased to 3 GHz. A very low specific attenuation was measured when the coal gas-air flame was not seeded with alkali metal salts.

Flames produced from combusting solid grains also significantly attenuated X-band microwaves. An average attenuation of 18 dB was measured when the flame was traversed by microwaves at a propagation frequency in the range of 2-15 GHz (Xu *et al*., 2006). The microwave attenuation produced from burning chemicals has been observed to increase with the increase in microwave propagation frequency in the frequency bands 2-7 GHz and vice-versa for the frequency band 8-15 GHZ (Yuan et al., 2007). Microwave attenuation in the chemical flame at 2-8 GHz increased from 16.89 GHz to a maximum of 33.83 dB over the chemical flame of depth 10 cm. In the 8-15 GHz band, microwave attenuation decreased from a maximum of 30.04 dB to minimum of 21.56 dB over the same fire thickness.

Schneider and Hoffman (1959) investigated the effect of alkali seeded acetylene-air flame on K-band (23.10 -92.96 GHz) microwaves. They observed that microwave attenuation decreased with the increase in propagation frequency. It decreased from 1.44 dB at 23.10 GHz to 0.33 dB at 92.96 GHz. Low attenuations were observed when the flame was not seeded.

Hata *et al.,* 1983 carried a propagation test over vegetation material fire at the microwave frequencies of 23 - 40 GHz. Insignificant microwave attenuation was measured over cool regions of the fire plume. Williams *et al*., 1970 also performed a propagation test over a vegetation mass fire at UHF and X-band. They also observed attenuations of less 5 dB over a propagation distance of about 40 m when propagation was about 1.7 m above the fuel.

Gibbins *et al*., 1985 traversed EHF (37-250 GHz) microwave through a hydrocarbon flame of temperature 1000 K and about 0.5 m thick. They measured attenuation generally less than 5 dB and concluded that at this frequency band the most significant signal loss mechanism is through scintillations rather than through signal absorption.

2.9. Summary of major points from the literature

- Potassium content in Australian vegetation could be in the range of 0.05-2.71%. Vegetation in southwest Western Australia can have potassium content up to 2.0% while those in south eastern Australia potassium content could reaches up to 2.71%.

- Bushfires are most intense in southern Australia where fire-line intensity can reach a maximum of 100 MWm^{-1}. High fuel loads in the ranges of 10 $tha^{-1}yr^{-1}$ sustain the catastrophic fires. A summary of typical fuel characteristics and fire intensities in the fire-prone vegetation is given in Table 2.1.

- Butler *et al.* 2004 measured the peak temperature of a crown fire to be 1330°C. The measured temperature is close to that estimated by Radojevic (2003). Radojevic estimates peak temperatures in bushfires to be around 1530°C. Nevertheless, Chandler e*t al.* 1983 estimate peak bushfire temperatures to be in the range of 875 to 2000°C. This implies that very high intensity bushfire flames are very hot gaseous media with temperature range as given by Chandler *et al.*

- The high temperature environment during flaming volatilises the omnipresent alkalis in vegetation into gaseous species that are dominated by K atoms, KCl, K_2SO_4 and/or KOH. The domination of either KOH or KCl species depends on the presence of water vapour in the combustion and the combustion temperature. The presence of water vapour and low temperatures favour the emission of gaseous KOH (Westberg *et al.* 2003). KOH is unstable at very high temperatures. It dissociates into potassium atoms. Conversely KCl is a very stable salt. It persists to higher temperatures.

- Global chemical equilibrium calculations using MINGTSYS and CHEMSAGE 3.0 software programs predict the formation of gaseous potassium and sodium atoms at temperatures above 800°C. However, at temperatures below 800°C, the chemical equilibrium calculations are not able to predict the existence of alkali atoms because they neglect the existence of oxygen associated alkalis in the combusting fuel's functional groups. The oxygen-attached alkalis are displaced by hydrogen radical from their attachment sites. The alkalis also need little thermal energy to be decomposed into atoms and other particulates. The concentration of the atoms increases rapidly with the increase

in temperature (Jensen *et al.* 2000). Atoms of magnesium and calcium are not predicted to be present at temperatures less than 1600°C (Ljung *et al.* 1997).

- The green to near infrared spectrum of bushfire (Latham 1998 and Vodacek *et al.* 2002) supports the predictions made by the chemical equilibrium softwares on the existence of sodium and potassium atoms in the bushfires. Doublet Line emissions of potassium and sodium are notable in the bushfire spectrum (Vodacek *et al.* 2002). The most prominent of the line emissions is that of potassium as it is the most abundant of the two in vegetation and has the lowest ionisation energy (4.34eV).

- It can be concluded from the literature that potassium is a very important alkali in bushfire ionisation at least at temperatures below 1600°C. Of the amount that is present in plant matter about 10-20% is ionised in the combustion zone of the bushfire (Vodacek *et al.* 2002).

- Radio wave signal attenuation at cool regions of a vegetation fire plume is insignificant (< 5 dB) but may be significant at the hottest region of the fire.

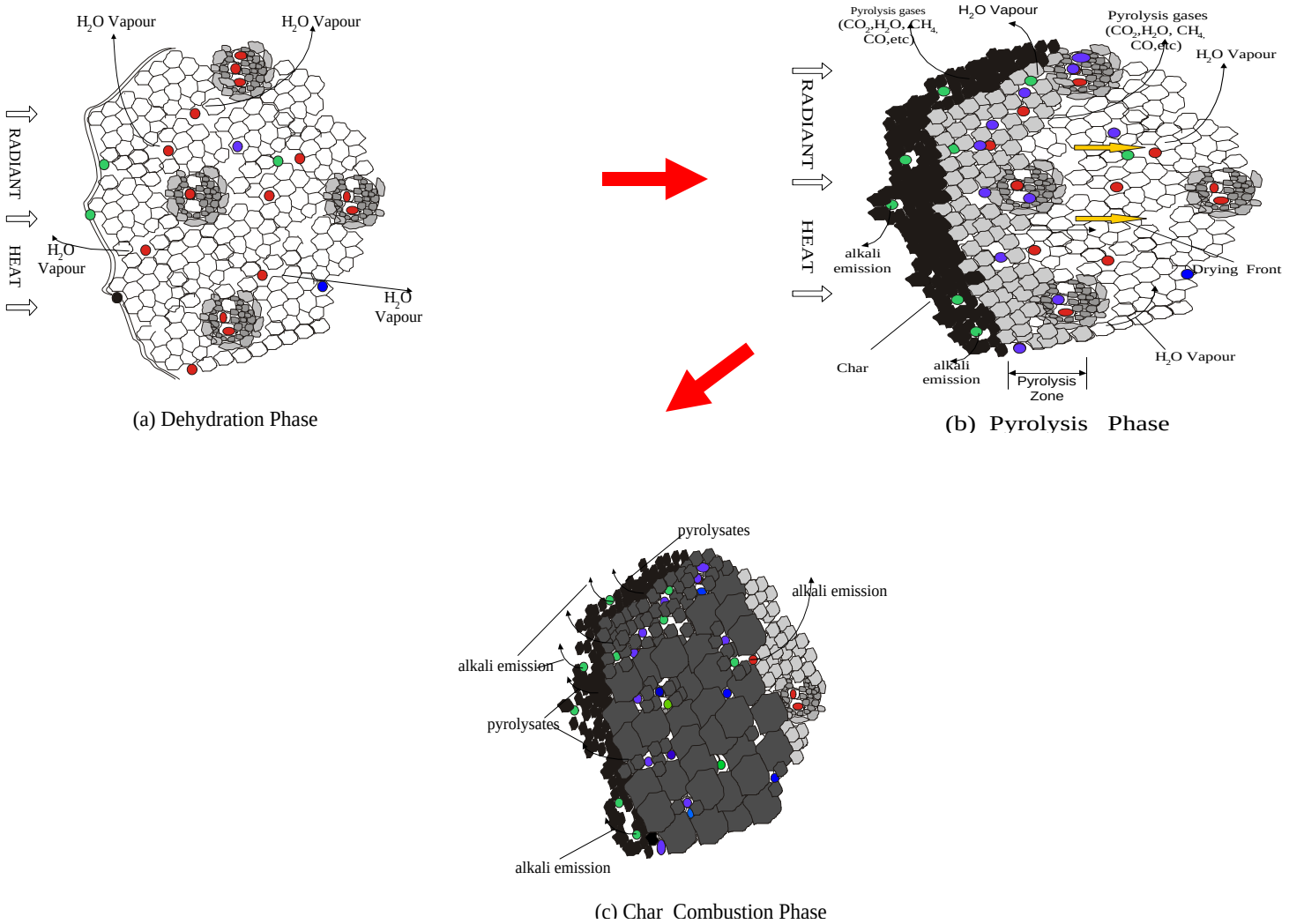

Figures 2.5(a) - (c). *Alkali emissions from burning vegetation*

Table 2.1. *Summary of fuel characteristics, potassium content and fire-line intensity in Australian fire prone vegetation*

Region:	**Southern Australia**			**Northern Australia**
	Southwest Western Australia	**South-eastern Australia**		
Vegetation Type:	Forest	Forest	Shrublands and heathlands	Tropical savanna
Climate:	Mediterranean	Temperate/Quasi-Medi	Semi-arid/Medi.	Tropical
Dominant species Dominant overstorey spp:	*E. marginata* *E.diversicolor* *Corymbia callophylla*	*E. obliqua* *E. regnans* *E. globus, E. Seiberi,* etc.	*E. socialis* *E. foecunda* *E.dumosa*	*E. tretonda* *E. miniata* *E.porrecta*
Dominant understorey spp:	*Macorzamia riedle* *Bossiacea laidlawina* *Xanthorrhea* spp.	*Accia dealbata* *Tetrarhena juncea* *Prostanthera lasianthos*	*Triodia irritans* *Acacia* spp. *Melaleuca* spp.	*Sorghum intrans* *Hetropogon triticeus* *Acacia* spp.
Observed Annual Litterfall ($tha^{-1}yr^{-1}$**):**	**11** (in *E. diversicolor* forests)	**9.4** (in *E. regnans*)	**7** (in heaths)	**6.1** (in late fire season)
Range of K Content Live foliage:	0.59-1.28%	0.32-0.78%	0.35-2.71%	0.13-1.80%
Litterfall and understorey:	0.08-2.00%	0.05-0.15%	Up to 0.1%	Up to 0.2%
Maximum Observed Bushfire Intensity:	60-100 MWm^{-1}	60-100MWm^{-1}	Up to 40MWm^{-1}	Up to 20MWm^{-1}

CHAPTER 3

Numerical prediction of very high frequency radio wave propagation characteristics in a grassfire

3.1. Introduction

Alkalis can be released from burning vegetation at temperatures as low as 400ºC. High heating rates in the range of about $100ºCs^{-1}$ as in bushfires (Engstrom *et al.* 2004) and forced airflow through combusting vegetation promote the release of atomic potassium (K) and sodium (Na) into vegetation fire flames as major component of Alkali and Alkaline Earth Metal (A-AEM) species emissions (Okuno *et al.* 2005). Predictions from thermodynamic equilibrium calculations are that atomic alkali species are emitted as major components of volatiles only at temperatures as high as 1100ºC (Jensen *et al.* 2000). At temperatures lower than 1100ºC, thermodynamic calculations identify potassium chloride (KCl) as a major component of the emissions (e.g. Jensen *et al.* 2000).

The thermodynamic equilibrium calculations however neglect char-attached alkali atoms such as in K-O-C, where O-C is a char attachment site for alkalis. When char-attached K is considered, high atomic K emission is predicted and has been observed in conditions similar to that of a bushfire. Under these conditions, atomic K species predominate over KCl particles. Vodacek *et al.* 2002 have estimated that about 10-20 % of K in vegetation is ionized in bushfires (flame temperature around 1200 K). Theoretical predictions of ionization under Local Thermodynamic Equilibrium (LTE) state suggest that a mole fraction of at least 2.42×10^{-3} of K atoms in a combustion zone is necessary to cause ionization density of the order of 10^{15} m^{-3} at 900 K, an electron density not attainable with gaseous KCl particles under the same conditions.

The main objective of this chapter is to predict radio wave propagation characteristics in grassfire flames of varying heat intensity and dimensions. The grassfire flames are not in complete thermal equilibrium state, however LTE state can be assumed in order to predict electron density in the bushfire flames. Section 3.2 discusses the necessary conditions for LTE to hold. Ionization under LTE state is discussed in section 3.3. Theory of radio wave propagation through a weakly ionized medium is discussed in section 3.4. A sub-slab model of grassfire flame with varying dielectric permittivity across the fire depth is proposed in Section 3.5. Numerical experiment results are given and discussed in Section 3.6 of the chapter. The chapter is concluded in Section 3.7 with summary statements.

3.2. Thermal equilibrium in grassfire flames

If an ionized gas is enclosed in a cavity with isothermic wall temperature and no spatial thermal gradients therein, then it can be said to be in Complete Thermodynamic Equilibrium (CTE). The physical state of the CTE system can be described by the Maxwell, Boltzmann and Saha equations, which respectively predict velocity of the gas particles, the extent of excitation and ionization in the gas. Planck's law governs radiation distribution.

Grassfires are open thermodynamic systems with temperature gradients and are most likely not in the ideal CTE state. The combustion reaction is exothermic with the hottest part being at the combustion zone and temperature decreases exponentially with height above the combustion zone. Across the grassfire depth, temperature assumes a Rayleigh profile with peak temperature at the combustion zone. The grassfire flame allows radiation to be emitted to the environment without being reabsorbed back into the system. This violates the Planck Law, which requires that radiation be in equilibrium with matter. A system that does not obey Planck's law cannot be in CTE state (Cabannes *et al.* 1971).

A grassfire flame volume can be divided into elementary small volumes (ΔV) whose physical parameters such as velocity and temperature can be described by their statistical averages. For this to hold, gas particles within the elementary volumes must be involved in a lot of collisions. With average kinetic temperature assigned to the elementary volumes, predictions of excitation, gas velocity and degree of ionization using Maxwell-Boltzmann statistics and Saha-Eggert equations are possible. The physical state of the elementary gas volumes can be assumed to be in Local Thermodynamic Equilibrium (LTE). There are conditions for the LTE to exist. One of the conditions is that electron density should be more than 10^{21} m^{-3} (Tendero *et al.* 2006). A condition that is clearly not possible with unseeded flames below 2000 K. Normal unseeded flames at this temperature have electron density up to 10^{15} m^{-3} (Drawin, 1971).

Studies of ionization in seeded flame have assumed the LTE condition despite the inherent low ionization density (see Gaydon *et al.* 1979, Belcher *et al.* 1950 and Frost, 1961). Using the assumption, ionization was predicted with a fair amount of accuracy when electron-scavenging radicals such as hydroxyl (OH) are taken into account (Belcher *et al.* 1950 and Frost, 1961). When predicting the amount of ionization in a grassfire, we will follow these authors and use LTE assumption for a *first approximation* of ionization density.

3.3. Ionisation in a grassfire

3.3.1. Thermal ionisation

Volatiles from vegetation combustion contain atoms, ionic and organometallic salts of Alkali and Alkaline Earth Metals (A-AEM). High concentrations of A-AEM particulates, especially those of potassium have been detected in bushfire plumes e.g. in Heil, 1998; Crutzen *et al.* 1990; Maenhaut *et al.* 1996 and many others. During a grassfire, the volatiles are often drawn from combusting litter, tree bark and leaves (see Figure 3.1) into the combustion zone of the fire by convective up-draughts. For moderate intensity grassfire, temperatures may be up to 900ºC (Clark *et al.* 2003). The heat in the combustion zone may thermally dissociate and ionize A-AEM particulates to produce electrons in the grassfire. At normal grassfire temperatures (≈1200 K), ionization is predominately due to elementary potassium (K) and sodium (Na). Spectroscopic studies of bushfire have revealed the dominance of Na and K in thermal ionization (Vodacek *et al.* 2002 and Latham, 1998). This is explained by the fact that salts of Na and K need a small amount of energy to thermally dissociate and ionize. Ionization energies are 4.34 eV and 5.14 eV for K and Na respectively.

3.3.1.1. Dissociation

The number concentrations of singly ionized and neutral particles in the plume may also depend on disassociation of the volatilized diatomic and polyatomic molecules according to the following relation (Maouhoub *et al.* 1999);

$$AB\ (g) \Leftrightarrow A\ (g) + B\ (g) \qquad \text{(Equation 3.1)}$$

Where: AB (g) = pyrolysate parent molecule

A (g), B (g) = daughter particles.

If thermal equilibrium is assumed, the number concentration of dissociated particles can be determined by using the Guldberg-Waage Law. Koalaga *et al.* (1999) gave the law as:

$$\frac{N_A N_B}{N_{AB}} = \frac{P_{Aint} P_{Bint}}{P_{ABint}} \left(\frac{2\pi\ kT}{h^2} \right)^{3/2} \left(\frac{m_A m_B}{m_{AB}} \right)^{3/2} \exp\left(\frac{-E_d}{kT} \right) \qquad \text{(Equation 3.2)}$$

Where: N_A, N_B and N_{AB} = number concentration of A, B and AB respectively,

P_{Aint}, P_{Bint} and P_{ABint} = internal partition function of A (g), B (g) and AB (g),

E_d, = dissociation energy,

k = Boltzmann constant,

h = Planck constant,

m_A ,m_B, m_{AB} = masses of particles,

T = thermodynamic temperature.

Exothermic chemical reactions that occur in the combustion zone render it hot enough to cause thermal disintegration of some pyrolysed species including the A-AEM based salts into atoms and their associated species. Alkali metal salts in the pyrolysate are more likely to be thermally decomposed due to low dissociation energies; for an example potassium hydroxide and sodium chloride have dissociation energies 3.51 and 4.24eV respectively. The dissociation energy could be much less for complex organic salts of alkali such as *malate* or oxalate.

3.3.1.2. Ionisation

The resulting atoms A (as in Equation 3.1) are electronically excited by the thermal energy in the reaction zone making them very unstable, thus giving atoms in the state A*. On collision with other flame species (S) the atoms may give out their outer shell electron to produce singly ionized particles (A^+). Reaction Equation 3.3 gives an account of ionization of excited atoms on collision with species S (Butler *et al.* 1998);

$$S\,(g) + A^*\,(g) \Leftrightarrow A^+\,(g) + e^-\,(g) + S\,(g) \qquad \text{(Equation 3.3)}$$

However, the overall equation for Equation 3.3 is:

$$A\,(g) \Leftrightarrow A^+\,(g) + e^-\,(g) \qquad \text{(Equation 3.4)}$$

Similarly an equation that represent the ionization of diatomic species such NO is given by Koalaga *et al.* (2001) as;

$$AB\,(g) \Leftrightarrow AB^+(g) + e^-\,(g) \qquad \text{(Equation 3.5)}$$

To quantify the approximate amount of ionization due to thermal ionization and the composition of the flame, the application of Saha and Guldberg-Waage equations is sufficient as long as the flame is assumed to be in LTE (Koalaga *et al.* 2003). Chen *et al.* 1999 gave the Saha equation in as:

$$\frac{N_{m^+} N_e}{N_m} = \frac{2P_{m^+int}}{P_{mint}} \left(\frac{2.\pi.m_e kT}{h^2} \right)^{3/2} \exp\left(\frac{-(E_i)}{kT} \right) \qquad \text{(Equation 3.6)}$$

Where: N_{m^+} N_e and N_m = number concentration of singly ionized particles, electrons and neutral particles,

P_{mint} and P_{m^+int} = internal partition function of particles,

E_i, and m_e = ionization energy and mass of an electron. The rest of the variables are as defined earlier in the chapter.

Equation 3.6 is the ionization equilibrium constant (K_1). Electron density (N_e) due to thermal ionization of K atoms is related the ionization equilibrium constant and the total number of ionised K particles (N_p) in the flames as (Frost, 1961);

$$N_e = (K_1 N_p)^{1/2} \left[\left(1 + \frac{K_1}{4N_p} \right)^{1/2} - \left(\frac{K_1}{4N_p} \right)^{1/2} \right] \qquad \text{(Equation 3.7)}$$

The total number of ionised K particles (N_p) is related to the potassium atoms in the flame by the equation (Frost, 1961);

$$N_p = \frac{7.335 \,.\, 10^{21} \tau}{T} \text{ cm}^{-3} \qquad \text{(Equation 3.8)}$$

Where τ is the number density of K atoms into the bushfire combustion zone.

3.3.2. Internal partition functions

3.3.2.1. Single atoms

Internal partition functions of particles can be calculated from the relations given in Joint Army, Navy, and Air Force (JANAF) tables (Chase *et al.* 1985). For single atoms and ions, Chase *et al.* 1985 gave the internal partition function of single atoms and ions as;

$$Q_{int}(T) = \sum_n \omega_n \exp\left(\frac{-E_n}{kT}\right) \qquad \text{(Equation 3.9)}$$

Where: E_n = energy at excited level,

ω_n = Statistical weight at level n.

k = Boltzmann constant.

T = temperature.

3.3.2.2. Diatomic molecules and ions

Using a Rigid-Rotor Model (e.g. in Andre, 1995), the internal partition function of ideal diatomic molecules is given by Maouhoub *et al.* 1999 as:

$$Q_{int}(T) = \sum_n \frac{kT}{hcB_e\sigma} \frac{\omega_n \exp\left(\frac{-E_n}{kT}\right)}{\left[1-\exp\left(-\frac{hc\omega_e}{kT}\right)\right]} \qquad \text{(Equation 3.10)}$$

Where: B_e and ω_e = rotational and vibration constants.

σ = symmetry number,

h = Planck's constant,

c = speed of light.

3.3.2.3. Poly-atomic molecules and ions

Gibbs free energy is used to calculate the internal partition energy of these particles. Chase *et al.* 1995 relates Gibbs free energy (G^0) to the total partition function (Q_t) of a particle by;

$$-\left[G^0(T) - H^0(0K)\right]/RT = \ln Q_t \qquad \text{(Equation 3.11)}$$

Where: H^o = enthalpy of formation of a particle,
R = gas constant.

Total partition function of a particle (Q_t) is a product of internal and translational partition functions and is given as (Maouhoub *et al.* 1999);

$$Q_t = Q_{int}.Q_{tr} \qquad \text{(Equation 3.12)}$$

From Equation 3.12, the internal partition function of a polyatomic particle is given by Maczek, 1998 as;

$$Q_{int} = \frac{Q_t}{\left[\frac{2\pi kT}{h^2}\right]^{2/3}\frac{kT}{P}} \qquad \text{(Equation 3.13)}$$

Where P is the total plasma pressure, given by Dalton's Law of partial pressures of individual gases in plume as (Maouhoub *et al.* 1999);

$$P = \sum_{i=1}^{\alpha} N_i kT \qquad \text{(Equation 3.14)}$$

Where N_i is species number concentration of a plume gas.

3.3.3. Chemi-ionization

According to Alkemade *et al.* 1979, this ionization process is brought about by exothermic chemical reactions. Some of the energy released during exothermic reactions goes to supplementing the ionization energy required to release electrons. Latham 1999 has observed that in premixed diffusion flames with no alkali impurities, chemi-ionization is a predominate mechanism which yields electrons and positive ions. In hydrocarbon flames chemi-ionization predominately yields CHO^+ ions and electrons according to the reaction given by Alkemade *et al.* 1979; as in premixed diffusion flames. The ionization process can also be connected to the radical recombination processes in which part of the energy goes to ionizing the a third party alkali metal as is given by Alkemade *et al.* 1979 as:

$$K(g) + CO(g) + O(g) \Leftrightarrow K^+(g) + e^-(g) + CO_2(g) \qquad \text{(Equation 3.15)}$$

In reactions where chlorine is in co-existence with alkali metals such as sodium, chlorine may play a catalytic role in ionization of the former by hydrogen atoms to produce electrons and metal ions. The process occurs according to the reaction equation (Alkemade *et al.* 1979):

$$Na(g) + H(g) + H(g) \Leftrightarrow Na^+(g) + e^-(g) + H_2(g) \qquad \text{(Equation 3.16)}$$

Chemi-ionization is also associated with the decomposition of metal oxides as a reaction equation below (Alkemade *et al.* 1979):

$$CO(g) + MO(g) \Leftrightarrow M^+(g) + e^-(g) + CO_2(g) \qquad \text{(Equation 3.17)}$$

The quasi-neutrality condition must hold. Thus the sum of all charges in the plasma system must be equal to zero. This condition is given as (Maouhoub *et al.* 1999);

$$\sum_{i=1}^{\alpha} n_i^+ = N_e \qquad \text{(Equation 3.18)}$$

3.4. Theory of radio wave propagation in a grassfire.

3.4.1. Average drift velocity of flame gases

In the prediction of radio wave propagation prediction in a grassfire the following assumptions are made: grassfire is weakly ionised, quasi–neutral and spatially nonhomogeneous in electron density; the fire is stationary with respect to speed of propagating radio wave; gravitational forces are negligible in comparison with applied and induced electromagnetic forces; neutral particles and heavy ions are considered stationary with respect to the light electrons and that only collision between electrons with neutrals are considered.

This is actually a propagation problem which has been thoroughly dealt with from various perspectives in past (see Wade 1961, Vandrey 1963, Laroussi *et al.* 1993 and Dowden *et al.* 2001, just to mention a few). By taking the above assumptions into consideration, the propagation problem is simplified a great deal. Solving such a problem requires the use of equation of motion for electrons that are under the influence of electromagnetic fields propagating in the weakly ionised plasma medium. The basis for this is Maxwell's equations. The relevant Maxwell's equations are mathematically expressed as (Guo *et al.* 2005):

$$\nabla X \vec{E} = -i\omega\mu_o \vec{H} \qquad \text{(Equation 3.19)}$$

$$\nabla X \vec{H} = \left[\sigma + i\omega\varepsilon\right]\vec{E} \qquad \text{(Equation 3.20)}$$

In the right hand side (RHS) of Equation 3.20 the quantity $\sigma\vec{E}$ is the conduction current density $\vec{J}$.

Assuming the neutral mobility to be very small compared to that of electrons, the conduction current density can be expressed as (Jiang *et al.* 2007);

$$\vec{J} = nq_e\vec{v}_d. \qquad \text{(Equation 3.21)}$$

Where: n = number density of the conducting electrons,

q_e = electron charge,

$\vec{v}_d$ = average drift velocity of an electron.

The drift velocity can be worked out from the Langevin Equation (see Molmud, 1959 and Margenau, 1946). The Langevin equation is used to describe the random motion of a particle in a fluid and is expressed as (e.g. in Isaacs, 2000);

$$\frac{d\vec{u}}{dt} = -\varphi\vec{u} + \beta(t) \qquad \text{(Equation 3.22)}$$

Where the first and last terms in the RHS of the Equation 3.22 are friction and force terms respectively. $\vec{u}$ is the average velocity of the particle.

Using the Langevin equation with Lorentz force replacing β(t) and $\vec{u}$ replaced by drift velocity of an electron ($\vec{v}_d$), the equation to describe the motion of an electron in an unmagnetised, cold weakly ionized plasma is given by the Langevin-Lorentz force equation which takes the form given below (see Molmud,1959);

$$\frac{d\vec{v}_d}{dt} + \varphi\vec{v}_d = \frac{q}{m}\left[\vec{E} + \frac{\vec{v}_d}{c} X \vec{H}\right] \qquad \text{(Equation 3.23)}$$

Where: φ = dissipative term,

$\vec{v}_d$ = average drift velocity of an electron respectively.

Other variables have their usual meaning in electromagnetism. $\vec{v}_d$ is negligibly small compared to the speed of light *c*, hence the contribution of the magnetic force component in the Langevin-Lorentz equation is very much smaller than that of electric force component. By neglecting the magnetic force component contribution Equation 3.23 reduces to;

$$\frac{d\vec{v}_d}{dt} + \varphi\vec{v}_d = \frac{q}{m}\vec{E} \qquad \text{(Equation 3.24)}$$

Assuming the time harmonic dependence of $\vec{v}_d$ and $\vec{E}$ so that they become $\vec{v}_d = \vec{v}_{do}e^{i.\omega.t}$ and $\vec{E} = \vec{E}_0 e^{i.\omega.t}$ (Epstein, 1962), Equation 3.24 can be solved for $\vec{v}_d$ .The solution of Equation 3.24 is;

$$\vec{v}_d = \frac{q}{m(\varphi + i\omega)}\vec{E} \qquad \text{(Equation 3.25)}$$

The dissipative term φ, is taken to be equal to the collision frequency (ν_c) for electron - neutral interaction which are Maxwellian (Albini *et al.* 1961; Schneider *et al.* 1959 and Epstein, 1962). Molmud observed that Equation 3.25 could also be used for non-Maxwellian interactions with Maxwellian distributions provided φ is complex. Noticeably, the Langevin Equation is used for deriving average drift velocity $\vec{v}_d$ for particles with Maxwellian distributions of energy or velocity, as it requires the momentum transfer collision frequency(ν_c) to be constant, which is not the case for non-Maxwellian interactions. Molmuld suggested a general average drift velocity relation which is in the form of Equation 3.25, for Maxwellian and non- Maxwellian gases may be given as;

$$\vec{v}_d = \frac{q}{m(\varphi_c + i\omega)}\vec{E} \qquad \text{(Equation 3.26)}$$

Where the complex collision frequency φ_c is given as;

$$\varphi_c = \varphi_r + i\varphi_i \qquad \text{(Equation 3.27)}$$

with $\varphi_r = B \Big/ \left(B^2 + D^2\right)$ and $\varphi_i + \omega = D \Big/ \left(B^2 + D^2\right)$

B and D are complex functions of collision frequency ν_c and the radio frequency ω. B and D take the forms;

$$B = \frac{4\pi}{3}\int_0^\infty f^1(u)\,u^4 du$$

$$D = \frac{4\pi}{3}\int_0^\infty \frac{\omega}{nQu}u^4 f^1(u)du$$

Where n is the density of neutral particles and $f^1(u)$ is a velocity distribution function. Assuming that the flame particle distribution is Maxwellian, then according to Molmud the velocity distribution function can be expressed as;

$$f^1(u) = \frac{NQu\beta\left(\beta \Big/ \pi\right)^{\frac{2}{3}} e^{\left(-\beta u^2\right)}}{N^2Q^2u^2 + \omega^2} \qquad \text{(Equation 3.28)}$$

Where $\beta = \frac{m}{2kT}$.

3.4.2. Effective collision frequency, conductivity and propagation constant for weakly ionized plasma with different electron- neutral interactions

Assuming Maxwellian velocity distribution for flame particles, average collision frequency for different transport phenomena can be expressed as (Itikawa, 1973):

$$\nu = \int NQ^{(m)}(u)f.u.du \qquad \text{(Equation 3.29)}$$

Ionized gases with same chemical composition, distribution function and temperature, but with different interactions, assume different average collision frequencies (Molmud, 1959). Average collision frequency depends on variation of momentum transfer cross section with electron velocity. However, Itikawa (1973) has worked out collision frequencies that can be used in many transport phenomena or to approximate such cases. For these "effective" collision frequencies Itikawa used momentum transfer cross section data from many authors such as Crompton *et al.* 1969; Hake *et al.* 1967 and Pack *et al.* 1962. Assuming Maxwellian energy distribution, Itikawa has used the following relation to calculate the effective collision frequency for alternating (A.C.) electromagnetic field,

$$\langle \varphi_{eff} \rangle = \frac{8}{3\pi^{1/2}} N \left(\frac{m_e}{2kT_e} \right)^{5/2} \int_0^\infty u^5 Q^{(m)}(u) \exp\left(-\frac{m_e u^2}{2kT_e} \right) du \qquad \text{(Equation 3.30)}$$

Where:

φ_{eff}	=	effective collision frequency,
m_e	=	mass of an electron,
k	=	Boltzmann's constant,
T_e	=	electron temperature,
N	=	number density of neutrals,
U	=	velocity of the electron,
$Q^{(m)}$	=	momentum transfer collision cross section.

Non-linear regression can be performed on Itikawa's data to interpolate effective collision frequency at temperatures between those given in the data. Average collision frequency can also be calculated for different interactions from the relation given by Molmud (1959). Momentum transfer collision cross section data from Engelhardt *et al.* 1964; Hake *et al.* 1967 and many others can be used to calculate the average collision frequency.

High accuracy in effective collision frequency values is not important in the simulations; therefore regression relations obtained from Itakawa's data are sufficient for calculating collision frequency to be used in the numerical prediction.

As current density $\vec{J} = \sigma\vec{E}$ (Guo *et al*. 2005) and is also related to the drift velocity by (3.21), one can write,

$$\sigma = \frac{nq_e^2}{m(\varphi_c + i\omega)} \qquad \text{(Equation 3.31)}$$

Where σ is the electronic conductivity for the weakly ionised plasma subjected to A.C. electric field. An attempt to derive the propagation constant for the fields in the weakly ionised plasma calls for the decoupling of Maxwell's equations so that they are in terms of one parameter ($\vec{H}$ or $\vec{E}$) only.

Decoupling follows by taking curl of Equation 3.21, which gives,

$$\nabla X\left(\nabla X\vec{E}\right) = -i.\omega\,\mu_o\left(\nabla X\vec{H}\right) \qquad \text{(Equation 3.32)}$$

Substituting Equation 3.22 into Equation 3.32 gives,

$$\nabla X\left(\nabla X\vec{E}\right) = \left(\omega^2\mu_o\varepsilon_r\varepsilon_o - i\,\sigma\,\omega\,\mu_o\right)\vec{E}$$

$$\nabla X\left(\nabla X\vec{E}\right) = \omega^2\varepsilon_o\mu_o\left(\varepsilon_r - \frac{i\sigma}{\omega\varepsilon_o}\right)\vec{E} \qquad \text{(Equation 3.33)}$$

Using the vector identity $\nabla X\left(\nabla X\vec{E}\right) = \nabla\left(\nabla.\vec{E}\right) - \nabla^2\vec{E}$ then Equation 3.33 becomes;

$$\nabla^2\vec{E} - \frac{\omega^2}{c^2}\tilde{\varepsilon}\vec{E} = 0 \qquad \text{(Equation 3.34)}$$

Where $\tilde{\varepsilon} = \varepsilon_r\left(1 - \frac{i\sigma}{\omega\varepsilon}\right)$ is the complex permittivity constant (Equation 3.35)

Equation 3.34 is the wave equation in electric field only. The equation can also be written as;

$$\nabla^2\vec{E} - \gamma^2\vec{E} = 0 \qquad \text{(Equation 3.36)}$$

Where γ^2 is complex and $\gamma^2 = \left[\frac{\omega^2}{c^2}\tilde{\varepsilon}\right]$ (Equation 3.37)

3.4.3. Complex radio relative permittivity of a grassfire flame

Relative permittivity constant for a plane electromagnetic wave propagating in a cold magnetised plasma incident at an arbitrary angle θ has been derived by Appleton and is given by Laroussi *et al.* 1993 as;

$$\tilde{\varepsilon}_r = 1 - \frac{\frac{\omega_p^2}{\omega^2}}{\left[1 - i\frac{\upsilon_c}{\omega} - \frac{\frac{\Omega^2}{\omega^2}\sin^2\theta}{2\left(1 - \frac{\omega_p^2}{\omega^2} - i\frac{\upsilon_c}{\omega}\right)}\right] \pm \left[\frac{\frac{\Omega^4}{\omega^4}\sin^4\theta}{4\left(1 - \frac{\omega_p^2}{\omega^2} - i\frac{\upsilon_c}{\omega}\right)^2} + \frac{\Omega^2}{\omega^2}\cos^2\theta\right]^{1/2}} \qquad \text{(Equation 3.38)}$$

Where $\omega_p^2 = \left(\frac{Ne^2}{m\varepsilon_o}\right)$ is the plasma frequency,

θ = angle of incidence,

Ω = gyrofrequency.

Adapting Equation 3.38 to an unmagnetised cold plasma with electric field incident normally at the plasma – air interface then we have,

$$\tilde{\varepsilon}_r = 1 - \frac{\frac{\omega_p^2}{\omega^2}}{\left[1 - i\frac{\upsilon_c}{\omega}\right]} \qquad \text{(Equation 3.39)}$$

When Equation 3.39 is expanded and simplified we then have;

$$\tilde{\varepsilon}_r = \left[\left(1 - \frac{\psi^2}{1+\zeta^2}\right) - i\left(\frac{\psi^2\zeta}{1+\zeta^2}\right)\right] \qquad \text{(Equation 3.40)}$$

Where: $\psi^2 = \left(\frac{\omega_p^2}{\omega^2}\right)$

$\zeta = \left(\frac{\upsilon_c}{\omega}\right)$.

3.4.4. Phase and attenuation coefficients for radio waves

The complex wave number can be expressed in terms of phase and attenuation factors as (Edwards *et al.* 1971):

$$\kappa = \beta - i\alpha \qquad \text{(Equation 3.41)}$$

Where α is attenuation factor and β is phase factor.

Complex wave number is related to refractive index by the relation (Akhtar *et al.* 2003):

$$\eta = \frac{c}{\omega}\kappa = \frac{c}{\omega}(\beta - i\alpha) \qquad \text{(Equation 3.42)}$$

The complex refractive index (η) also relates to relative permittivity ($\tilde{\varepsilon}_r$) by the equation (Akhtar *et al.* 2003):

$$\eta = [\tilde{\varepsilon}_r]^{1/2} = (\mu - i\chi) \qquad \text{(Equation 3.43)}$$

By comparing Equations (3.42) and (3.43);

$$\mu = \frac{c}{\omega}\beta \qquad \text{(Equation 3.44)}$$

$$\chi = \frac{c}{\omega}\alpha \qquad \text{(Equation 3.45)}$$

From Equation (3.43),

$$\tilde{\varepsilon}_r = (\mu - i\chi)(\mu - i\chi)$$

$$\tilde{\varepsilon}_r = (\mu^2 - \chi^2) - i(2.\mu.\chi) \qquad \text{(Equation 3.46)}$$

Let φ be the real part of Equation 3.46; therefore,

$$\varphi = \left(\mu^2 - \chi^2\right) \quad \text{(Equation 3.47)}$$

and let Γ be the imaginary part of Equation 3.46, thus

$$\Gamma = \left(2.\mu.\chi\right) \quad \text{(Equation 3.48)}$$

Equation 3.46 becomes,

$$\tilde{\varepsilon}_r = \eta^2 = \varphi - i\Gamma \quad \text{(Equation 3.49)}$$

Squaring Equation 3.41 gives;

$$\eta^2 = \frac{c^2}{\omega^2}\left[(\beta - i\alpha)(\beta - i\alpha)\right]$$

$$\eta^2 = \frac{c^2}{\omega^2}\left[\left(\beta^2 - \alpha^2\right) - i\left(2\,\alpha\,\beta\right)\right] \quad \text{(Equation 3.50)}$$

Comparing Equation 3.49 with Equation 3.50;

$$\varphi = \frac{c^2}{\omega^2}\left[\beta^2 - \alpha^2\right] \quad \text{(Equation 3.51)}$$

and

$$\Gamma = \frac{c^2}{\omega^2}\left[2\,\alpha\beta\right] \quad \text{(Equation 3.52)}$$

Squaring Equations 3.51 and 3.52 gives;

$$\varphi^2 = \frac{c^4}{\omega^4}\left[\left(\alpha^4 + \beta^4\right) - 2\alpha^2\beta^2\right] \quad \text{(Equation 3.53)}$$

and

$$\Gamma^2 = \frac{c^4}{\omega^4}\left[4\alpha^2\beta^2\right] \quad \text{(Equation 3.54)}$$

Adding Equation 3.53 and Equation 3.54 gives

$$\varphi^2 + \Gamma^2 = \frac{c^4}{\omega^4}\left[\alpha^4 + \beta^4 + 2\alpha^2\beta^2\right] \quad \text{(Equation 3.55)}$$

Square root of Equation 3.55

$$(\varphi^2 + \Gamma^2)^{1/2} = \frac{c^2}{\omega^2}\left[\alpha^2 + \beta^2\right] \quad \text{(Equation 3.56)}$$

Subtracting Equation 3.51 from Equation 3.56 gives

$$(\varphi^2 + \Gamma^2)^{1/2} - \varphi = \frac{c^2}{\omega^2}\left[\alpha^2 + \beta^2 + \alpha^2 - \beta^2\right]$$

$$(\varphi^2 + \Gamma^2)^{1/2} - \varphi = 2\alpha^2$$

Therefore $$\alpha = \left[\frac{((\varphi^2 + \Gamma^2)^{1/2} - \varphi)}{2}\right]^{1/2}$$ (Equation 3.57)

Equation 3.57 gives the **attenuation coefficient (α).**

Adding Equation 3.51 to Equation 3.56 gives

$$(\varphi^2 + \Gamma^2)^{1/2} + \varphi = \alpha^2 + \beta^2 - \alpha^2 + \beta^2$$

$$(\varphi^2 + \Gamma^2)^{1/2} + \varphi = 2\beta^2$$

Therefore $$\beta = \left[\frac{((\varphi^2 + \Gamma^2)^{1/2} + \varphi)}{2}\right]^{1/2}$$ (Equation 3.58)

Equation 3.58 gives the **phase shift coefficient (β).**

Attenuation per unit length (A/L) is related to the attenuation coefficient by;

Attenuation per unit length (A/L) = 0.868 α (dB/m) (Equation 3.59)

Where L is the width of plasma-producing grassfire.

Phase change (ΔΦ) per meter given by the relation below

$$\Delta\Phi / L = \beta - \beta_0$$ (Equation 3.60)

Where $\beta_0 = 2\pi/\lambda_0$

3.4.5. Transmission and reflection coefficient

From the Fresnel equations, Pozar, 1993 gives reflection coefficient for plane wave at oblique incidence as;

$$R_c = \frac{E_r}{E_o} = \frac{n_2\cos\theta_i - n_1\cos\theta_t}{n_2\cos\theta_i + n_1\cos\theta_t} \qquad \text{(Equation 3.61)}$$

Dividing the numerator and the denominator of Equation 3.61 by n_1 gives;

$$R_c = \frac{E_r}{E_o} = \frac{\frac{n_2}{n_1}\cos\theta_i - \cos\theta_t}{\frac{n_2}{n_1}\cos\theta_i + \cos\theta_t} \qquad \text{(Equation 3.62)}$$

But $\cos\theta_t$ can also be written as $\cos\theta_t = \left(1 - \frac{n_1^2}{n_2^2}\sin^2\theta_i\right)^{1/2}$ (Equation 3.63)

Taking out the factor $\frac{n_1^2}{n_2^2}$ from the brackets of Equation 3.63 gives;

$$\cos\theta_t = \frac{n_1}{n_2}\left(\frac{n_2^2}{n_1^2} - \sin^2\theta_i\right)^{1/2} \qquad \text{(Equation 3.64)}$$

Substituting Equation 3.64 into Equation 3.62,

$$R_c = \frac{E_r}{E_o} = \frac{\frac{n_2}{n_1}\cos\theta_i - \frac{n_1}{n_2}\left(\frac{n_2^2}{n_1^2} - \sin^2\theta_i\right)^{1/2}}{\frac{n_2}{n_1}\cos\theta_i + \frac{n_1}{n_2}\left(\frac{n_2^2}{n_1^2} - \sin^2\theta_i\right)^{1/2}}$$

Multiplying the denominator and the numerator by $\frac{n_1}{n_2}$ we then have

$$R_c = \frac{E_r}{E_o} = \frac{\left(\frac{n_2}{n_1}\right)^2\cos\theta_i - \left(\frac{n_2^2}{n_1^2} - \sin^2\theta_i\right)^{1/2}}{\left(\frac{n_2}{n_1}\right)^2\cos\theta_i + \left(\frac{n_2^2}{n_1^2} - \sin^2\theta_i\right)^{1/2}} \qquad \text{(Equation 3.65)}$$

But $n_2^2 = \varepsilon_2$ and $n_1^2 = \varepsilon_1$ (Equation 3.66)

Substituting Equation 3.66 into Equation 3.65 gives;

$$R_c = \frac{E_r}{E_o} = \frac{\left(\frac{\varepsilon_2}{\varepsilon_1}\right)\cos\theta_i - \left(\frac{\varepsilon_2}{\varepsilon_1} - \sin^2\theta_i\right)^{1/2}}{\left(\frac{\varepsilon_2}{\varepsilon_1}\right)\cos\theta_i + \left(\frac{\varepsilon_2}{\varepsilon_1} - \sin^2\theta_i\right)^{1/2}} \quad \text{(Equation 3.67)}$$

Equation 3.67 is reflection coefficient of a radio wave incident obliquely on air- fire plasma interface.

Transmission coefficient is given by Fresnel equation (Pozar, 1993);

$$T_c = \frac{E_t}{E_o} = \frac{2n_2\cos\theta_i}{n_2\cos\theta_i + n_1\cos\theta_t} \quad \text{(Equation 3.68)}$$

Dividing the numerator and the denominator of Equation 3.68 by n_1 gives;

$$T_c = \frac{E_t}{E_o} = \frac{2\frac{n_2}{n_1}\cos\theta_i}{\frac{n_2}{n_1}\cos\theta_i + \cos\theta_t} \quad \text{(Equation 3.69)}$$

Substituting Equation 3.64 into Equation 3.69 gives;

$$T_c = \frac{E_t}{E_o} = \frac{2\frac{n_2}{n_1}\cos\theta_i}{\frac{n_2}{n_1}\cos\theta_i + \frac{n_1}{n_2}\left(\frac{n_2^2}{n_1^2} - \sin^2\theta_i\right)^{1/2}} \quad \text{(Equation 3.70)}$$

Multiplying numerator and denominator of Equation 3.70 by $\frac{n_2}{n_1}$ gives;

$$T_c = \frac{E_t}{E_o} = \frac{2\left(\frac{n_2}{n_1}\right)^2 \cos\theta_i}{\left(\frac{n_2}{n_1}\right)^2 \cos\theta_i + \left(\frac{n_2^2}{n_1^2} - \sin^2\theta_i\right)^{1/2}} \qquad \text{(Equation 3.71)}$$

Substituting Equation 3.66 into Equation 3.71 gives;

$$T_c = \frac{E_t}{E_o} = \frac{2\left(\frac{\varepsilon_2}{\varepsilon_1}\right) \cos\theta_i}{\left(\frac{\varepsilon_2}{\varepsilon_1}\right) \cos\theta_i + \left(\frac{\varepsilon_2}{\varepsilon_1} - \sin^2\theta_i\right)^{1/2}} \qquad \text{(Equation 3.72)}$$

Equation 3.72 is transmission coefficient for a Radio wave incident obliquely on the air–fire interface.

The above derivations were done for oblique incidence, but for normal incidence θ_i and θ_t are zero (0) therefore the reflection coefficient reduce to;

$$R_c = \frac{E_r}{E_o} = \frac{\left(\frac{\varepsilon_2}{\varepsilon_1}\right) - \left(\frac{\varepsilon_2}{\varepsilon_1}\right)^{1/2}}{\left(\frac{\varepsilon_2}{\varepsilon_1}\right) + \left(\frac{\varepsilon_2}{\varepsilon_1}\right)^{1/2}} \qquad \text{(Equation 3.73)}$$

The transmission coefficient reduces to;

$$T_c = \frac{E_t}{E_o} = \frac{2\left(\frac{\varepsilon_2}{\varepsilon_1}\right)}{\left(\frac{\varepsilon_2}{\varepsilon_1}\right) + \left(\frac{\varepsilon_2}{\varepsilon_1}\right)^{1/2}} \qquad \text{(Equation 3.74)}$$

3.4.7. Transmission and reflection power fractions

Fractions of energy transmitted and reflected are expressed in field intensity (I). As intensity is defined as the average power per unit area, it can be given by Pozar, 1993 as;

$$I = 0.5\ \varepsilon u E_0^2 \qquad \text{(Equation 3.75)}$$

Where ε, u, E_0 are medium permittivity, energy wave velocity and amplitude respectively.

The reflected power fraction is therefore given by;

$$P_{rf} = \frac{I_{or}}{I_{oi}} = \frac{0.5\varepsilon_1 u_1 E_{or}^2}{0.5\varepsilon_1 u_1 E_{oi}^2} \qquad \text{(Equation 3.76)}$$

Simplifying Equation 3.76 gives;

$$P_{rf} = (R_c)^2 \qquad \text{(Equation3.77)}$$

Equation 3.77 is **Reflection Power Fraction.**

Transmitted power fraction can be worked out to be;

$$P_{tf} = \frac{I_{ot}}{I_{oi}} = \frac{0.5\varepsilon_2 u_2 E_{ot}^2}{0.5\varepsilon_1 u_1 E_{oi}^2} \qquad \text{(Equation 3.78)}$$

Simplifying Equation 3.78 further gives;

$$P_{tf} = \frac{I_{ot}}{I_{oi}} = \frac{\varepsilon_2 \sqrt{\varepsilon_1} E_{ot}^2}{\varepsilon_1 \sqrt{\varepsilon_2} E_{oi}^2}$$

$$P_{tf} = \frac{I_{ot}}{I_{oi}} = \left(\frac{\varepsilon_2}{\varepsilon_1}\right)^{1/2} T_c^2 \qquad \text{(Equation 3.79)}$$

Equation 3.79 is **Transmission Power Fraction** of an incident radio wave.

3.5. Numerical simulation of attenuation of radio waves in a moderate intensity grassfire

This section models the propagation of radio signals polarized perpendicular to the fire direction of a moderate intensity grassfire (Figure 3.1). Moderate intensity grassfires are a common phenomenon in Northern Australia during late dry season (Williams *et al.* 1999). Most of these fires occur in *Sorghum spp*. grasslands or in open woodland where the grasses are the dominant understorey vegetation. During the season, intensity of the fires could be up to 18 MWm^{-1}(Williams *et al.* 2003). Potassium and other omnipresent nutrients such as phosphorus and nitrogen are volatized from the combusting vegetation into the fire plumes. At combustion efficiency of about 98 %, about 23 % of potassium is volatilized (Raison *et al.* 1985). The fire simulated here has similar physical dimensions and characteristics to those simulated by Clark *et al.* 2003. The behavior and the dimensions of the grassfire used in the simulation are given in Table 3.1.

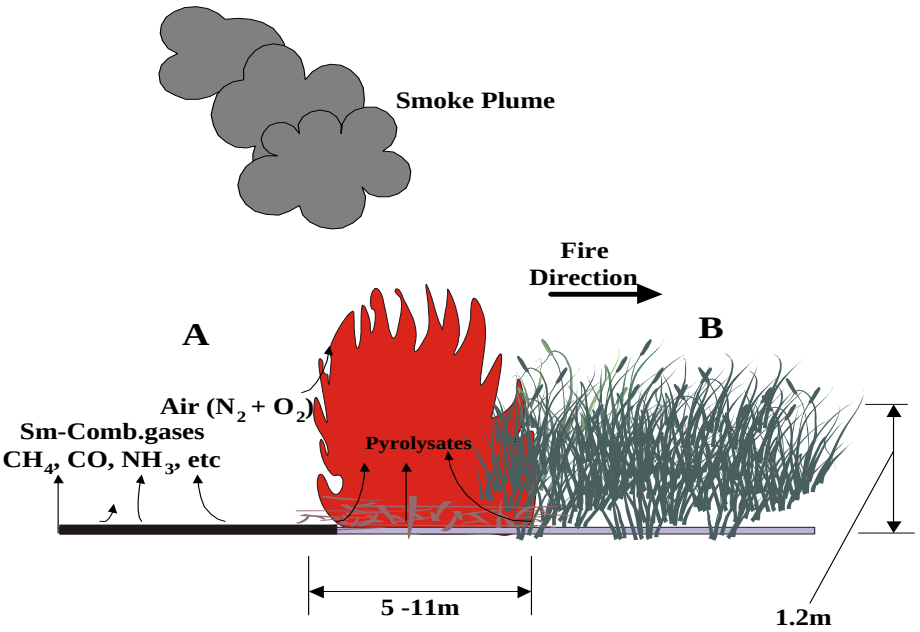

Figure 3.1. *Physical dimensions of the grassfire considered in the simulation experiment*

3.5.1. Temperature of the grassfire flame

The maximum temperature of 1240 K is assumed to occur near the grass canopy. The temperature decreases exponentially with height to a value of 998 K at 1.50 m. Figure 3.2 shows the decrease of temperature with height. Across the grassfire, the temperature is fitted to a Rayleigh profile (Fig. 3.3).

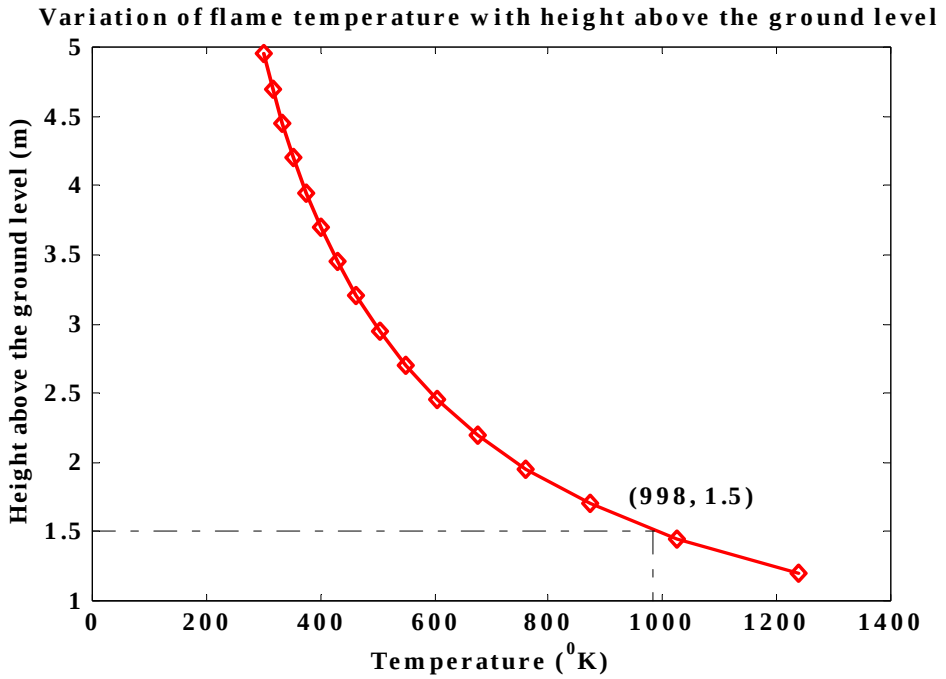

Figure 3.2. *Variation of temperature with height above ground of the grassfire plume*

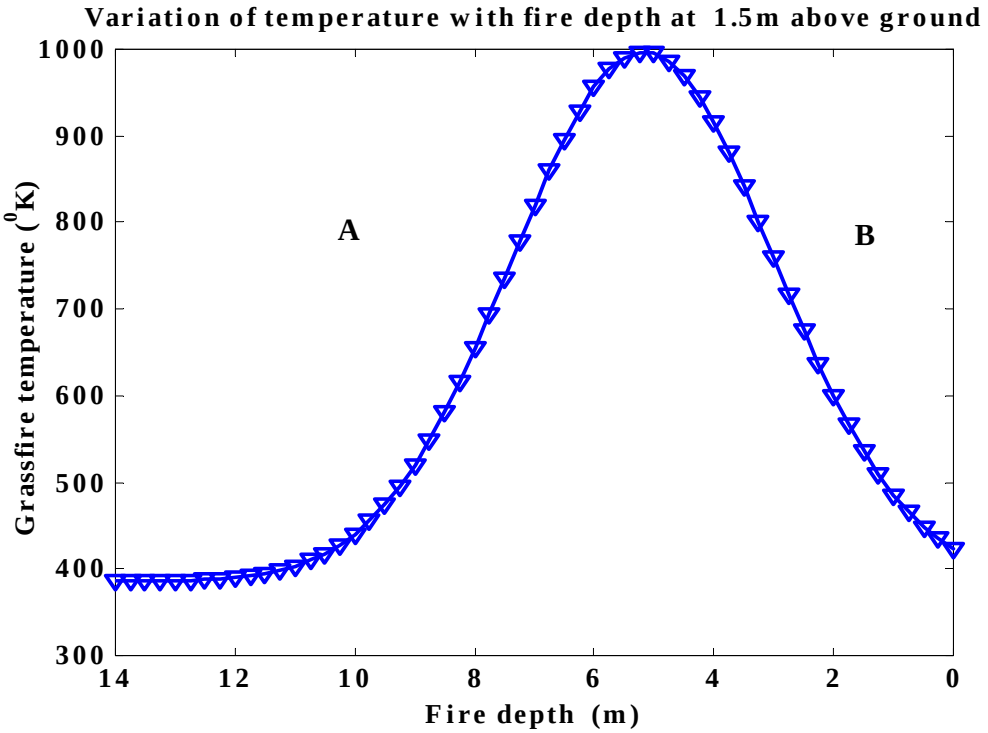

Figure 3.3. *Temperature variation across the grassfire depth at 1.5m above ground*

3.5.2. Step function approximation of temperature at 1.50 m above ground

One of main objectives of this chapter is to make predictions of the extent of ionization that causes radio wave loss in the grassfire. This is done by assuming the existence of LTE state in the flame. The LTE assumption calls for the flame to be divided into elementary volumes of average temperature (T). A line grassfire is considered in the experiment. Temperature along the width of the fire-line is assummed to be invariant at any height above the grass canopy. Temperature only varies across the fire depth. A step function approximation of temperature variation is shown in Figure 3.4.

3.5.3. Number of alkali atoms in the grassfire flame

Let us consider for simplicity, an infinite fire front ravaging through a uniform grass fuel bed as in Figure 3.5. As the fire line is very wide compared to its depth, the velocity of entrainment of the pyrolysis products into the flame can be calculated from the conservation of energy principle. Let U_e be the velocity of entrainment of gases into the flame. Ignoring some other energy sources, then the kinetic energy lost by a mass of a buoyant pyrolyzate over height dh is equal to potential energy gained over the same height. Thus,

$$\frac{1}{2}U_e^2 = g.dh \qquad \text{(Equation 3.80)}$$

Where dh and g are height gained in a unit time and acceleration of free fall respectively. However, under normal conditions fire spread is wind aided. Let wind speed be U_w. Balancing the heat content over depth dh per unit time (heat intensity, I_f) with the heat content over depth dh due to gases streaming into the combustion zone per unit time gives (Fendell *et al.* 2001);

$$I_f = \rho_a C_p T_a U_w .dh \qquad \text{(Equation 3.81)}$$

Where I_f, T_a, , C_p and ρ_a are heat intensity, ambient temperature, specific capacity at constant pressure and air mass density, respectively. For an infinite fire front, entrainment velocity is related to wind speed by the relation (Fendell *et al.* 2001);

$$U_w = 2\beta U_e \qquad \text{(Equation 3.82)}$$

For a steady state condition with $U_e > U_w$, $2\beta \cong 1$ (Fendell *et al.* 2001).

Substituting the above condition and Equation 3.82 into Equation 3.81 and simplifying gives,

$$U_e = \left(\frac{2gI_f}{\rho_a c_p T_a} \right)^{1/3} \qquad \text{(Equation 3.83)}$$

With entrainment velocity calculated as per Equation 3.83, the amount of potassium atoms in an elementary volume can be calculated by considering vegetation potassium content and combustion efficiency. Consider a section of a fire front which is *dw* meters wide as shown it is shown in Figure 3.5. In a unit time, fuel area consumed by a bushfire (*A*) is given by;

$$A = dw \text{ x Rate of Fire Spread } (RoS) \qquad \text{(Equation 3.84)}$$

Area *A* forms the base for the elementary volume drawn in dotted lines in Figure 3.5. Let the mass of potassium drawn into the flame per second be $M_{p,}$ its percentage in vegetative matter be P_k and the fuel loading be L_f. Therefore the mass of potassium in fire flame is;

$$M_p = A \text{ x } P_k \text{ x } L_f \text{ x } \tau \qquad \text{(Equation 3.85)}$$

The number of potassium atoms (K_a) swept into the volume V in 1 second is

$$K_a = (M_p / 39.10) \text{ x } 6.02 \text{ x } 10^{23} \qquad \text{(Equation 3.86)}$$

The volume swept by the pyrolysates in 1 second (V) = *A* x U_e. Therefore number of potassium atoms (τ) in a unit volume is K_a / V. However in vegetative matter, these potassium atoms do not exist as free atoms but are attached to other atoms in form of the ionic compounds or are organically bonded. The potassium compounds thermally dissociate into its respective atoms.

3.5.4. Dissociation and ionization in the elementary volume at 1.5m above ground

Volatiles are released from the vegetation's organic matrix and swept by convective currents into the combustion zone of flames (Raison *et al.* 1985 and Figure 3.5). In the elementary volume, alkali atoms released as volatiles from char (Okuno *et al.* 2005) are directly thermally ionised at the local

kinetic temperature into electrons and alkali ions. Potassium and sodium have ionization potential of 4.34 and 5.14 eV respectively. Alkali molecules such as KCl (g), KOH (g), etc. are thermally dissociated first and then ionized thereafter. Dissociation energy of potassium salts are low, they range from as low as 0.75 eV to about 4.51 eV (KCl). KOH has dissociation energy of about 3.51 eV. Electron density in the elementary volumes was calculated from the Saha equation (Equation 3.6). It is assumed that the most significant contribution to ionisation is from hydrogen displaced potassium atoms (K) from the charcoal. Potassium atoms released from char are from K-O-C (Okuno *et al.* 2005). Dissociated potassium atoms from KCl (g) and KOH (g) are also considered. KCl (g) is stable at temperatures below 1000K; however it dissociates significantly at temperatures around 1500 K.

3.5.5. Grassfire flame as a composite of dielectric slabs

The flame could be viewed as a composite of subslabs with varying dielectric permittivity governed by the electron density profile shown in Figure 3.7. The radio permittivity decreases to below unity with the increase in electron density and this is more likely at the combustion zone of the grassfire.

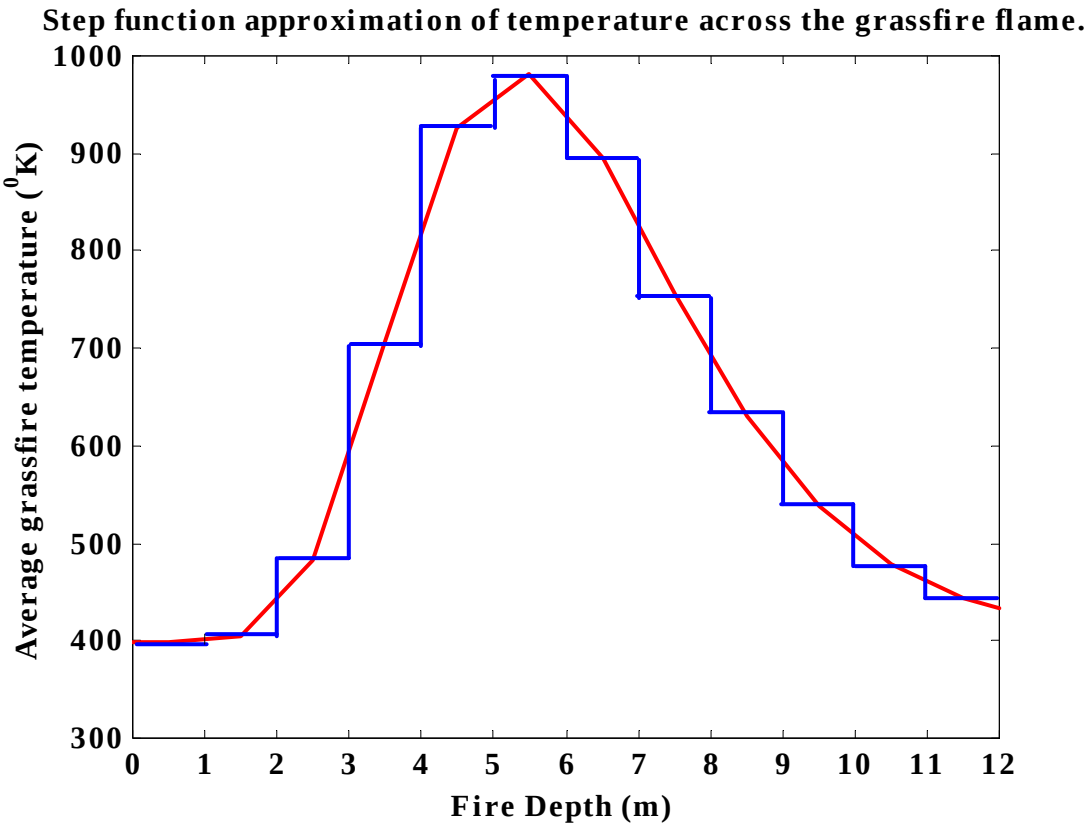

Figure 3.4. *Step function approximation of temperature across grassfire flame depth*

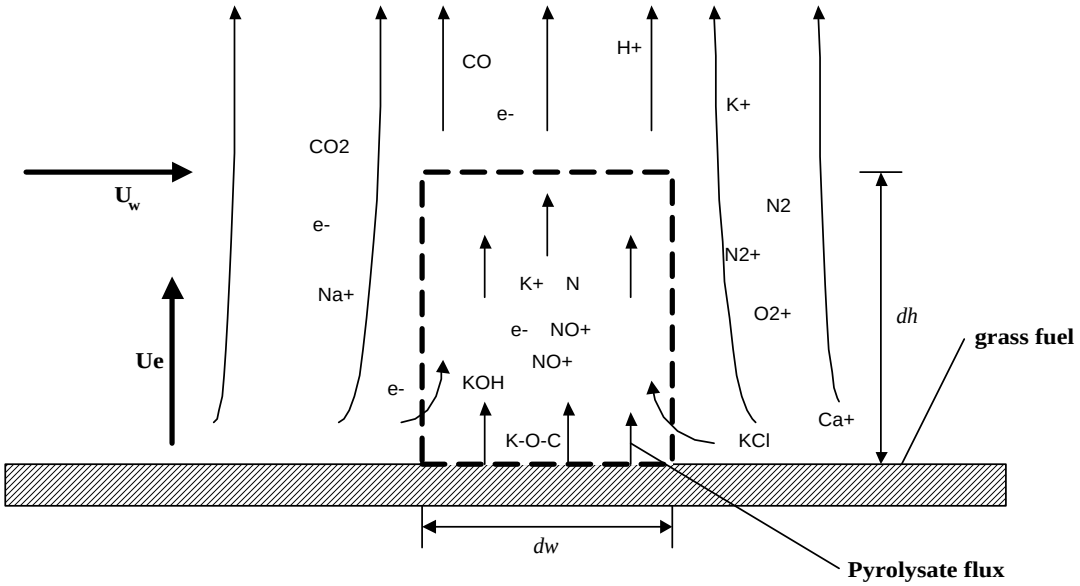

Figure 3.5. *Dissociation and ionization volatiles in the grassfire flame combustion zone*

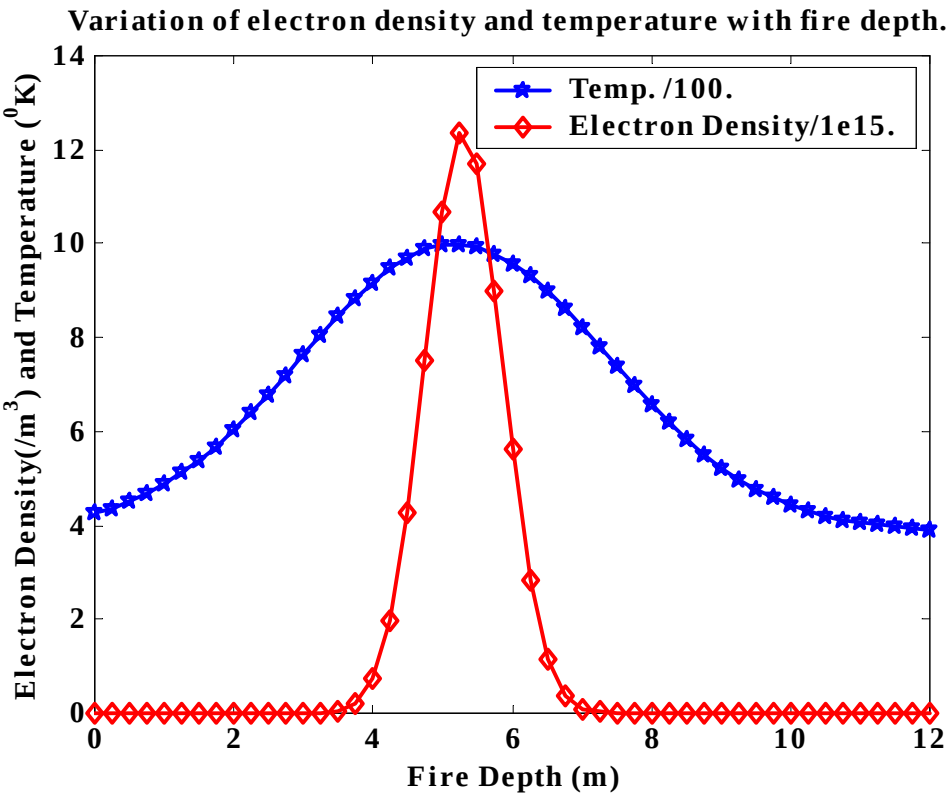

Figure 3.6. *Variation of electron density, temperature (Max.temp=1000K) with fire depth*

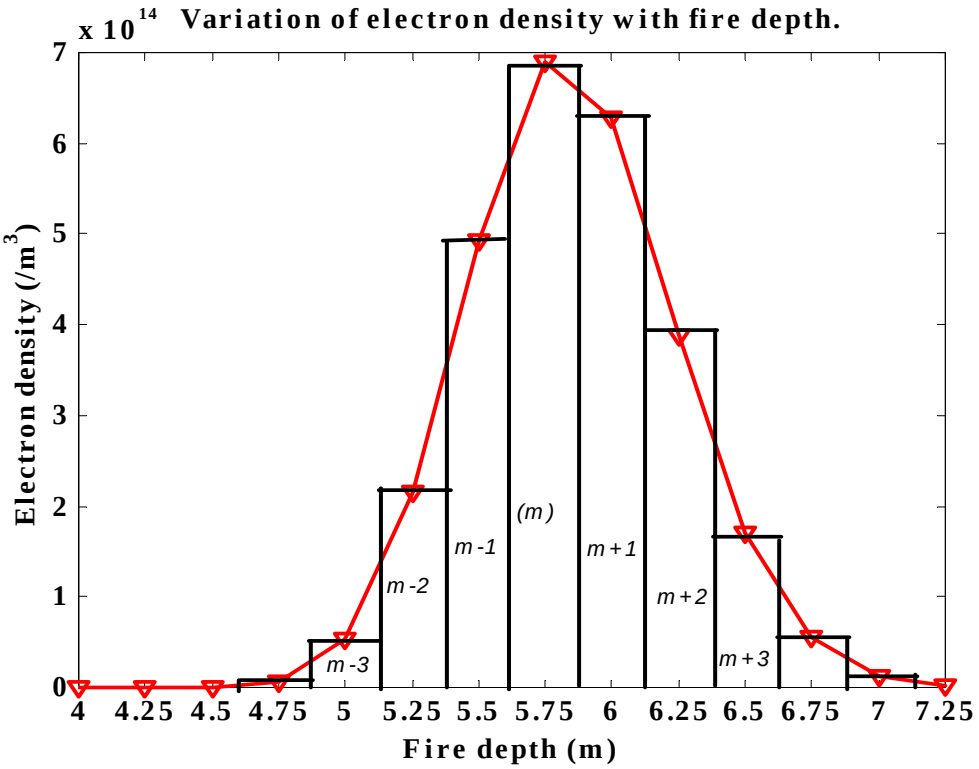

Figure 3.7. *Variation of electron density, temperature with fire depth*

3.5.6. Transmission and reflection power fractions

For a slab composite in Figure 3.7, the reflection coefficient equation at (*m+1*)th subslab is given by Equation 3.73 as;

$$R_{m+1} = \frac{E_r}{E_o} = \frac{\left(\frac{\varepsilon_{m+1}}{\varepsilon_m}\right) - \left(\frac{\varepsilon_{m+1}}{\varepsilon_m}\right)^{1/2}}{\left(\frac{\varepsilon_{m+1}}{\varepsilon_m}\right) + \left(\frac{\varepsilon_{m+1}}{\varepsilon_m}\right)^{1/2}} \qquad \text{(Equation 3.87)}$$

Total transmitted power for the whole slab arrangement as worked out from Equation 3.79 is given as;

$$P_{tf} = \prod_{1=1}^{sn} \left(\left(1 - |R_{m+1}|^2\right) \left[\exp(-2\alpha(i)d)\right] \right) \qquad \text{(Equation 3.88)}$$

Total reflected power for the composite as worked out from Equation 3.77 is given as;

$$P_{rf} = \left\{ R_1^2 + \sum_{i=2}^{sn} \left[(R_i)^2 \prod_{i=1}^{sn-1} \left(\left(1 - |R_i|^2\right) \left(\exp[-4(i)\alpha\, d]\right) \right) \right] \right\} \qquad \text{(Equation 3.89)}$$

3.6. Numerical Results and Discussions

Very High Frequency (VHF) radio wave propagation through a grassfire was simulated at various maximum temperatures 1.50 m above ground level. The depth of the fire front increased with the increase in maximum temperature at the height. A volatile flux of 0.10 kgm^{-2} s^{-1} from combusting grass is assumed. The use of the flux value is motivated by that obtained in experimental grassfires in Northern Australia (Clark *et al.* 2003).

Table 3.1. *Fire Depth at 1.50 m above ground for maximum temperature from 900-1200 K*

Maximum Temperature at 1.50 m (K):	900	1000	1100	1200
Fire depth(m):	5.10	6.40	8.10	11.20

3.6.1. Total transmitted, reflected and absorbed power fractions

The total transmitted and absorbed power fraction of radio waves in grassfire flames at maxiumum temperatures 900-1100 K were simulated for 2.00 and 10.00 %K (elemental) in the A-AEM volatiles (Figures 3.8 – 3.11). From the simulations, total reflected power of radio waves from flames was generally negligible; hence graphs of variation of total reflected power with fire depth are not shown. Total transmitted power fraction generally decreased with the increase in both the distance into the flame and potassium content in A-AEM volatiles. According to the slab model, a significant change in the power fraction was observed to be between about 3.00 m and 7.00 m of the fire front. This was due to high electron density in the region attributable to high temperature. This corresponded to temperature in the region of about 700 K.

The reduction of transmitted power in the flame was mainly brought about by collisonal damping of a radio wave since reflected power was negligible. Centerline electron densities in the flames ranged from 10^{14} to 10^{17} m^{-3}. At the maximum temperature of 900 K at 1.50 m above ground and 2.00 % K content in A-AEM volatiles, the power of the incident R-wave was reduced by 0.47 dB. The slab model predicts that at least 2.38 dB of the total power incident on the flame is lost at flame maximum temperature of 1000 K at the same height above ground and alkali concentration. At maximum temperature of 1100 K at 1.5 m above ground and 2.00 %K in the volatiles, the model predicts that the power of the incident R-wave will be decreased by 23.75 dB (see Figures 3.8 and 3.10).

At 900K, an increase in potassium content in A-AEM volatiles to 10.00 %, increased power loss to 0.60 dB. The absorption is much greater at higher temperatures as power loss of 4.84 and 52.99 dB were predicted for 1000 and 1100 K respectively. This represented an increase of 26.02, 92.00 and 34.56 % for 900, 1000 and 1100 K respectively from the values of 2.00 %K in A-AEM volatiles (see Figures 3.9 and 3.11). At higher percentages of potassium in the volatiles and a higher temperature, absorption can be much greater. If we consider 20.00 % of the A-AEM volatiles to be potassium atoms and the average grassfire temperature to be 1200 K, almost 184.21 dB of the incident power is predicted to be absorbed in grassfire which has a depth of 11 m.

Temperatures in a grassfire can be up to 1200 K and it is also possible to have 20.00 % of the A-AEM volatiles being potassium atoms (Vodaceck *et al.* 2002 and Okuno *et al.* 2005). Theoretically, under these conditions it possible to have a communication failure. Communication failure in grassfires have been documented, an example of such a failure is in the LARA grassfire of 1961(William *et al.* 1970).

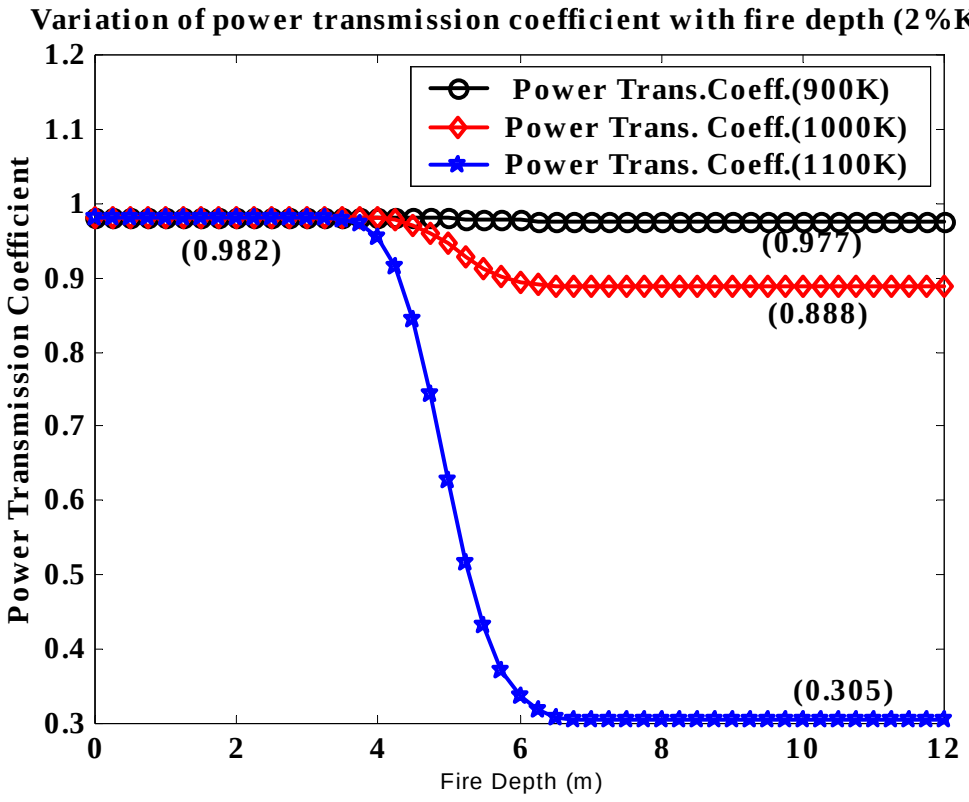

Figure 3.8. *Variation of total transmitted power coefficient with fire depth for 2%K conten*t

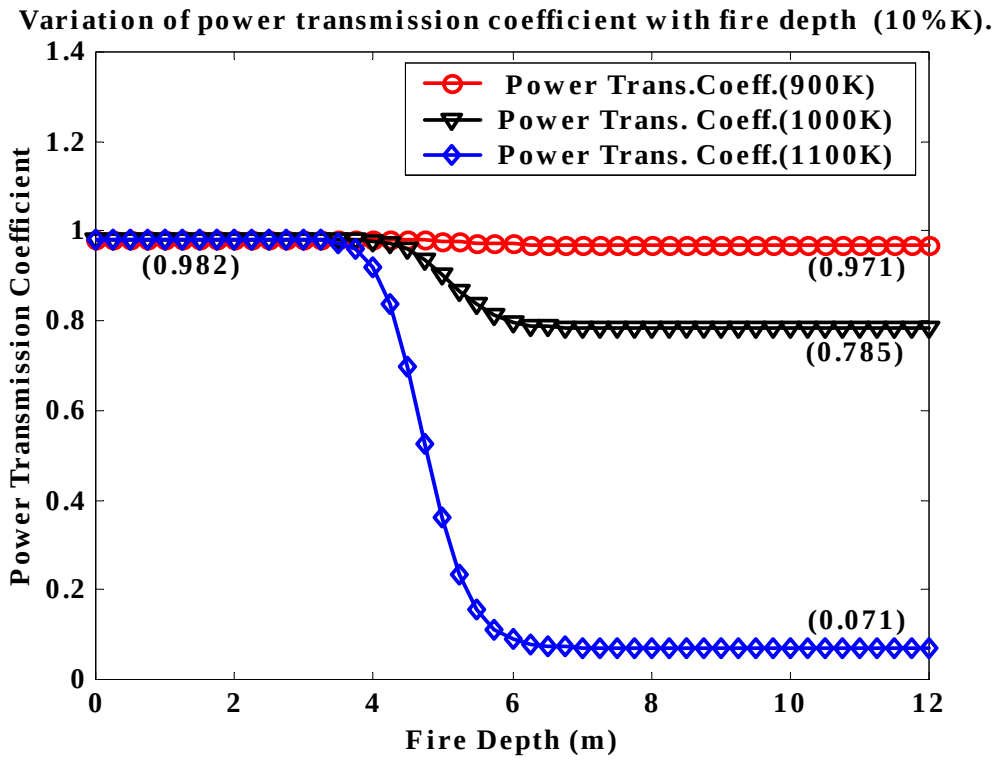

Figure 3.9. *Variation of total transmitted power coefficient with fire depth for 10%K content*

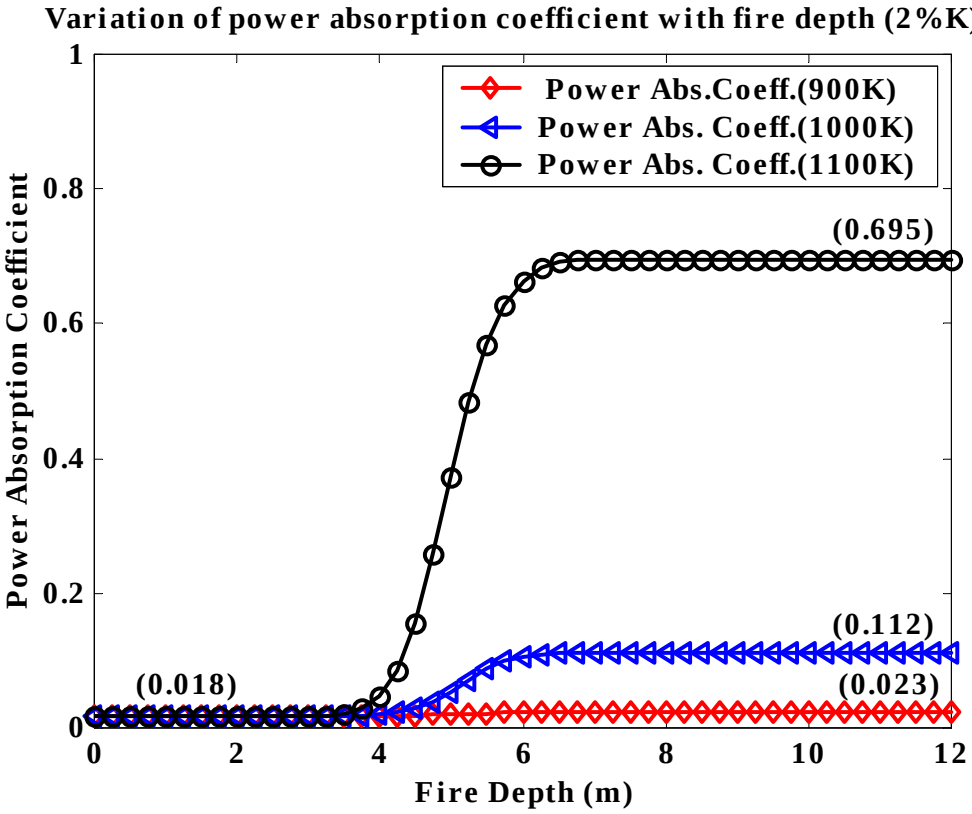

Figure 3.10. *Variation of total absorbed power coefficient with fire depth for 2%K content*

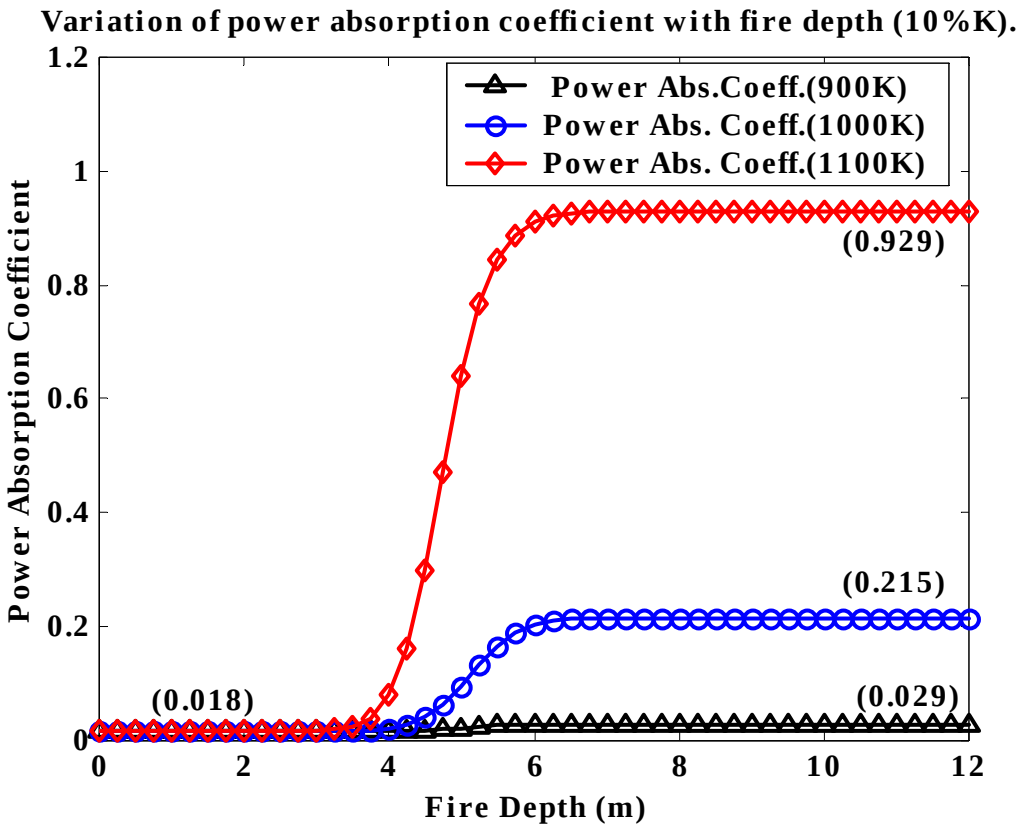

Figure 3.11. *Variation of total absorbed power coefficient with fire depth for 10% K content*

3.6.2. Total attenuation and phase shift due to grassfire flames.

Total attenuation of radio waves at 1.50 m above ground increased with the increase in maximum temperature and percentage of potassium in the A-AEM volatiles. It was observed from the simulation that at the maximum temperature of 900 K, total attenuation increased from 0.02 dB/m at 2.00 %K in the A-AEM volatiles to 0.03 dB/m at 20.00 %K in the volatiles (Figure 3.12). At the maximum temperature of 1000 K, the simulation predicted 0.08 dB/m at 2.00 %K in the volatiles whereas 20.00 %K in the volatiles gives 0.23 dB/m (Figure 3.13).A total attenuation of 0.64 dB/m was observed at 2.00 %K at the temperature of 1100 K which increased with the increase in potassium content in the volatiles to 2.28 dB/m at 20 %K in the volatiles (Figure 3.14). At 1200 K, total attenuation at 2.00 %K in the volatiles was predicted to be 3.62 dB/m which increased to 11.43 dB/m at 20 %K in the volatiles (Figure 3.15).

Phase shift imposed on radio waves due the flames was negligibly small for temperatures below 1000 K (Figure 3.16). For maximum temperatures above 1000 K, phase shift ranged from 1.82 -1036.03^0 for 1100 and 1200 K respectively.

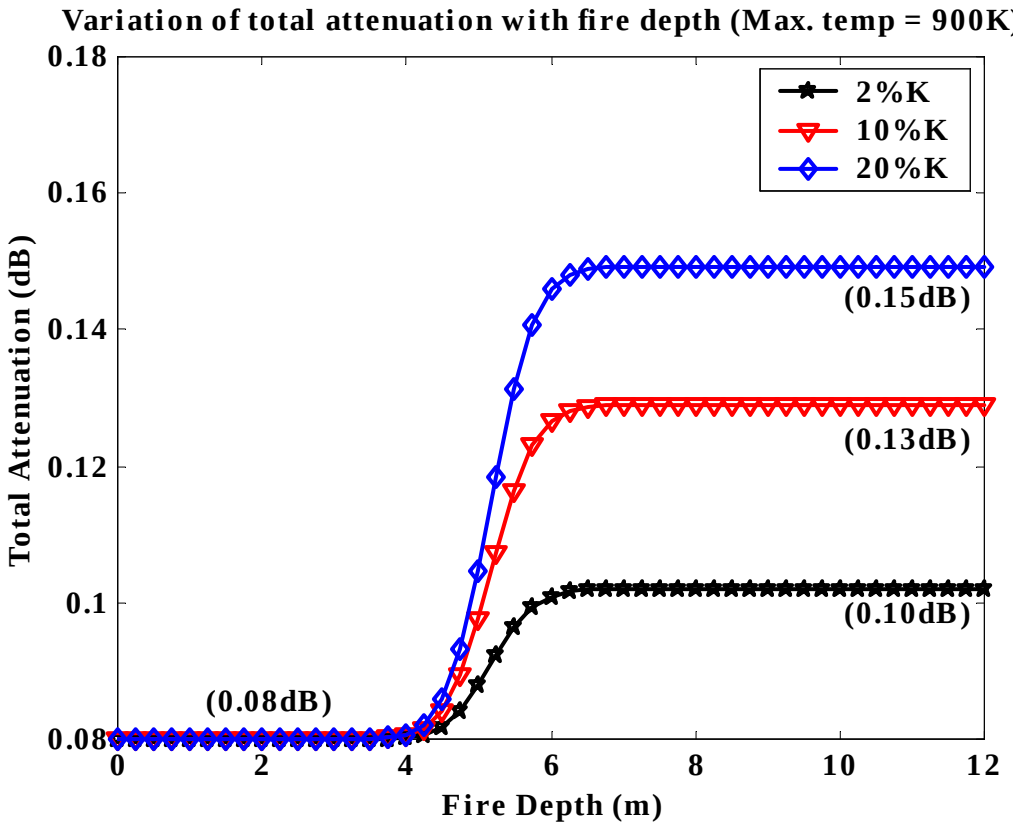

Figure 3.12. *Variation of total attenuation with fire depth for various K content at 900K*

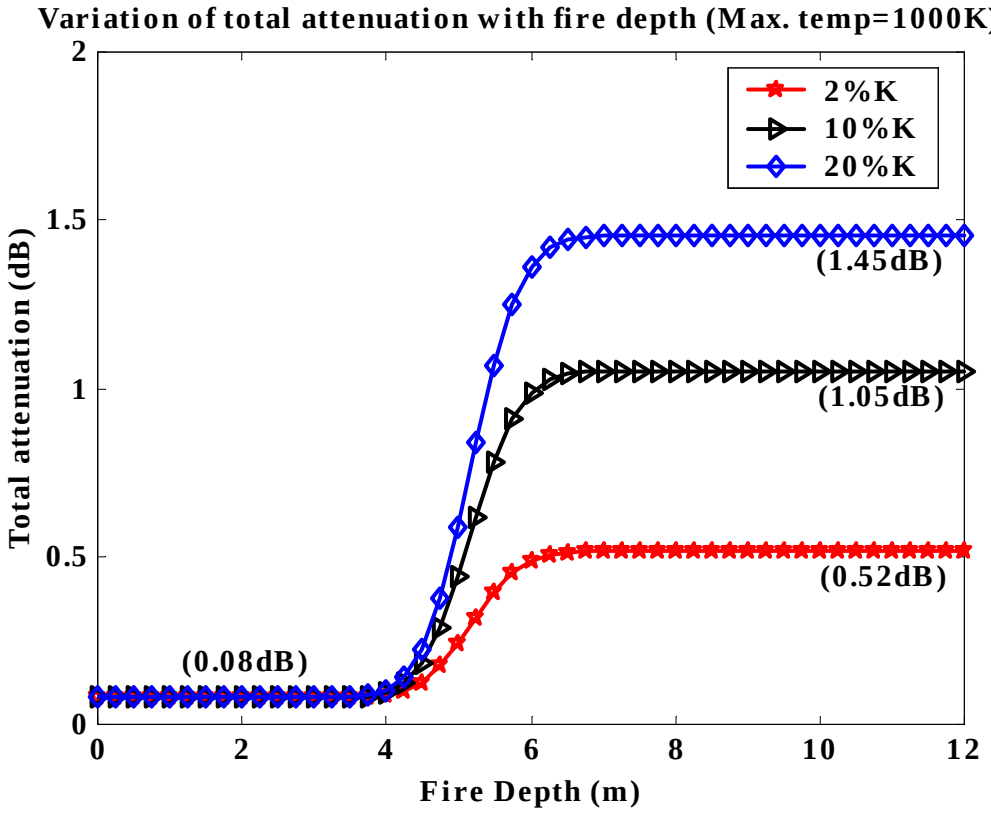

Figure 3.13. *Variation of total attenuation with fire depth for various K content at 1000K*

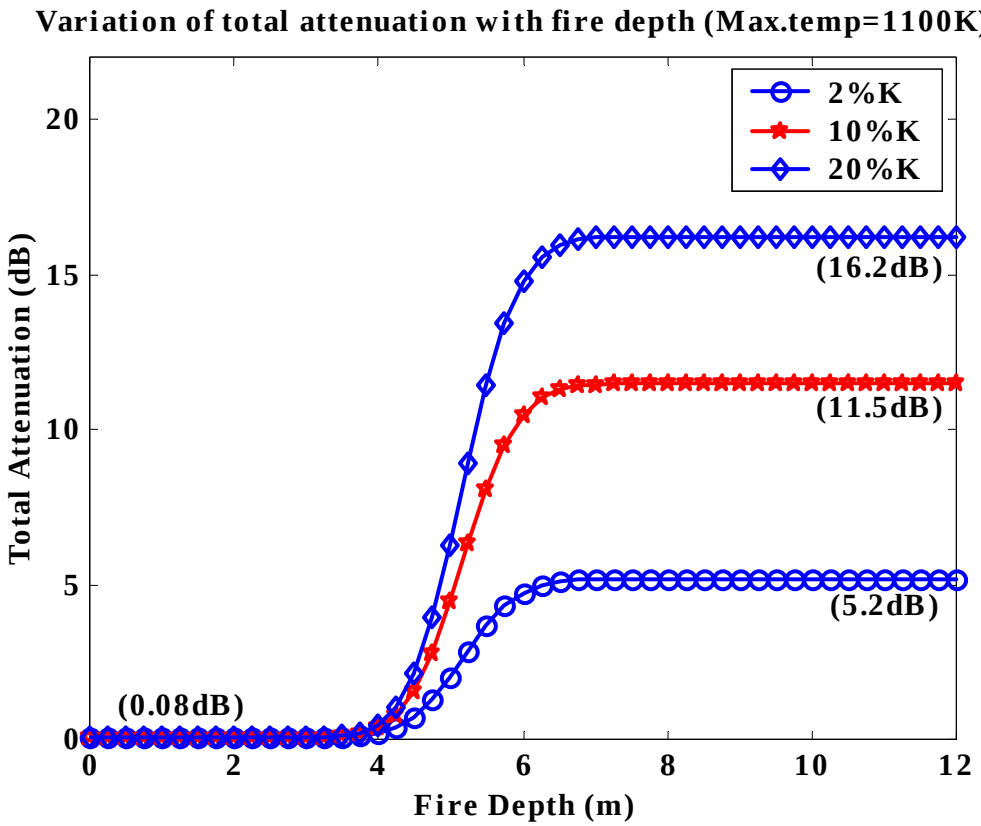

Figure 3.14. *Variation of total attenuation with fire depth for various K content at 1100K*

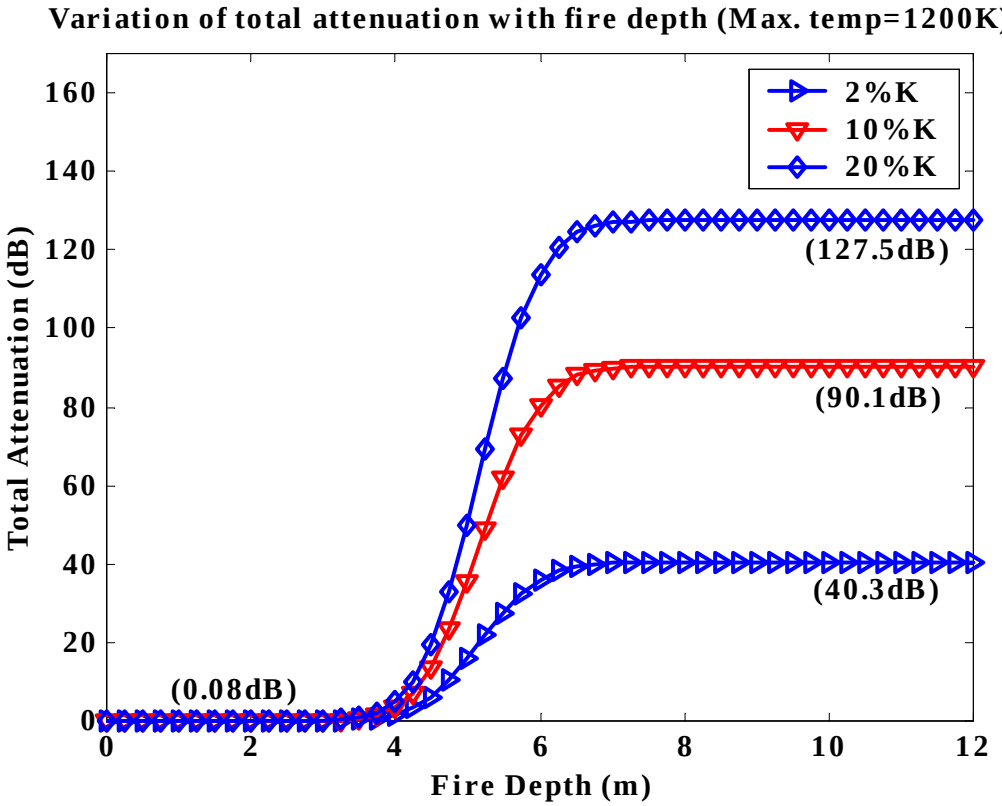

Figure 3.15. *Variation of total attenuation with fire depth for various K content at 1200K*

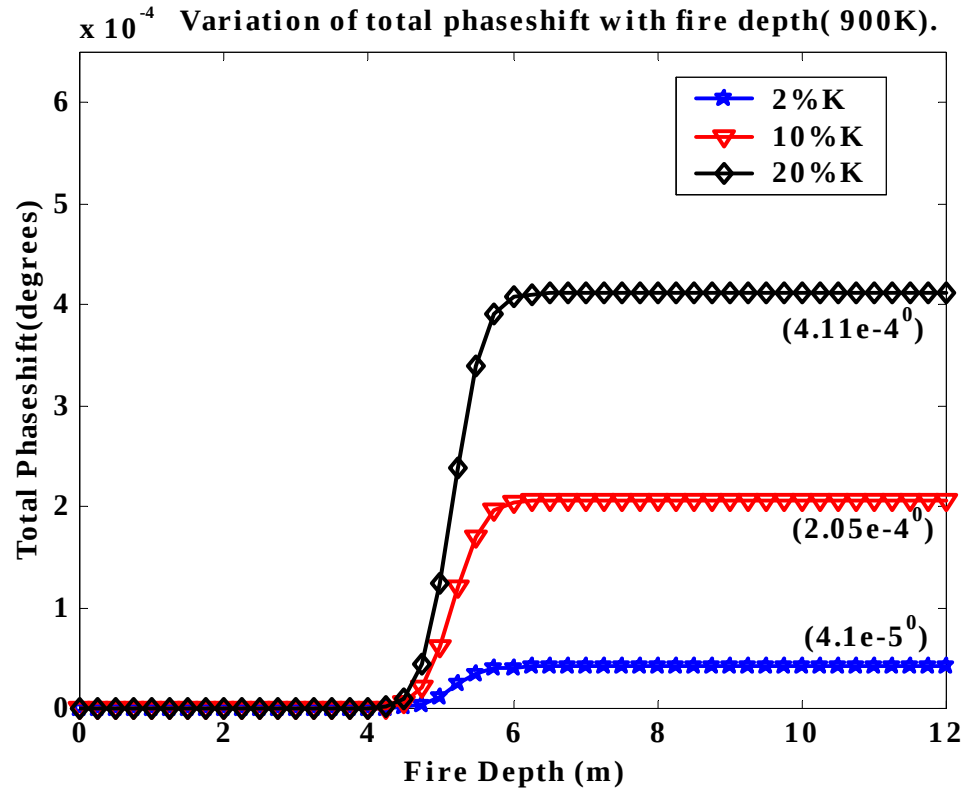

Figure 3.16. *Variation of phase shift with fire depth for various K content at 900K*

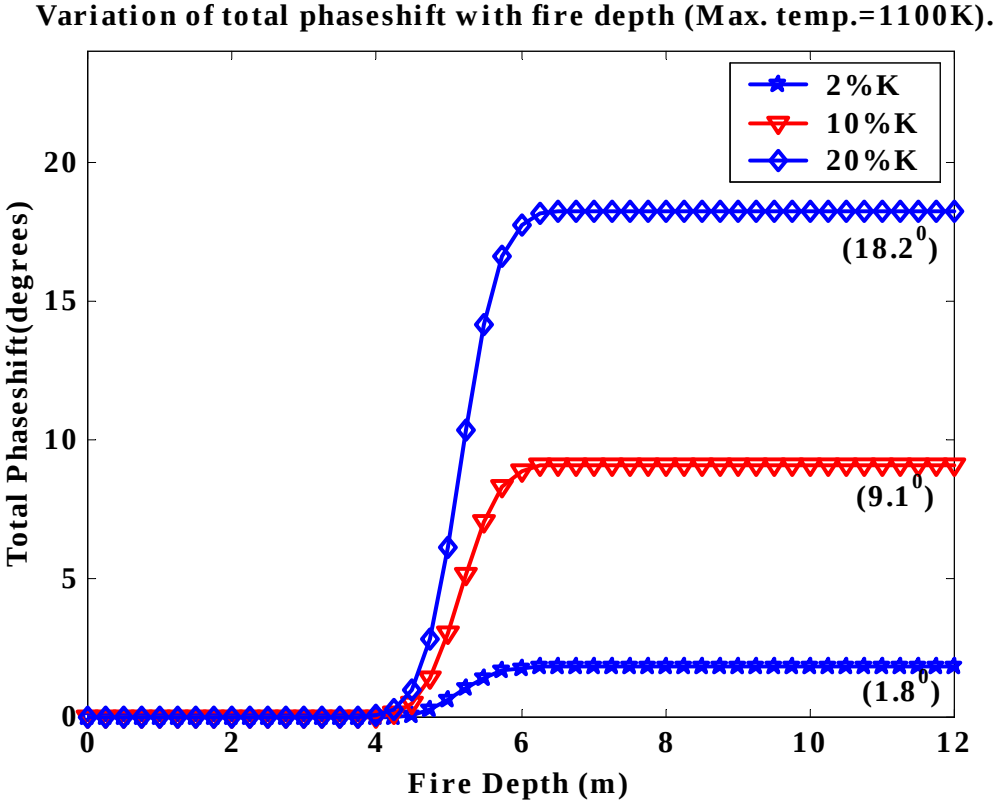

Figure 3.17. *Variation of phase shift with fire depth for various K content at 1100K*

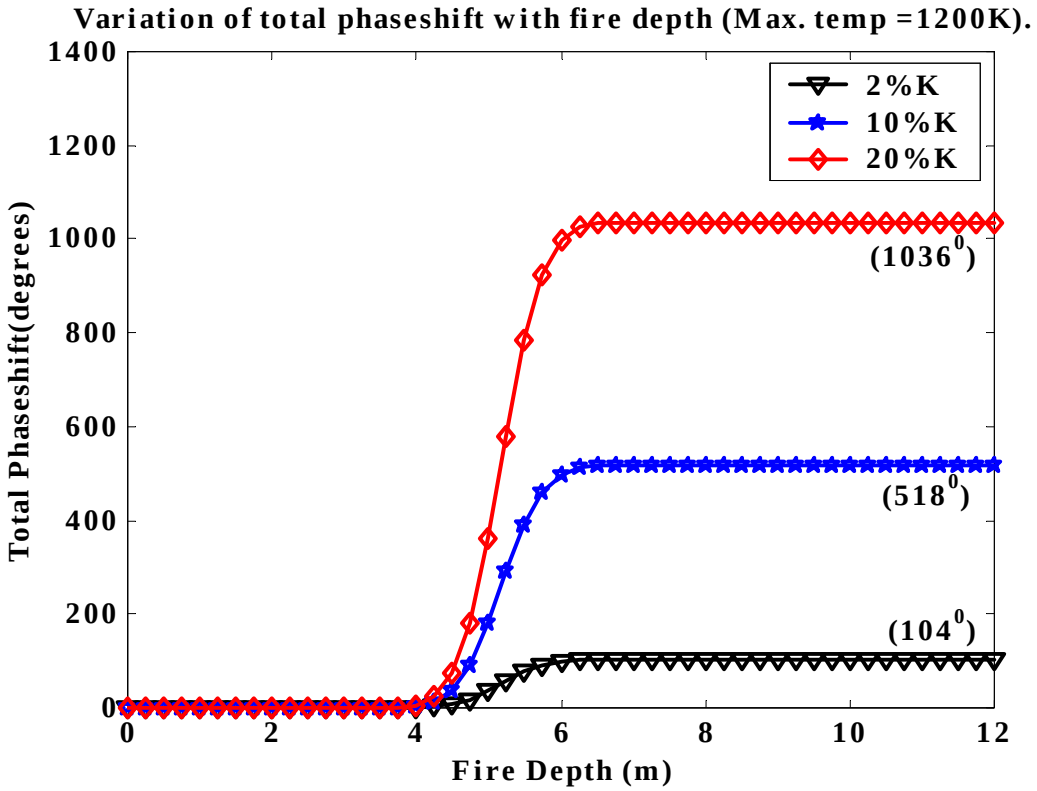

Figure 3.18. *Variation of phase shift with fire depth for various K content at 1200K*

3.7. Conclusions

- Grassfires are weakly ionized medium with electron density, which could be in the range of 10^{14}-10^{17} m^{-3}. The plasma significantly absorbs radio wave energy due to the high collisionality of the atmospheric pressure plasma. Atmospheric pressure plasmas have momentum transfer collision frequency of up to one Terahertz (10^{12} s^{-1}). From the numerical experiment, electron density of up to 10^{17} m^{-3} and electron-neutral collision frequency of about 10^{12} s^{-1} produce attenuations of up to 11.43 dB/m at the maximum temperatures of about 1200 K. This is high enough to cause radio wave communication failure.

- Phase shift also causes signal strength loss through interference of out of phase radio waves. The numerical simulation predicts phase shift as high as 1036.03º at maximum temperature of 1200 K. Considering the fact that phase change increases with temperature, the phase induced may impose a significant signal strength loss.

CHAPTER 4

Radio wave propagation measurements in a prescribed grassfire

4.1. Introduction

The omnipresent potassium in vegetation appears to be main source of ionization in grass and bushfires (Mphale *et al.* 2007). Moderate intensity grassfires with temperatures around 900°C in partially cured fuel are significantly ionized. This has been observed from attenuation and phase shifts measurements of high frequency and very high frequency radio waves in a moderate intensity controlled grassfire. Electron densities in the range of up to 10^{15} m^{-3} were measured.

The observed electrons density is partly due to the moist combustion environment and the presence of potassium (K) atoms in the fire plume. K atoms can be displaced by hydrogen radicals from alkalis attached oxidic functional groups such as K-O-C (Matsukata *et al*. 1989). Hydrogen radicals exist in appreciable amounts in bushfire flames. Moist combustion environment favors the emission of K species as hydroxide (KOH) and carbonate (K_2CO_3) (Westberg *et al*. 2003). Potassium chloride (KCl) emission is favored under dry and high chlorine combustion environment. If KCl, KOH and K_2CO_3 happen to coexist in the bushfire flame, most of the ionization will come from KOH and K_2CO_3 as they readily decompose into K atoms on heating. Compared to KCl, KOH and K_2CO_3 have low thermal dissociation energies. Bushfires that occur in partially cured vegetation are likely to have KOH and K_2CO_3 as predominant K species in the plume and are therefore likely to be significantly ionized.

The main objective of this chapter is to report on attenuation and phase change measurements carried out in a controlled moderate intensity grassfire at Plot B (see Figure 4.1) in James Cook University using a Radio Wave Interferometer (RWI). The instrument directly measures attenuation and phase change induced by a bushfire plume. The RWI was designed and built at the University as part of this project. The site studied had accumulated a lot of fuel over the past years and as safety precaution, the fuel load was being reduced to a level that would not support high intensity grassfires. This fire was controlled by the University's fire officers and offered a excellent opportunity for propagation measurements.

Section 4.2 describes the location, climate and the vegetation structure at Plot B. The vegetation in the study site is typical open woodland. Black spear grass (*Heteropogon Contortus*) and poplar gum (*Eucalyptus Platyphylla*) dominated the understorey and the overstorey vegetation respectively. There were occasional chinee-apple (*Ziziphus mauritiana*) shrubs in the understorey stratum. The design of the RWI is discussed in Section 4.3. RWI uses the same principles as a Microwave Interferometer (MWI) except that it has been designed to operate at much lower frequencies.

The theory relating attenuation and phase shift of R-Wave to ionization is briefly discussed in section 4.4. Section 4.5 explains how the experiments were carried out with the results and discussion presented in Section 4.6. The chapter is concluded in section 4.7.

4.2. Study site and vegetation structure

The study site is located at 147°58′56″E and 19°25′46″S on the western side of James Cook University's Main campus in Townsville, northern Queensland (Figure 4.1). Climate in Townsville region is warm and humid (Lokkers, 2000). Summers are hot with average maximum temperature of 30.7°C in January. An average minimum temperature of 15.4°C occurs in winter (July). The region receives an average annual rainfall of 1143 mm (Williams *et al.* 2003). Most of it falls during summer; a season that extends from December to March. The rainfall in this season is generally associated with the northeasterly trade winds, cyclones and depressions (Lokkers, 2000). Long dry periods during the winter and variable annual rainfall have resulted in the region being fire-prone and frequent fires have created mosaics of open forest, woodlands and grasslands in the region.

The vegetation structure in the study site is open woodlands of *eucalyptus* and grassy understorey. The understorey is mainly black spear grass and there are occasional 1.5-3 m high chinee-apple shrubs. An average grass density was about 150 plants per square meter. The average height of spear grass was about 1.02 m. The dominant overstorey tree species were poplar gums *eucalypts* (Figure 4.2).

The study site (Plot B, in Figure 4.1) was irregular in shape (see Figure 4.14) with a perimeter of 393.29 m. A propagation path of about 44.47 m long was chosen at the site in an area where there was minimum obstruction from trees and shrubs. The site was chosen along with Plot A by the

Physical Planning division of the University for Controlled burning in 2004, a preemptive exercise necessary for the control of high intensity bushfires occurrence on campus. Amount of fuel accumulated and proximity to building structures were the main reasons for the selection of these plots.

Figure 4.2. *Vegetation structure at the study area (Plot B)*

4.3. VHF radio wave interferometer

4.3.1. Microwave Interferometer

Measurement of phase shift and signal amplitude provides useful information for predicting the effect of bushfire on radio waves. A technique has long been used since the 1960s to diagnose line integrated plasma electron density and collision frequency of weakly ionized plasma. This technique, called microwave interferometry (see Whitmer, 1956; Zivanovic *et al.* 1964 and Gilchrist *et al.* 1997), has an advantage over conventional methods (e.g. the use of Langmuir probes) of being non-intrusive and provides a direct measurement of attenuation. The use of Langmuir probes is limited to measuring local electron density and carries with it some inherent problems such as probe heating and local plasma perturbation. Despite its advantages over Langmuir probe, a microwave interferometer is limited in its capability by plasma natural frequency. Microwave frequencies lower than its natural frequency cannot traverse the plasma.

At a suitable probe frequency, an interferometer can be arranged to measure both attenuation and phase shift (e.g. in Caron *et al.* 1968). RWI is an instrument designed to use the same principles as the microwave interferometer except that it works at a much lower frequency and is suitable for measuring ionization in large unbounded volumes at atmospheric pressure in a weakly ionized medium such as a bushfire.

4.3.2. Theory

Consider a plane polarized electromagnetic wave to travel in the positive x-direction such that its amplitude at any given time is given as (Heron *et al.* 2004):

$$E = E_0 e^{i(\omega.t-\gamma.x)} \qquad \text{(Equation 4.1)}$$

Where: γ = propagation constant,
ω = cyclic propagation frequency ($=2\pi f$),
E_0 = initial electric field strength of the radio signal.

From Chapter 3, propagation constant (γ) can also be given as: $\gamma=\alpha + i(\beta)$, therefore Equation 4.1 can be written as (Heron *et al.* 2004):

$$E = E_0 e^{-\beta z}\{\cos(\omega t - \alpha x)\} \qquad \text{(Equation 4.2)}$$

If the signal travels through a bushfire (a lossy medium), electromagnetic wave energy will be lost to the medium and phase shift will be induced by fire. The induced phase shift and loss in energy are due to dielectric permittivity of the fire being not equal to unity. The two effects are measurable and can be related to those in free space. The amplitude of the signal that traverses fire is attenuated and is given by;

$$E_f = E_0 e^{-\alpha_f x} \qquad \text{(Equation 4.3)}$$

Without the fire the amplitude of the signal that traversed air would not be attenuated, and would be given by:

$$E_a = E_0 \quad \text{(Equation 4.4)}$$

Attenuation of the signal that traverses fire expressed in dB is (Pozar, 1993);

$$\text{Attenuation (dB)} = 10\log_{10}\left\{\left(\frac{E_a}{E_f}\right)^2\right\}$$

$$\text{Attenuation (dB)} = 10\log_{10}\left[e^{2\alpha_f x}\right] \quad \text{(Equation 4.5)}$$

Induced phase shift ($\Delta\varphi$) depends on the phase constants of free space (β_0) and that of the fire (β_f) and is given by the expression (Chang *et al*. 2007):

$$\Delta\varphi = \int_0^x (\beta_0 - \beta_f).dr \quad \text{(Equation 4.6)}$$

The phase constants are related to propagation frequency (f_0) in the following manner;

$$\beta_0 = \frac{2\pi f_0}{c} \quad \text{(Equation 4.7)}$$

and

$$\beta_f = \frac{2\pi f_0}{c}.\text{real}\left(\sqrt{\varepsilon_f}\right) \quad \text{(Equation 4.8)}$$

4.3.3. Radio Wave Interferometer (RWI) Units

RWI has 6 units whose primary function is to synthesize, transmit, receives and process phase coherent radio signals. The units perform the above functions on 6, 30 and 150 MHz signals. Block diagram in Figure 4.3 shows all the units making up the instrument and some of them are separately shown in Figures 4.4-4.7.

4.3.3.1. Master oscillator and transmitter unit

The unit is responsible for generating phase coherent 6, 30 and 150 MHz radio wave signals from a 75 MHz master oscillator. A 75 MHz square wave signal is frequency divided by 5 using logic circuits, it is then doubled (x 2) to produce a 30 MHz sinusoidal signal. The 30 MHz signal is then amplified to a power rating of 250 mW and fed to a 30 MHz antenna. A part of the 30MHz signal is tapped, buffered and then divided by 5 to produce a 6 MHz reference signal. This reference signal is fed at low impedance to a 75 m long coaxial cable and connected to Receiver Unit (Rx). The 75 MHz was doubled to produce a 150 MHz sinusoidal signal. It was then amplified and fed to a 150 MHz Yagi antenna. The unit produced phase coherent signals since they are produced from one oscillator – the 75 MHz master oscillator.

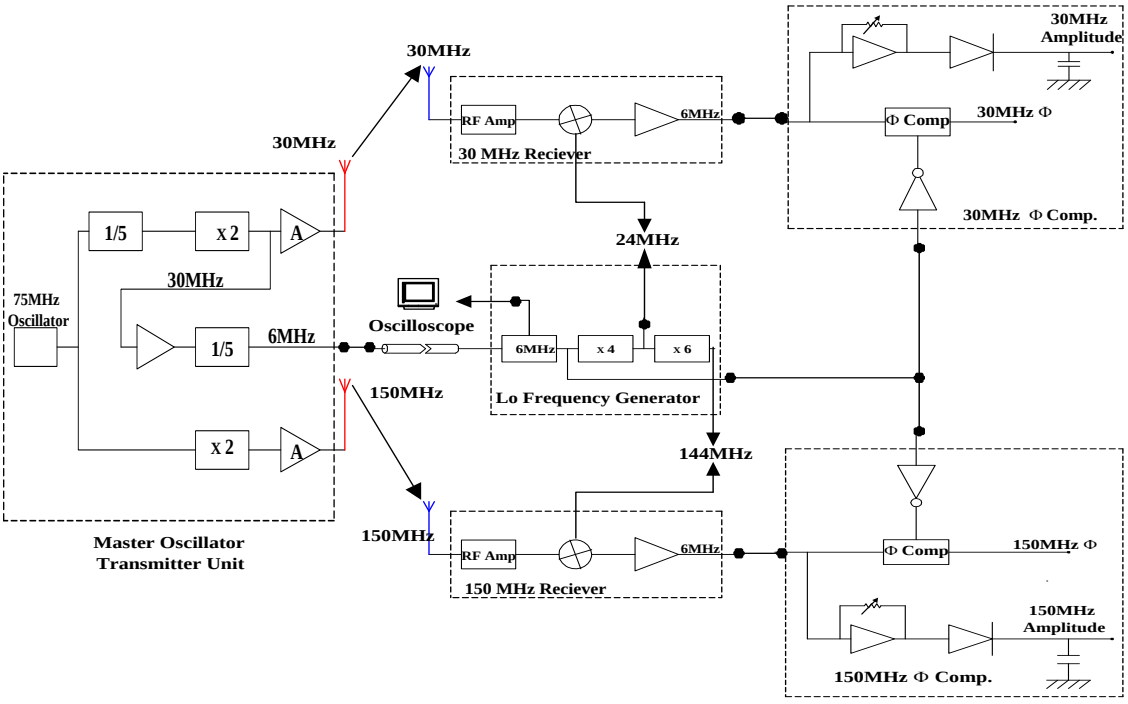

Figure 4.3. *A block diagram for a VHF Radio Wave Interferometer*

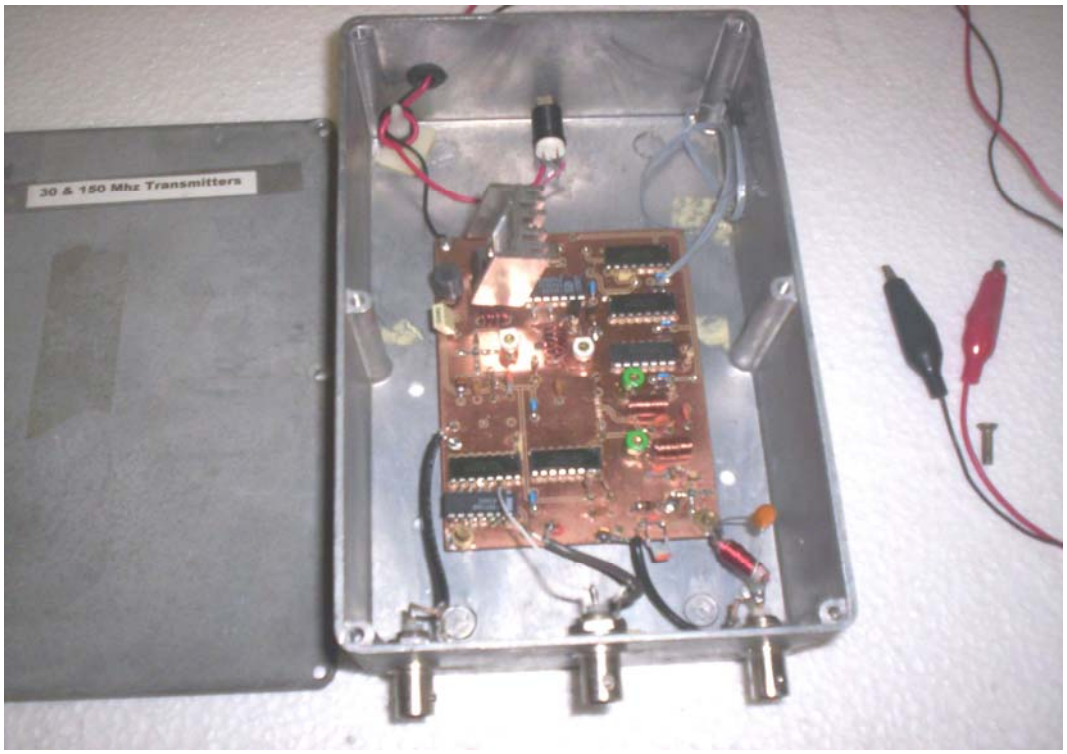

Figure 4.4. *30 and 50MHz transmitter circuits in protective casing*

Figure 4.5. *Local Oscillator Frequency Generator*

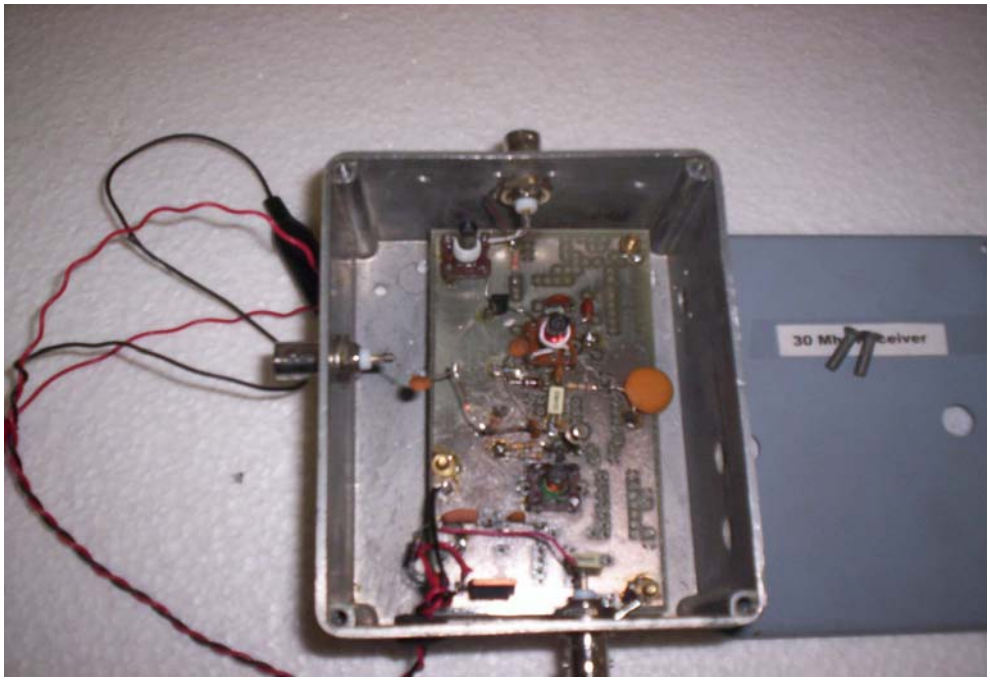

Figure 4.6. *30MHz receiver circuit in protective casing*

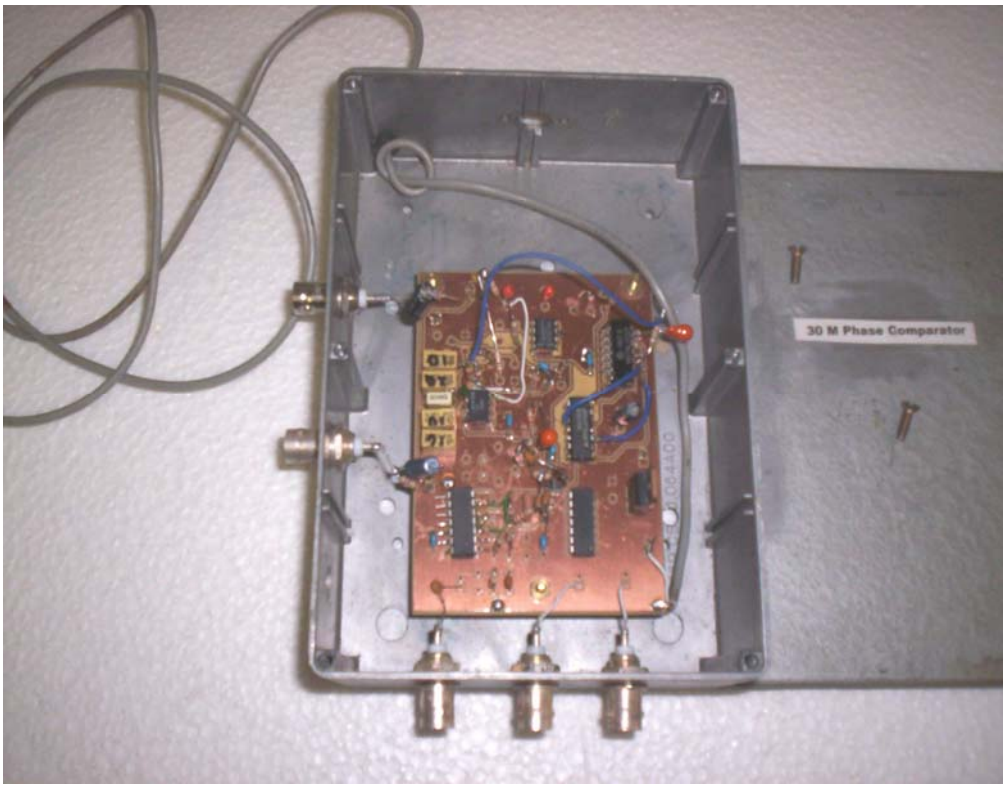

Figure 4.7. *30MHz Phase Comparator circuit in protective casing*

4.3.3.2. Local Oscillator Generator (LOG) and Receiver (Rx) units

The main function of these units is to receive the transmitted signals from master oscillator-transmitter unit and synthesize a 6 MHz signal for phase comparison. Generally LOG generates signals for mixing in the Rx units. The LOG unit is fed with the 6 MHz reference signal from the master oscillator and transmitter unit. The reference signal is frequency-multiplied by 4 and 6 respectively to produce 24 and 144 MHz signals (see Figure 4.3). In the 30MHz Rx unit, a received signal from 30 MHz antenna is mixed with a 24 MHz signal from the local oscillator frequency generator to produce 6 MHz. The 150 MHz signal received from a Yagi antenna is mixed with a 144 MHz signal from the LOG to produce 6MHz. The 6MHz signals and the reference 6 MHz are fed in respective phase comparators.

4.3.3.3. Comparators

These are 180° phase comparison circuits. Phase of 6 MHz signals from Rx units is compared with the phase of the 6 MHz reference. A D.C. voltage representative of this phase difference is registered in a HOBO®data logger. Initially a voltage of 2.50 V was set for 180° phase difference.

4.3.3.4. Antennae

Two types of antennae were used in the interferometer; a horizontal Yagi (Figure 4.8) and vertical quarter-wavelength whip (Figure 4.9). The Yagi antenna was designed to work at frequency range of 149-151 MHz, and the vertical quarter-wavelength whip at 30 MHz

Figure 4.8. *150MHz Yagi antenna.*

Figure 4.9. *Quarter-wavelength whip antenna*

4.3.4. Phase Change Tests

The interferometer was tested for sensitivity to phase changes using antenna position. In the tests, an oscilloscope was used to monitor the output from the 30 MHz comparator unit. The quarter wave dipole was initially set at Position A (PsA) so that the amplitude signal and the reference signal (shown as a square wave) are nearly in phase as in Figure 4.10(a). The antenna was moved a fraction of the wavelength away from PsA. When the antenna was moved 2.90 m (0.29λ) away from PsA, a phase shift of 53.03° was induced (see Figure 4.10(b)).

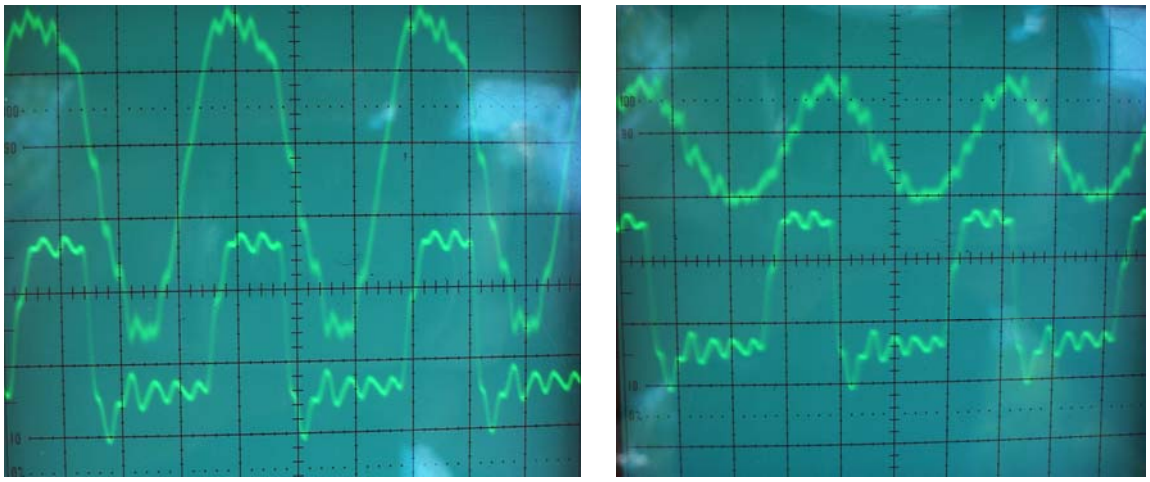

(a) (b)

Figure 4.10. *Phase change due to moving the antenna: (a) phase at starting position and (b) antenna moved 2.9m away from starting position*

When the antenna was moved 5.00 m (0.5λ) away from PsA, a phase shift of 95.30° was induced on the amplitude signal (see Figure 4.11(b) below).

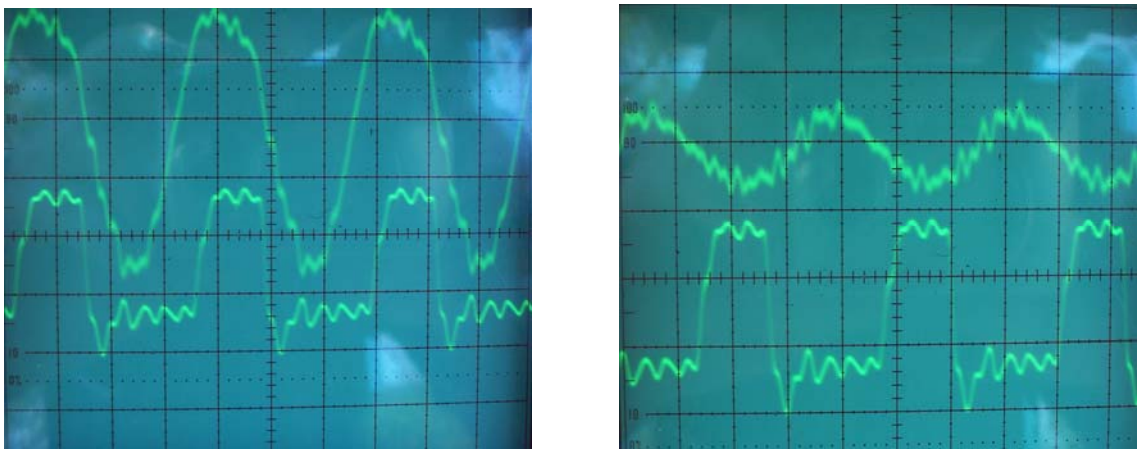

(a) (b)

Figure 4.11. *Phase change due to moving the antenna: (a) phase at starting position (PsA) and (b) antenna moved 5.0m away from starting position*

4.4. Electron density, phase change and radio wave attenuation.

By comparing Equations 3.40 and 3.46 together with Equations 3.47 and 3.48, it can be deduced that

$$\varphi = \left(1 - \frac{\omega_p^2}{\omega^2 + \varphi_{eff}^2}\right) \text{ and } \Gamma = \left(\frac{\omega_p^2}{\omega^2 + \varphi_{eff}^2}\frac{\varphi_{eff}}{\omega}\right) \qquad \text{(Equations 4.9)}$$

Substituting Equation 4.9 into Equations 3.57 and 3.58 gives;

$$\beta_f = \frac{\omega}{c}\left\{\frac{1}{2}\left(1 - \frac{\omega_p^2}{\omega^2 + \varphi_{eff}^2}\right) + \frac{1}{2}\left[\left(1 - \frac{\omega_p^2}{\omega^2 + \varphi_{eff}^2}\right)^2 + \left(\frac{\omega_p^2}{\omega^2 + \varphi_{eff}^2}\frac{\varphi_{eff}}{\omega}\right)^2\right]^{1/2}\right\}^{1/2}$$

(Equation 4.10)

$$\alpha_f = \frac{\omega}{c}\left\{-\frac{1}{2}\left(1 - \frac{\omega_p^2}{\omega^2 + \varphi_{eff}^2}\right) + \frac{1}{2}\left[\left(1 - \frac{\omega_p^2}{\omega^2 + \varphi_{eff}^2}\right)^2 + \left(\frac{\omega_p^2}{\omega^2 + \varphi_{eff}^2}\frac{\varphi_{eff}}{\omega}\right)^2\right]^{1/2}\right\}^{1/2}$$

(Equation 4.11)

Since grassfire flames are slightly ionized, at HF-VHF frequencies, $\varphi_{eff} >> \omega \geq \omega_p$ because atmospheric plasmas are highly collisional (Larroussi, 1995). Equations 4.10 and 4.11 then reduces to:

$$\beta_f \cong \frac{\omega}{c}\left[1 + \frac{\omega_p^4}{8\varphi_{eff}^2}\frac{1}{\omega^2}\right] \qquad \text{(Equation 4.12)}$$

$$\alpha_f \cong \frac{\omega}{c}\left[\frac{\omega_p^2}{2\omega\varphi_{eff}}\right] \qquad \text{(Equation 4.13)}$$

From Equations 4.5 and 4.6, a grassfire flame with an average electron density (N) induces phase change ($\Delta\Phi$) and attenuation on radio waves given by:

$$\Delta\Phi = \beta_o - \beta_f$$

$$\Delta\Phi = 0.00067\,\frac{N^2 d}{f_0\,\varphi_{eff}^2} \qquad \text{(Equation 4.14)}$$

$$\text{Attenuation} = 5.29\text{x}10^{-6}\,\frac{N\ d}{\varphi_{eff}} \qquad \text{(Equation 4.15)}$$

4.5. Experimental Methods

4.5.1. Fuel characteristics

Vegetation was sampled by means of $1m^2$ quadrants. Four $1m^2$ quadrants were randomly set up one hour before ignition in the prescribed burn area. 20 spear grass plants were randomly sampled in each quadrant. The height of each plant was measured by a 5m-measuring tape and then averaged to give the average fuel height (H_a). Surface litter and vegetation (clipped from just above the ground surface) were collected from the quadrants into separate bags (a bag for each quadrant) and then sealed for analysis. The mass of plant material from each quadrant was determined and the masses were then averaged to give M_{aw}. Weighed samples of plant material from each bag were then dried in an oven set at 60°C for 72 hours. The masses of the samples were averaged to give M_{saw}. The oven-dried plant materials were thereafter re-weighed to give dry mass, which averaged to give M_{sad}. The degree of curing (Dc) for the fuel was determined from the relation;

$$Dc = \left[1 - \left(\frac{M_{saw} - M_{sad}}{M_{sad}}\right)\right] x100\% \qquad \text{(Equation 4.16)}$$

Fuel load (F_L) for the study area was calculated from averaged biomass per unit area, thus:

$$F_L = M_{aw} \ \ Kg/m^2 \qquad \text{(Equation 4.17)}$$

4.5.2. Grassfire behavior

The fire front was produced by the wind from the northeast direction (60°E). The propagation equipment was set such that it propagates approximately in the West to East direction (see Figure 4.2). The rate of spread (RoS) for the grassfire was determined from running the CSIRO Fire Spread Calculator v.1. (CSIRO, 1998) This is a model that calculates rate of spread for different vegetation scenarios in Australia including northern Australia's open woodland vegetation. The inputs to this model are ambient temperature, relative humidity, curing percentage and wind speed (km/h) at 10m. From the output of this model, flame depth (F_d) of the grassfire was calculated by considering that the flame front intercepted the transmission path at angle of 30^0 taking account of the direction of the wind (see Figures 4.12).

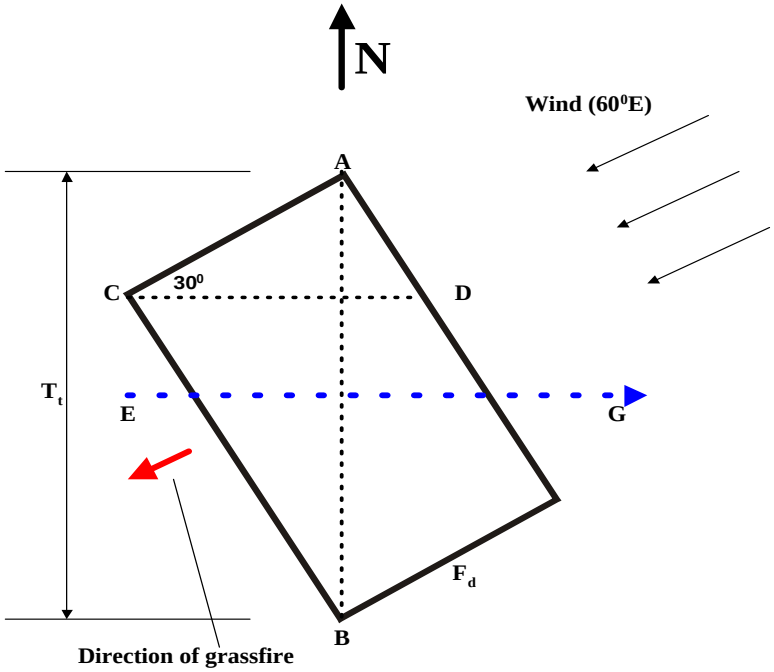

Figure 4.12. *Observed grassfire direction during the prescribed burn*

Assuming that the head fire is rectangular, then flame depth (F_d) is proportional to flame residence time (t_r) or the time when the flame was in the propagation path. The constant of proportionality is RoS, in this respect;

$$F_d = RoS \,.\, t_r \qquad \text{(Equation 4.18)}$$

Residence time for the flame is to be determined from propagation measurements. By inspection angle **DAB** is 30°, therefore flame depth (F_d) can be calculated as follows:

$$F_d = T_t \,.\, \sin(30°)$$

$$F_d = (1/2).T_t \qquad \text{(Equation 4.19)}$$

From Equations 4.18 and 4.19, the rate of spread (RoS) is given

$$RoS = \frac{T_t}{2.t_r} \qquad \text{(Equation 4.20)}$$

The intensity of the grassfire can be calculated from Byram's fire line intensity relation, thus:

$$I_{gf} = H \times (W-r) \times RoS \quad \text{(Equation 4.21)}$$

Where: H = heat of combustion for the grass fuel,
W = grass fuel load (F_L),
r = weight of grass remaining after the burn.

It was observed that during the controlled burn all of the surface fuel burnt, $r \approx 0$ in Equation 4.18

4.5.3. Temperature Measurements

A thermocouple tree about 1.25 m high was constructed from a steel pipe of diameter 0.025 m. Side "arms" of length 0.4 m were attached at every 0.25 m of tree's height to hold at least four thermocouples. Thermocouples were cut from a 100m double braided fiberglass insulated chromel-alumel (24-G/G) thermocouple wire 50 μm in diameter. The thermocouple wire had fiberglass shield which can withstand temperatures up to 450°C. At temperatures more than 450°C, the fiberglass shield fuses. Our tests showed that the insulation properties hold for higher temperatures but the material then becomes brittle on cooling, and therefore can be used only once.

The type K thermocouple wires were electro-fused at one end to make perfect junctions and tested with a hot air gun and a multimeter. The thermocouples were then fixed to tree "arms" by means of muffler tape and the electro-fused junctions were left protruding 1cm beyond the "arm" length into the flame. The thermocouple wires were buried in a shallow trench (10 cm deep) and connected to the thermocouple logger 3m away from the thermocouple tree at a spot that allowed access without trampling the fuel in the immediate vicinity of the thermocouples.

The thermocouples were wired to a SPECTRUM® SP 1700-51W thermocouple data logger to read the temperatures into the data logger's internal memory throughout the experiment. Operational cold junction temperature of the data logger ranges from –45 to 85°C; therefore it was necessary to protect the logger from heating beyond 85°C as this may invalidate the data. The data logger was dug 75 cm into ground and wrapped around with an insulating material (Fiberfrax®) to protect it from heat that may the produced in the grassfire. SP 1700-51w logger has the capability to read temperatures up to 1370°C, therefore is ideal for measuring bushfire flame temperatures. The setup for temperature measurement is shown in Figure 4.13.

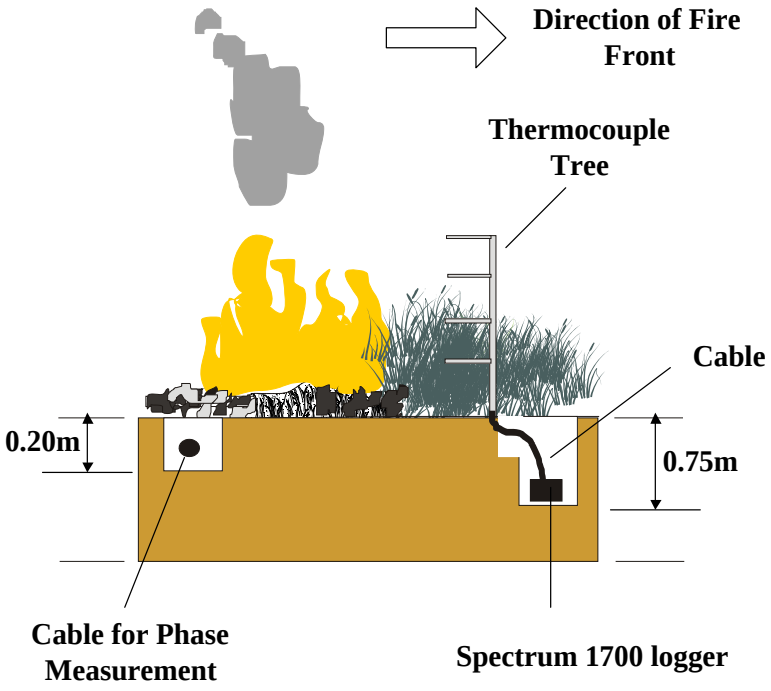

Figure 4.13. *Thermocouple tower set up-(not drawn to scale)*

4.5.4. Radio Wave propagation Measurements

4.5.4.1. Propagation and phase measurement path

The transmitters and receivers were set up on opposite sides of the plot, separated by a direct distance CA-CD (Fig. 4.14) of 44 m. A 75 m long 75 Ω coaxial cable used for phase change measurement was dug 0.25 m in the ground. The purpose of the trench was to protect the cable from the heat that may diffuse into the ground. At this depth, the heat from the grassfire is negligibly small that it cannot influence the phase measurements. During the propagation measurement the cable ran far from where the head fire intercepted the transmission path. The cable was set such that CD-CC was10.3 m, CC-CB was 25.5 m and CB-CA was 9.5 m to connect to both 30 MHz receiver and transmitter units.

The transmitter, receiver and the rest of the units were enclosed in polysterene boxes to prevent heat from the fire affecting the circuitry. A polystyrene board was placed over the boxes to act as shade for both the boxes and the cables that connect to the antennas. The boards were placed over

the boxes in such a way that it allowed circulation around the enclosures. A thermocouple was connected a HOBO® data logger and placed inside the boxes to monitor the temperature inside the boxes.

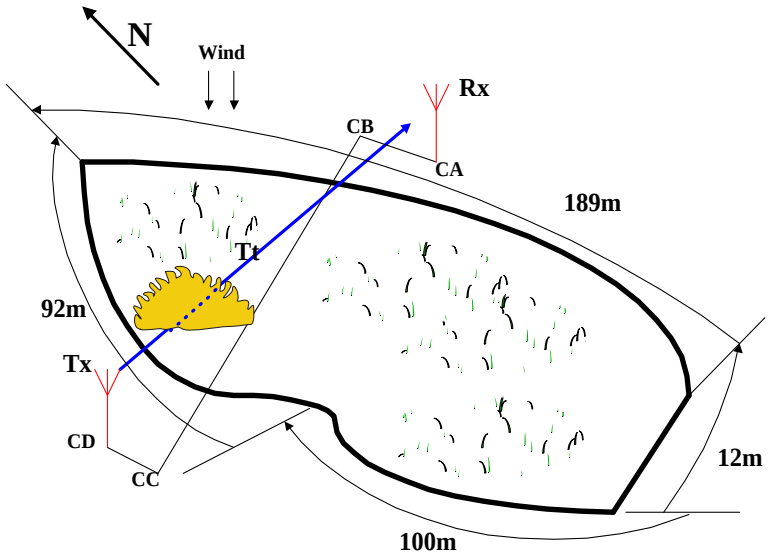

Figure 4.14. *Propagation paths and the shape of the study area plot (not drawn to scale)*

4.5.4.2. Signal amplitude measurement

The 150 and 30 MHz modules were tested for stability days before the controlled burn. It was noted that the 150MHz module was not stable, only 30MHz module passed the test. The 150 MHz module was replaced by a commercial 151.3 MHz module and we had to cancel the phase measurements at this frequency.

4.6. Experimental Results and Discussions

4.6.1. Grassfire temperature

The maximum flame temperature observed in the grassfire was 899K. This occurred at 75cm above the ground surface. The maximum temperature occurred at 10.44:50am.It coincided with maximum temperatures at heights 25 and 50 cm above ground. At 100cm the maximum temperature occurred between 10.44:45 and 10.44:50am. This was because the flame was wind-blown toward the thermocouple tree, therefore reaching the thermocouple at 100cm earlier than others at lower heights.

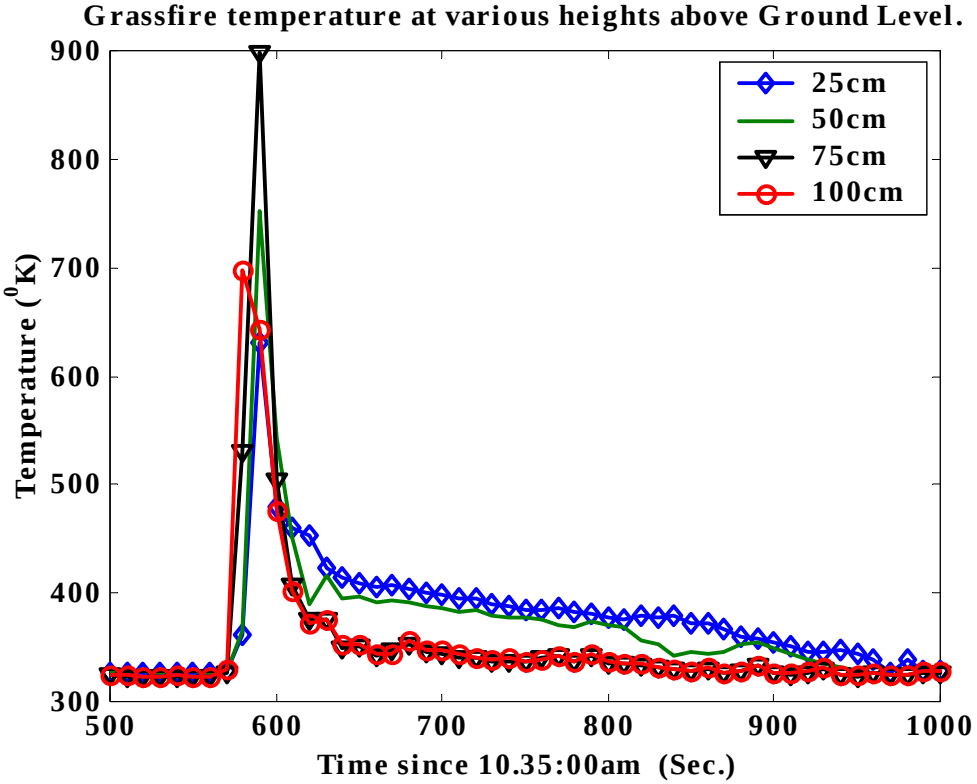

Figure 4.15. *Grassfire flame temperatures as they intercepted the propagation path*

Maximum temperature observed at 100 cm was 700K while at 50cm and 25 cm were 753 and 631K respectively. Flame occurs at temperatures above 500K, therefore from Figure 4.15 and data from the SPECTRUM® logger, it can be deduced that the flame residence time was on average 32 seconds. This can also be observed from attenuation measurements.

4.6.1.1. Errors in temperature measurements

There is a discrepancy between thermocouple measured fire temperatures and actual fire temperature. The error in temperature measurements, which could sometimes be more than 200 ºC, is a result of heat transfer from the thermocouple bead to the surrounding gas (Dupuy *et al.*, 2003 and Daniels, 1968). Convection and conduction heat transfer contribute but not significantly as radiation. Magnitude of the radiation error is mainly a function of thermocouple bead size and temperature of the radiating surfaces. Reducing the size of the thermocouple bead significantly reduces the measurement uncertainties. Martin *et al.* 2005 observed that the error is small for thermocouples with beads less than 0.13 mm. The errors are reduced when thermocouples are

inserted in the flame. We have put the upper limit of the uncertainty in *grassfire temperature measurement to 40 K as in Butler et al. 2003.

4.6.2. Attenuation of 151.3MHz Signal

From amplitude signal graph (Figure 4.16), it appears that there was a lot of commotion up to two minutes before the grassfire crossed the propagation path. The signal fluctuation between **A** and **B** were identified as those due to the University fire suppression crew moving up and down a fire break next to receiver units. Between **B** and **C** were identified as due to a crewmember intercepting the propagation path at 10.42am. A prominent drop in the signal amplitude **D-E** was observed when the grassfire flame cross the propagation path. A minute or two after the fire crossed the propagation path, the fire crew moved in to extinguish it before it got out of control. This was observed in the drops that occurred in the region E to G of the signal amplitude graph.

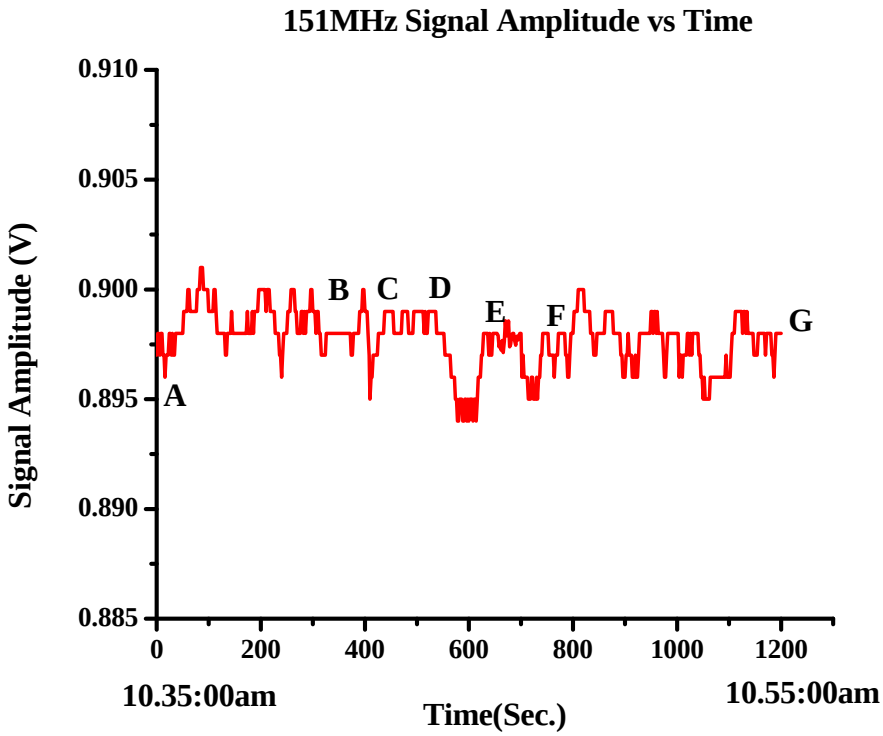

Figure 4.16. *151.3MHz signal amplitude versus time*

A 10-point adjacent averaging smoothing algorithm was applied on the data to give the blue graph (Figure 4.18). The time between 10.42:30am and 10.46:30am was considered for

attenuation calculation. Based on the smoothed amplitude at D and E, attenuation (dB) was calculated using the Equation 4.5 as signal intensity is directly proportional to voltage.

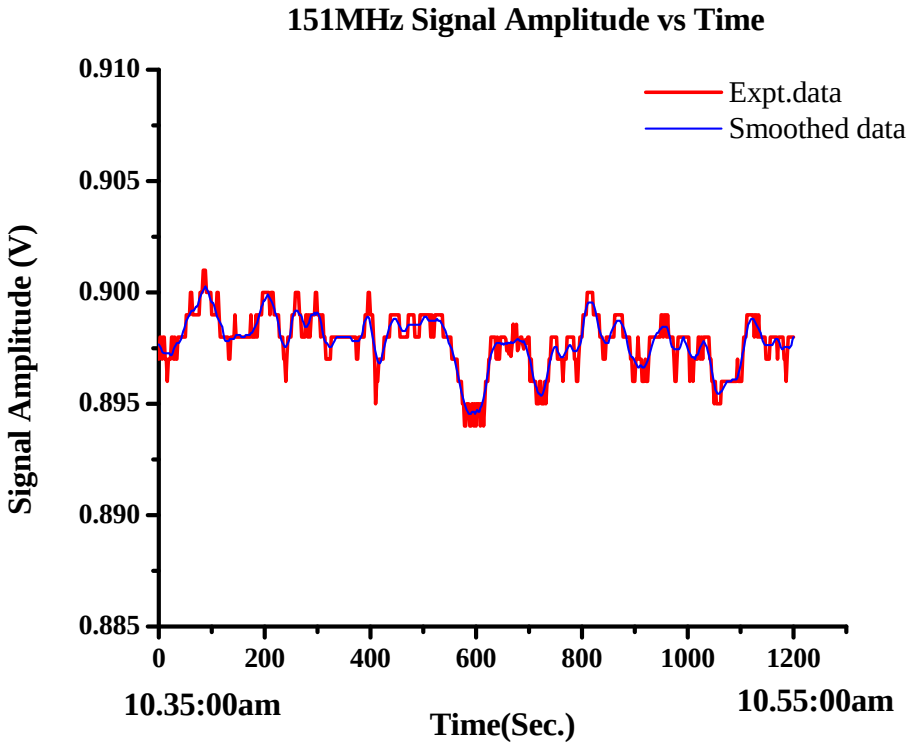

Figure 4.17. *Smoothed Signal amplitude vs. time graph*

Possible source of error in the experiment is multiple reflections of radio wave signals from fire crew members, who were not stationary during the burn, to fall onto the receiver. To minimize this error, the crew members were asked to remain calm two (2) minutes before and after the grassfire has intercepted the propagation path. Another possible source of error in the experiment is the effect of temperature changes on the signal transmission and reception modules. This was minimizes by placing the modules in polystyrene heat insulating boxes.

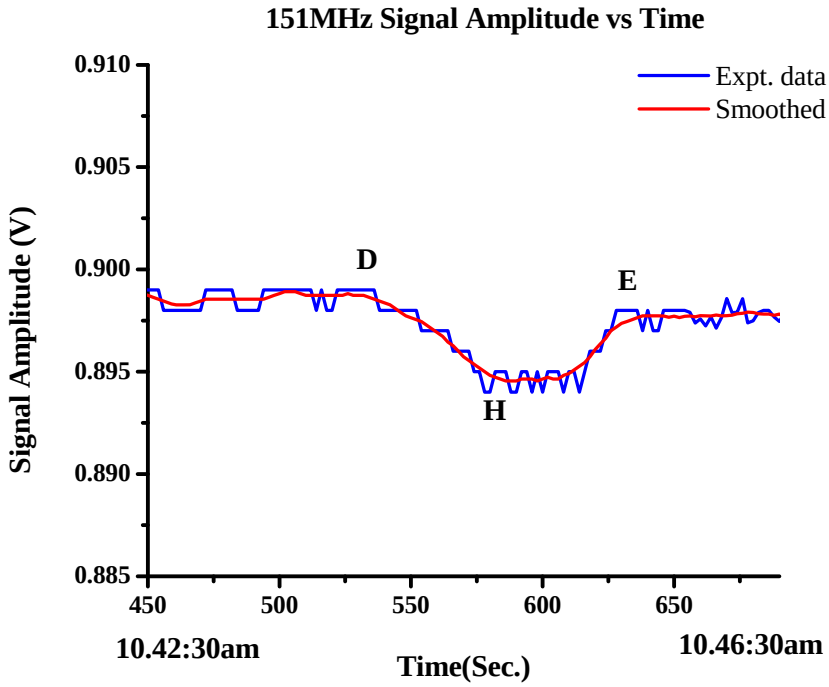

Figure 4.18. *Expanded signal amplitude vs. time graph*

From Equation 4.5 and using the smoothed data attenuation of the 151.3 MHz signal due to the flame is:

$$\text{Attenuation due to the flame}\,(\text{dB}) = 20\log_{10}\left[\frac{0.899}{0.8943}\right]$$

$$= 0.05\ \text{dB}.$$

Observations reveal that soon after the flame has passed, signal amplitude remained lower than at D. Hot air from the hot ground surface refracts radio waves away from the ground causing a reduction in signal intensity at antenna height. This attenuation is due to reduced air density rather than ionization. This will be discussed in Chapter 7. Attenuation due to the hot ground surface can be estimated to be:

$$\text{Attenuation due hot surface}\,(\text{dB}) = 20\log_{10}\left[\frac{0.899}{0.8977}\right]$$

$$= 0.01\ \text{dB}.$$

4.6.3. Attenuation of 30MHz signal

The 30 MHz signal responded to path interception in the same way as the 151.3 MHz signal. Unlike the Yagi antenna used in 151.3 MHz transmission, the quarter-wavelength whip used for 30 MHz signals spreads energy in all directions as results reflections from fire crew and their equipment during **A-C** affected the signal strength more significantly than at 151.3 MHz. A prominent drop in the signal amplitude due to the fire was also observed between **D** and **E**. It occurred at the same time as that of the 151.3 MHz signal.

By the looking at the graphs, one of the major differences is that after the grassfire, 151.3MHz signal remained below its average level before the fire while the 30MHz signal quickly regained its strength after the 3mins after the fire.

Attenuation of a 30MHz signal due to the flame as calculated from Equation 4.5 is:

$$\text{Attenuation due to the flame}\,(\text{dB}) = 20\log_{10}\left[\frac{2.011088}{2.005}\right]$$

$$= 0.03\text{dB}.$$

Similarly that due to the hot ground is 0.006dB.

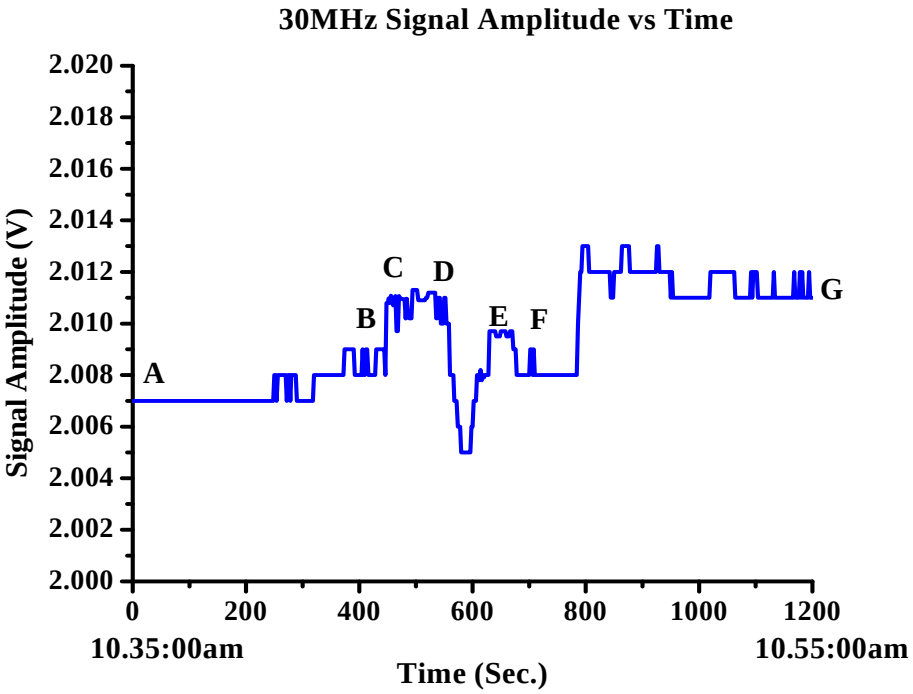

Figure 4.19. *30MHz Signal amplitude versus time*

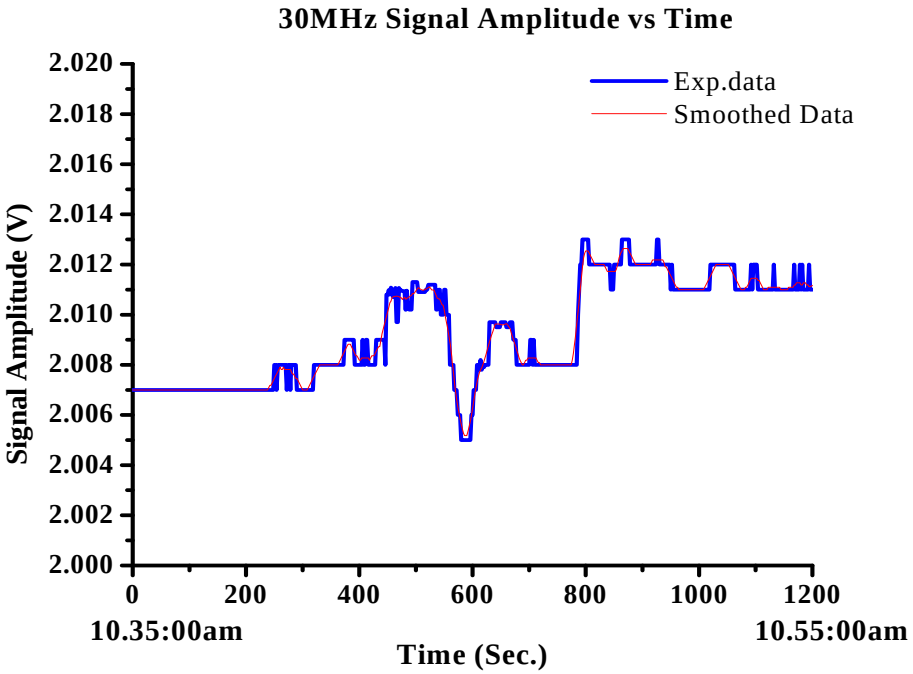

Figure 4.20. *30MHz Smoothed signal amplitude versus time*

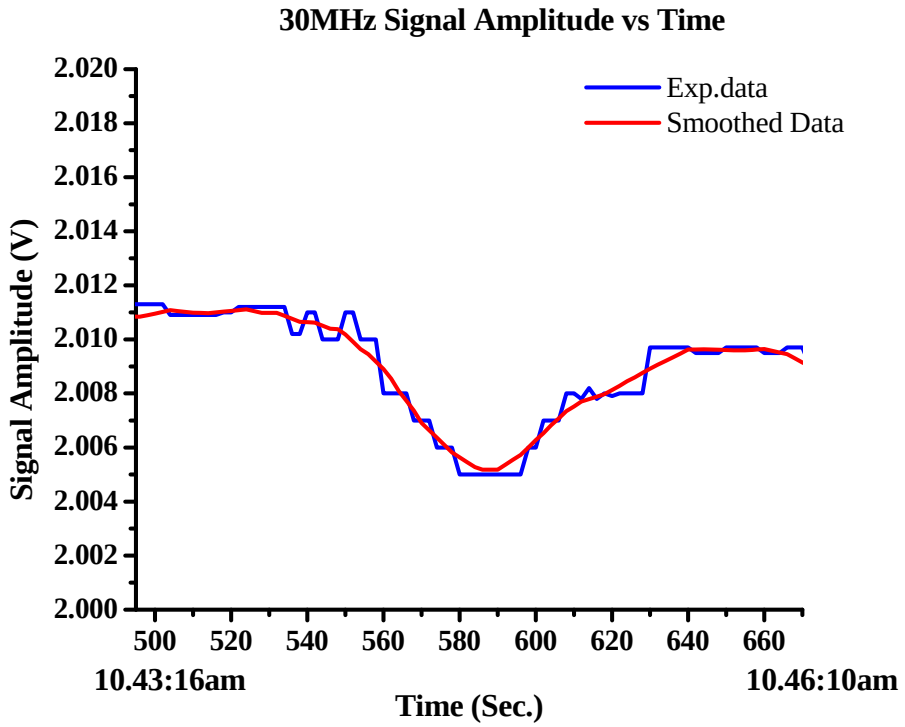

Figure 4.21. *Expanded signal amplitude vs. time graph*

4.6.4. 30MHz signal phase change

The phase on the 30 MHz signal responded in much the same way to path interception by the grassfire front as the amplitude of both 30 and 151MHz signals. A prominent drop in the signal phase due to the grassfire was observed to be at about 10.44:34am. It occurred at nearly the same time as the drop between **D** and **E** for amplitude attenuation measurement at the two frequencies. The maximum drop for the 30MHz amplitude occurred at 10.44:45am while that of 151.3 MHz occurred at 10.44:43am.

The calculated phase shift induced on the 30MHz signal as worked out from Figure 4.23 is 32.0mV. From calibration measurement it was observed that 10.4mV represents 1° of phase change, therefore 32 mV is 3.08°.

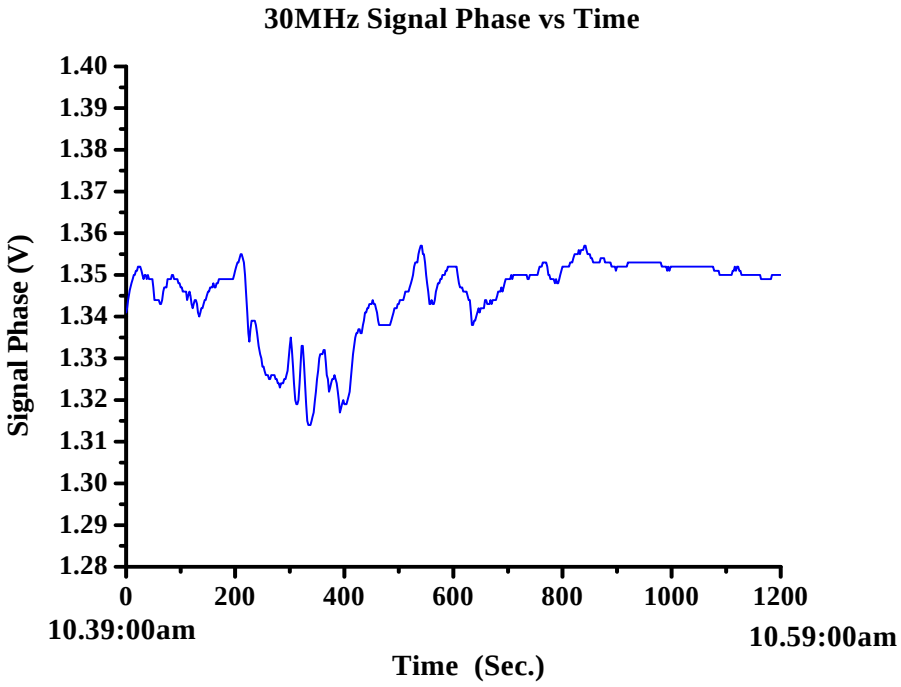

Figure 4.22. *30MHz signal phase vs. time graph*

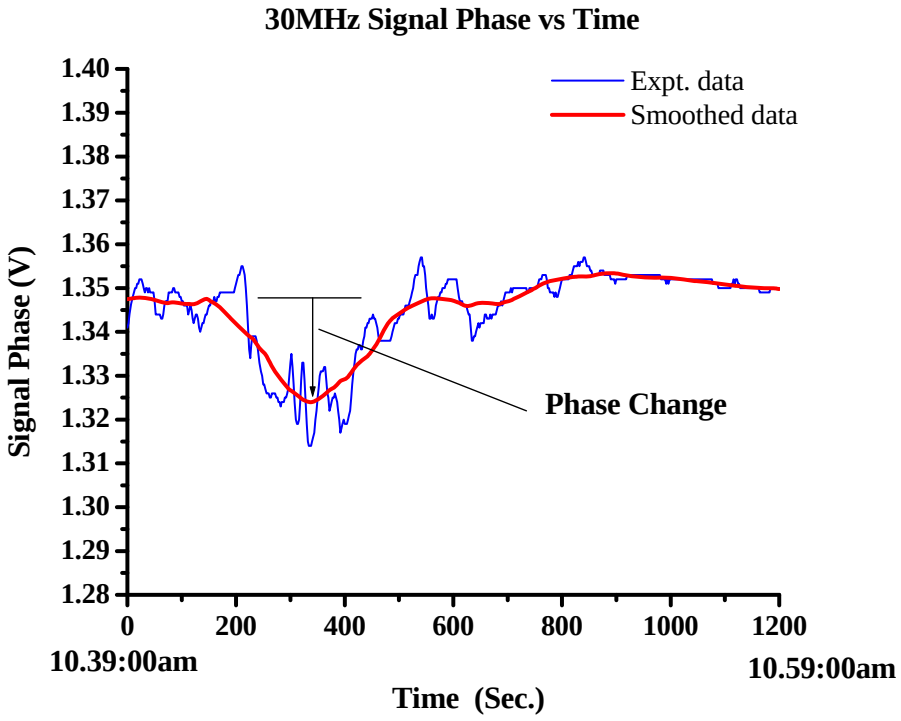

Figure 4.23. *Smoothed signal phase vs. time graph*

4.6.5. Fuel characteristics and grassfire behavior

The fuel characteristics have been calculated from Equations 4.16 and 4.17 while CSIRO Fire Spread Calculator was used to predict grassfire spread. The inputs to the calculator are: relative humidity; degree of curing; wind speed at 10m and ambient temperature. Equations 4.18 - 4.20 were used to estimate the grassfire front depth. The intensity of the grassfire was calculated using the Byram's fire-line intensity Equation 4.21.

From the ground data collected at the time of the experiment, it was noted that relative humidity was 37.8%, wind at 1.5 m was 1.0 m/s and ambient temperature was noted to be 28.9°C. Since the fire spread calculator requires wind speeds measurements at 10m, the wind speed at 2m can be used to estimate that at 10m by the use of the relation (CSIRO Fire Spread Calculator, 1998):

$$U_{10} \approx 1.25U_2 \qquad \text{(Equation 4.22)}$$

From the wind speed at 1.5 m, a correction for wind speed at 2m can be done according to the relation given by Cheney *et al.* 1995 as:

$$U_2=0.017 + 1.056\, U_{1.5} \qquad \text{(Equation 4.23)}$$

Table 4.1 is a compilation of fuel characteristics and fire behavior as worked from the equations stated.

Possible errors in this section could arise from inaccurate determination of wind direction. This could give wrong values of ROS and ultimately wrong values of ionization in the grassfire. The heat of combustion value used to calculate grassfire intensity is from theory.

Table 4.1. *Fuel characteristics and fire behavior at Plot B*

Fuel Load (kg/m^2)	Curing Deg. (%)	RoS. (m/min)	Flame Depth. (m)	Estimated. Flame height (m)	Intensity (kW/m)
0.462	90.1%	3.33	0.89	2.5	554

4.7. Conclusions

The grassfire considered was of moderate intensity, thus Byram's grassfire intensity was observed to be 554 kWm^{-1}. The maximum temperature measured was 899 K at 75 cm above the ground inside the grass fuel stratum. The rate of spread for this fire was approximately 3.33 m/min. The flame was slightly tilted in the direction of the wind. The grass was 90.12 % dry. The depth of the flame was around 0.89 m.

Potassium is volatilized during vegetation fires (Raison *et al.* 1984 and Vodacek *et al.* 2003). It is emitted in different forms but the most prominent forms are potassium atoms and ionic bonded potassium chloride (KCl). However, the water vapor influences the type of potassium salt emitted from the vegetation. Potassium hydroxide (KOH) and potassium carbonate (K_2CO_3) are favored when there is high moisture content in combustion (Westberg, 2001). Local thermal equilibrium theory for ionization in flame containing traces of alkalis (as in Chapter 3) predicts an average electron density of about 5.35 x 10^{15} m^{-3} when it is assumed that the flame contains 10-20% of atomized K species (as in Vodacek *et al.* 2003)..

At 151.3 MHz, maximum attenuation of the signal intensity due to the grass fire flame was observed to be 0.05 dBm^{-1}. Hot ground surface after the fire refracted the radio waves and induced a 0.02 dBm^{-1} signal loss. The loss was slightly lower for a 30 MHz signal with a maximum attenuation of 0.03 dBm^{-1} when the flame intercepted it. The hot ground surface also slightly affected the 30 MHz signal as it attenuated the signal by 0.01 dBm^{-1}.

The phase shift induced on the 30 MHz signal was significant. A maximum phase shift of 3.08^0 was observed as the signal path was intercepted by the grassfire. With this amount of phase shift and the geometry of the experiment it is estimated from Equation 4.14 that the electron density in flame was 5.29 x10^{15} m^{-3} when effective collision frequency of 1x10^{11} s^{-1} is assumed. The effective electron–neutral collision frequency used is from the regression relations interpolated from Itikawa's data at temperatures up to 900 K (Chapter 3).

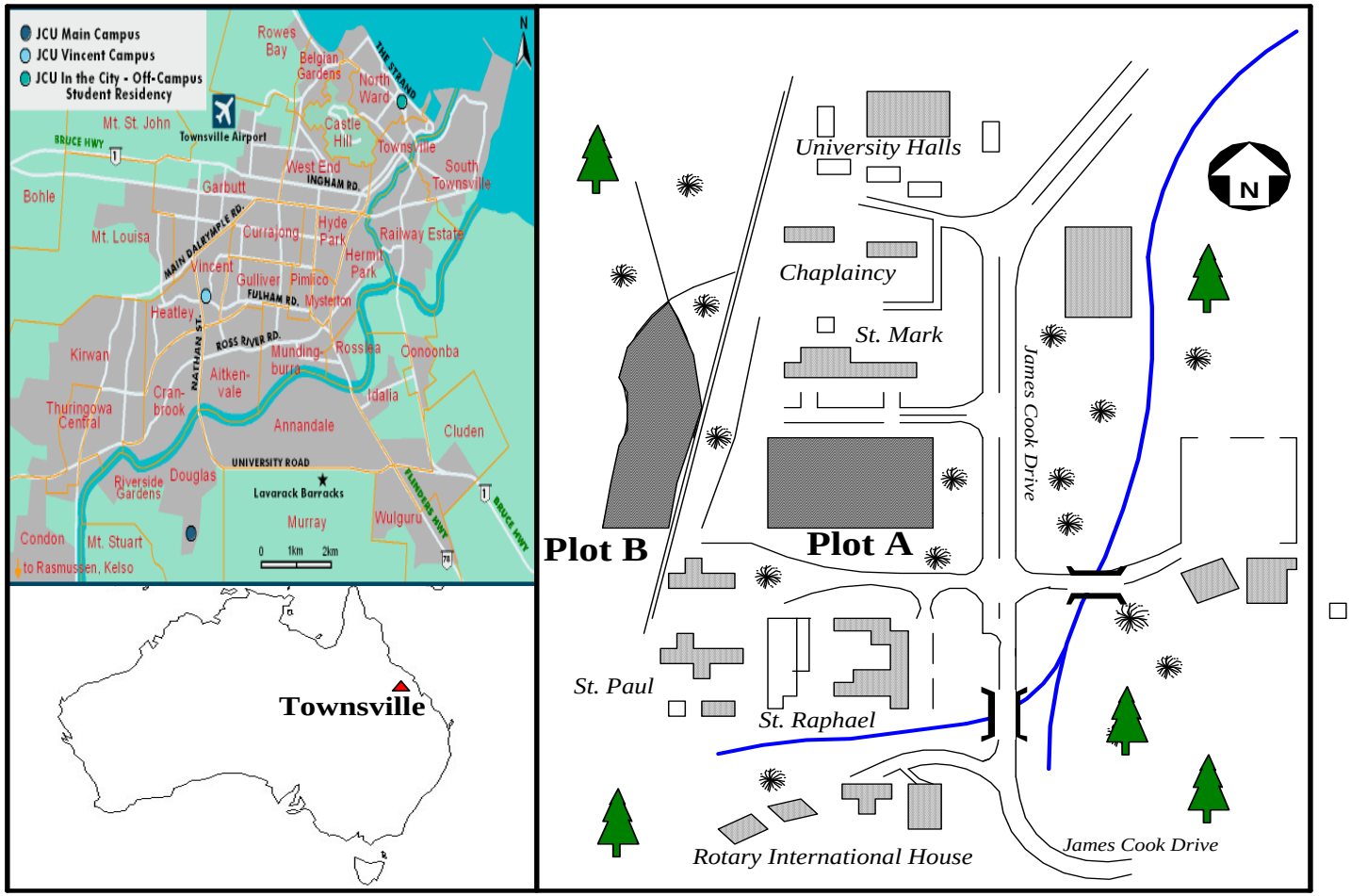
JCU Main Campus
JCU Vincent Campus
JCU In the City - Off-Campus Student Residency
Rowes Bay
Belgian Gardens
North Ward
THE STRAND
Mt. St. John
Townsville Airport
BRUCE HWY
Castle Hill
Townsville
West End
South Townsville
INGHAM RD.
Garbutt
Bohle
Mt. Louisa
MAIN DALRYMPLE RD.
Currajong
Hyde Park
Railway Estate
Vincent
Hermit Park
Gulliver
Pimlico
FULHAM RD.
Mysterton
Heatley
NATHAN ST.
ROSS RIVER RD.
Kirwan
Mundingburra
Rosslea
Oonoonba
Aitkenvale
Cranbrook
Idalia
Thuringowa Central
Annandale
Cluden
UNIVERSITY ROAD
Riverside Gardens
Douglas
Lavarack Barracks
FLINDERS HWY
Wulguru
Murray
BRUCE HWY
Condon
Mt. Stuart
to Rasmussen, Kelso
0 1km 2km
Townsville
University Halls
Chaplaincy
St. Mark
James Cook Drive
Plot B
Plot A
St. Paul
St. Raphael
Rotary International House
James Cook Drive
N

CHAPTER 5

Radio wave propagation measurements in a cane fire

5.1. Introduction

The Burdekin Delta is known for its high sugar cane (*Saccharum* spp.) crop yield in Australia (Qureshi *et al.* 2002). High annual rainfall, which is over a 1000mm and high soil fertility, makes it suitable for sugar cane farming. Potassium enriched nutrients such as *potash* are often used to supplement soil fertility in cane paddocks in order to increase crop yields. Potassium content in sugar cane may be up to 2.2% on dry weight basis. In northeast Queensland, it is a common agricultural practice to burn foliage before harvesting sugar cane (Ayers, 2005). The cane burning is done when weather conditions do not favor the development of very high intensity cane fires. It is for this reason burning is normally done at dusk when atmospheric instability is low. Otherwise the cane fires, which are often massive (see Figure 5.1), may burn out of control.

Cane fire flame temperatures are in the range of 600-1000°C (Meyer *et al.* 2004). Potassium that exists in cane foliage is volatilized by the intense heat and drawn by convective currents into the flame where it is thermally ionized to give electrons. The fires move rapidly and turbulently mix with convected surrounding air. The cool night air quenches the heat in the flame to temperatures lower than 1000°C. Moist combustion conditions prevailed in the cane fire. The moist conditions and up draughts promote the release of potassium into the flame as hydroxide (KOH) and K atoms (Westberg *et al*. 2003 and Okuno *et al*. 2005). The species contribute significantly to ionization in the cane fire flames.

The main objective of this chapter is to report on attenuation measurements carried out in a prescribed agricultural fire in a sugar cane field at Australian Tropical Agriculture College in Clare, Lower Burdekin. The measurements were carried out using RWI (see Chapter 4). The instrument directly measures both attenuation and phase change induced by a fire plume; however it was not possible to measure phase change in this case as the sides of the sugar cane paddock were

THIS IMAGE HAS BEEN REMOVED DUE
TO COPYRIGHT RESTRICTIONS

Figure 5.1. *Massive sugar cane fire (*Photo: John Maddocks, 2003*)*

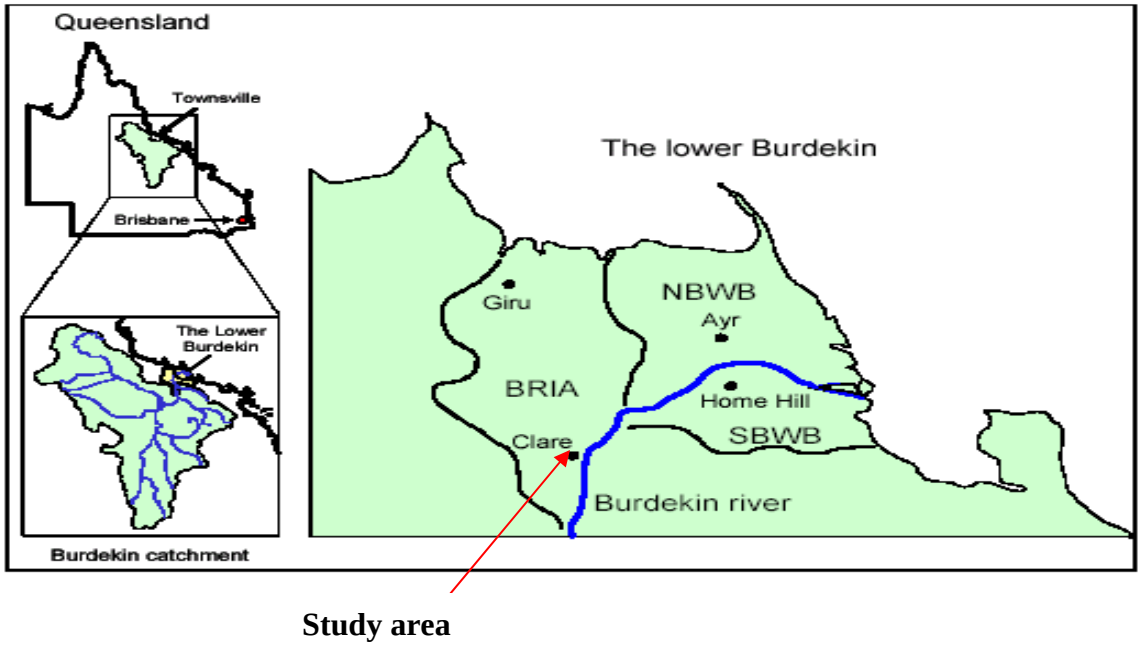

Figure 5.2. *The location of the study area* (adapted from: Charlesworth *et al.* 2002)

very long to consider running a reference signal cable. A 151.3 MHz radio frequency was used in the experiment. The location and climate of the cane fire site is described in Section 5.2 of the chapter. Section 5.3 discusses the set up of the measurement apparatus (RWI) at the paddock and attenuation measurements are reported in Section 5.4 of the chapter. Section 5.5 discusses the results and concludes the Chapter.

5.2. The study area

The sugar cane paddock where the prescribed burn was carried out is at the Burdekin Agricultural College in Clare. Clare is 90 km south of Townsville in the Burdekin Delta (19°35`S and 147°24`E). It is 40 km from Ayr and 30 km from Home Hill. The paddock is one of the 400 ha of sugar cane paddocks owned by the Agricultural College. The climate in the area is monsoonal with hot wet summers and warm dry winters. Average rainfall in the region is 1032 mm. The soils are fertile alluvial with variable layering (Charlesworth *et al.* 2002). This fertile soils and the high rainfall in the regions makes it suitable for sugar cane farming.

5.3. Experimental methods

5.3.1. Fuel characteristics

The sugar cane considered for harvesting was mature and nearly 6m tall. Its leaves in the bottom 3m were fully dried while those in the rest of height of straw were half dried. The separation between the cane rows was 1m. The crops were closely packed and almost impossible for one to walk across the rows. Though the cane was mature, most of it had not flowered. The length of the paddock was roughly 1000 m and it was 100 m wide. Figure 5.3 shows sugar cane before burning.

Figure 5.3. *Sugar cane paddock before burning.*

5.3.2. Sugar cane fire behavior

The cane fire was ignited along side **AB** of Figure 5.4 with liquid flame-throwers. At the time for ignition a mild wind blew from the easterly direction. The wind forced the fire to propagate along the length of the paddock thus intercepting the propagation path at an angle of approximately 79°. As the cane fire front raced across the paddock from the east, it left leafless and charred cane straws standing behind. The chaff was completely burnt. The flames of the cane fire were observed to be about 5-10 m high (see Figure 5.5). The flames were hottest at the cane canopy and its temperature decreased with the increase in height above the canopy as it can be deduced from Figure 5.6. The cane fire took 21 minutes to burn through the whole paddock. This gives an average Rate of Spread of (*ROS*) of 0.79ms^{-1}. If is assumed that flaming occurs at temperatures more than 300°C (e.g. Stott, 2000) then the resident time of flames above the canopy is 17s as obtained from thermocouple tower temperature measurements. It can be estimated from Equation 4.14 that cane fire flame depth was on average 13.43 m. Visual estimation puts flame depth at about 10 m.

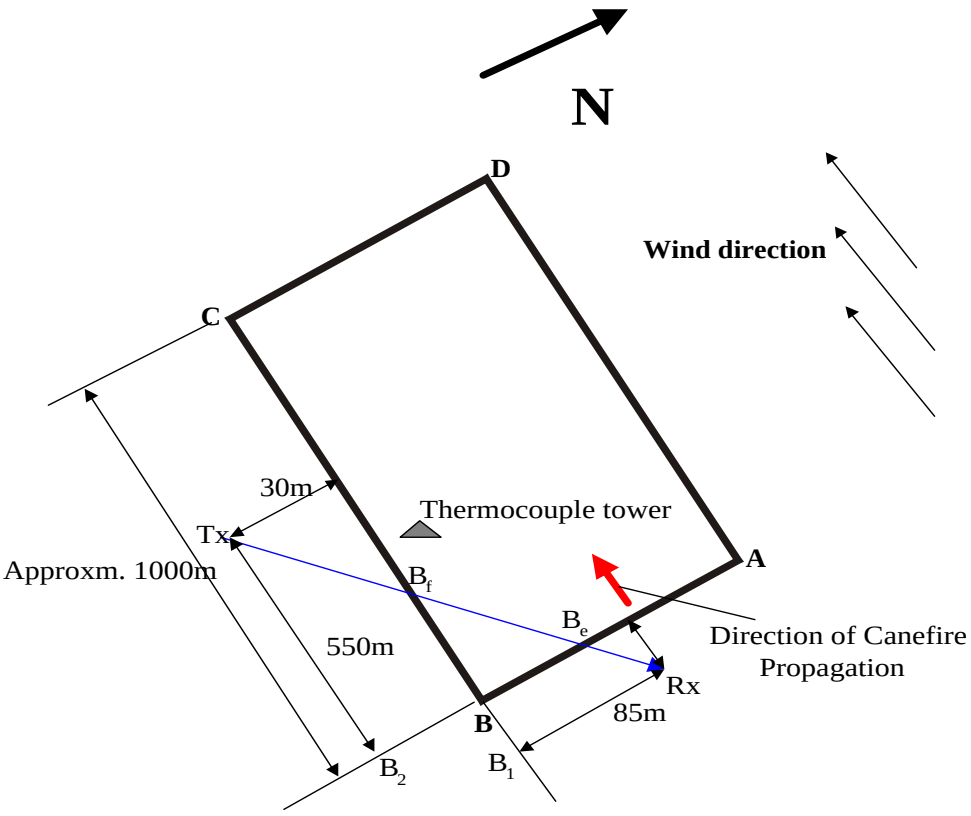

Figure 5.4. *Set up of the transmitter and receiver units at the study site*

Figure 5.5. *Sugar cane flames 5-10m tall.*

Figure 5.6. *Flame height from which we estimate a decrease in heat intensity from the sugar cane canopy.*

5.3.3. Temperature measurements

A thermocouple tower of height 6.1 m was constructed from a steel pipe (stem) of diameter 0.15 m and erected in the cane field a few meters from the edge. Six steel pipes of diameter 20 cm were screwed horizontally into the steel pipe stem forming "branches" at every 1.0 m of the steel stem's height. Thermocouples were mounted at every branch of the stem. Thermocouples were also cut from a 100 m roll of double braided fiberglass insulated chromel-alumel (24-G/G) thermocouple wire 50 μm in diameter as in Chapter 4. The type K thermocouple wires were electro-fused at one end to make perfect junctions and tested with a hot air gun and a multimeter. The thermocouples were then fixed to branches by means of muffler tape and the electro-fused junctions were left protruding 2.5 cm beyond the branch length into the flame. The thermocouples wires were buried in a trench 20 cm deep and connected to the SPECTRUM® data logger 50 cm away from the tower.

The thermocouples were wired to a SPECTRUM® SP 1700-51W thermocouple data logger to read the temperatures into the data logger's internal memory throughout the experiment. Operational cold junction temperature of the data logger ranges from – 45 to 85°C; therefore it was necessary to protect the logger from heating beyond 85°C as this may invalidate the data. The data logger was dug 75 cm into ground and wrapped around with an insulating material (Fiberflex®) to protect it from heat that may the produced in the canefire. SP 1700-51w logger has the capability to read temperatures up to 1370°C, therefore is ideal for measuring bushfire flame temperatures. The setup for temperature measurement is shown in Figure 5.7.

5.3.4. Radio wave propagation measurements

5.3.4.1. Propagation path

Receiver (*Rx*) and transmitters (*Tx*) units were set up on adjacent sides of the sugar cane paddock (sides **AB** and **BC** in Figure 5.3). The distance separating the units (*Tx*-*Rx*) was 581.59 m. The units were set some distance away from the paddock so that they would not the affected by heat from the burning sugar cane. *Rx* was set 20 m from AB such that from B_1 to the *Rx* was 115.20 m. *Tx* was 30.00 m from BC such that *Tx* was 570.43 m from B_2. The distance $\mathbf{B_e}$ to $\mathbf{B_f}$ was 556 m. The *Rx* and *Tx* antennas were set 3.2 m high from the ground facing each other to maximize the amount of signal strength received. The antennas were tuned such that the maximum possible signal strength on the meter was 689 mV.

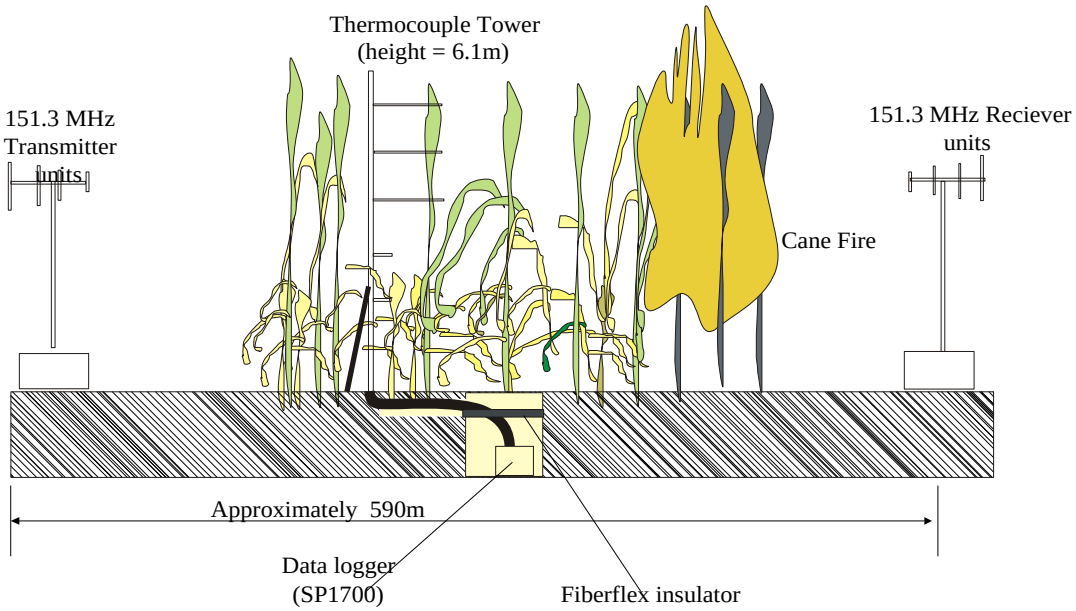

Figure 5.7. *Set up for temperature measurement tower, logger, transmitter and receiver units*

5.3.4.2. Signal amplitude measurement

The field experiment considered only signal amplitude measurement as there was a limitation of phase comparison cable which must run between *Tx* and *Rx* units. The units were enclosed in polystyrene boxes wrapped with aluminum foil to reflect heat from cane fire. The RWI was switched on at 6.20pm and the HOBO data logger was switched on at 6.24pm. The antennas were then set for maximum signal reception.

5.4. Experimental Results and Discussions

5.4.1. Sugar cane fire temperature

Temperature of the cane fire increased with the increase in distance above the ground. The maximum temperature was observed 904 K at 6.00 m above the ground. The next highest was observed to be at 5.00 m above and was recorded to be 810 K (Figure 5.8). These temperatures occurred at 6.49:20pm. The flames above the canopy were windblown as temperature maxima for other heights occurred 10s later. The minimum temperature recorded was 680 K and this was at 2 m above ground. At 4.00 m above the ground temperature was observed to be 707 K. From the temperature measurements, it appears that the northeasterly winds that blew across the paddock affect the flame as much as 1m deep into the sugar cane canopy.

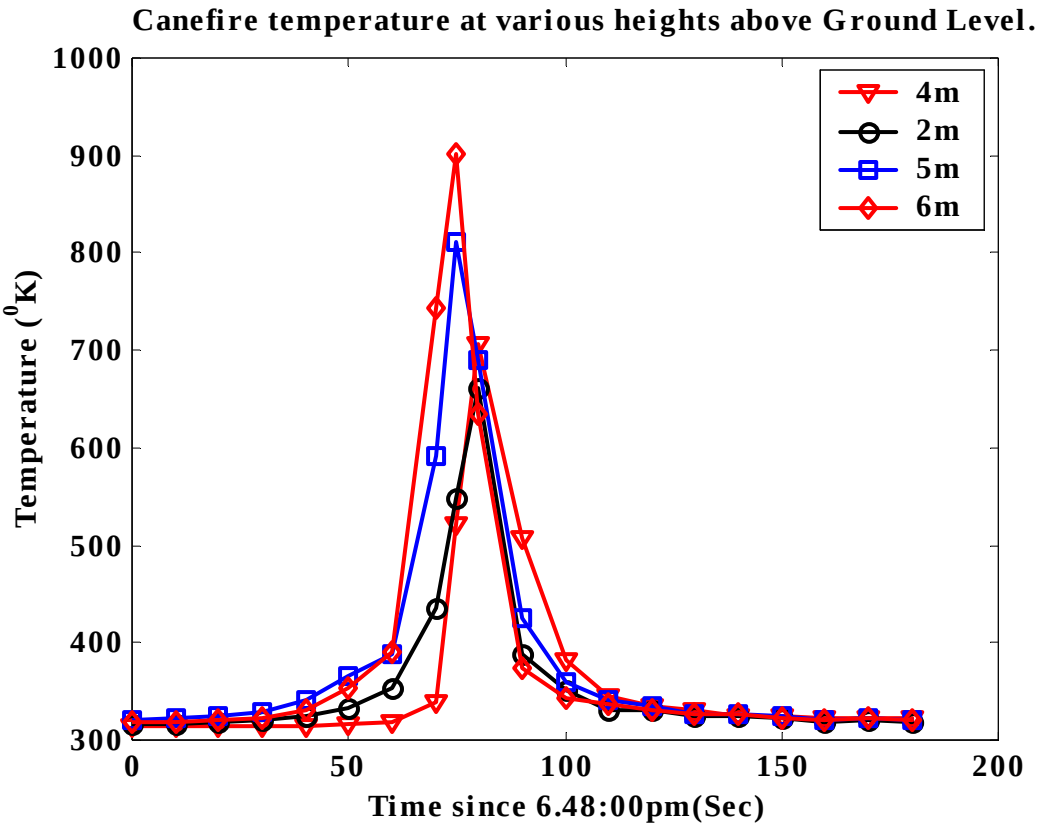

Figure 5.8. *Sugar cane fire flame temperatures as the flame front temperature tower*

5.4.2. Attenuation of 151.3MHz signal

Movements by the research team in the first 4mins after the logger was switched on reduced the signal strength. This is shown by signal dip **AB** in Figure 5.9. Figure 5.9 is a result of a 10-point adjacent averaging smoothing of real time data, which is in the background (blue). Signal strength increased soon after that to a value of 686 mV. The ACTA fire crews moved in to set the sugar cane paddock alight at 6.36pm. As they intercepted the propagation path the signal strength decreased to a minimum of 666 mV, which is show by a prominent dip at **C** in the same figure. As the crew moved out of the propagation path, the cane fire grew. The signal never re-gained its reception strength of 686 mV. It only rose to a maximum strength of about 682 mV (shown as **D** in Figure 5.9). As the fire gained strength and intercepted the propagation path the signal strength fell to a minimum of 653 mV at 6.48:32pm (**E**). Soon after the fire had passed the propagation path, signal strength slowly rose to an average value of 660 mV at 6.55pm (**F** in Figure 5.9) until the instruments were disconnected at 7.10pm.

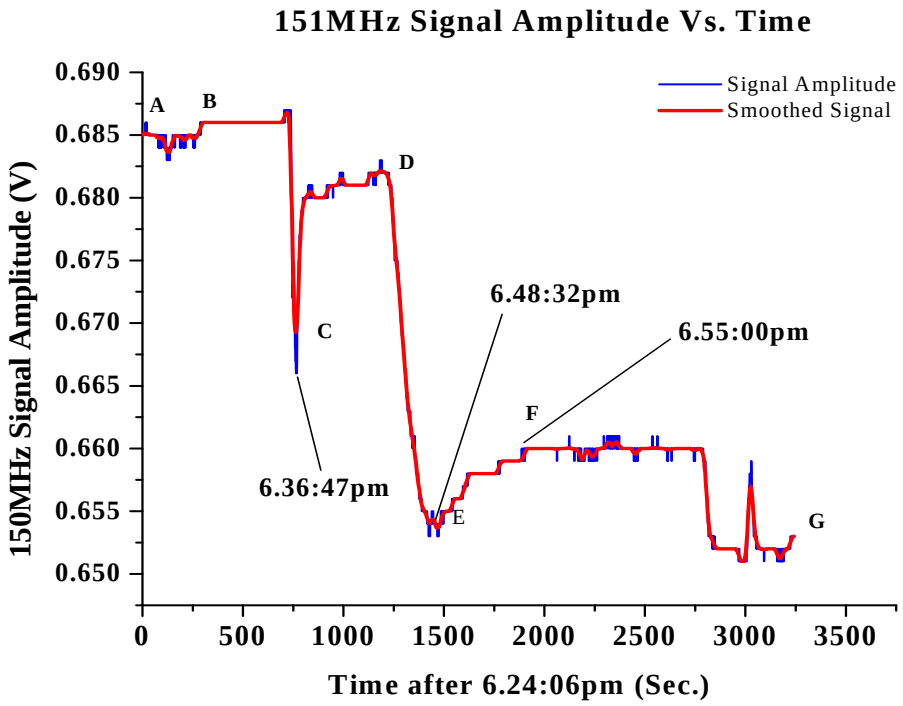

Figure 5.9. *Signal strength response to crew and cane fire interception of the propagation path*

Using the smoothed data attenuation of the 151.3 MHz signal due to the cane fire flame as per Equation 4.5 is:

$$\text{Attenuation due to the flame}\,(\text{dB}) = 20\log_{10}\left[\frac{0.686}{0.653}\right]$$

$$= 0.43 \text{ dB}.$$

Considering the fire depth of 13.4 m, then attenuation per unit length is 0.03 dB/m.

After the dry chaff has been consumed by then cane fire, stalks of sugar cane remained standing in the propagation path of the 151.3 MHz signal. The carbon covered stalks together with the hot air in the environment attenuated the signals markedly. Before the fire, the stalks are there with leaves and have the same water/sap content but do not have the carbon coating. As leaves do not

attenuate radio signals at the frequency, carbon covered stalks may be the main cause of attenuation after the fire. The attenuation induced on the signal was observed to be:

$$\text{Attenuation due hot surface}\,(\text{dB}) = 20\log_{10}\left[\frac{0.686}{0.660}\right]$$

$$= 0.34 \text{ dB}.$$

Through the cane fire depth of 13.4 m bring attenuation per unit length to 0.02 dB/m

5.5. Conclusions

The fire front was 13.4 m deep and there were strong up draughts, which cooled the flame intensity to maximum temperatures of 904 K at the cane canopy. Within the cane stratum, temperature increased from maximum of 680 K to a maximum of 810 K at 5.00 m above the ground surface. The rate of spread for this fire was approximately 0.79 ms^{-1}.

At 151.3 MHz, maximum attenuation of the signal intensity due to the canefire flame was observed to be 0.03 dBm^{-1}. Hot ground surface after the fire, the carbon covered stalks and multipath effects induced a 0.02 dBm^{-1} signal loss.

CHAPTER 6

Microwave attenuation in forest fuel litter flames

6.1. Introduction.

The presence of electrons in a vegetation fire creates slightly ionised gaseous medium. In the weakly ionised gas, particles collide with each other. Electron-neutral particle collision is the dominant form of particle interaction. The reason for the insignificance of other forms of interactions, such as electron-ion, electron-electron, ion-neutral, etc., is that: (a) compared to electrons, other particles are far much heavier and therefore less mobile; and (b) electrons and ionised particles are less numerous than the neutrals and therefore, the interaction of electrons with ionised particles is infrequent. When fire is illuminated with microwaves, electrons are accelerated by the electric field of the incident waves. Assuming that interaction between electrons and neutrals is elastic, the neutrals gain little kinetic energy during collisions mainly because they are relatively massive. Electrons are scattered isotropically such that the average velocity after collision is zero. In this way, energy is transferred from microwaves to the neutral gas causing signal attenuation.

Vegetation fires are essentially hydrocarbon flames seeded with alkali-based species (Mphale *et al.* 2007). The absorption of energy by electrons in the flame can significantly attenuate signals (e.g., in Belcher *et al.* 1950 and Schneider *et al.*1959). Microwave absorption in a flame is a factor of both the quantity of ionisable impurities and flame temperature (Schneider *et al.*1959). Belcher et al., 1950 have observed that X-band microwave signals propagating in alkali halide seeded coal-gas/air flame at a temperature of 2200 K are attenuated by up to 1 $dBcm^{-1}$. The absorption was observed to be very small when the flame was not seeded. Schneider *et al.*1959 have recorded microwave attenuation of 1.8 $dBcm^{-1}$ in a potassium chloride seeded acetylene-air flame of thickness 0.8 cm at the temperature of 2480 K.

The chapter reports on X-band microwave propagation measurements in a controlled fire in which natural vegetation litter is used as fuel. Section 6.2 discusses microwave propagation constants for a weakly ionized flame. It also discusses a method of obtaining signal attenuation

from network analyzer measured S-parameters. A simulation of X-band microwaves attenuation and phase coefficients in weakly ionized flame is carried out in Section 6.3. Line integrated average electron density and momentum transfer collision frequency for gases in the reaction zone of the fires are estimated in Section 6.5, as they are important for numerical propagation prediction of microwaves in forest fires environments.

6.2. Microwave Propagation Constant for a Weakly Ionized Fire

6.2.1. Microwave Attenuation Coefficient

The signal attenuation can be mathematically extracted from experimentally determined microwave propagation constant for vegetation fire. The propagation constant (γ) of a dielectric medium such as the weakly ionized flame is given by the following relation (Whitmer, 1956):

$$\gamma = \alpha_f + i\beta_f \qquad \text{(Equation 6.1)}$$

where α_f and β_f are attenuation and phase coefficients. When X-band microwaves illuminate weakly-ionised, highly-collisional atmospheric pressure flame plasma, α_f and β_f are related to electron-neutral collision frequency (φ_{eff}) and ionisation by the expressions derived from equations 4.10 and 4.11 as:

$$\alpha_f \cong \frac{\varphi_{eff}}{2c}\left[\frac{\omega_p^2}{\left(\omega^2+\varphi_{eff}^2\right)}\right] \qquad \text{(Equation 6.2)}$$

and

$$\beta_f \cong \frac{\omega}{c}\left[1+\frac{\omega_p^4}{8\left(\omega^2+\varphi_{eff}^2\right)^2}\frac{\varphi_{eff}^2}{\omega^2}\right] \qquad \text{(Equation 6.3)}$$

where $\omega_p = \left(\frac{Nq_e^2}{M_e\varepsilon_0}\right)^{1/2}$, ε_0, N, q_e, M_e are the plasma collision frequency, free space, permittivity, electron density, charge and mass, respectively. ω and c are propagation cyclic frequency and speed of light in vacuum, respectively.

Inverting (6.2) gives

$$\frac{1}{\alpha_f} = \frac{\varsigma\left(\omega^2 + \varphi_{eff}^2\right)}{\varphi_{eff}}, \qquad \text{(Equation 6.4)}$$

where $\varsigma = \frac{2c}{\omega_p^2}$. Equation (6.4) is used to analyse experimental data by plotting $\frac{1}{\alpha_f}$ versus ω^2 in order to get the observed values of electron density and collision frequency.

6.2.2. Determination of Propagation Constant from S-Parameters

The propagation constant (γ) can be measured indirectly using a Vector Network Analyser (VNA). The VNA measures scattering parameters (S-parameters) from which γ can be determined. S-parameters measured from a two-port VNA are elements of 2x2 matrices that relate the intensity of the outgoing to the incoming waves [see Seeger, 1986]. The matrix is given as:

$$\begin{bmatrix} B1 \\ B2 \end{bmatrix} = \begin{bmatrix} S_{11} & S_{12} \\ S_{21} & S_{22} \end{bmatrix} \begin{bmatrix} A1 \\ A2 \end{bmatrix} \qquad \text{(Equation 6.5)}$$

where B1, B2 are outgoing wave amplitude and A1, A2 are incoming wave amplitudes.

Figure 6.1 shows the set-up to measure these S-parameters. If the flame is matched so that A1 and A2 are set to zero alternately, then we have $S_{21} = \left.\frac{B2}{A1}\right|_{A2=0}$ and $S_{11} = \left.\frac{B1}{A1}\right|_{A2=0}$. S_{12} and S_{22} are determined in a similar way when A1 is set to zero.

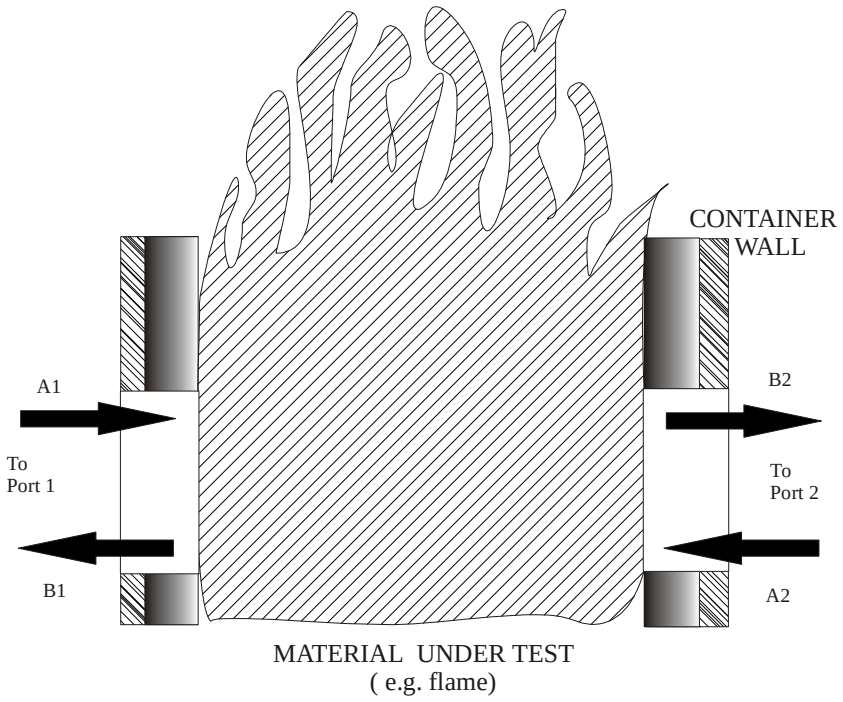

Figure 6.1. Illustration of s-parameter measurement using a two-port network analyser

Propagation factor (P) is the ratio of the transmitted microwave amplitude transmitted to the incident and is related to γ through the relation;

$$P = e^{-i\gamma d} \qquad \text{(Equation 6.6)}$$

where d is the length of the path traversed by the electromagnetic beam through the flame.

The S-parameters determined from the VNA (S_{11} and S_{21}) are then used to determine P from the relation (Boughriet *et al.* 1997):

$$P = \left[\frac{S_{11}^2 + S_{21}^2 - \Gamma}{1 - (S_{11} + S_{21})\Gamma} \right] \qquad \text{(Equation 6.7)}$$

where Γ is the reflection coefficient given by

$$\Gamma = \Omega \pm \sqrt{\Omega^2 - 1} \qquad \text{(Equation 6.8)}$$

where $\Omega = \left(\frac{S_{11}^2 - S_{21}^2 + 1}{2S_{11}} \right)$.The sign in (6.8) is chosen so that the magnitude of Γ is less than 1.

With P determined, γ which is complex can be worked out from Equation 6.6 as:

$$\gamma = [\ln(1/P)]/d \qquad \text{(Equation 6.9)}$$

The real part of γ gives the attenuation per unit propagation path length (α_f).

6.3. Simulation of Microwave Propagation Characteristics in Forest Fuel Flames.

Collision frequency and electron density of coal gas-air flames (temperature 2200K) at X-band microwave frequencies have been determined by Belcher *et al.* 1950. Belcher *et al.* determined the electron density and collision frequency to be 8.8 x 10^{10} s^{-1} and 2.0 x 10^{17} m^{-3} respectively. The coal gas-air flames were seeded with alkali salts to increase ionization and therefore conductivity. Adler (1954) also conducted a similar experiment, even though he used a cavity to determined electron-neutral momentum transfer collision frequency and electron density of pure Jet flames (temperature up to 1920K) at VHF. Adler observed the two parameters to be 6.5 x 10^{8} s^{-1} and 1.9 x 10^{12} m^{-3} respectively. Forest fuel naturally contains alkali metals salts in their organic matrix incorporated during growth as macronutrients. During combustion, the salts are given out as volatiles into the flames, making them impure. Very hot flames from forest fuel can have high electron densities due to the pyrolysed alkalis.

Electron densities and collision frequency values between those of coal gas-air and pure Jet flames but closer to those of coal gas-air flame are good enough to be used in the simulation of propagation characteristics of microwaves in forest fuel flames. For the numerical simulation, a collision frequency of 1.1 x 10^{10} s^{-1} and electron densities in the range of 1 - 3.2 x 10^{16} m^{-3} are used in conjunction with equations (6.2) and (6.3). For every meter of the flames with the above electromagnetic properties, attenuation is observed to range from 0.8 - 4.2 dB while phase shift ranges from 6 - 34 degrees. Figures 6.2 and 6.3 show the variation of attenuation coefficient, phase shift with frequency.

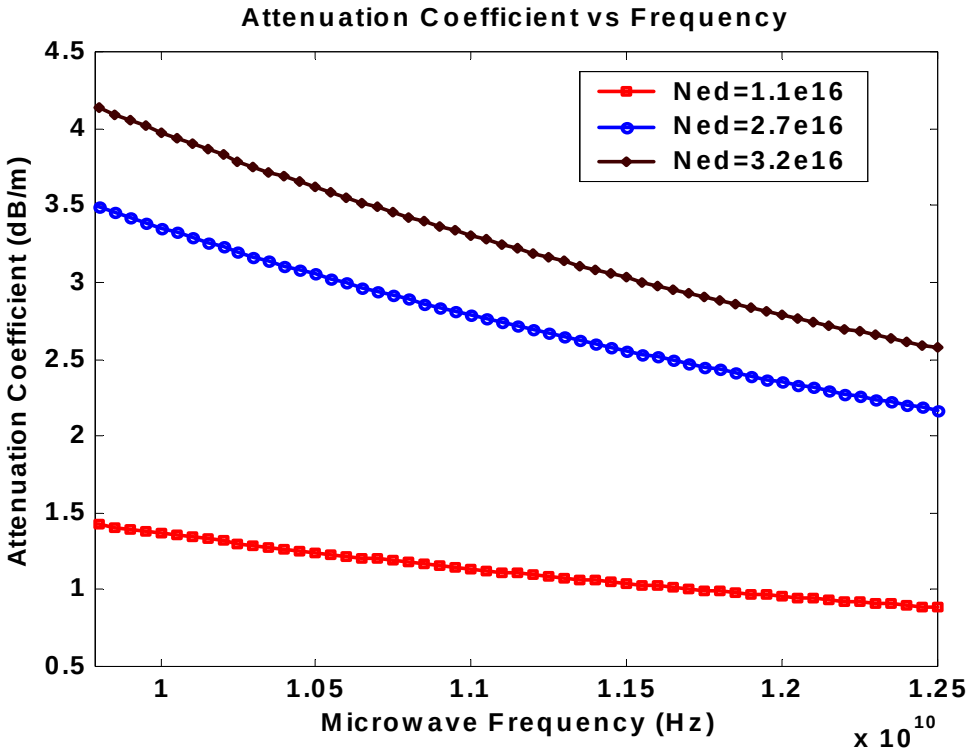

Figure 6.2. *Attenuation coefficient versus microwave frequency for collision frequency 1 x 10^{10} s^{-1} and electron densities in the range 1.1 - 3.2 x 10^{16} m^{-3}.*

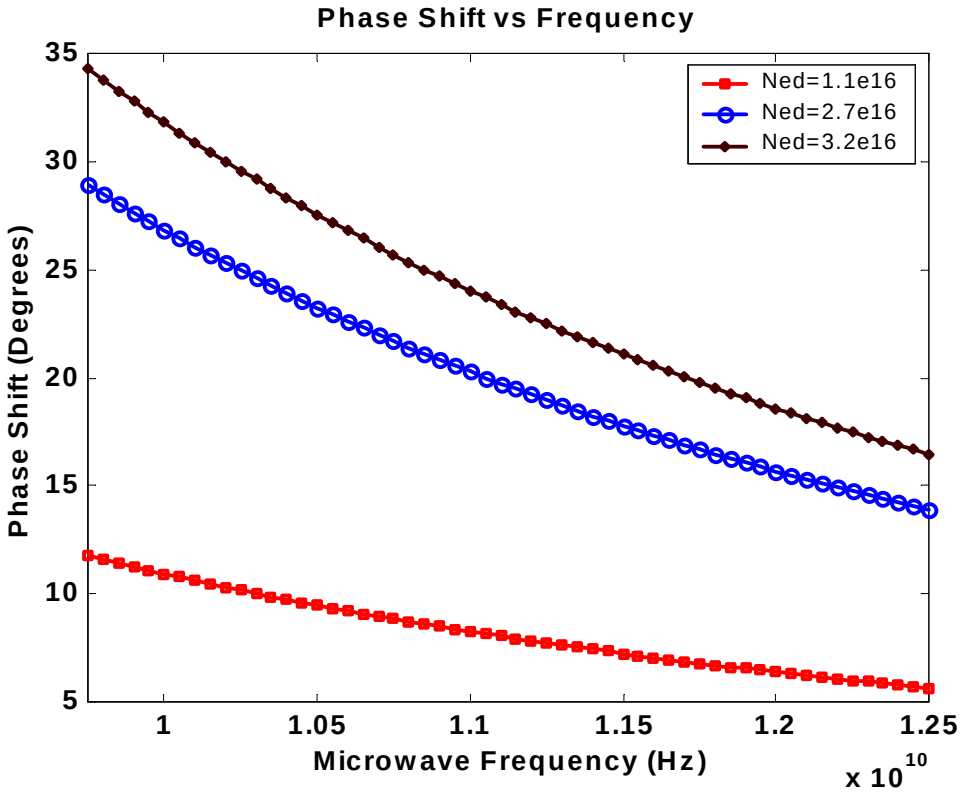

Figure 6.3. *Phase shift versus Microwave frequency for Collision frequency 1 x 10^{10} s^{-1} and electron densities in the range 1.1 - 3.2 x 10^{16} m^{-3}.*

6. 4. Experimental methods

6.4.1. Natural forest fuel samples

Samples used in the experiment consisted of litterfall from *Eucalyptus platyphylla* (poplar gum or eucalyptus), *Panicum maximum* (Guinea grass) and *Pinus Caribea* (pine) from the vegetation in and around the James Cook University campus in northern Queensland. Eucalyptus trees are endemic to most parts of Australia, while guinea grass grows mainly in the tropics. Pines grow naturally in the eastern parts of Australia. The litterfall were collected and left to dry in the laboratory for about 10 days before being used for the experiment so as to improve combustion efficiency during the experiment.

6.4.2. Forest fuel flame temperature measurement

A thermocouple "tree" of about 1.25 m high was constructed from a steel pipe of diameter 0.025 m. Side "arms" of length 0.4 m were wielded at every 0.25 m from the base of the tree to hold four thermocouples, TCA - TCD (see Fig.6.5). The thermocouples used were constructed from a 100 m double braided fiberglass insulated chromel-alumel (24-G/G) wire 50 μm in diameter. The wire had a fibre glass shield which can withstand temperatures up to 450 °C. The type K thermocouple wires were electro-fused at one end to make perfect junctions. Beads were made small to minimise error in temperature readings due to heat transfer processes. The thermocouples were tested for accuracy and consistency in generated thermoelectric voltage using a hot air gun, thermometer and multimeter. They were then threaded in the steel pipe and then fixed to the tree arms by means of a muffler tape. The electro-fused junctions were left protruded 1 cm beyond the arm length into the flame. The thermocouple tree was placed so that it measures temperature at the burner centreline. The thermocouples were wired to a PICO® Tech TC-O8 data logger and a laptop for on-line temperature measurement. In this experiment, temperatures of interest were those taken from the bottom thermocouple, TCA, and its position coincided with fuel surface.

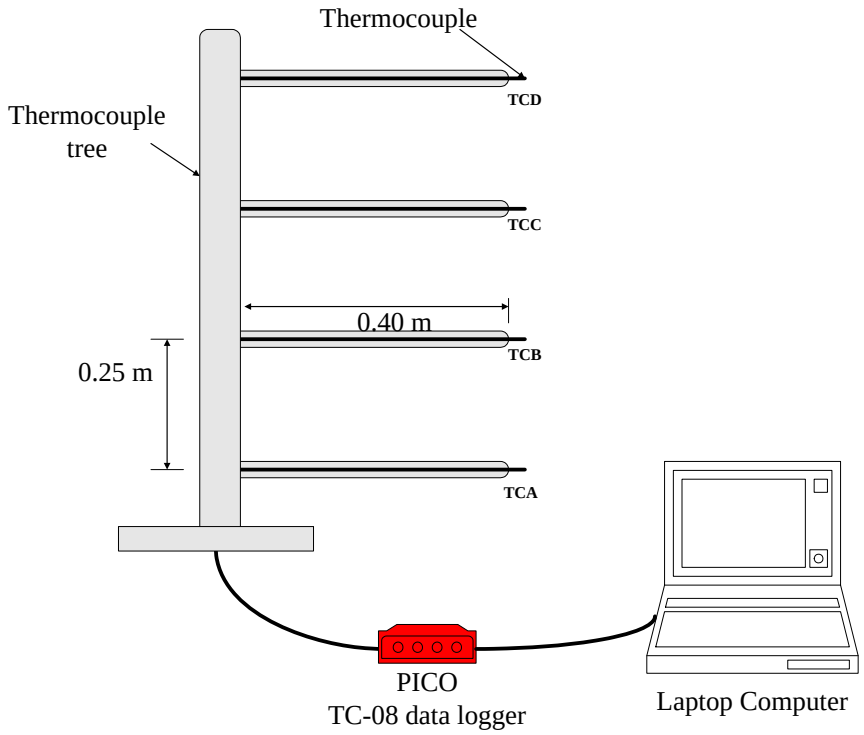

Figure 6.4. *Thermocouple tree used for temperature measurement in the cylindrical burner*

6.4.3. Determination of alkali and alkaline metal content in samples

Vegetation samples were thoroughly washed with high purity deionized water and dried for 72 hours in an oven set at 343 K. The dried samples were then ground in a mill to a fine powder (< 0.5 mm) to prepare them for acid digestion. The fine sample powders were then digested in a mixture of ultra-pure hydrogen peroxide (H_2O_2) and super-pure nitric acid (HNO_3) in a microwave oven as in Asfaw *et al.,* 2005. Standard solutions were prepared from the digests following Cai *et al.,* 2004. A blank sample with the same amount of acid as the standard solutions was prepared with the same procedure for quality assurance. All samples including the blank were introduced into Inductively Coupled Plasma-Atomic Emission (ICP-AE) spectrophotometer for alkali and alkaline earth metal content determination.

6.4.4. S-parameter measurements

The equipment used to measure the S-parameters for the fire consisted of a hexagonally shaped burner (see Fig.6.5) with an insulated wooden casing, Hewlett-Packard 8577C network analyzer

with X-band horns and a computer. The burner casing was hexagonally shape so as to allow easy conversion from one base cross section to another e.g. rectangular to circular without reconstructing the wooden casing. On the inside of the burner, a thick (8 cm thick) Fiberfrax® insulation was used to protect wood from the fire and heat. The material was lined to form a combustion area that was circular in base cross section. Two vent holes of 25 mm diameter were drilled on each of the sides, except the ones with horn inlets, to allow air to enter and mix with fuel during combustion. Two holes of horn dimensions were also cut out from the burner casing directly opposite each other and wooden supports were provided to secure the horns firmly to the wooden casing. The internal diameter of the burner lined with Fiberfrax® was set to 50 cm.

In this experiment, X-band transmit-receive horns were used for microwave propagation. They were connected to a network analyzer through the two-port S-parameter test set by coaxial cables. High quality mode transition adapters were used to make the connections between coaxial cables and the horns. The set up is shown in Figure 6.6.

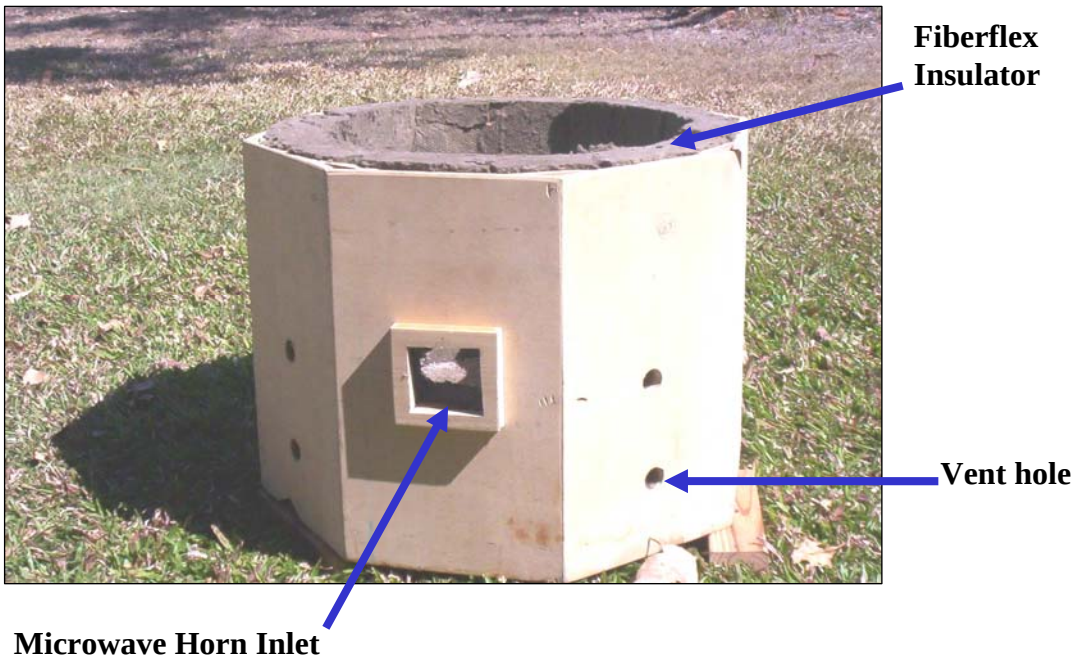

Figure 6.5. *Hexagonal burner used in the experiment*

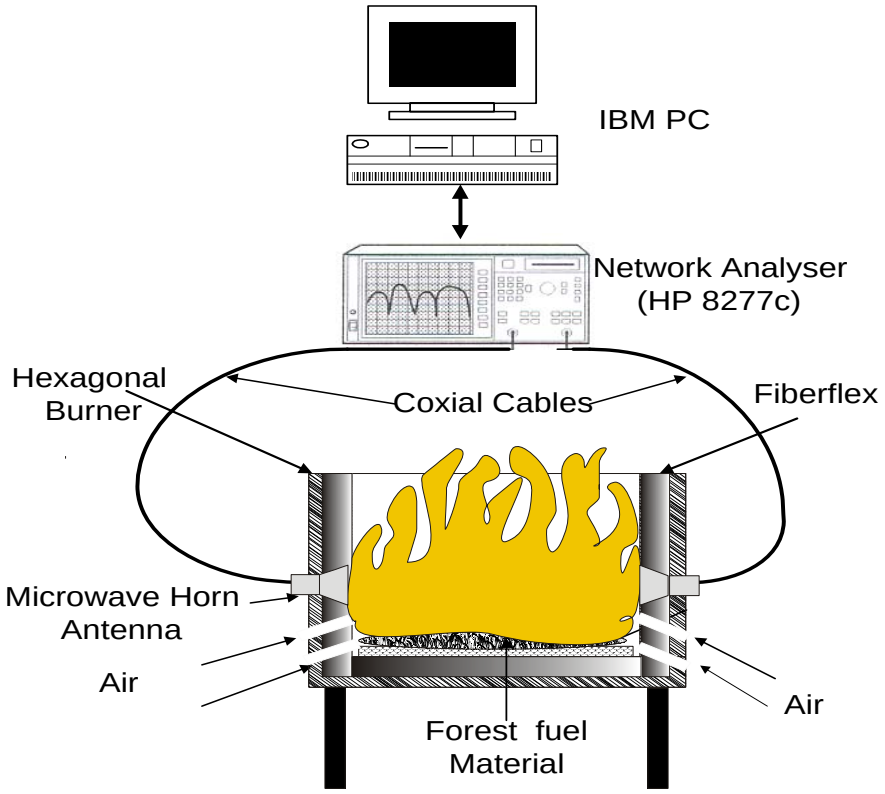

Figure 6.6. *Network Analyzer set up for S_{21} and S_{11} parameter measurements*

The 8577C network analyzer set is designed to sweep from 50 MHz to 40 GHz, logging in 601 S-parameter data points in each and every sweep. The data are then uploaded to the computer. The analyzer takes 2 s to sample over one sweep, and then there is a latency of about 50 s before the next sweep can be initiated. The network analyzer was initially calibrated using the Transmit, Reflect and Line (TRL) method. *Varadan et al.* [2000] give a full account of how the TRL calibration method is done. Several logging of S-parameters were carried out but only those in which flames covered the whole burner volume (by visual inspection) were chosen for S-parameter analysis, e.g., flames similar to that shown in Figure 6.7.

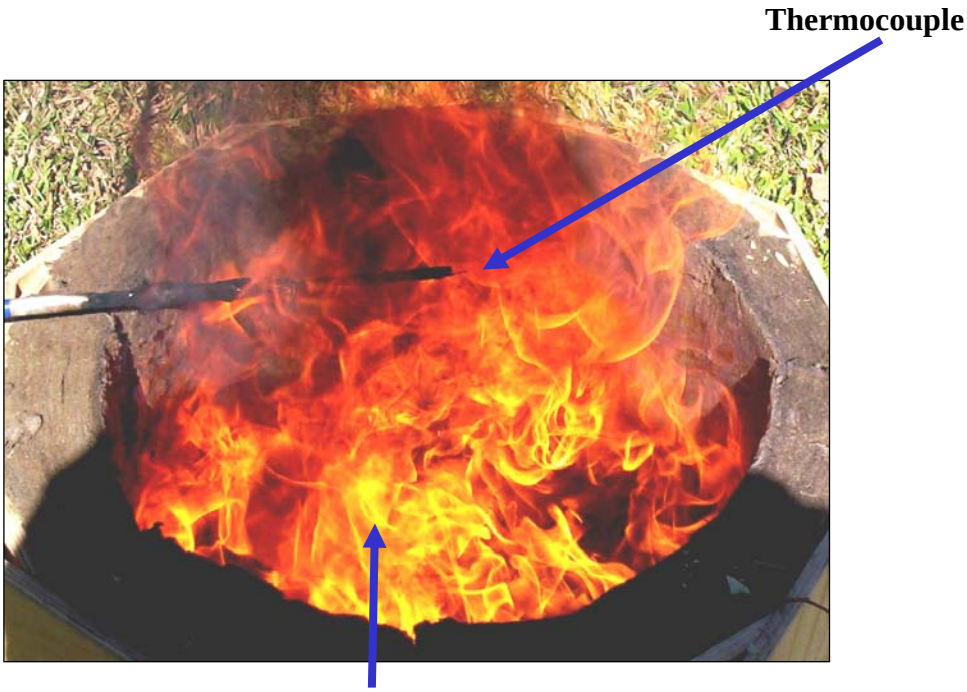

Figure 6.7. *An example of selected burns used for S-parameter measurements.*

6.5. Results and Discussions

6.5.1. Thermocouple temperature correction

Actual flame temperatures could be reconstructed from thermocouple readings using the energy balance equation. If it is assumed that flame gas is transparent to radiation, steady state energy balance for a thermocouple bead is given as [Daniels, 1968];

$$\dot{q}_{cond} + \dot{q}_{rad} + \dot{q}_{conv} = 0 \qquad \text{(Equation 6.10)}$$

where $\dot{q}_{cond}$, $\dot{q}_{rad}$ and $\dot{q}_{conv}$ are rate of heat transfer by conduction, radiation and convection, respectively. The terms are positive or negative depending on whether the sensor is warmer or colder than its surroundings or its support. When it is assumed that conduction is symmetric about the burner centerline, equation (6.10) becomes

$$hA_b\left[T_g - T_b\right] - \varepsilon_{th}\sigma A_b\left[T_b^4 - T_\infty^4\right] - 2k_w A_w\left(\frac{dT_w}{dx}\right)\Bigg|_b = 0 \qquad \text{(Equation 6.11)}$$

where T_g , T_b and T_w are temperatures of the local flame gas, bead and thermocouple wire, respectively. A_w and A_b are surface areas of thermocouple wire and bead, respectively. Convective heat transfer coefficient, thermocouple emissivity and Stefan-Boltzmann constant are represented by h, ε and σ, respectively. K_w represents thermal conductivity of the thermocouple wire. The last part of equation (6.11) is negligible for long thermocouple wires therefore equation (6.11) becomes

$$hA_b\left[T_g - T_b\right] - \varepsilon_{th}\sigma\left[T_b^4 - T_\infty^4\right] = 0 \qquad \text{(Equation 6.12)}$$

Re-arranging equation (6.12) gives;

$$\left[T_g - T_b\right] = \frac{\varepsilon_{th}\sigma}{h}\left[T_b^4 - T_\infty^4\right] \qquad \text{(Equation 6.13)}$$

Heat transfer coefficient $(h) = \frac{kNu}{d_{th}}$, where $k = \frac{\mu C_p}{Pr}$, Nu and d_{th} are thermal diffusivity, nusselt number and diameter of thermocouple bead. C_p, μ and Pr are specific heat capacity, viscosity and prandtl number respectively.

Prandtl number for the flame gas is 0.71. Nusselt number for forced convection for a cylinder is given by Dupuy *et al.*, 2003 as;

$$Nu = 0.43 + 0.53Re^{0.5}Pr^{0.31} \qquad \text{(Equation 6.14)}$$

where $Re = \frac{\rho_g v_g d_{th}}{\mu}$ and $v_g = \left[\frac{2gI}{\rho_0 C_p T_0}\right]^{0.33}$. Flame intensity (I) is given by $q_{comb}/\sqrt{A_s}$ where also q_{comb} and A_s are heat of combustion and flaming area, respectively. Dupuy *et al.*, gives the error (Eq. (6.13)) as $\left[T_g - T_b\right] = \frac{\sigma\varepsilon_{th}\left(1-\varepsilon_g\right)T_g^4}{h + 4\sigma\varepsilon_{th}T_g^3}$ and response time of the thermocouple sensor as $\tau = \frac{\rho_{th} C_{th} d_{th}}{4\left(h + 4\sigma\varepsilon_{th}T_g^3\right)}$. The actual flame temperatures are determined by

the use of iterative methods given in Welch *et al.*, 2007 and Pal et al. In this work, errors in flame temperatures were calculated following Welch *et al*, and Dupuy *et al.*, 2003. A typical correction to eucalyptus fire thermocouple measured temperature is given in Figure 6.8. The blue graph shows the actual flame temperature (corrected) while red graph is temperature variation as measured by a thermocouple.

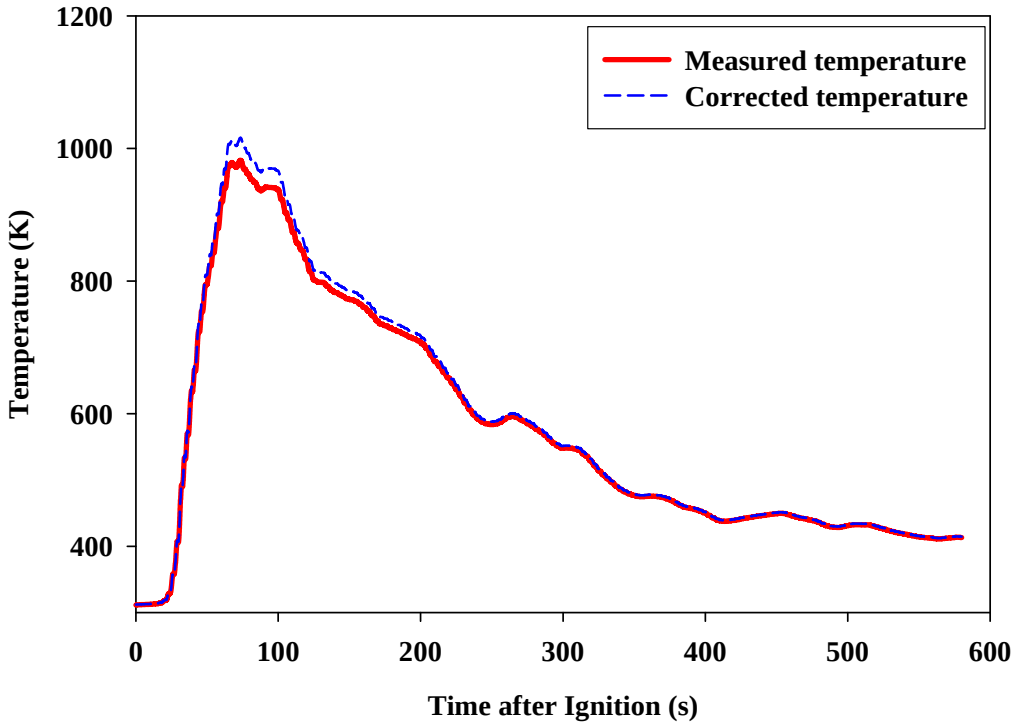

Figure 6.8. *A typical thermocouple measured temperature correction*

6.5.2. Fire Temperatures

Flames heights of about 75 cm were observed during the experiment. The flames from the combustion of pine needles and guinea grass took 2-3 minutes to extinguish while those from eucalyptus leaves took about 6 minutes. Pine needle and Guinea grass flames took about 5 s to fill the whole burner inner space. It took a little longer (approximately 10 s) for eucalyptus leaves fire to fill the space. Radiation corrected 5 s moving average of temperatures measured during fuel combustion at the fuel-flame interface by thermocouple TCA are shown in Figs. 6.9 – 6.11.

It is observed from Fig 6.9 that in the first 5 s after ignition, the pine needle flame temperature rose rapidly to reach a maximum temperature (TP_{max}) of 1069 K after 53 s. The figure shows that

guinea grass temperature rose steadily to reach a maximum position (TG_{max}) of 931 K after 44 s. Eucalyptus flame temperature also rose steadily to reach a maximum value (TE_{max}) of 1015 K after 74 s. The first sets of S-parameters were logged in after 60 s and that corresponded to Guinea grass, eucalyptus and pine leaves flame temperatures of 848, 946 and 1035 K, respectively.

After reaching the maximum value, the temperature for the pine leaves flame decreased rapidly to a value of 547 K after 140 s (see Fig 6.10). However, Guinea grass and eucalyptus leaf flame temperatures decreased steadily to 465 and 796 K, respectively, over the same period. After 111 s, second sets of analysed S-parameters were logged in and corresponded to Guinea grass, pine needle and eucalyptus fire temperatures of 542, 652 and 894 K, respectively.

The last sets of S-parameters were obtained when eucalyptus leaves were only fuel flaming and this was after 178 s (see Fig 6.11). The temperatures of the eucalyptus leaves flame, pine and Guinea grass ambers were 730, 489, and 438 K, respectively, at this time.

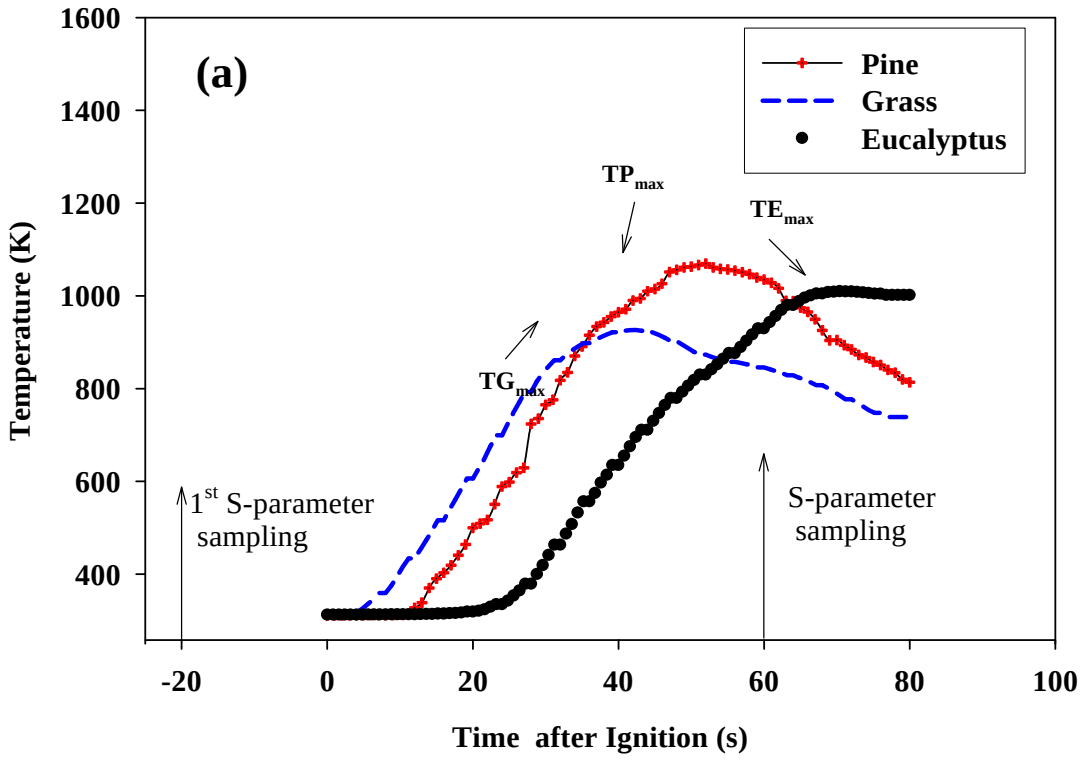

Figure 6.9. *Vegetation litter temperature (corrected) in the first 80 s after ignition*

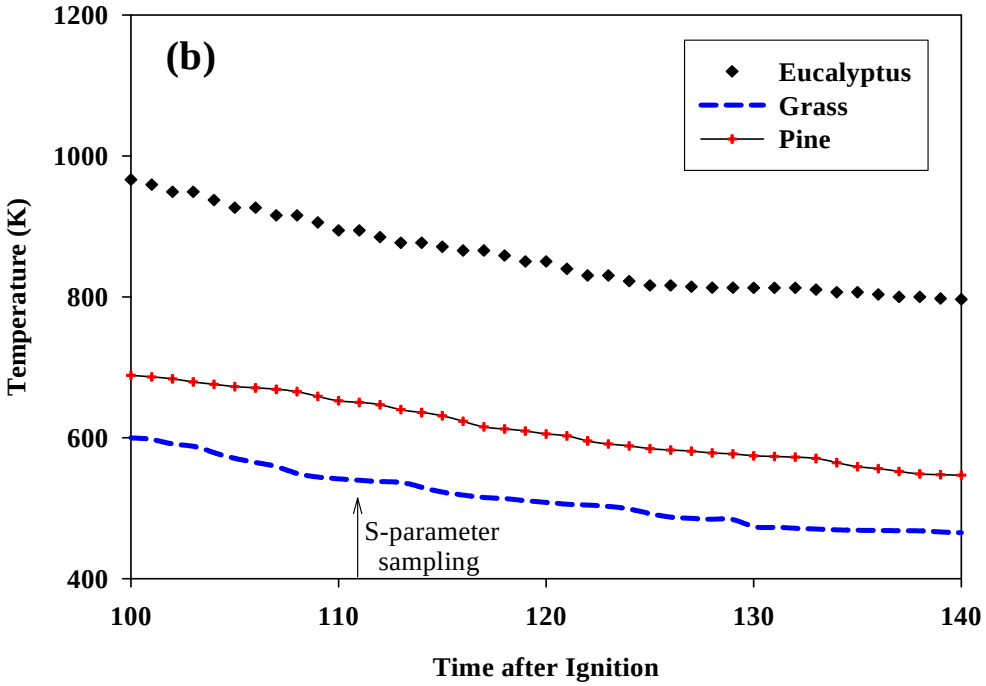

Figure 6.10. *Vegetation litter temperature (corrected) up to 140 s after ignition*

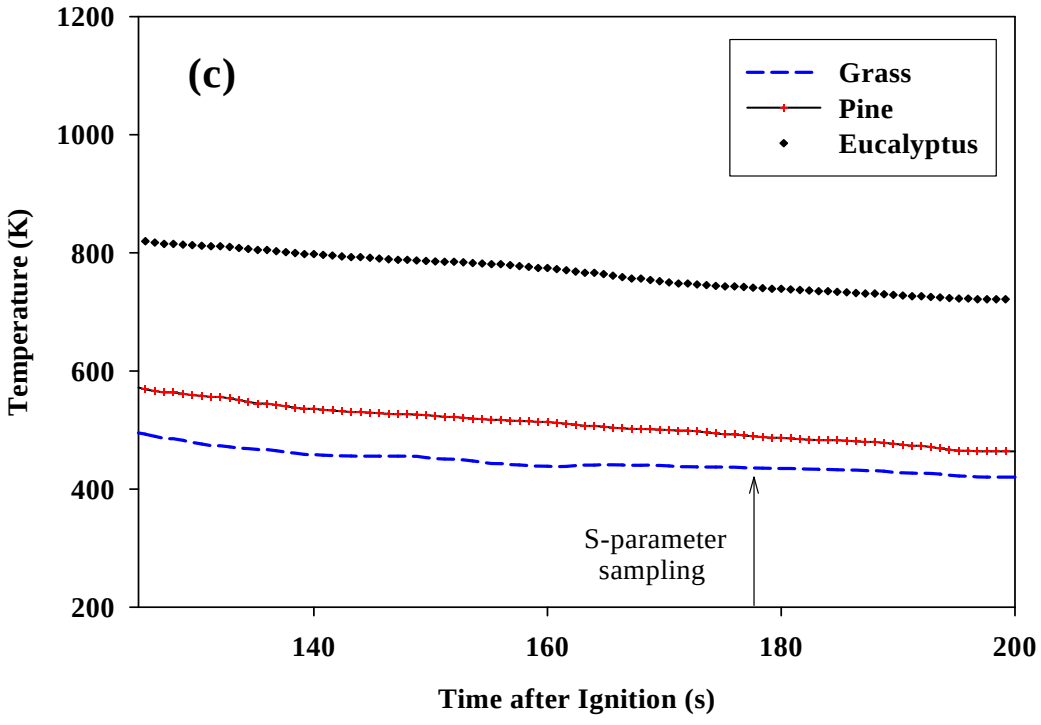

Figure 6.11. *Vegetation litter temperature (corrected) up to 200 s after ignition*

During combustion, air more easily mixed with pine needles than other fuels as its packing ratio was 5.76 x 10^{-3} and it is lowest ratio as read from Table 1. This implies that the volume of air around each pine fuel particle was higher than for other fuels. This rendered pine needle combustion to be more efficient than with other fuels hence the highest maximum flame temperature observed in the experiment. Guinea grass had packing ratio of 6.18 x 10^{-3} (Table 1). It burned spontaneously during the experiment. Despite the rapid combustion, a much lower maximum temperature was recorded for this fuel. This could be explained by the fact that by nature grass is a light fuel with a lower heat of combustion compared to the other two fuels. Therefore, the heat produced during combustion was not sufficient to raise its temperature beyond the maximum temperature of pine leaves. The burning of eucalyptus leaves was slowest as the leaves were closely packed and had the highest packing ratio of all the fuels with a value of 9.21 x 10^{-3} (Table 1). Air could not mix well with the fuel as with the combustion of pine needles, therefore the maximum temperature observed for this fuel was lower than that observed in the combustion of pine leaves. The high packing ratio in eucalyptus leaves ensured low combustion efficiency and longer combustion duration.

Table 1. Fuel properties and combustion behaviour in the burner

Fuel	**Bulk Density** (Kg m^{-3})	**Specific Gravity** (Kg m^{-3})	**Packing Ratio** (x 10^{-3})	**Max.Emissive Power** (kWm^{-2})
Eucalyptus	6.46	702	9.21	46.93
Pine	4.79	831	5.76	56.58
Grass	5.09	823	6.18	33.11

6.5.3. Microwave Attenuation

Propagation of microwave in the combustion zone of the leaves and grass flames has revealed that the zone is significantly ionized. Pine leaves burned fiercely and efficiently to produce the highest relative attenuation per meter of the flame during the experiment. The burner cavity with no flame and network analyzer system caused an average system's loss of about 7.1 dB per meter as shown in Fig. 6.12. Fluctuations in Figures 6.13, 6.14 and 6.15 are due to resonance in the chamber. At a frequency of 11.11 GHz, there are 18.5 wavelengths in the 50 cm chamber (in free

space). This combined with a 180 degree per meter phase change on reflection gives a standing wave. As the frequency is increased, the next standing wave occurs at 19.5 wavelengths, which corresponds to 11.72 GHz. The frequency difference of 0.61 is characteristic of the fluctuations in the figures. The amplitude of the fluctuations is less than the amplitude variations due to attenuation. Fitting the solid lines shown in the figures has filtered the effects of resonance.

Attenuation measurements during flaming (Figs 6.13-6.15) are relative to the system's loss. Relative attenuation observed after 60 s (see Fig 6.13) shows that over the X-band frequency range of 9.8–12.5 GHz, the relative attenuation per meter of flame due to pine needles was 4.45-2.73 dB. Guinea grass and eucalyptus leaf flames produced attenuations of 3.36-2.27 dB and 2.00-1.32 dB respectively over the same frequencies. From the results, it appears that temperature is not the only factor that affects attenuation. At 111 s (see Fig 6.14), the loss due to eucalyptus leaves was lower than that due to Guinea grass even though the temperature of eucalyptus leaves flame was higher than of Guinea grass.

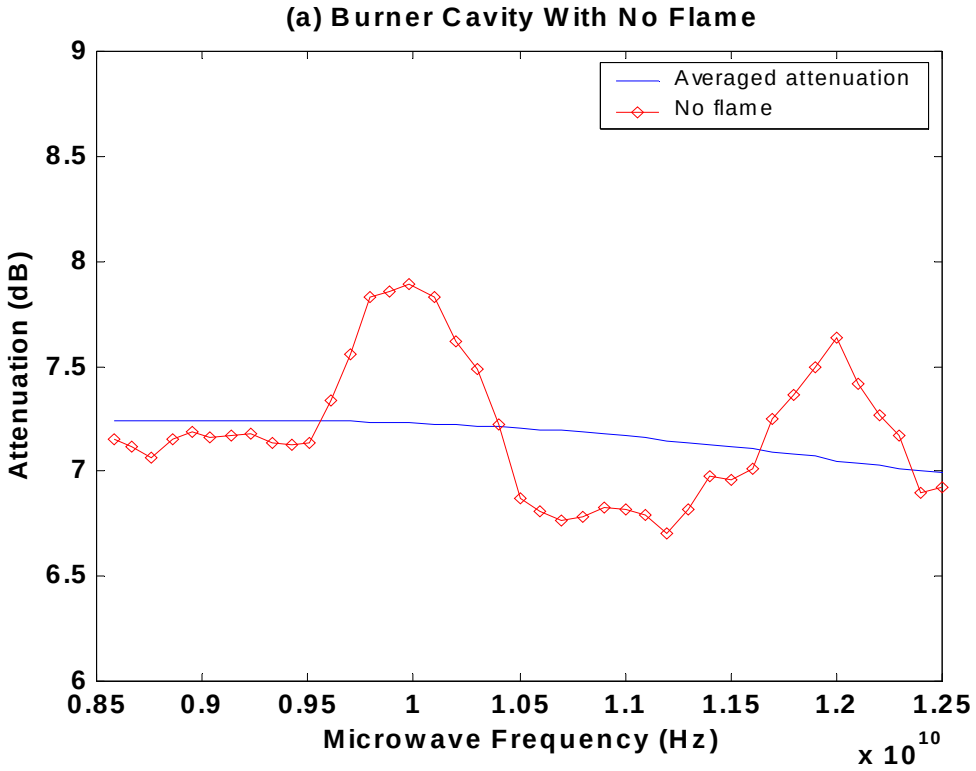

Figure 6.12. . *Variation of attenuation per meter with microwave frequency for a burner cavity during without flame*

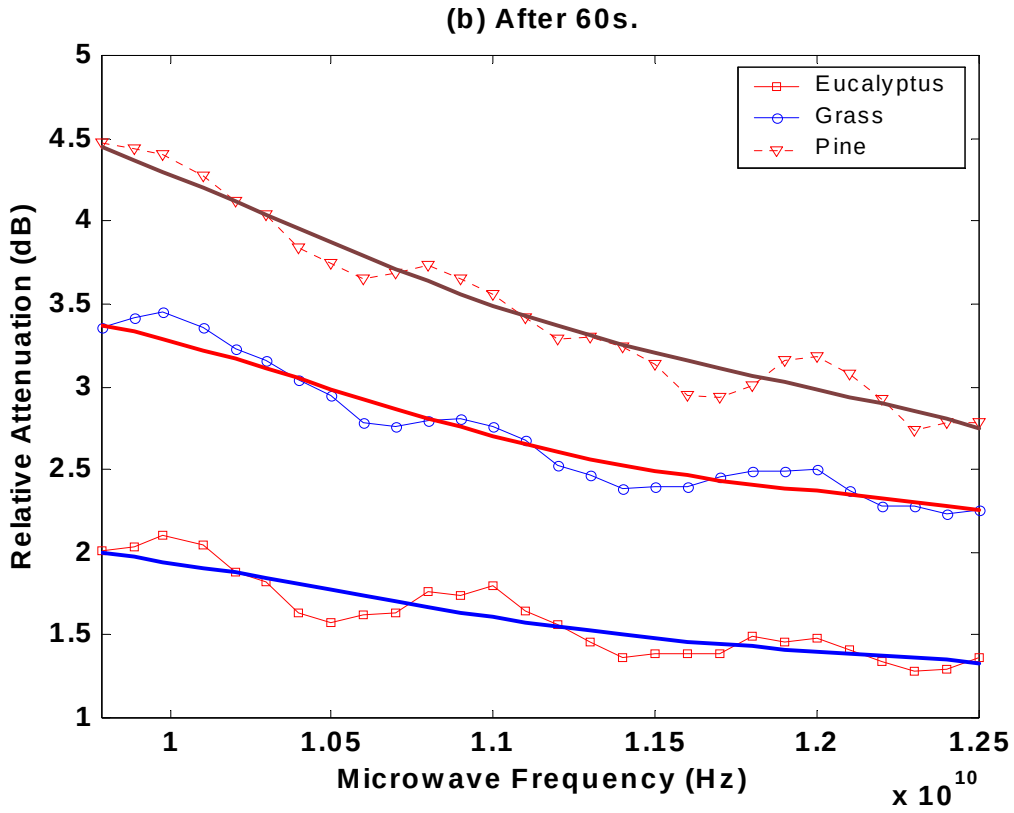

Figure 6.13. *Variation of attenuation per meter with microwave frequency during flaming of three vegetation litter after 60 s*

At 111 s (see Fig 6.14), relative attenuation per meter of the flame due to pine needles decreased to 2.84 -1.50 dB while that due to the eucalyptus and guinea grass had fallen to 2.70 - 1.25 dB and 2.00 - 1.09 dB, respectively, for the whole frequency range.

At 178 s, guinea grass and pine needles had stopped flaming (see Fig 6.15). The surface of the fuels glowed red hot with some small naked flames at the sides. Eucalyptus leaves still burned with flames but there were parts which did not flame but glowed fiercely. Eucalyptus leaf flames attenuated the microwaves by about 0.96 - 2.22 dB per meter of flame whereas Guinea grass and pine needles weakened the power of the microwaves by 2.28 - 1.36 dB and 2.20 - 1.09 dB per meter respectively at this frequency range.

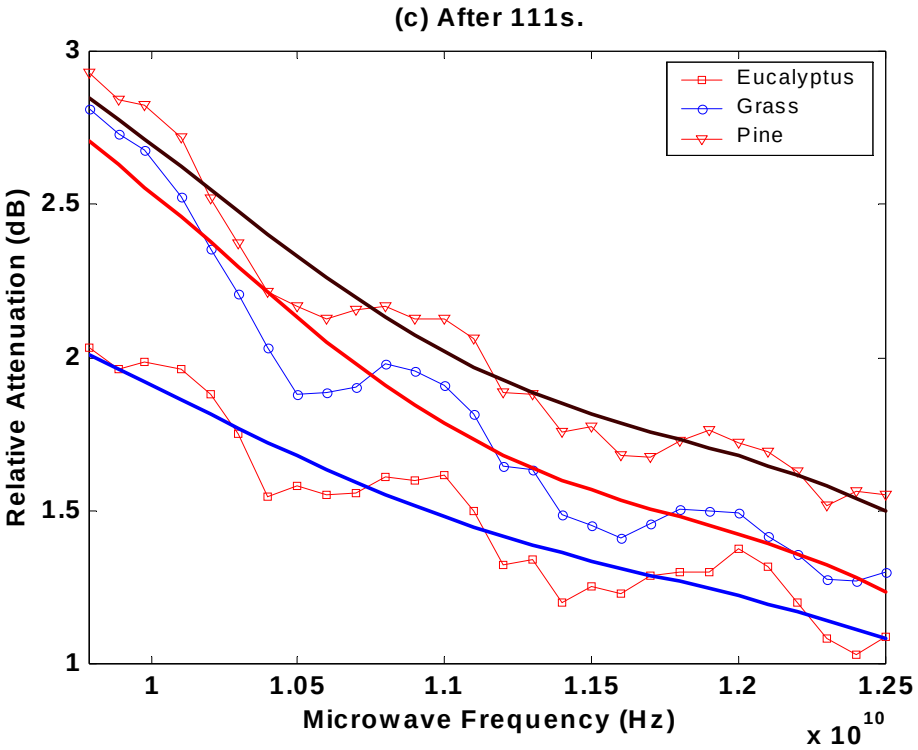

Figure 6.14. *Variation of attenuation per meter with microwave frequency during flaming of three vegetation litter after 111 s*

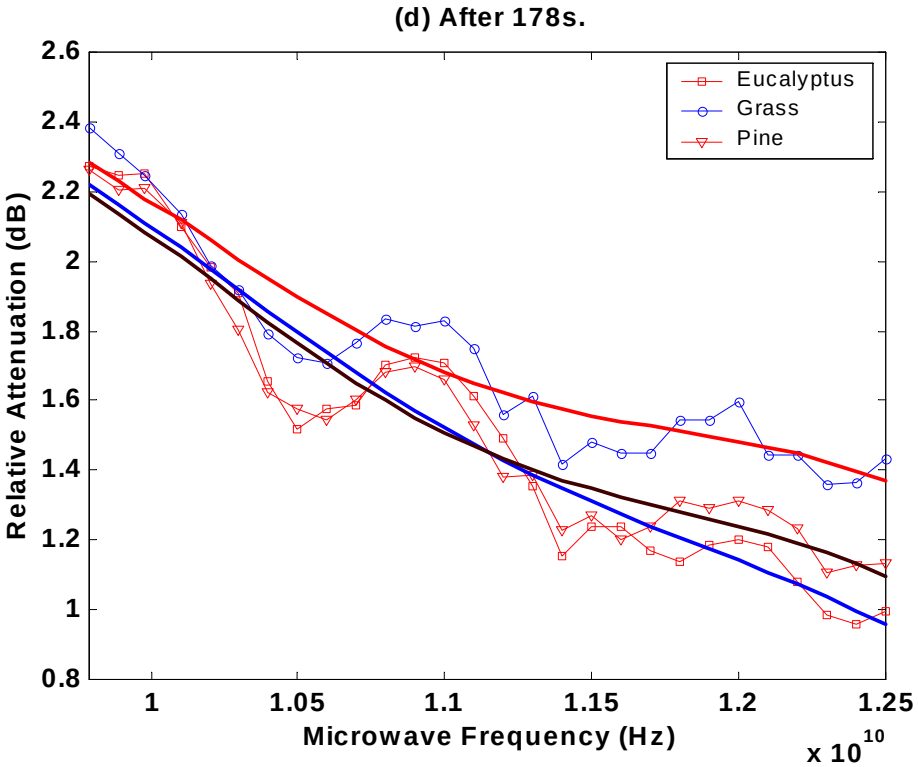

Figure 6.15. *Variation of attenuation per meter with microwave frequency for when only eucalyptus litter was flaming after 178s*

6.5.4. Measured Phase Shift.

The measured phase shifts due to the flames decreased with increasing frequency. Pine needle flame had a higher impact than grass and eucalyptus leaves flames. Generally, the flames imposed a phase shift less than 180 degrees per meter. After 60 s, phase shift due to the pine needle flame decreased from 29.3 - 18.3 degrees per meter of flame over the X-band frequency range of 9.8 -12.5 GHz (see Fig 6.16). A similar trend was also observed was observed for the two other flames. For eucalyptus leaves and guinea grass the phase shift decreased from 13.1 - 8.8 and 22.1 - 5.0 degrees per meter of flame respectively.

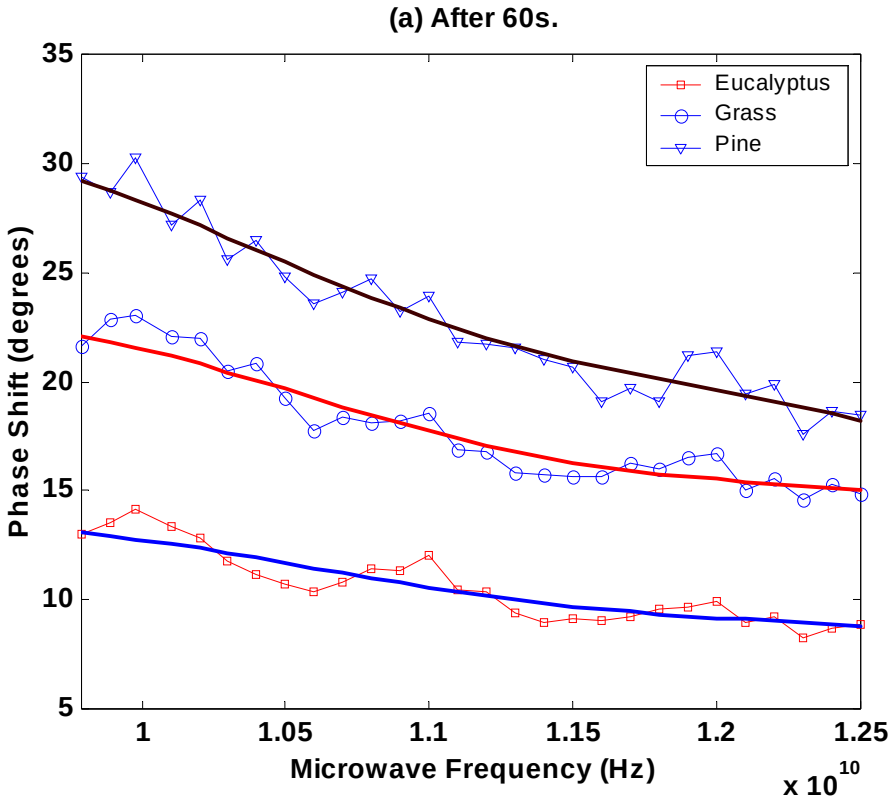

Figure 6.16. *Variation of phase shift with microwave frequency during flaming of three vegetation litter after 60 s*

After 111 s, microwave phase shift continued to decrease with frequency. Phase shift measured for eucalyptus leaves flame decreases from 13.1 - 7.1 degree per meter over 9.75 - 12.5 GHz frequency range (see Fig 6.17). For Guinea grass and pine needles the phase shift decreased from 17.8 - 8.3 and 18.8 -10.0 degrees per meter, respectively.

After 178s, phase shift due to eucalyptus leaves flame decreases from 14.5 - 6.3 degrees per meter over the frequency range (see Fig 6.18). Guinea grass and pine needles phase shift decreased from 14.9 - 9.1 degrees and 14.5 - 7.3 degrees per meter, respectively, over the frequency range.

From the measurements, microwave phase shift in the vegetation flames seems to be related to temperature and fuel type. The rate of decrease of phase shift with frequency for eucalyptus leaves flame was got steeper with time while that of grass and pine needles flames got steadier during the experiment. This could be explained by the amount of ionisation in the flames since phase shift is directly dependent on electron density. It took longer time for the organic structure eucalyptus leaves to thermally disintegrate, a process that release the organically bound alkalis in to combustion zone, than for pine needles and grass.

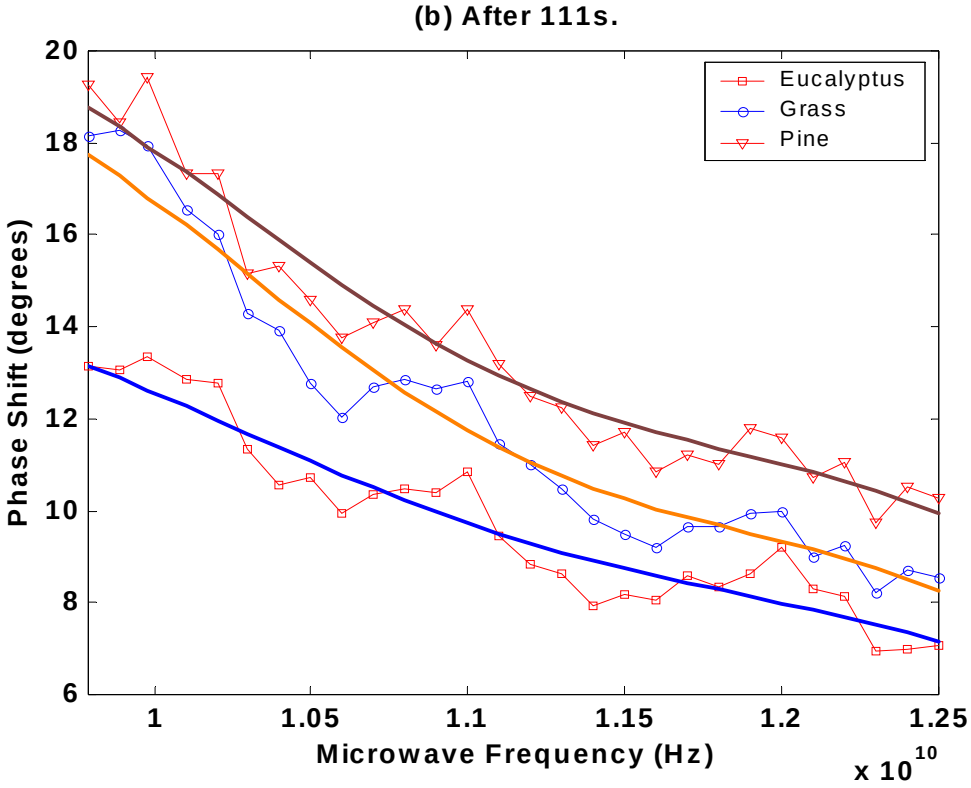

Figure 6.17. *Variation of phase shift per meter with microwave frequency during flaming of three vegetation litter after 111 s*

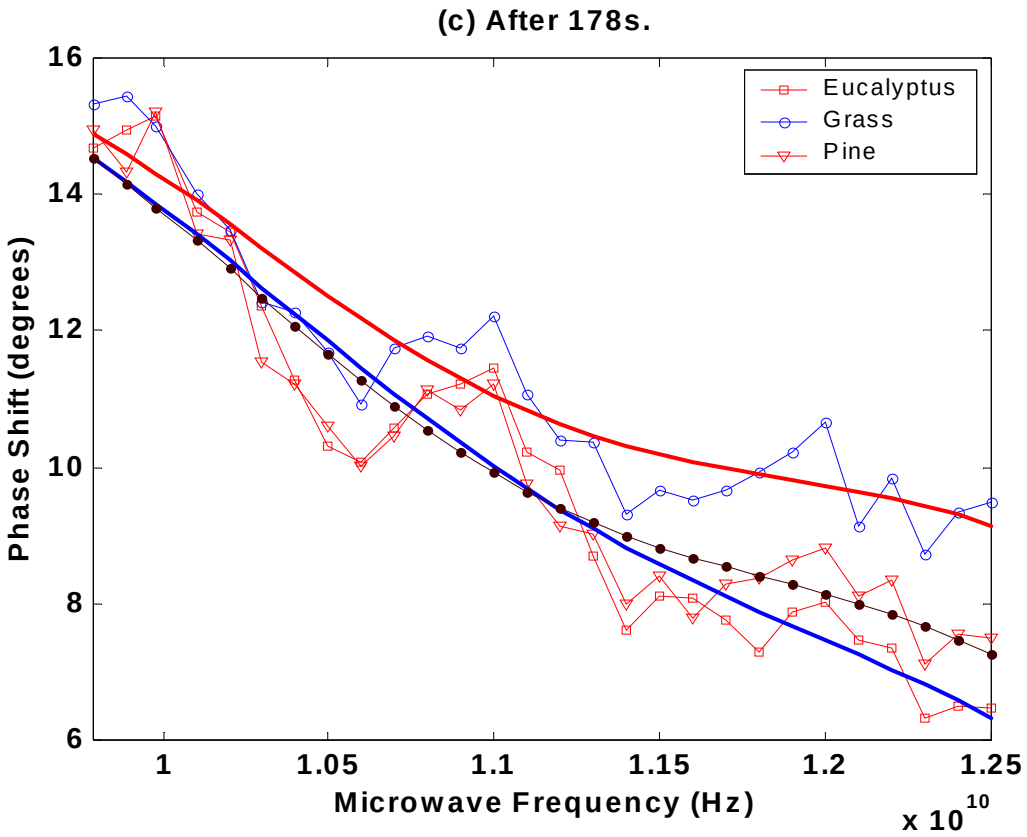

Figure 6.18. *Variation of phase shift per meter with microwave frequency during flaming of eucalyptus litter after 178 s*

6.5.5. Alkali and alkaline metal content in the forest fuel sample

Alkali and alkaline earth metal content in vegetation samples was determined using Inductively Coupled Plasma-Atomic Emission (ICP-AE) spectrophotometer and the results of the analysis are shown in Table 2. Guinea grass has the highest potassium content of 1.29 % while pine litter fall has the lowest content of 0.40 %. Sodium content was the highest in eucalyptus leave with a percentage of 0.2%. The lowest sodium content was in pine needles with a value of about 0.01%. The highest calcium content was in eucalyptus with a percentage of 0.77 %.

Table 2. Alkali content in forest fuels used in the burner (ICP-AES method)

Fuel	Alkali content (mg/g)		
	Sodium (Na)	Potassium(K)	Calcium (Ca)
Eucalyptus	0.188	6.62	7.67
Grass	0.132	12.9	4.64
Pine	0.092	3.50	1.65

6.5.6. Electron Density and Collision Frequency during Flaming.

Electron density and collision frequency were calculated by plotting the inverse of attenuation $(1/\alpha_f)$ against cyclic frequency (ω^2). This gave a linear graph with $(\varsigma / \varphi_{eff})$ as the gradient and $\varsigma\varphi_{eff}$ as the ordinate at zero abscissa (see Equation 6.4). At 60 s (see Fig 6.19), the gradient of the graph for eucalyptus flame was observed to be 9.98 x 10^{-22} and the ordinate was 5.98 x 10^{-1}. For the pine needles, the gradient of the plot was 5.31 x 10^{-22} and the ordinate was noted to be 6.5x10^{-2}. The Guinea grass plot showed a gradient of 5.70 x 10^{-22} and the ordinate was noted to be 4.48x10^{-1}. The gradient and ordinate values gave electron density and collision frequency for the eucalyptus leaves, pine needles and Guinea grass to be 7.73 x 10^{15} m^{-3} and 2.41 x 10^{10} s^{-1}; 3.21 x 10^{16} m^{-3} and 1.11 x 10^{10} s^{-1}; and 1.18 x 10^{16} m^{-3} and 2.80 x 10^{10} s^{-1} (Tables 3 and 4), respectively.

At 111 s (see Fig 6.20), the gradient and the ordinate for eucalyptus leaves are 1.19x10^{-21} and 2.57 x 10^{-1}. Pine needles and Guinea grass gave 1.02 x 10^{-21} and -6.04 x 10^{-1}; and 1.50 x 10^{-21} and -2.34 x 10^{-1} as their gradient and the ordinate, respectively. The gradients and ordinate gave calculated electron density and collision frequency as; 1.08 x 10^{16} m^{-3} and 1.47 x 10^{10} s^{-1}; 7.62 x 10^{15} m^{-3} and 2.44 x 10^{10} s^{-1} (Tables 3 and 4), respectively.

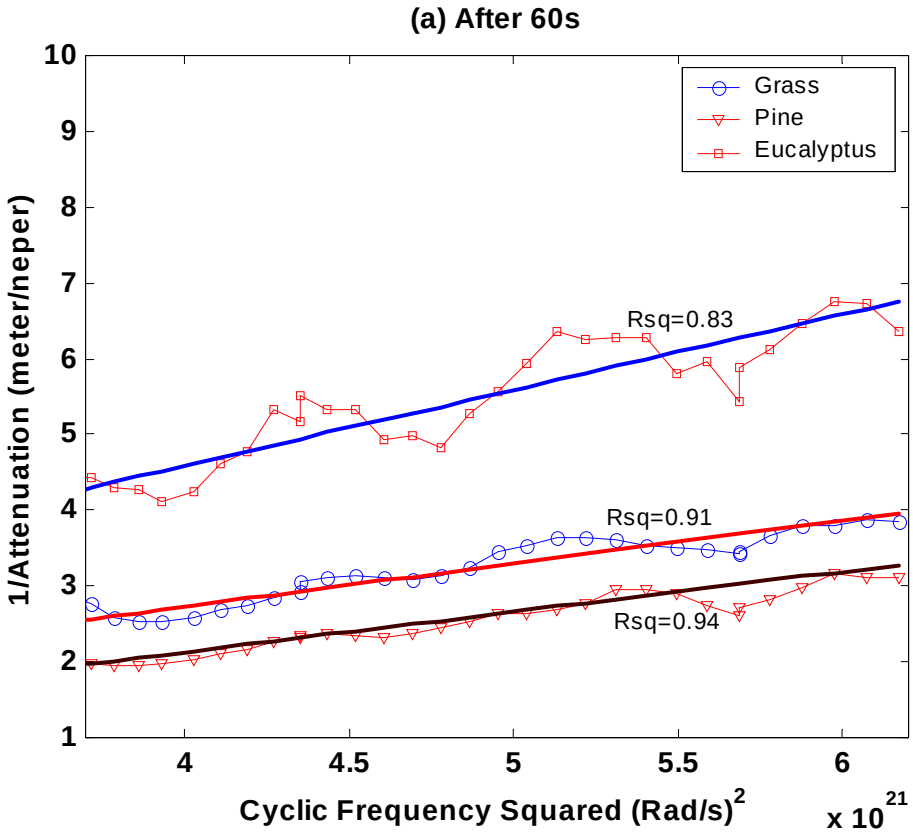

Figure 6.19. *Variation of 1/attenuation with cyclic frequency squared during flaming of three vegetation litter after 60 s*

and 5.50 x 10^{15} m^{-3} and 1.47 x 10^{10} s^{-1} for eucalyptus leaves, pine needles and Guinea grass respectively. After 178 s (see Fig 6.20), the gradient and ordinate for eucalyptus leaf flame were 1.69 x 10^{-21} and –2.09 respectively. These gave the collision frequency and electron density as 3.52 x 10^{10} s^{-1} and 3.18 x 10^{15} m^{-3}. The collision frequency values were observed to increase slightly during smoldering. This was due to the fact that neutrals moved into the space that was previously occupied by flame particles in order to balance the pressure to the atmospheric pressure.

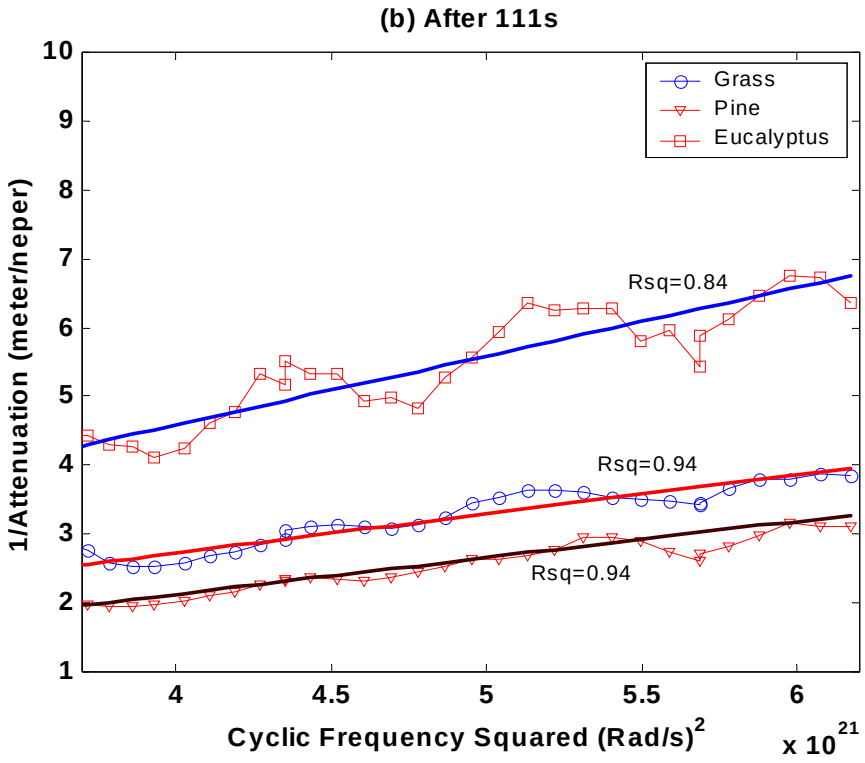

Figure 6.20. *Variation of 1/attenuation with cyclic frequency squared during flaming of three vegetation litter after 111 s*

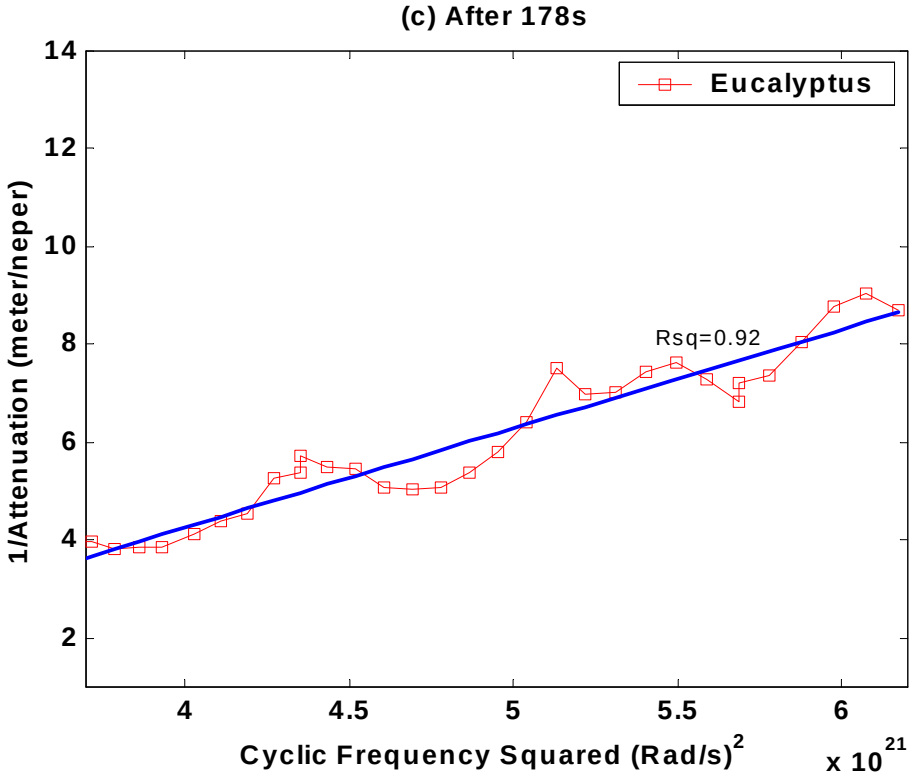

Figure 6.21. *Variation of 1/attenuation with cyclic frequency squared during flaming of eucalyptus litter after 178 s*

Collision frequency as determined from the graphical method is inversely related to flame temperature. Thus, it increased with the decrease in fire temperature. After 60 s, fire collision frequency was low for pine and guinea grass fires. However, it increased as the flames got cooler (less then 800 K) after 111 s. A similar behaviour was observed for Eucalyptus fire which was low near fire temperature maximum and higher after 60 and 178 s.

Electron density in the fire increased with flame temperature, an inverse relationship to collision frequency. It was observed that ionization was low for eucalyptus flame at 60 s and higher after 111 and 178 s. The electron density was high for pine and grass fires after 60s and lower after 111 s. Eucalyptus has a high heat of combustion than the other two fuels. Comparatively, a lot of heat was required to thermally decompose the eucalyptus leaves so that they could release organically bound alkalis than grass and pine needles.

The pine needle fire was the hottest and spread more quickly down the fuel bed than the other two flames (see Table 1.). Large air spaces between the fuel particles ensured sufficient oxygen for efficient combustion, hence the highest maximum radiant heat flux observed. The effect of the flames on X-band microwaves does not seem to be directly related on the heat flux produced from combustion. Even though flames from guinea grass have the least maximum radiant heat flux, its attenuation effect is higher than that of eucalyptus leaves throughout flaming combustion. At these radiant heat fluxes, the contribution from thermal ionization of alkali metals may be significant. Alkalis have been observed to be emitted from the solid fuel matrix during char combustion [e.g., *Knudsen et al.,* 2004]. The amount of alkalis emitted per unit time is a factor of both temperature and fuel particle size. Heat is required to thermally decompose the fuel so that the alkalis organically attached or in the transport vessels are freed first. Alkalis then thermally dissociate and consequently give electrons and positively charged ions.

The combined effect of both electrons in the flame and collision frequency absorbs energy from the microwaves. For example, pine needles in the experiment have low potassium content (see Table 2) but the combined effect of collision frequency and electron density was able to attenuate the microwaves much more than the other flames. As the temperature decreased, the effect of collision frequency was reduced, and the combination with electron density was not strong enough to weaken the X-band microwaves as much as the other two flames, for example, see Figure 6.14.

Two cases can be used to compare values of attenuation and phase indices calculated from propagation theory and those determined from the experiment. The cases are flames of pine and eucalyptus leaves at 111 and 60 s respectively. At times, the momentum transfer collision frequency was 2.4 x 10^{10} s^{-1} and electron densities of pine and eucalyptus leaves were 7.7 x 10^{15} m^{-3} and 7.6 x 10^{15} m^{-3} respectively. Using the values to back calculate attenuation and phase change indices gives attenuation index of 2.6 - 1.3 dB/m and phase change index of 15°-10 degree/meter in the frequency range of 8 -12 GHz.

Table 3. Electron density in forest fuel flames

	Fuel Flame electron density (x10^{16})		
Time(s)	**Eucalyptus**	**Grass**	**Pine**
60	0.77 ± 0.03	1.18 ± 0.05	3.21 ± 0.08
111	1.08 ± 0.05	0.32 ± 0.02	0.76 ± 0.04
178	1.47 ± 0.06	Not flaming	Not Flaming

Table 4. Collision Frequency in forest fuel flames

	Fuel Flame collision Frequency (x10^{10})		
Time(s)	**Eucalyptus**	**Grass**	**Pine**
60	2.40 ± 0.06	2.80 ± 0.07	1.11 ± 0.05
111	1.47 ± 0.06	3.95 ± 0.09	2.44 ± 0.09
178	3.52 ± 0.08	Not Flaming	Not Flaming

6.5.7. Errors in Electron Density and Collision Frequency Estimations

As electron density and collision frequency were determined by a graphical method, gradient and ordinate values and their associated errors could be used to determine the errors for the parameters, e.g., in Baird, 1988. Using this method, error in the electron density (ΔNed) and error in effective momentum transfer collision frequency ($\Delta\varphi_{eff}$) are determined from the following expressions:

$$\Delta\text{Ned} = \frac{\text{Ned}}{2\ \text{x grad.x ord}}\left\{\frac{\Delta\text{ord}}{\text{ord}} + \frac{\Delta\text{grad}}{\text{grad}}\right\} \qquad \text{(Equation 6.21)}$$

and

$$\Delta\varphi_{\text{eff}} = \frac{\varphi_{\text{eff}}}{2\ \text{x grad.x ord}}\left\{\frac{\Delta\text{ord}}{\text{ord}} + \frac{\Delta\text{grad}}{\text{grad}}\right\} \qquad \text{(Equation 6.22)}$$

where grad. is the difference between the best and the worst fit slopes and ord. is the difference in the ordinate intercepts of the best and the worst fits. They errors range from 3.2 - 4.8 %.

6. CONCLUSIONS

The electron density of forest fuel flames with radiant heat up to about 57 kWm^{-2} was calculated to range from 0.32 to 3.21 x 10^{16} m^{-3}. The electron densities determined in the experiment were lower than those produced from non vegetation fuel flames at temperatures which are around 2000 K. The amount of ionisation in the vegetation fires was a factor of fuel, combustion behaviour as well as flame temperature. We can be sure, however, that when forest fire temperatures get up to 2000 K [e.g., in *Viegas*, 1993; *Chandler et al.*, 1983] the electron densities will be higher for the same fuel type.

The collision frequency of the vegetation fires was in the ranges 1.1- 4.0 x $10^{10}s^{-1}$. The range is lower than electron-neutral collision frequency for flames in *Belcher and Sugden*, 1950, which was up to 8.8 x 10^{10} s^{-1}. Collision frequency is directly related to the electron, neutral gas densities and inversely related to flame temperature. For example, at ambient air temperature (approx.

300K), electron-neutral collision frequency is about 2.3 x 10^{12} s^{-1} [see *Akhatar et al.,* 2003] which is far higher than that of the flames at 2000 K.

Attenuation in forest fuel flames is, however, related in a complex way to both electron density and collision frequency, which are related to both the alkali content and flame temperature. From the experiment, X-band microwaves suffered a relative attenuation in the range of 1.0 - 4.5 dB/m when propagating in a line-of-sight mode through flame of radiant heat up to 57 kWm^{-2}. A phase shift of 29.3 - 6.3 degrees per meter was imposed on the microwaves.

The theory of electromagnetic wave propagation in weakly ionised plasma [*Koretzky et al.,* 2003 and *Akhatar et al*., 2003] predicts attenuation index in the range of 35.7 - 33.6 dB/m for the HF-UHF frequency band when mean values of the measured collision frequency and electron density are used. This implies that a UHF signal caused to propagate along the fire-fuel interface of a very intense ionised fire may be strongly attenuated.

CHAPTER 7

Radio wave refraction in bushfire plumes

7.1. Introduction

Three regions are distinct in a bushfire plume. The distinction lies in variations in temperature, plume velocity and implicitly in dielectric permittivity. These regions are the: continuous and intermittent flames and the thermal plume (Santoni *et al.* 2002 and Marcelli *et al.* 2004) and are shown in Figure 7.1. There is an immense literature on the behavior of these regions more especially the continuous flame and the thermal plume regions (e.g. in Balbi *et al.* 1999; Viegas, 1998; Porterie *et al.*1999 and Webber *et al.*1995). Most of the literature on the continuous flame region concerns its intensity (I), rate of spread (RoS) under various conditions, velocity and thermal properties. The application of these flame properties is in their relevance to fire suppression and firefighter safety. Very few people have studied the physical properties of the intermittent region e.g. Marcelli *et al.* There is lack of interest in the region among fire management scientists because its properties do not directly relate to a safety concern.

Bushfire plumes interact with the atmosphere (e.g. in Potter, 2002). The interaction comes in form of fire–induced circulation that facilitates mass exchange between the atmosphere and the plume, and enormous amount of heat energy released by the fire into the atmosphere through radiation and convection. The heat released from a bushfire causes surface air to rise convectively into the atmosphere creating a thermal bubble.

The main objective of this chapter is to theoretically study the refractive behavior of the thermal bubble on radio waves propagation by ray tracing schemes. Radio wave deflections and attenuation due to density gradients are calculated in the schemes using Snell's law of refraction. The chapter starts in Section 7.2 by reviewing the literature on physical characteristics of plumes from line-bushfire and circular flaming areas. Plume physical characteristics such as temperature and density variations are used as inputs to the ray-tracing schemes.

Maximum temperatures in very high intensity bushfires (90MWm^{-1}) can be up to 1400°C. Above the fuel canopy and under steady state conditions, plume temperatures decrease exponentially with height. Within the fuel stratum, temperatures behave in a complex way, however they generally increase almost constantly from ground surface to the fuel canopy for high fuel stratum (e.g. in crown bushfires); and are nearly constant for lower strata (e.g. in surface fires). Across a bushfire plume depth, temperature may be assumed to have a Rayleigh profile (following Oliveira, 1994). Gas velocity behaves in a similar manner as temperature. These variations in temperature produce radio refractivity gradients in the plume.

Plume constituents concentrations are a very important factor in radio refractivity. Water vapor concentration and ionization significantly affect radio refractivity. The issue is explored by varying plume water vapor and potassium concentration in Section 7.3. Models simulating radio wave refraction in bushfire environments are also constructed in this section. The models are applied for a typical eucalyptus crown fire in Section 7.4. Section 7.5 considers a case history of multinational *Operation Euroka* mass fire experiment. Radio wave propagation experiments carried out during the *mass fire* experiment are modeled and the results compared with those reported in Williams *et al.* 1970. The chapter is concluded in Section 7.6.

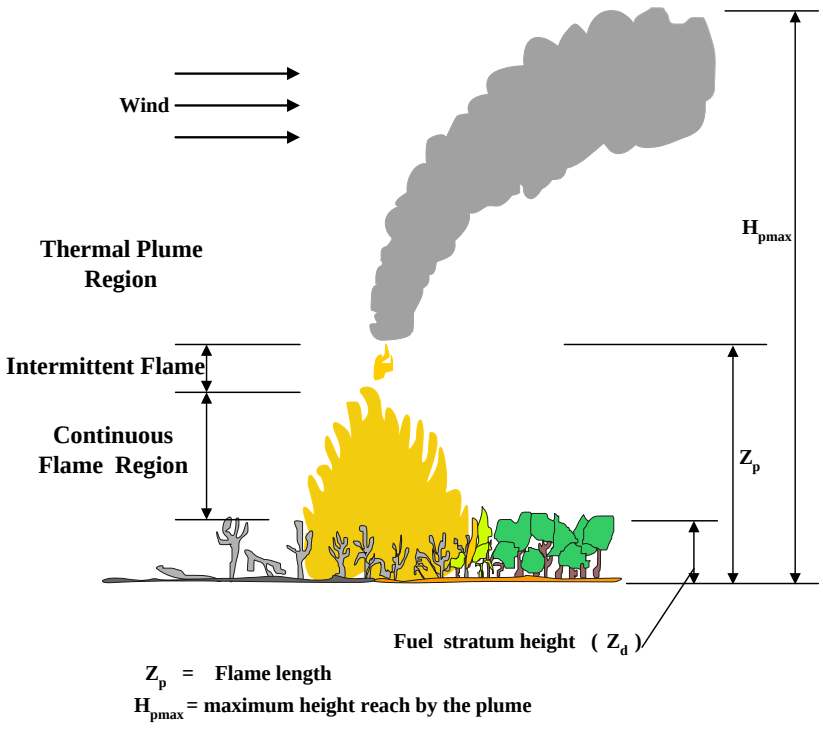

Figure 7.1. *Bushfire's continuous, intermittent flame and thermal plume regions*

7.2. Physical characteristics of circular and line bushfires

7.2.1. Line Bushfire plume

7.2.1.1. Continuous flame region

(a) Temperature variation

Spatial variation of temperature with time in the continuous flame region of a bushfire plume has been documented (e.g. in Weber *et al.*1995, Simeoni *et al.* 2001 and Venturi *et al.* 1994). According to Venturi *et al.*, Oliveira *et al.* (1994) gave an empirical relation that describes experimental data on temperature-time variation in the bushfire front with a fair amount of accuracy. The relation is a Rayleigh Distribution fit of the temperature–time curves such as that given in Figure 7.1. Oliveira *et al.* gave the relation as:

$$T_{fl} = T_{amb} + \frac{\alpha\beta}{\varsigma'} e^{-\left[\frac{\beta}{\varsigma'}\right]^2} \qquad \text{(Equation 7.1)}$$

Where: α and β = empirically determined constants,

ς' = distance from arbitrary origin of the Gaussian curve.

Heat radiated from the flame heats up the air ahead of the bushfire front. The energy causes air temperature to vary exponential from a maximum value (T_{max}) at the flame-fuel interface to the ambient (T_{amb}) some distance away in front of the flame. Catchpole *et al.* 2002 modeled this exponential decrease in air temperature as:

$$T_{air} = T_{amb} + \left(T_{max} - T_{amb}\right) e^{-\left[\frac{x}{\lambda_d}\right]} \qquad \text{(Equation 7.2)}$$

Where: x = distance from the bushfire front,

λ_d = gas temperature characteristic distance.

Catchpole *et al.* 2002 also related T_{max} and λ_d to packing ratio (β_p), surface to volume ratio (σ), heating distance (d), Byram's convection number (N_c) and wind speed (U) respectively as:

$$T_{max} = e^{(a - b\sigma - c\beta - dU)}; \qquad \text{(Equation 7.3)}$$

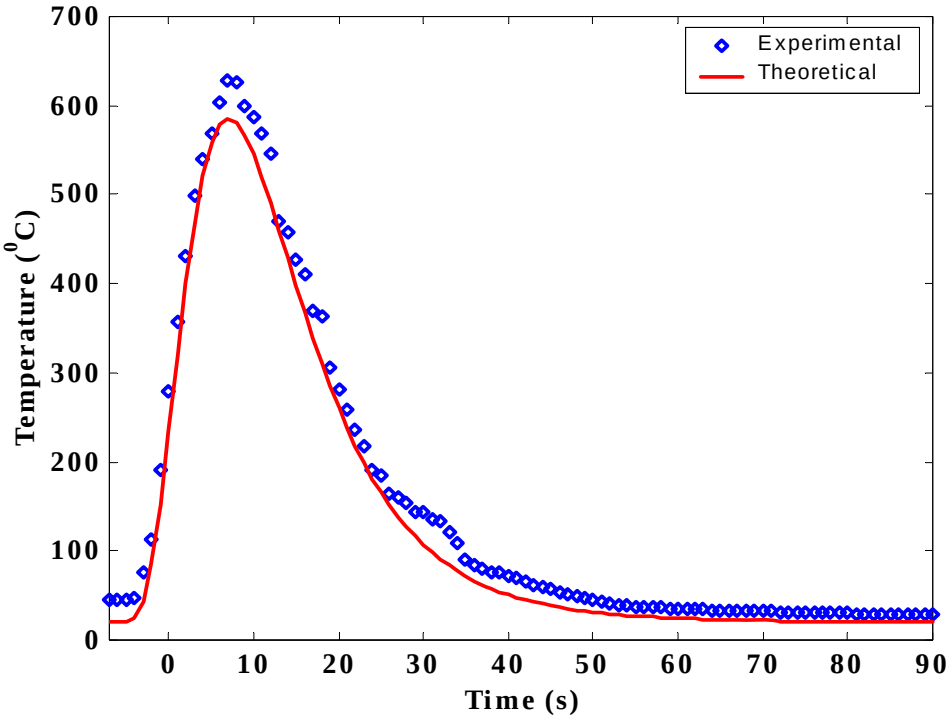

Figure 7.2. *A Rayleigh distribution fit of temperature – time variation in a line-fire front (adapted:* Moradini *et al.* 2001*)*

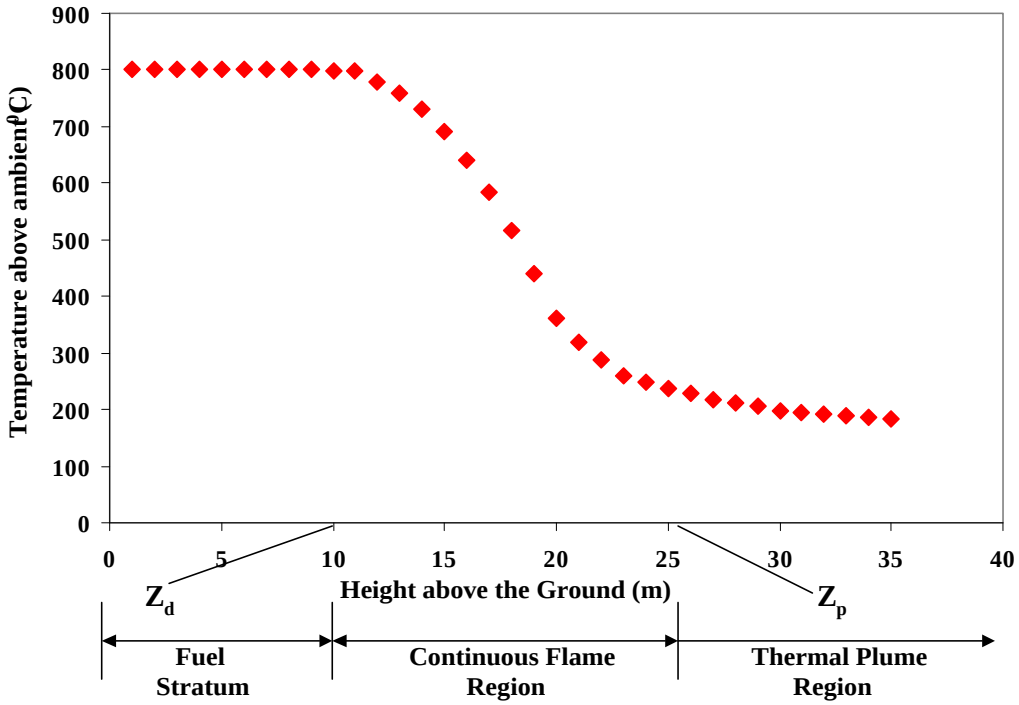

Figure 7.3. *Example of temperature variation with height in a bushfire plume (adapted:* Weber *et al.* 1995*)*

and

$$\lambda_d = d + a\left(N_c\right)^b e^{\left(-c\beta\sigma\right)} \qquad \text{(Equation 7.4)}$$

Where: a, b and c are empirical constants.

Vertical temperature variation in the flame above fuel layer decreases exponential with height. The decrease in temperature with height in the fire plume is given by Weber *et al.* 1995 as:

$$T_{fl} = T_\infty + Ke^{\left(-\alpha_f (z-z_d)^2\right)} \qquad \text{(Equation 7.5)}$$

Where: K = an empirical constant,

z_d = a constant related to fuel height,

α_f = $1/\left(2z_p(z_p - z_d)\right)$.

z_p = a constant related to flame height,

An example of such a variation is given in Figure 7.3 above.

Maximum temperature in both the vertical and horizontal sense occurs at about the center of the bushfire. Visible flaming edges are noted to be at much low temperatures of around 450°C than at the center of the combustion zone, which can be up to 1300°C (e.g. in Santoni *et al*. 2002). This produces temperature gradients between the edges and fire center. The temperature gradient sets a flow of ambient air into the flame, a process that lowers the combustion temperature by turbulent mixing (Nelson, 2003 and Dickinson *et al.* 2001).

Velocity at base of a line bushfire flame

The chapter considers a line bushfire to be semi-infinite in its width compared to its depth and also to burn in steady state conditions. Under steady state conditions the vertical velocity at the base of the base of a line bushfire has been derived by R. Nelson (1993) as:

$$\upsilon_{lf} = \left[\frac{2gI_b}{\rho_\infty C_p T_{amb}}\right]^{1/3} \qquad \text{(Equation 3.6)}$$

Where: I_b = Fire line intensity

C_p, = specific heat capacity at constant pressure

T_{amb} = ambient air temperature

ρ_∞ = ambient air density

g = acceleration of free fall respectively.

7.2.1.2. Thermal plume above a line bushfire

Line bushfires liberate enormous amount of heat energy into the atmosphere in the form of a thermal plume (Viegas, 1998). Combustion products and aerosols are transported into the atmosphere through the convection column. Air from the surrounding atmosphere entrains into the column as it rises. The entraining air dilutes the smoke and makes it spread with height (see Figure 7.4). Mercer *et al.* 1994 developed a model that relates plume temperature, density, vertical and entrainment velocities to plume radius. The model's governing equations are derived from balancing mass, momentum and energy fluxes. Mercer *et al.*'s model assumes top-hat distribution of the variables, thus a variable such as velocity is assumed to be constant across a cross section perpendicular to the plume's centerline. From the conservation of thermal energy, Mercer *et al.* 1994 gave temperature variation in the convection column as:

$$\frac{d\left(\rho_p b w T_p\right)}{ds} = \rho_a \upsilon_e T_{amb} \qquad \text{(Equation 7.6)}$$

Where: ρ_a = ambient air density,

ρ_p = plume density,

T_{amb} = ambient temperature,

T_p = plume temperature,

w = vertical velocity of the plume,

b = plume radius,

υ_e = Entrainment velocity.

Assuming ideal gas behavior of the plume, its density can be related by;

$$\rho_p = \rho_a \frac{T_{amb}}{T_p} \qquad \text{(Equation 7.7)}$$

When Gaussian distribution is fitted on the top-hat data, it gives temperature distribution of the form (Mercer *et al*. 1994):

$$T_G = T_a + \frac{N}{\lambda^2}\left(T_p - T_a\right)e^{-\frac{r^2}{\lambda^2 b^2}} \qquad \text{(Equation 7.8)}$$

Where: r = radial distance normal to the centerline trajectory,

N = plume edge criterion, which is usually taken to be 2,

λ^2 = spread ratio, also usually taken to be 1.

Weber *et al.* 1993 also fitted a Gaussian distribution on the experiment data and gave the temperature–time variation in the plume to be in the form:

$$T' = \frac{A}{z}\exp\left(\frac{-t^2}{B^2 z^2}\right) \qquad \text{(Equation 7.9)}$$

Where: z = height above the ground.

A and B = empirically determined factors.

Weber *et al.* 1995 observed that Equation 7.9 can be explicitly written as:

$$\Delta T = \frac{kI^{2/3}}{z}\exp\left(\frac{-x^2}{\beta^2 z^2}\right) \qquad \text{(Equation 7.10)}$$

Where *A* has been replaced with the product of fire-line intensity (*I*) to the power of 2/3 and proportionality constant k. Entrainment constant (β) and horizontal distance (*x*) from the line source replace *B* and *t* respectively.

Figure 7.4. *A thermal plume rising from a bushfire* (photo: S. Warzler)

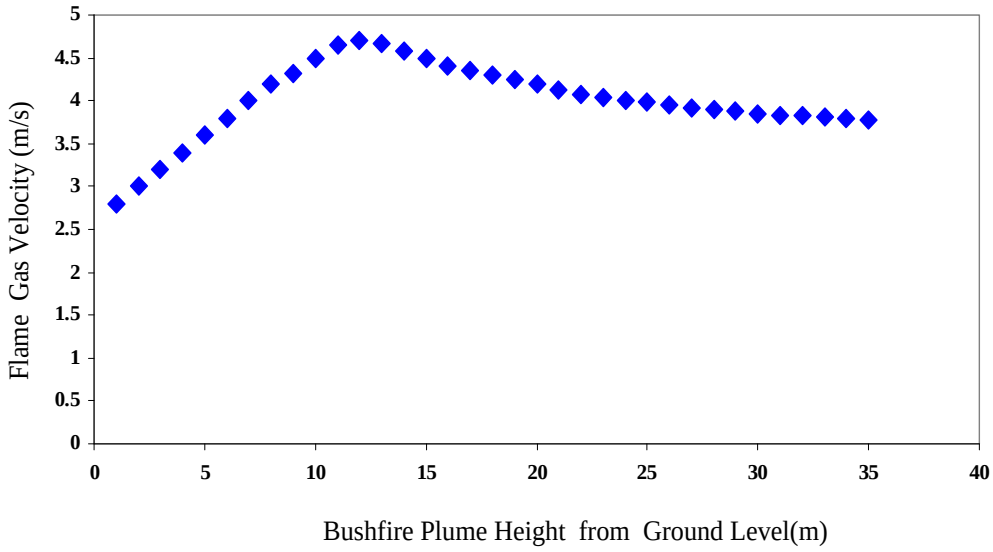

Figure 7.5. *Typical variation of velocity with height above a circular bushfire plume* (Adapted: Heskestad, 1998)

7.2.2. Circular fire plumes

7.2.2.1. Continuous flame region

(a) Temperature and velocity variation circular fire flame.

Temperature variation in a circular fire has also been a subject of intense study (e.g. Hiroshi Koseki *et al.* 2000; Dupuy *et al.* 2003; etc.). Temperature above ambient (excess temperature) has been noted to have a Gaussian profile and varies as (Dupuy *et al.* 2003):

$$T_{exc}(r,z) = (T_{max}(z) - T_{amb}) + ke^{-a\left[\frac{r}{z}\right]^2} \qquad \text{(Equation 7.11)}$$

Where: r = radial position,
$T_{max}(z)$ = center line fire temperature at height z,
k and a = empirical constants.

Dupuy *et al*. also studied the vertical temperature in forest material flames produced from a cylindrical burner. Normalized height Z (Z=height/height of flame) was used as a vertical variable. According to Dupuy *et al.* the three fire behavior regions are distinct. It is assumed that the intermittency region starts at when Z is equal to Z_1. The thermal plume starts at when Z is Z_2. Z_0 is the position of the pyrolysis zone. Dupuy *et al.* modeled the vertical temperature profile from when Z is greater than 0.3 and obtained the following model equations:

(i) In the continuous flame region, thus $Z_0 \le z < Z_1$: $T_{exc}(r,z) = T'$.

(ii) In the intermittent flame region, thus $Z_1 \le z < Z_2$: $T_{exc}(r,z) = T'\left(\frac{z_1}{z}\right)^b$

(iii) In the thermal plume region, thus $z < Z_2$: $T_{exc}(r,z) = T'\left(\frac{z_2}{z_1}\right)^b\left(\frac{z_2}{z}\right)^c$

(Equation 7.12)

Where T' is defined by Equation 7.11. A plot of excess temperature with normalized height (Dupuy *et al*.) reveals that in the continuous flame region of a cylindrical burner, the temperature decreases steadly with height (slope of –0.9) and then decreases faster in the intermittent and thermal plume regions with slopes of –2.2 and –5/3 respectively.

Heskestad (1998) has shown a general behavior of gas velocity in a circular fire plume (see Figure 7.4). Measurement of upward gas velocity in the continuous flame region reveals a steady increase to a maximum value then a slow decrease thereafter.

7.2.2.2. Thermal plume above circular fires

Emissions from bushfires are more concentrated at the centerline of the plume and fade out at the edges. The flow pattern is empirically fitted by a Gaussian shape e.g. Dickinson *et al*. 2001 (Figure 7.6). There is a similar pattern for temperature, density and velocity of the plume particles.

Most of bushfires occur when the atmosphere is in neutral-stable condition (Nelson, 2004). Under these conditions, the physical parameters (e.g. density, velocity and temperature) of the plume produced from a circular fire are related to the entrainment coefficient (β) and altitude z.

Under a neutral atmosphere and assuming top-hat profile, the radius of the plumes (R_p) is given by Viegas 1998 as;

$$R_p = \frac{6}{5}\beta z \qquad \text{(Equation 7.13)}$$

Under stable conditions the maximum height reached by the thermal plume is given by Viegas as:

$$z_{max} = 5F_0 G^{-1/4} \ . \qquad \text{(Equation 7.14)}$$

Where G is the Brunt Vaisala frequency. This frequency is given by; $G = \frac{-g}{\rho_1}\left[\frac{d\rho_0}{dz}\right]$.

7.3.2. Thermal bubbles and roll vortices in very high intensity bushfires

Heat transfer by convection in the atmosphere is driven by large values of Rayleigh Number (Ra). Ra is a dimensionless ratio between the product of buoyancy forces and heat advection and the product of viscous forces and heat conduction in a fluid. It is given by Nikolaenko *et al*. 2003 as:

$$Ra = \frac{g.\alpha.\Delta T.L^3}{\upsilon.\kappa} \qquad \text{(Equation 7.16)}$$

Where: g = acceleration of gravity,

α = isobaric thermal expansion coefficient,

ΔT = temperature difference,

L = characteristic length

ν = kinematic viscocity.

κ = thermal diffusivity

Low values of Ra favor heat transfer in the fluid by conduction mode.

The earth surface absorbs radiation from sun and re-emits it in form of long waves into the atmosphere. The emitted long waves continually warms up the air the near the ground surface with the consequence of troposopheric temperature decreasing with the increase in altitude. The temperature difference between the air masses has a potential to trigger convection. The initiation of convective heat transfer is releasable when there is an intense heat source such as bushfire, which sets up a large temperature gradient. A large temperature gradient between the local surface air and air aloft significantly increases the value of Ra as per Equation 7.16.

When surface air is heated by a bushfire, it bulges upwards. Continuous heating from the fire bulges the air into a bubble, which displaces some of the cooler air aloft and finally breaks away from the surface air mass to form a thermal bubble (Figure 7.6). This occurs when the Ra exceeds a critical value of 1708. As the thermal bubble ascends through the atmosphere its size increases with the decrease in atmospheric pressure. Hot gaseous combustion products from the bushfire are sucked into the bubble as it ascends. This makes temperature and velocity highest at the centerline of the thermal bubble. Due to high velocity at the bubble centerline, internal buoyant forces produce vortex tubes that are circular rings concentric with the vertical axis (Church *et al.* 1970 and Burrows 1984). Figure 7.7 shows the concentric vortex rings.

The vortices suck in cool atmospheric air along the plume periphery. The sucked in cool air mixes in a turbulent manner with the combustion products. This ultimately leads to loss of momentum in plume, buoyant forces losing their strength and finally the plume spreads as it rises.

Fluid buoyancy can be defined by a parameter called the bulk Richardson number, which is given by the relation:

$$Ri_b = \frac{g\left(d\bar{\theta}/dz\right)}{\bar{T}\left(d\bar{u}/dz\right)^2} \qquad \text{(Equation 7.16)}$$

Where: g = acceleration due to gravity

$d\bar{\theta}/dz$ = average potential temperature gradient,

$d\bar{u}/dz$ = average velocity gradient

$\bar{T}$ = average fire temperature.

According to Haines *et al.* 1987, low values of Ri_b favor the generation of roll vortices while large values of Ri_b favor the cellular convection. Convective roll vortices such as those observed in crown fires have Ri_b values as low as –0.022 (Haines *et al.* 1982).

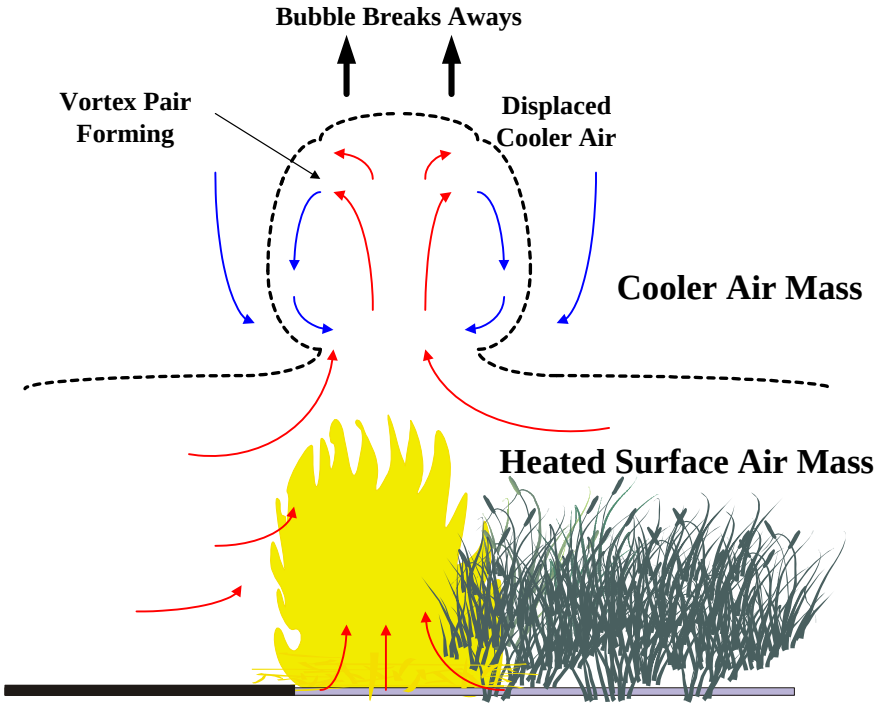

Figure 7.6. *Gaussian distribution of plume velocity over a circular fire*

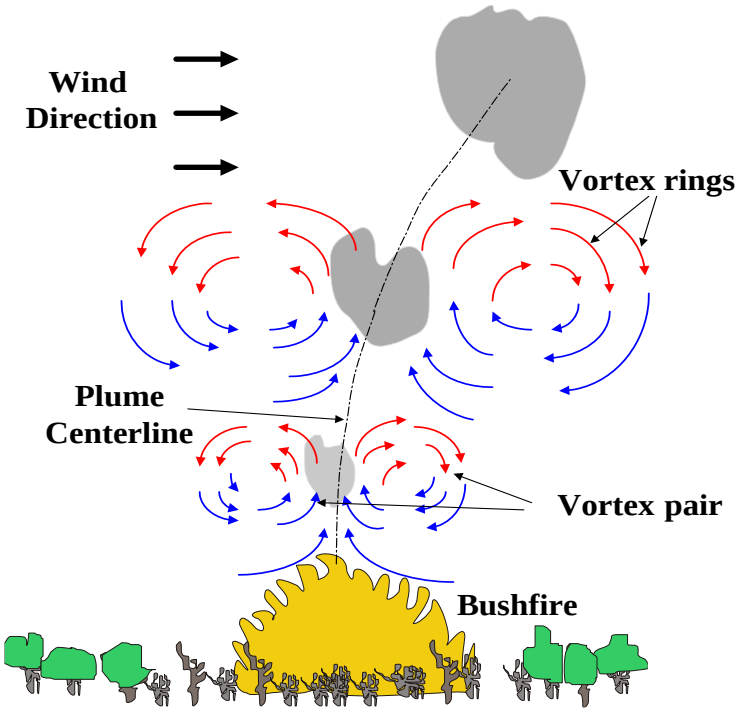

Figure 7.7. *Concentric vortex rings above circular fire* (Adapted: Church *et al.* 1980)

7.2.3.1. Occurrences of roll vortices in bushfire environments

The occurence of Roll Vortices (RV) in very high intensity bushfires and grass fires has been documented (e.g. in Church *et al.* 1970; Byram *et al.* 1970; Haines *et al.* 1987 and Haines *et al.* 2003). Vortices can exist as: Vertical Roll Vortices (VRV), which takes the form of fire-whirls; and Horizontal Roll Vortices (HRV). HRVs are a result of bending of VRV in light to moderate speed wind. The bending results in the reduction in angular velocity and loss of ferocity (Haines *et al.* 2003). HRVs exist in at least three forms: longitudinal vortex pair, single longitudinal vortex and transverse roll vortex (Haines *et al.*1987). The most common HRV in bushfire environment is the longitudinal vortex pair, thus that which is shown in the thermal bubble. The longitudinal vortices are considered one of the ways by which crown fires spread; at least in coniferous forests (Haines *et al.*1987).

The interaction of the plume with the winds creates vortex tubes that are bent and stretched along the flanks of the plume (Church *et al.* 1970). Counter rotating roll vortex pairs are then formed over the flaming area provided the wind speeds are light to moderate. Further downwind of the plume, strong vorticity and weak buoyancy effects may exist. The counter-rotational vortices that still exist in this region lie almost parallel to the surface.

7.2.3.2. Conditions for the occurrence of HRV

At least three conditions are critical to the occurrence of HRVs. HRVs are hard to form in rough terrain as a result of complex airflow and turbulence (Haines *et al.* 2003). High wind speed breaks up the roll vortices. Very high temperatures are very important for the formation of the HRVs. This can be inferred from equations 7.17 and 7.16 in which high temperature gradient and high average temperature are very important for low Richardson and high Raleigh numbers respectively. This of course restricts the formation of HRVs to fire burning extreme bushfire weather. Roll vortices formed from crown fire are dependent on temperature gradient in the burning area. This causes a wind to flow transverse to the burning area, a very important component to the initiation of horizontal vortices. Light to moderate ambient wind of 6 ms^{-1} is a necessity for the formation of longitudinal pair and transverse vortices while single longitudinal vortices require winds up 22 ms^{-1}.

Longitudinal vortex pair is the most common HRV in crown fires. They are considered the most common method by which crown fires spread. They create "crown streets" whenever they occur in a grassland or forests. Crown streets are rows of unburned vegetation, which remain after a crown fire. The crowns are saved by cool air in the descending arm of counter-rotational vortex pair (see Figure 7.8). The air circulation in the vortices drives fire in opposite directions so much that it is only the tree stems that are charred. The char heights are low and in opposite directions on either sides of the crown streets.

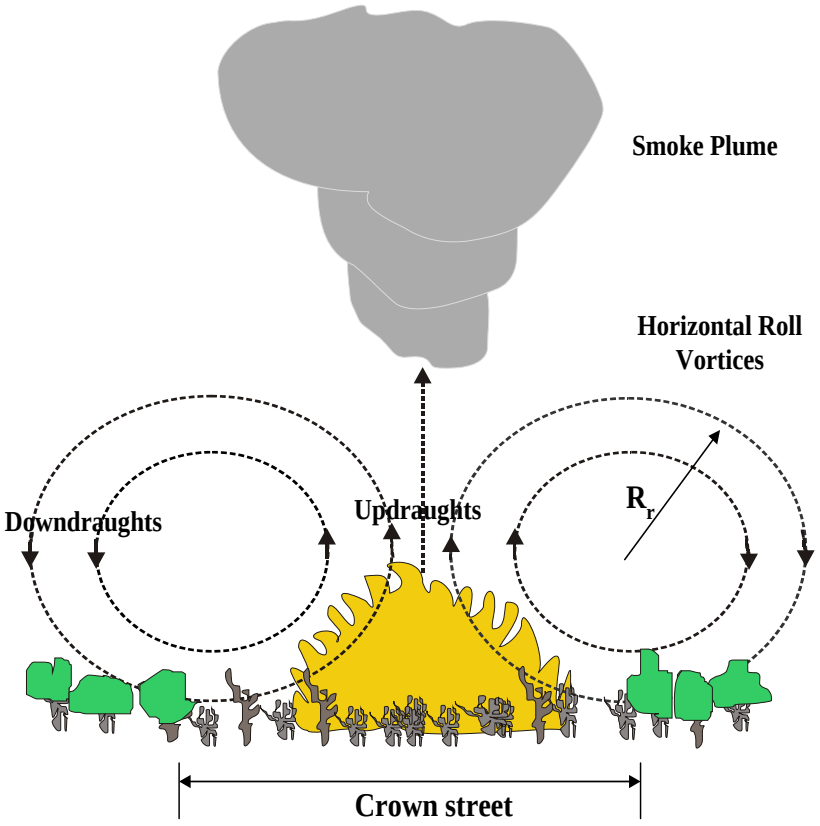

Figure 7.8. *Formation of crown streets by HRV pair*

7.3. Radio refractivity in bushfire plume

A bushfire plume is a non-homogeneous dielectric medium. The continuous flame region of the plume is characterized by high enough temperatures to cause thermal ionization of plume constituents. The ionization may be intense if the flame contains alkali metal particulates. Alkali metals have low ionization potential. The effect of high ionization is to decrease the radio refractive index of the flame to below unity (1). Considering the amount of ionization in the seat of the fire as measured and predicted in Chapters 3 to 6, the contribution of electrons to the radio refractivity cannot be neglected, more especially in the combustion zone of continuous flame region. Beyond the combustion zone, concentration of electrons falls rapidly mainly because of a decrease in temperature and recombination with incumbent ions. Some of the electrons attach to the soot macromolecules (e.g. in Latham, 1999) and as the electrons are not free anymore their effect on an impressed electric field is no longer significant.

A large number of gases (>100) exist in the smoke plume. The gases contribute to the radio refractivity through their dipole moments and their ability to be polarized by an impressed electric field. Apart from nitrogen of the ambient air and soot particles (carbon), water vapor (H_2O) content in the smoke plume is high. This is because water is one of the major products of combustion. In fact, the content can be as high as 1g of water vapor produced in every 1g of fuel burnt (Palmer 1981). Water vapor is a very important particulate in radio refractivity. Its dipole moment and polarization ability are very high compared to other common plume gases therefore has a significant contribution to bushfire plume radio refractivity. At high concentrations, its refractivity is dominant over that due to ionization in the bushfire flame. As for other particles such as nitrogen and carbon, low or absence of dipole moment and polarization ability make them less important than water at normal smoke concentrations.

7.3.1. Contribution of polarization and density gradients to radio refractivity of bushfire plume

Refractivity of air is constituent and frequency dependent. It takes different forms for visible and radio wave frequencies. At visible frequencies, refractivity of air has the form (Néda e*t al.* 2001):

$$N_{air} = \frac{P}{T}\left(776.2 + 4.36 \times 10^{-8} \kappa^2\right) \qquad \text{(Equation 7.18)}$$

Where: P = atmospheric pressure
T = temperature
κ = visible light wave number.

At radio wave frequencies up to 20GHz, equation 7.18 takes a form that is frequency independent but dependent on the constituents more especially water vapor (Thayer, 1974 and Gossard, 1977).

Bushfire smoke is made up products of vegetation combustion, which are primarily water vapor (H_2O), carbon monoxide (CO) and carbon dioxide (CO_2). Nitrogen (N_2) from the air and other by-product of incomplete combustion form a significant portion of the mixture. Oxygen (O_2) is also present in significant quantities due to the entrainment of ambient air into the smoke column as it rises up into the atmosphere.

Dry air is mainly composed of N_2, O_2, CO_2 and trace gases such as argon (Ar). From the principles of Classical Mechanics, polarizability (P(ω)) of a medium impressed upon by an electric field is given by Debye relation in the form (see Bean *et al.*, 1966].

$$P(\omega) = \frac{4N_a \pi}{3}\left[\alpha_0 + \frac{\mu^2}{3kT}\left(\frac{1}{1+i\omega\tau}\right)\right] \qquad \text{(Equation 7.19)}$$

Where: ω = electric field frequency,
τ = relaxation time of the molecules to return to their random distribution after an impressed electric field is removed
α_0 = polarization factor for a plume gas,
μ = electric moment dipole of the plume gas,
k = Boltzmann's constant,
N_a = Avogadro's constant,
T = plume temperature.

Polarizability is also related to the dielectric permittivity (ε) of a gas by the relation:

$$P(\omega) = \left(\frac{\varepsilon - 1}{\varepsilon + 2}\right)\left(\frac{M}{\rho}\right) \qquad \text{(Equation 7.20)}$$

Where : M and ρ = Molecular weight and density of a gas

Therefore Equation 7.19 can be written as:

$$\frac{\varepsilon - 1}{\varepsilon + 2} = \frac{4N_a \pi\rho}{3M}\left[\alpha_0 + \frac{\mu^2}{3kT}\left(\frac{1}{1 + i\omega\tau}\right)\right] \qquad \text{(Equation 7.21)}$$

At frequencies less than 100GHz, $\omega\tau \ll 1$ (Bean *et al*.) and for most gases, $\varepsilon \cong 1$, therefore Equation 7.21 can be approximated to;

$$\varepsilon - 1 = \frac{4N_a \pi\rho}{M}\left[\alpha_0 + \frac{\mu^2}{3kT}\right] \qquad \text{(Equation 7.22)}$$

Assuming that air and thermal plume behave ideally, pressure of a specific volume is related to absolute temperature by,

$$P = \rho RT \qquad \text{(Equation 7.23)}$$

Substituting Equation 7.23 into Equation 7.22 then we have,

$$\varepsilon - 1 = \frac{4N_a \pi P}{RT}\left[\alpha_0 + \frac{\mu^2}{3kT}\right] \qquad \text{(Equation 7.24)}$$

A compact form of Equation 7.24 can be written as;

$$\varepsilon - 1 = \frac{k_{a/p} P}{T} \qquad \text{(Equation 7.25)}$$

Where $k_{a/p}$ is constant for air or thermal plume.

As the thermal plume and air are composed of many gases, the constant $k_{a/p}$ can be broken down to account for each constituent, each having its own constant. Therefore Equation 7.25 can be written as;

$$\varepsilon - 1 = \sum_{1}^{r} \frac{k_{gr} P_{gr}}{T} \qquad \text{(Equation 7.26)}$$

Where: k_{gr} = constant for air or plume gas constituent

P_{gr}, = its partial pressure.

Permittivity (ε) is related to refractive index by the relation: $\varepsilon - 1 = n^2 - 1$. Using binomial expansion, $\varepsilon - 1 \approx 2(n-1)$.

Therefore Equation 7.26 becomes,

$$n - 1 = \frac{2\pi\pi_{a} P}{RT} \sum_{1}^{r} \left[\alpha_{0r} + \frac{\mu_r^2}{3kT} \right] \qquad \text{(Equation 7.27)}$$

In modified refractivity units (N), Equation 7.27 can be expressed as;

$$N_{p/a} = \frac{2.\pi.{}_{a}P}{RT} . 10^6 . \sum_{1}^{r} \left[\alpha_{0r} + \frac{\mu_r^2}{3kT} \right] \qquad \text{(Equation 7.28)}$$

For temperature range of 294 to 522 K (Bean *et al.,* 1966), refractivity of air takes the form (Solheim *et al*.1999):

$$N_{p/a} = 77.6 \frac{P_d}{T} + 64.8 \frac{P_{wv}}{T} + \left(3.776 \text{ x } 10^5\right) \frac{P_{wv}}{T^2} \qquad \text{(Equation 7.29)}$$

Where: P_d = hydrostatic pressure in millibars

P_{wv} = partial pressure of water vapor in millibars.

At approximately 300 K, Equation 7.29 reduces to (Gossard, 1977):

$$N_{p/a} = 77.6 \frac{P_d}{T} + \left(3.73 \text{ x } 10^5\right) \frac{P_{wv}}{T^2} \qquad \text{(Equation 7.30)}$$

Equation 7.30 is normally written as (Bean *et al.* 1966 and Burrows 1968);

$$N_{p/a} = \frac{77.6}{T}\left[P_d + 4810\frac{P_{wv}}{T}\right] \qquad \text{(Equation 7.31)}$$

In Equation 7.31, 77.6 is k_a for dry air which is mainly nitrogen (78%) and oxygen (≅21%). In the thermal plume, where temperatures can be more than 522 K, radio refractivity is calculated from Equation 7.28.

7.3.2. Contribution of ionization to radio refractivity of bushfire plume

Refractive index of the flame is related to the radio wave phase shift per meter by the equation;

$$n_f = \frac{c}{\omega}\beta_f - i\frac{c}{\omega}\alpha_f \qquad \text{(Equation 7.32)}$$

Where n_f, c, ω, β_f , α_f are refractive index of the flame, speed of light, phase and attenuation constants of an electromagnetic wave due to the flame. Phase shift and attenuation per unit length induced by weakly ionized plasma such as a bushfire is expressed by Akhtar *et al.* 2003 as;

$$\beta_f = \frac{\omega}{c}\left\{\frac{1}{2}\left(1-\frac{\omega_p^2}{\omega^2+\varphi_{eff}^2}\right)+\frac{1}{2}\left[\left(\underbrace{1-\frac{\omega_p^2}{\omega^2+\varphi_{eff}^2}}_{a}\right)^2+\left(\underbrace{\frac{\omega_p^2}{\omega^2+\varphi_{eff}^2}\frac{\varphi_{eff}}{\omega}}_{b}\right)^2\right]^{1/2}\right\}^{1/2}$$

(Equation 4.10)

$$\alpha_f = \frac{\omega}{c}\left\{-\frac{1}{2}\left(1-\frac{\omega_p^2}{\omega^2+\varphi_{eff}^2}\right)+\frac{1}{2}\left[\left(\underbrace{1-\frac{\omega_p^2}{\omega^2+\varphi_{eff}^2}}_{a}\right)^2+\left(\underbrace{\frac{\omega_p^2}{\omega^2+\varphi_{eff}^2}\frac{\varphi_{eff}}{\omega}}_{b}\right)^2\right]^{1/2}\right\}^{1/2}$$

(Equation 4.11)

For frequency range from HF to UHF and considering that the wildfire flame is weakly ionized with electron densities up to 10^{16} m^{-3} and highly collisional (collision frequency in the range of 10^{11}-$10^{12}s^{-1}$), $Q_{eff} >> \omega > \omega_p$. In Equations 4.10 and 4.11, a >> b within the frequency range and therefore reduce to:

$$\beta_f = \frac{\omega}{c}\left(1 - \frac{\omega_p^2}{2\varphi_{eff}^2}\right) \qquad \text{(Equation 7.33)}$$

and

$$\alpha_f = \frac{\omega}{c}\left(-\frac{\omega_p^2}{2\omega\varphi_{eff}}\right) \qquad \text{(Equation 7.34)}$$

Therefore complex refractive index (Equation 7.32) due to the flaming part of the plume can be written as:

$$n_f = \left(1 - \frac{\omega_p^2}{2\varphi_{eff}^2}\right) - i\left(\frac{\omega_p^2}{2\,\omega.\varphi_{eff}}\right) \qquad \text{(Equation 7.35)}$$

Refractivity (N_f) is defined by, ((n_f -1) x 10^6). Refractivity in the flaming region of the bushfire plume can be expressed as:

$$N_{fl} = \left[-\frac{1}{2}\left(\frac{\omega_p^2}{\varphi_{eff}^2}\right) - i\left(\frac{\omega_p^2}{2\omega\varphi_{eff}}\right)\right].10^6 \qquad \text{(Equation 7.36)}$$

In general, radio refractivity for the bushfire plume can be given as:

$$N_{p/a} = \left\{\left[\frac{2.\pi.\ {}_aP}{RT} \cdot \sum_1^r\left[\alpha_{0r} + \frac{\mu_r^2}{3kT}\right] - \frac{1}{2}\left(\frac{\omega_p^2}{\varphi_{eff}^2}\right)\right] - i\left[\frac{\omega_p^2}{2\omega\varphi_{eff}}\right]\right\}.10^6 \qquad \text{(Equation 7.37)}$$

7.3.3. Thin biconcave thermal lens model for radio wave refraction

7.3.3.1. Temperature-height variation in a crown fire

The horizontal vortices that form at the edges of an intense line bushfire (Figure 7.9) emulate two cylinders, which form two curvatures of a biconcave lens. The bushfire plume provides a dielectric material for the lens configuration (in Figure 7.9). Temperature gradients that exist in the crown bushfire plume though complex can be modeled by appropriate equations in Section 7.2. Unlike when the fuel layer is thin, temperatures in the fuel stratum of a crown bushfire seem to rise steadily from a minimum value of about 300°C to a maximum value at near fuel-air interface within the fuel stratum. Beyond the fuel canopy, plume temperature falls exponentially with height until it reaches the ambient air temperature. To illustrate this, temperature data obtained during International Crown Fire Modeling Experiment (ICFME) for Plot 9 (Butler *et al.* 2004) is used. The data are from near ground level (3.1 m) to 13.2 m (above canopy). Beyond 13.2 m, an extrapolation of temperature was made using Weber *et al.*'s relation (Equation 7.5). The temperature-height variation up to 22m above ground level for the crown bushfire is shown in Figure 7.10. Plume constituents and temperature variation influence the refractivity of the plume. If we consider plume constituents with concentrations given by *nria* (see Table A2 in the Appendices), then its variation with height may behave as in Figure 7.11.

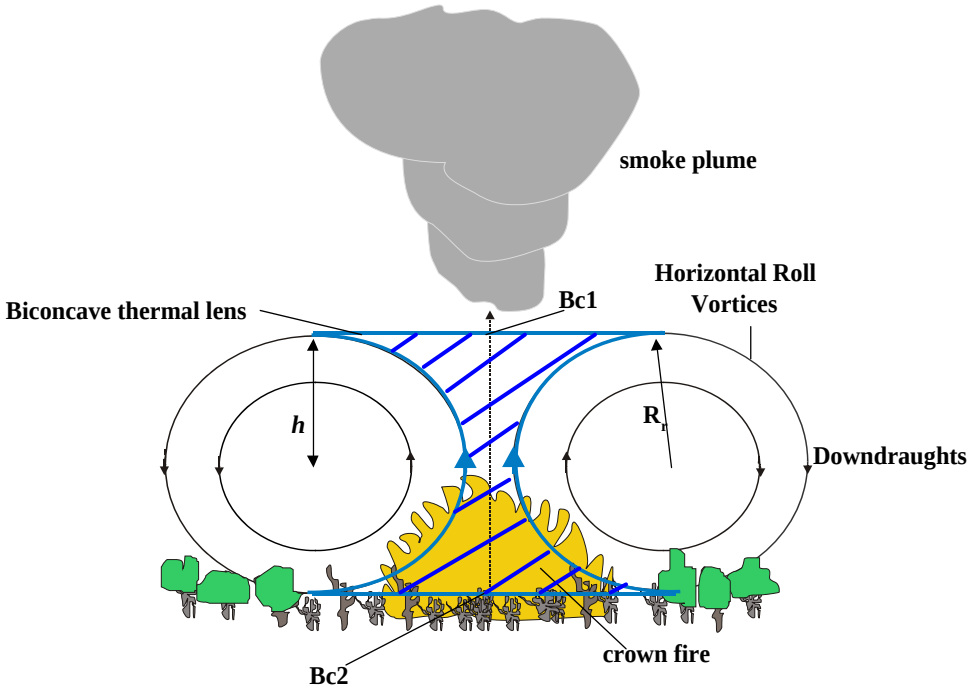

Figure 7.9. *Thermal biconcave lens formed by horizontal roll vortices*

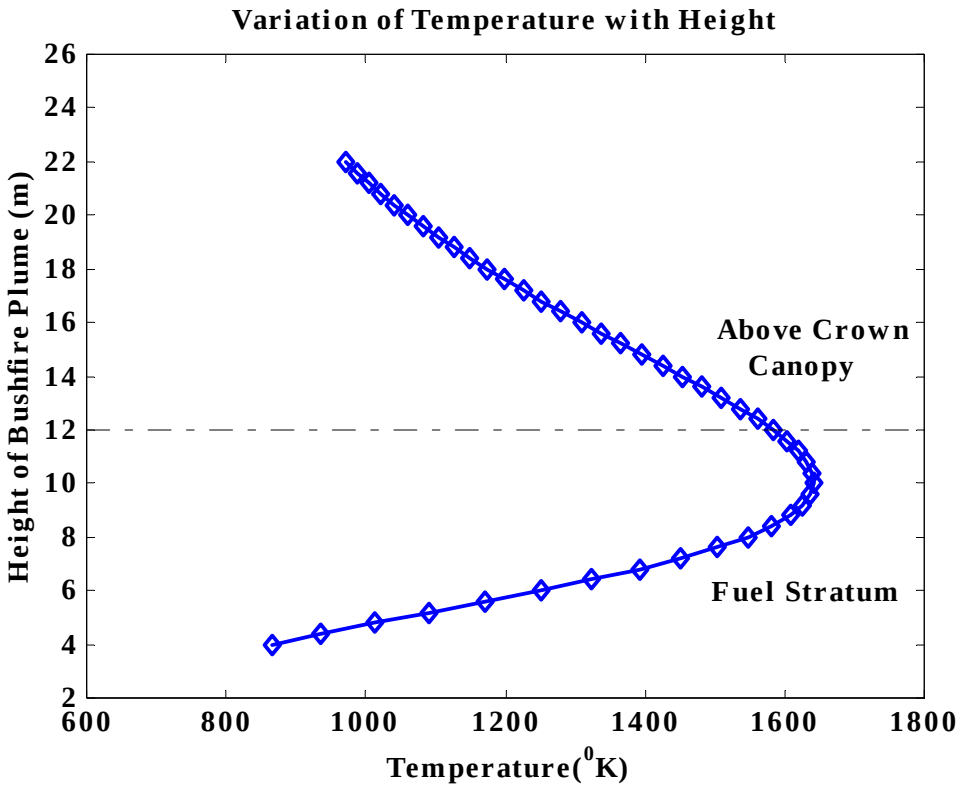

Figure 7.10. *Temperature variation with height for a crown fire* (adpt'd: Butler *et al*. 2004)

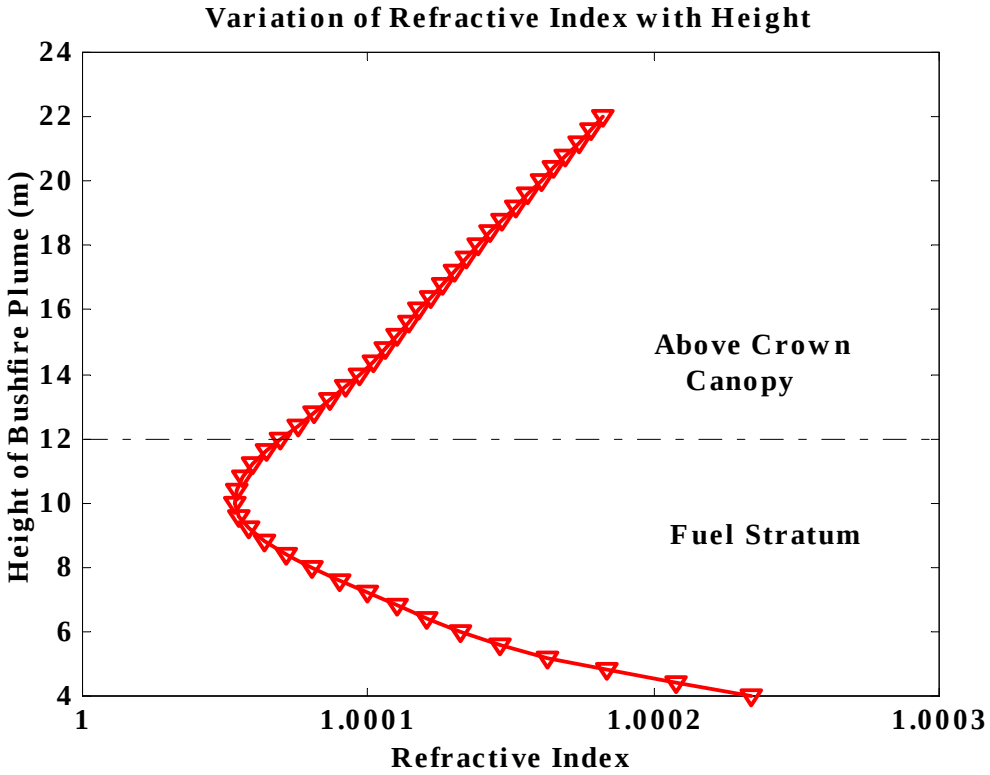

Figure 7.11. *Refractive index variations with height for a crown fire*

The configuration of the vortices and the plume form a biconcave thermal lens (shaded in blue). Its focal length is expected to be some kilometers away form the bushfire because the thermal lens is dielectrically "thin". According to the lens maker equation, the power of the vortex made lens (1/f) is given by:

$$\frac{1}{f} = \left(\mu_p - \mu_a\right)\left[\frac{1}{R_{r1}} + \frac{1}{R_{r2}}\right] \qquad \text{(Equation 7.38)}$$

Where: μ_a = radio refractive index of air,

μ_p = radio refractive index of the plume,

R_{r1}, R_{r2} = radius of curvature of a vortex,

f = focal length of the lens.

Assuming that the vortices are of the same radius, Equation 7.38 becomes;

$$\frac{1}{f} = \frac{2\left(\mu_p - \mu_a\right)}{R_{rc}} \qquad \text{(Equation 7.39)}$$

Where R_{rc} is the common radius for the vortices. A typical radius for a vortex is 200m e.g. Mack Lake crown fire (Haines, 1982). In Geometrical optics, rays projected parallel to the principal axis to a bi-concave lens are diverged by angle (δ) related by;

$$\delta = \tan^{-1}\left[\frac{h}{f}\right] \qquad \text{(Equation 7.40)}$$

Where h is the height relative to the principal axis of the lens. However the deviation angles are small, therefore equation 7.40 can be written as;

$$\frac{1}{f} = \frac{\delta}{h} \qquad \text{(Equation 7.41)}$$

Equating Equations 7.39 and 7.41 gives;

$$\delta = \frac{2h\left(\mu_p - \mu_a\right)}{R_{rc}} \qquad \text{(Equation 7.42)}$$

The implication of Equation 7.42 is that deviations are small at cooler parts of the thermal lens where μ_p are close to μ_a and high for the hottest part where μ_p is less than μ_a.

7.3.4. 2-D Ray-tracing scheme for radio wave propagation in a bushfire plume

In Geometrical Optics (GO), the propagation of an electromagnetic ray through a non-homogeneous medium is governed by the eikonal equation (Deschamps, 1972). The equation can derived from Maxwell equations and is given by Ling *et al.* 1991 as:

$$\frac{d}{ds}\left(n\hat{t}\right) = \nabla n \qquad \text{(Equation 7.43)}$$

Where n, s and $\hat{t}$ are refractive index, arc length along the ray trajectory and unit tangent vector respectively. The solution to this equation gives the trajectory of the radio ray. In most cases this equation is solved numerically. The common method is finite differencing (e.g. Ling *et al.*). The solution to the eikonal equation using finite differencing gives the solution:

$$n(\vec{r} + \Delta\vec{r})\hat{t}(\vec{r} + \Delta\vec{r}) = n(\vec{r})\hat{t}(\vec{r}) + \Delta s \nabla n(\vec{r} + \Delta\vec{r}/2) \qquad \text{(Equation 7.44)}$$

Once the position and the direction of a ray are given at $\vec{r}$, its trajectory can be determined in subsequent positions. Using Fermat's principle phase and the intensity of the radio ray can also be determined from the following equations (Ling *et al.*):

$$k_0\left[S(P_1) - S(P_2)\right] = k_0 \int_{p_1}^{p_2} n\,ds \qquad \text{(Equation 7.45)}$$

and

$$\vec{E}(P_2) = \bar{e}_2 \vec{E}(P_1)\sqrt{\frac{n_1}{n_2}}(DF)\exp\left\{-jk_0\left[S(P_1) - S(P_2)\right]\right\} \qquad \text{(Equation 7.46)}$$

Where k_0, DF, n_n, $\vec{E}(P_n)$ are free space wave number, Divergence factor, refractive index at point *n*, and electric field at point *n*.

Divergence factor is given by the following equation:

$$DF = \exp\left\{-\frac{1}{2}\int_{p_1}^{p_2}(\nabla.\hat{t})ds\right\} \qquad \text{(Equation 7.47)}$$

This factor accounts for the spreading of the ray tube.

7.3.4.1. Graphical ray tracing method.

Unlike other methods, Ling *et al.*'s method has an advantage of not relying on an analytical refractive index profile such as those developed by Marchand 1972 and Streifer *et al*. 1971. However, this method is rigorous and relies on solving the ordinary differential equations by finite differencing scheme. A much simpler method is that developed by Richerzhagen, (1996). This method combines the finite element and ray tracing techniques. Though this method can be used for an arbitrary refractive index profile, it has the disadvantage of assuming planar stratification. A method that does not assume any stratification is discussed below. Its strength depends on the calculation of the gradient in the direction of the ray trajectory.

7.3.4.2. A 2-D ray tracing procedure

A ray is traced in small steps (segments) through a medium of inhomogeneous refractive index. The ray is projected horizontally or any direction with respect to the horizontal into the medium. The unit vector of the ray segment (r_u) is determined as it propagates through the medium.

The head of the ray segment determines the refractive index of a medium in which the next ray segment will be travelling. The refractive index of the starting ray segment is assumed known (n_0). Figure 7.12 shows the ray tracing procedure. At the end of the ray segment a vector normal to a surface of constant refractive index at that point is calculated. The normal at the end of the ray segment is a gradient in refractive index at the point. In 2D, a gradient of refractive index is calculated from the relation:

$$\nabla n = \vec{i}\frac{\partial n}{\partial x} + \vec{j}\frac{\partial n}{\partial y}$$

Where $\frac{\partial n}{\partial x}$ and $\frac{\partial n}{\partial y}$ are x and y derivatives. The derivatives are calculated from the following expression, e.g in x-direction;

$$\frac{\partial n(x,y)}{\partial x} = \frac{n\big((x+\Delta s),y\big) - n\big((x-\Delta s),y\big)}{2\Delta s} \qquad \text{(Equation 7.48)}$$

Where Δs is a very small step or offset point either side of a ray head. The y derivate can be calculated in a similar way as in Equation 7.50. Angles of incidence are determined from the dot product of r_u and gradient unit vector (g_u). From Figure 7.12, angle of incidence (Φ_i) is the sum of α and β. Angle of refraction (Φ_r) is calculated from Snell's law:

$$\Phi_r = \arcsin\left[\frac{n_{\rho-1}}{n_\rho}\sin(\Phi_i)\right] \qquad \text{(Equation 7.49)}$$

Where $n_{\rho-1}$ and n_ρ are the refractive indices in the trajectory of the previous and present segments. Angle of refraction is also the sum of α, β and δ. The increment in the horizontal and vertical direction are given by r.cos(α+δ) and r.sin(α+δ) respectively.

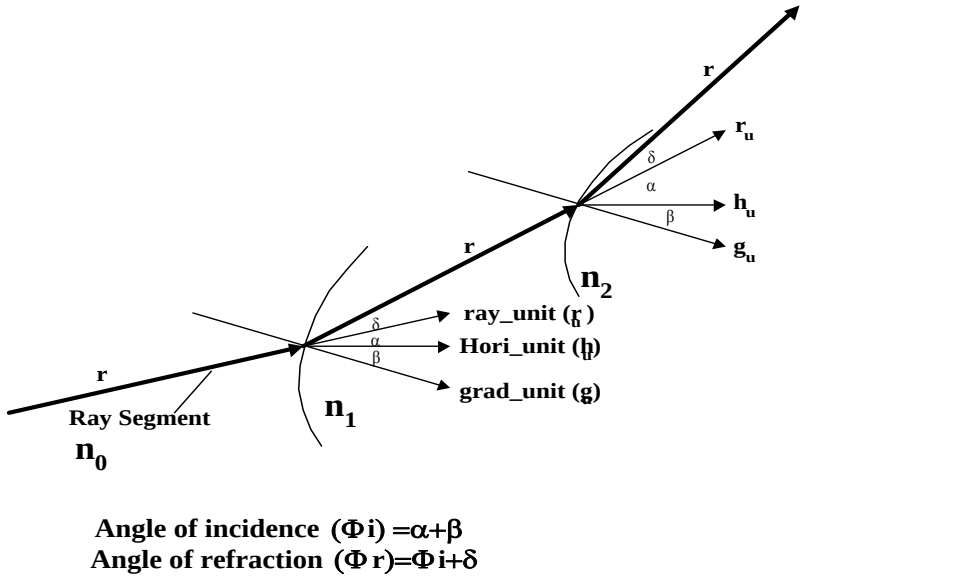

Figure 7.12. *A ray trace through a non-homogeneous plume*

7.3.4.3. Validation of the 2-D Ray Tracing Scheme

A dielectric pothole with rapidly varying refractive index with radial symmetry was used to validate the 2-D ray-tracing scheme. The pothole's refractive index (n(ρ)) varies as:

$$n(\rho(= \begin{cases} \sqrt{0.75\left[1 - \frac{1}{3}\cos\left(\frac{\pi\rho}{10}\right)\right]}, & \rho < 10 \\ 1, & \rho > 10 \end{cases} \qquad \text{(Equation 7.50)}$$

Where ρ is the radial distance from the center of the pothole calculated from the x and y coordinate points and is given by;

$$\rho = \sqrt{x^2 + y^2} \qquad \text{(Equation 7.51)}$$

The permittivity at the center of the pothole is $\sqrt{\frac{1}{2}}$ and is shown in Figure 7.13.

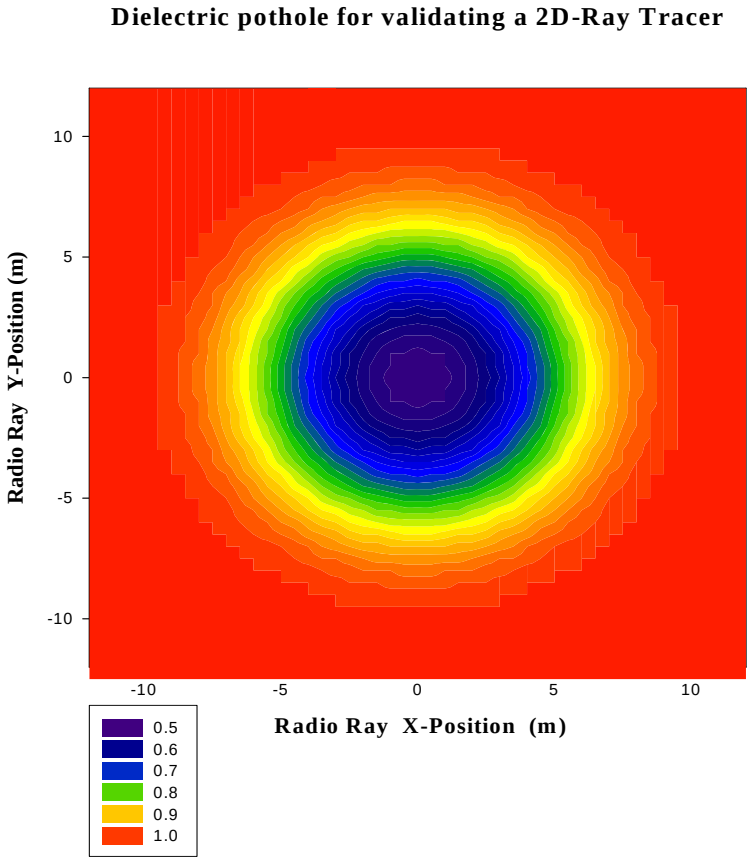

Figure 7.13. *A dielectric pothole with variable refractive index*

A similar structure was used by Ling *et al.* to validate their ray-tracing scheme. Rays that pass through the center (0,0) and edge (0,10) are not deflected, as expected. Figs 7.14a and 7.14b show the validation results. Deviations increase from center (Y-position =0 to Y-Position = 10. The results are very similar to those of Ling *et al.*

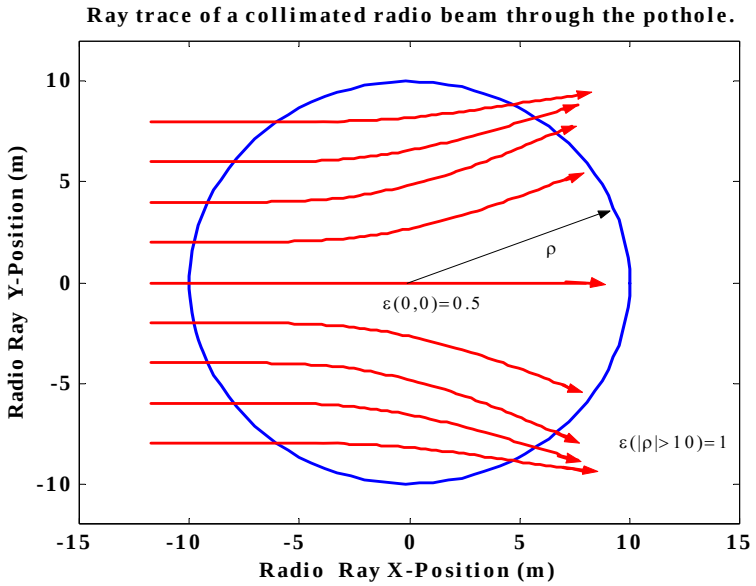

Figure 7.14a Rays (excluding rays at edges) refraction in a dielectric pothole

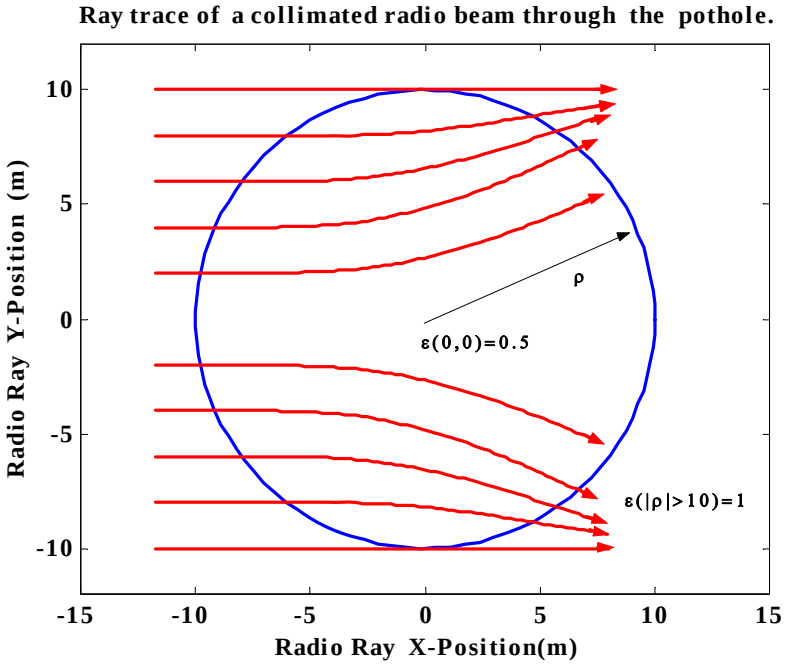

Figure 7.14b Rays (excluding ray at center) refraction in a dielectric pothole

7.4. Numerical Results and Discussions

7.4.1. Thermal biconcave lens model.

7.4.1.1. Application of the thermal lens model to Mack Lake crown fire

The thermal lens model is applied to predict radio wave deviation in a crown fire that occurred in the Mack Lake in Huron National Forest, Michigan, USA (Haines, 1982). The fire consumed 10040 ha of jack pine forest (height: 6–18 m) and also created crown streets 11km long and maximum width of 200m. The maximum distance between streets was observed to be 850m. The fire behavior is given in Table 7.1

Table 7.1 *Mack Lake crown fire behavior and horizontal roll vortex properties*

Range of RoS (m/s)	Range of Flame Height (m)	Range of Roll radius(m)	Range of Fireline Intensity (MWm^{-1})
0.04-3.14	10-25	11-200	1.83-103

Equation 7.42 gives divergence as;

$$\delta = \frac{2h(\mu_p - \mu_a)}{R_{rc}} \qquad \text{(Equation 7.42)}$$

For a thermal cell, the ratio of h and R_{rc} is approximately 1.6 (Burrows, 1984), therefore Equation 7.42 can be simplified to:

$$\delta = 3.2 \times 10^6 \times \left|\mu_p - \mu_a\right| \ (\text{mrads}) \qquad \text{(Equation 7.52)}$$

Radio refractive index of air at standard temperature and pressure is 1.000272 (Burrows, 1984).

Mack Lake crown bushfire had a wide range of behavior, and ICFME's Plot 9-crown fire is taken as a case study. Plot 9's fire-intensity was about 90 MWm^{-1}, RoS and observed flame heights were 1.16 m/s and 20-30m respectively. An HRV radius of 20m, a range of potassium content in the jack pine of 0.9-2.0% and fire behavior identical to that of Plot 9 are assumed and the divergence was calculated for the thermal lens.

The thermal lens model was run for a region 4 – 22 m above ground. The results are shown in Figure 7.15. For potassium content of 0.5%, deviation increases from 1.20×10^{-4}rad at 4.0m to a maximum of 6.80×10^{-4} rad at 10.0 m. Deviation due a plume that contains 2.0% K followed a similar trend. It increased from minimum of 1.20×10^{-4} rad at 4.0 m to a maximum of 7.75×10^{-4} rad at 10.0 m.

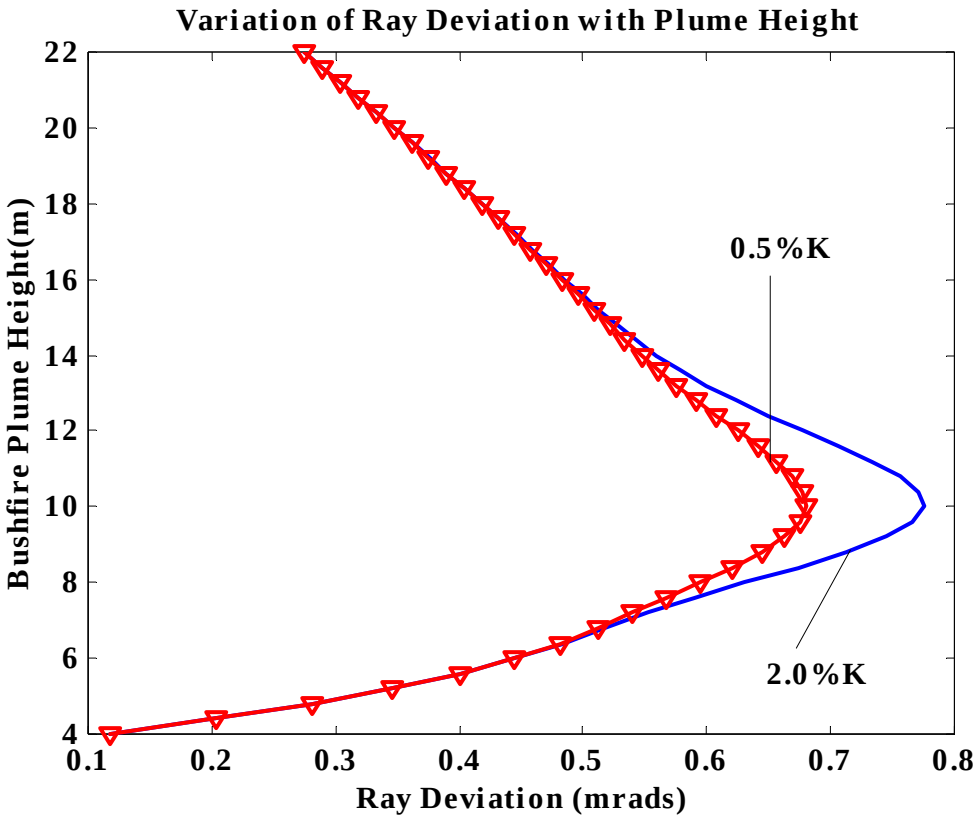

Figure 7.15. *Variation of ray divergence with height at 0.5 and 2%K*

7.4.2. Radio ray tracing through a typical Eucalyptus forest crown bushfire

Most bushfires occur under stable atmospheric conditions. Under these conditions, pressure gradient force balances gravity, thus the atmosphere is under hydrostatic balance;

$$\frac{dP}{dz} = -g\rho \qquad \text{(Equation 7.53)}$$

Assuming ideal gas behavior of the atmospheric air, the density of the air is related to pressure by the ideal gas equation, thus;

$$\rho = \frac{P}{RT} \qquad \text{(Equation 7.54)}$$

Substituting Equations 7.56 into 7.55 and re-arranging leads the hydrostatic balance to be represented as:

$$\frac{dP}{P} = \frac{-g}{RT}dz \qquad \text{(Equation 7.55)}$$

Temperature of atmospheric air decreases with height as;

$$T(z) = T_{sl} - \lambda z \qquad \text{(Equation 7.56)}$$

Where: T_{sl} = ambient temperature at z =0

λ = environmental lapse rate.

Substituting 7.58 into 7.57 and integrating over the entire height of the atmosphere gives:

$$P(z) = P_{sl}.e^{-\frac{g}{R}\int_0^{\infty}\frac{dZ}{T(z)}} \qquad \text{(Equation 7.57)}$$

Which simplifies to;

$$P(z) = P_{sl}\left[1 - \frac{\lambda z}{T_{sl}}\right]^{\frac{g}{R\lambda}} \qquad \text{(Equation 7.58)}$$

A typical eucalyptus forest (Jarrah) crown bushfire is that shown in Figure 7.16 below. Crown bushfires more intense (≈100 MWm^{-1}) that the one shown are known to occur in Mountain Ash forests in eastern Australia (Gill *et al.*, 1990).

Figure 7.16. *A 30m high flames in Crown fire burning through a 15-year-old jarrah forest in Western Australia.*

7.4.2.1. Crown bushfire behavior for the ray tracing scheme

A high intensity crown fire is considered to be able to burn in jarrah forest under steady state idealistic conditions. The crown fire behavior is given in Table 7.2 below. The data were chosen to replicate that given by de Groot *et al.* 2004 (for Plot 9) though there are some differences in wind behavior and fuel type and dimension. De Groot *et al.* collected the data on the crown fire behavior during the International Crown Fire Modeling Experiment (ICFME) which ran from 1997 to 2000 in jack pine-black spruce forest in Canada's Northwest Territories.

Some of the data were obtained from Butler *et al.*, 2004. Butler *et al.* also participated in the same experiment but reported on temperature and emissive power of the crown fire that occurred on Plot 9. Intensity of the crown fire was calculated from Byram's fire line relation, thus:

$$I_{crown} = Hw(RoS) \qquad \text{(Equation 4.17)}$$

Where: I_{crown} = crown fire intensity,
H = heat of combustion (18 000 kJ/Kg),
RoS = rate of spread,
w. = weight of the fuel consumed.

Crown flame depth (D_{crown}) was calculated from the ROS and average residence time, vis:

$$D_{crown} = RoS.t_r \qquad \text{(Equation 5.27)}$$

Where t_r is the flame residence time.

Table 7.2 *Crown bushfire behavior for the radio ray tracing experiment*

Avg. Intensity (I_{crown}) (kW/m)	Avg. RoS (m/s)	Avg Residence time(t_r) (s)	Avg. Canopy height (m)	Max. Flaming temp.(^{0}C)	Flame height(m)
89 681	1.16	30	12	1202	18

A slight ambient wind of about 0.5 m/s at 10 m height was assumed so that flame tilt is small and negligible. This is an idealistic situation as crown fires of this intensity often occurs in moderate to high wind velocities.

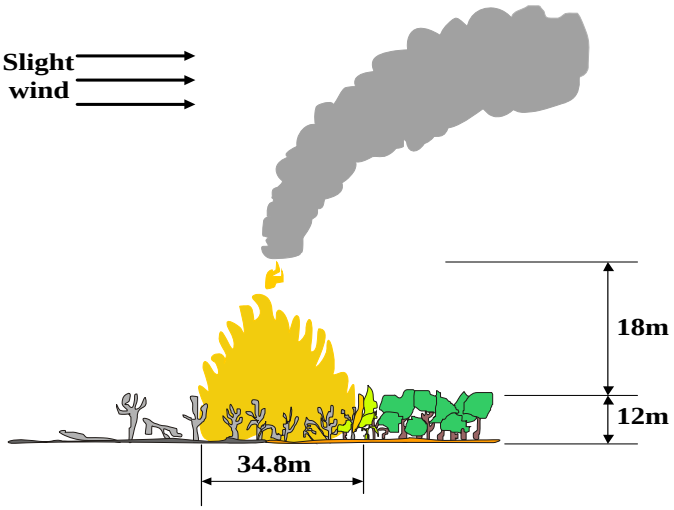

Figure 7.17. *Physical dimensions of the crown fire to used in the ray tracing simulation*

7.4.2.2. Physical properties of plume area considered for ray tracing

The ray tracing experiment considered the continuous flame region and part of the thermal plume region, thus from 12 m to 52 m above ground level. The flame is up 30 m above the ground and 20 m of the smoke plume was considered.

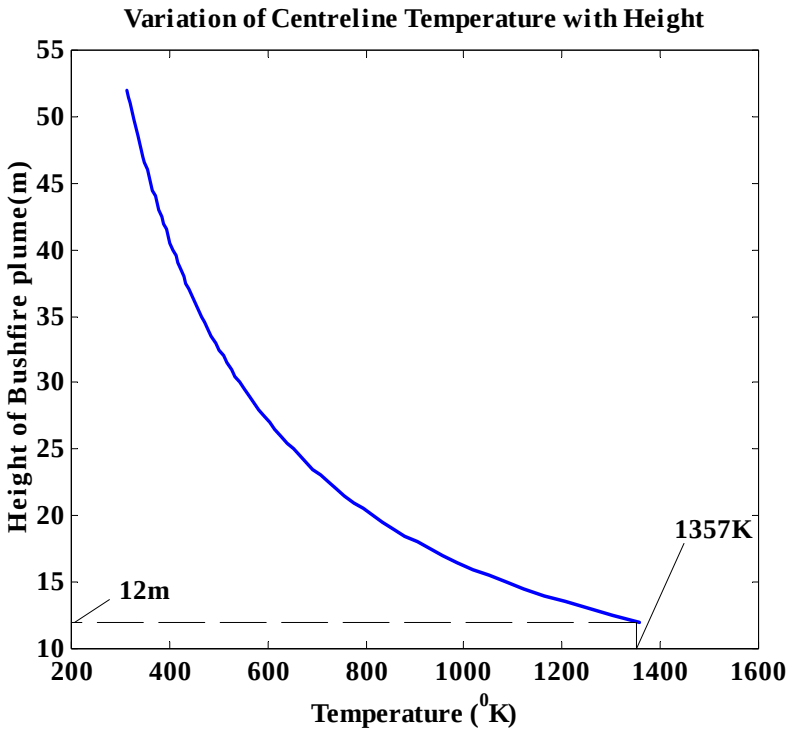

Figure 7.18. *Temperature variation in the region considered for ray tracing*

(a) Temperature and influence of constituents on refractive index variation in the plume

The temperature of the area considered ranged from 1357 K at 12m to 313 K at 52 m above ground level (Figure 7.18). It decreases exponentially as it is governed by the empirical Weber *et al.*'s relation. The temperature variation and plume constituents influence the variation of refractive index in the region considered. The influence of the constituents on the refractivity of the plume was explored by the use of the relations;

$$N_{p/a} = \left\{ \left[223\rho - \frac{1}{2}\left(\frac{\omega_p^2}{\varphi_{eff}^2} \right) \right] - i\left[\frac{\omega_p^2}{2\omega\varphi_{eff}} \right] \right\}.10^6 \qquad \text{(Equation 7.59)}$$

and

$$N_{p/a} = \left\{ \left[\frac{2.\pi._a P}{RT} \cdot \sum_1^r \left[\alpha_{0r} + \frac{\mu_r^2}{3kT} \right] - \frac{1}{2}\left(\frac{\omega_p^2}{\varphi_{eff}^2} \right) \right] - i\left[\frac{\omega_p^2}{2\omega\varphi_{eff}} \right] \right\}.10^6 \qquad \text{(Equation 7.36)}$$

Equation 7.59 assumes that the flame is dry, thus contains no water vapor. For ionization, potassium content of 2.7% is assumed. High temperatures in the combustion zone cause significant ionization of potassium. Refractive index variation in the plume was then deduced from (10^6 x N) +1. Electric dipole moments (μ_r) and polarization ability (α_{or}) of the dry air constituents at combustion temperatures obtained from Kuei-Chiao[a], 1970 and Kulemin[b] *et al.*, 1997 and are given in the Table 7.3.

Table 7.3 *Dipole moments and polarizabilities of plume gases(adapted from a and b)*

Combustion gas:	N_2	H_2O	CO	O_2	CO_2
Dipole Moment (μ_r)					
(Debye)	-	1.65[b]	0.112[b]	-	0.1[b]
Polarization Ability(α_{or})	1.76[a]-1.84[b]	1.5$_b$	1.95[a]-2.02[b]	1.6[a]	2.6[b]

The constants were used in equation (7.36) to calculate refractive index of the plume under the same conditions as in equation 7.59. Calculations reveal that refractive index values from equations 7.36 and 7.59 do not vary very much. They differ at most by 1 N-unit. Table 7.4 and Figure 7.19 show the variations.

Table 7.4 *A comparison of refractive index (n) derived from density and dipole moments*

Height (m)	12	22	32	42	52
n. (ρ derived)	0.999375	1.000094	1.000131	1.000165	1.000197
n (μ and α derived)	0.999376	1.000094	1.000131	1.000165	1.000197

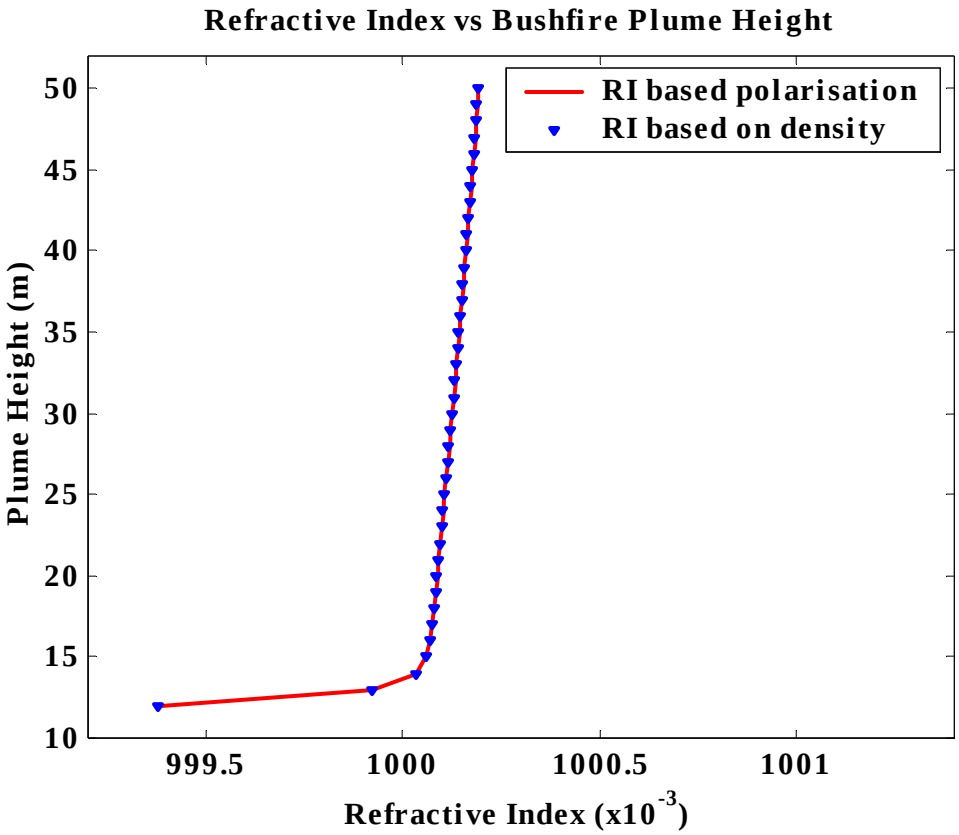

Figure 7.19. *Refractive indices (n) derived from plume density and polarisation*

This indicates that where the constituents of air do not differ very much from the ambient (dry), equation 7.59 is appropriate but where there is a difference equation 7.36 should be used and the electric dipole moments and polarizabilities of the constituent gases need to be known.

During *Flambeau project* (Palmer 1981), the air 2 m above ground was sampled for plume constituents. At maximum fire energy output, Palmer observed that the plume contained about 5.6% H_2O, 0.24% CO, and 0.25% CO_2 by volume. These concentrations decreased as the fire progressed until the fire stopped burning. At least 70% of the constituents can be assumed to be N_2 and the rest are carbon particulates (e.g. graphitic carbon) and hydrocarbon by-products. If the relative proportions of the gases are assumed to be representative of what is inside the plume, then the refractive index of the plume can be calculated using equation 7.36 and dipole and polarization ability data (Table 7.3).

(b) The effect of ionization on radio refractivity

If the plume is assumed to be wholly weakly ionized plasma, then equation 7.36 reduces to 7.35. With equation 7.35, it is observed that the influence of ionization at the plume centerline is only limited to a region below 16.0 m above ground level. Thus its refractivity (N) becomes zero (n =1) at height 16.0 m. This occurs when potassium content is at 2.0%. At 0.1% potassium content, refractivity reduces to zero at 15.5 m. This is because of low available potassium atoms for ionization. Figure 7.20 illustrates the reduction in height at which N is equal to 0 brought about by the reduction in potassium content.

Away from the centerline (say 5 m), at the same height as the centerline, the height at which refractivity becomes zero is reduced for respective potassium contents because of the influence of temperature. Temperatures are lower at the same height but some distance away from the centerline (Rayleigh profile influence). When reduction in height at which N=0 are compared with those at the centerline, reduction at the centerline are smaller. This is explained by the fact that ionization is not only a factor of potassium content but it is also related in a complex way with temperature. A decrease of 1m is observed 5 m away from the centerline compared to 0.5 m at the centerline of the plume. This is shown in Figures 7.21.

(c) The effect major plume constituents on radio refractivity

Apart from ionization, dipole moments and polarization ability of plume gases may also increase the radio refractivity of the plume. This means that height at which N is reduced to zero is decreased by the inclusion of the constituent in the refractivity equation. Figures 7.22, 7.23 and 7.24 show the decreases 2(Ia=14 m), 2.5, 2.5 for constituent compositions *nria*, *nrib* and *nric* respectively. The plume compositions *nria*, *nrib* and *nric* are given in the Table A2 in the appendix. Water is the very important constituent in the plume that affects radio refractivity significantly. The experiment has revealed that increasing the percentage of water 5-fold (*nrib* composition) increases the refractivity ($(n-1).\ 10^6$) of the plume by on average 2.74 times. Increasing the density of CO and CO_2 by six times, and H_20 by five times (*nric* composition) the concentration in *nria,* and decreasing the density N_2 by 0.82 the density in *nria* has an effect of increasing refractivity of *nria* nearly by the same amount as *nrib*. The effect is summarized in Table 7.5.

Table 7.5 *Plume properties at different heights above ground level*

Height above ground level(m)	Refractivity of *nria* ($H_{N=0}$ =14m) N-units	Refractivity of *nrib* ($H_{N=0}$=13.5m) N-units	Refractivity of *nric* ($H_{N=0}$ =13.5m) N-units
12	-2860.00	-2802.78	-2801.13
14	-50.02	24.74	26.72
22	95.87	281.51	284.66
32	205.83	504.74	509.29
42	295.00	777.02	783.74
52	392.00	1091.11	1098.03

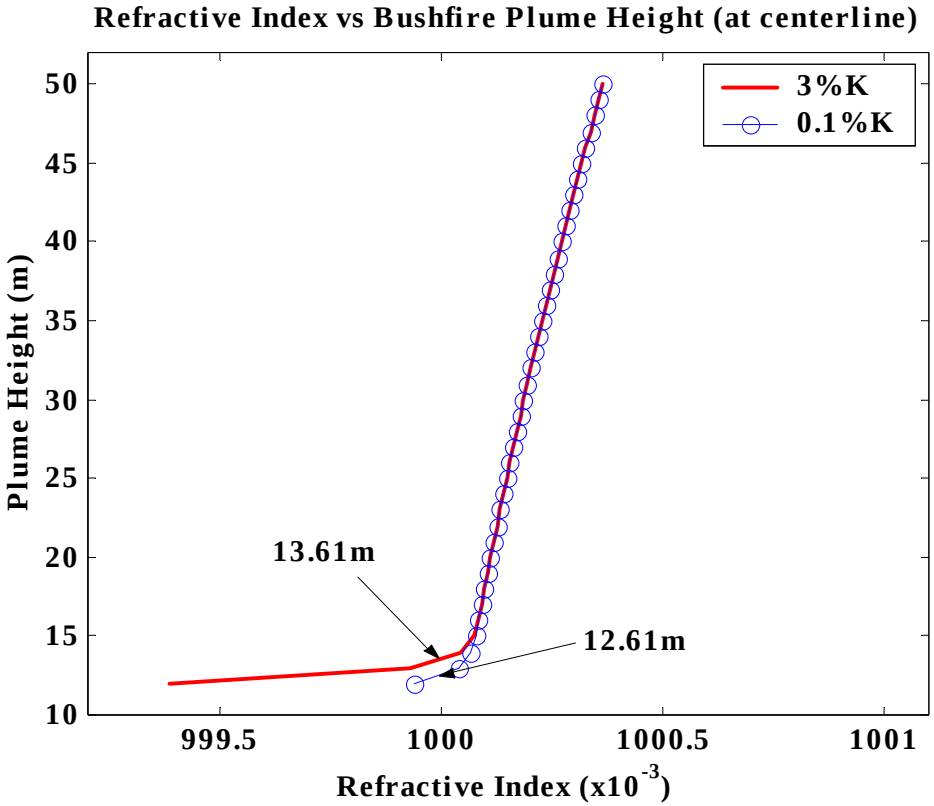

Figure 7.20. *Influence of K-content on the refractivity due to ionization only at centerline*

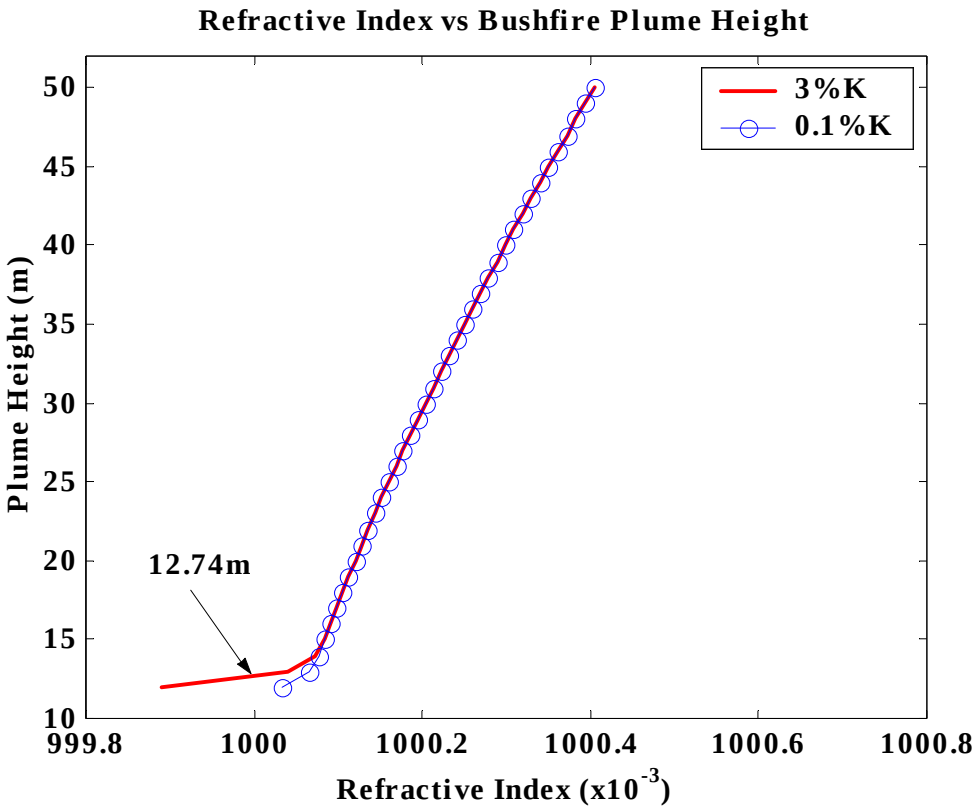

Figure 7.21. *Influence of distance away from centerline on the refractivity due to ionization*

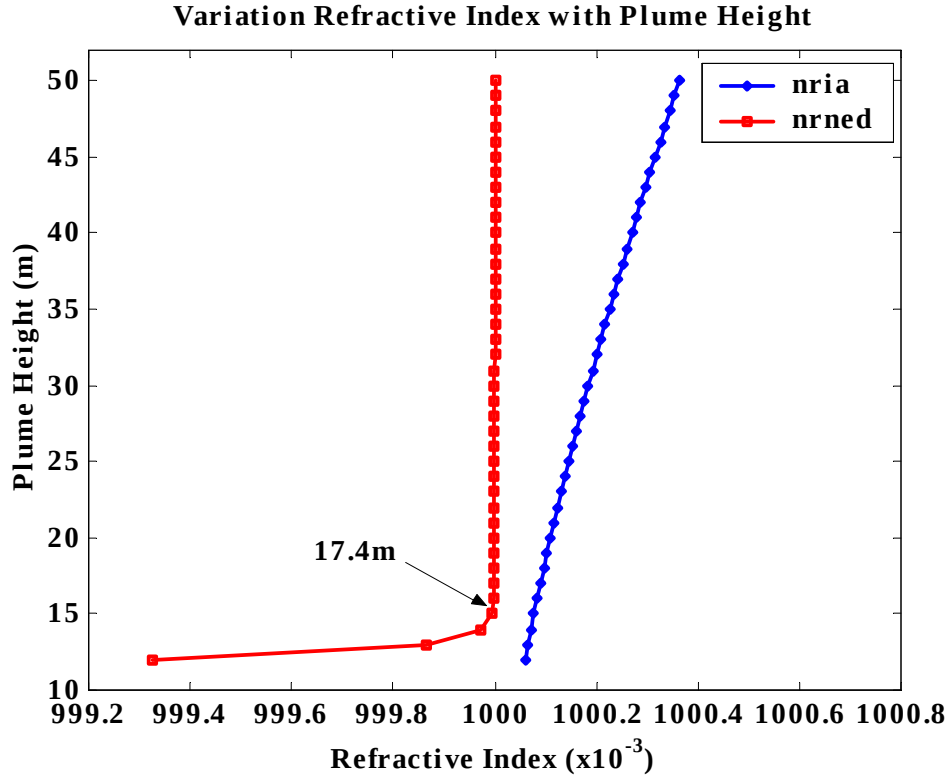

Figure 7.22. *Influence of plume gases on the radio refractivity at 2.0%K and nria*

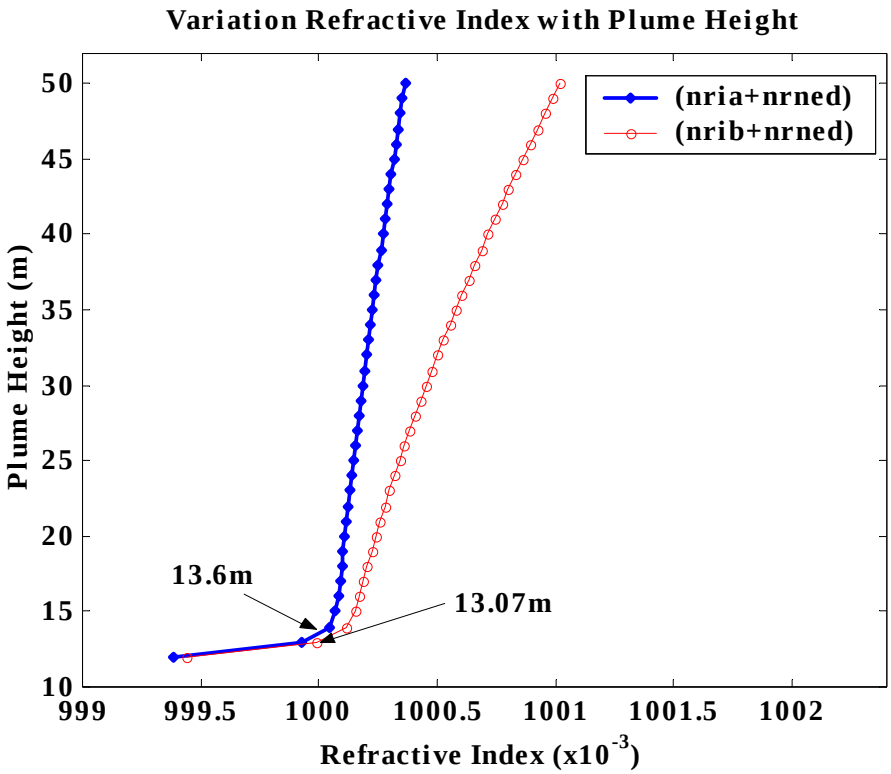

Figure 7.23. *Influence of plume gases on the radio refractivity at 2.0%K and nrib*

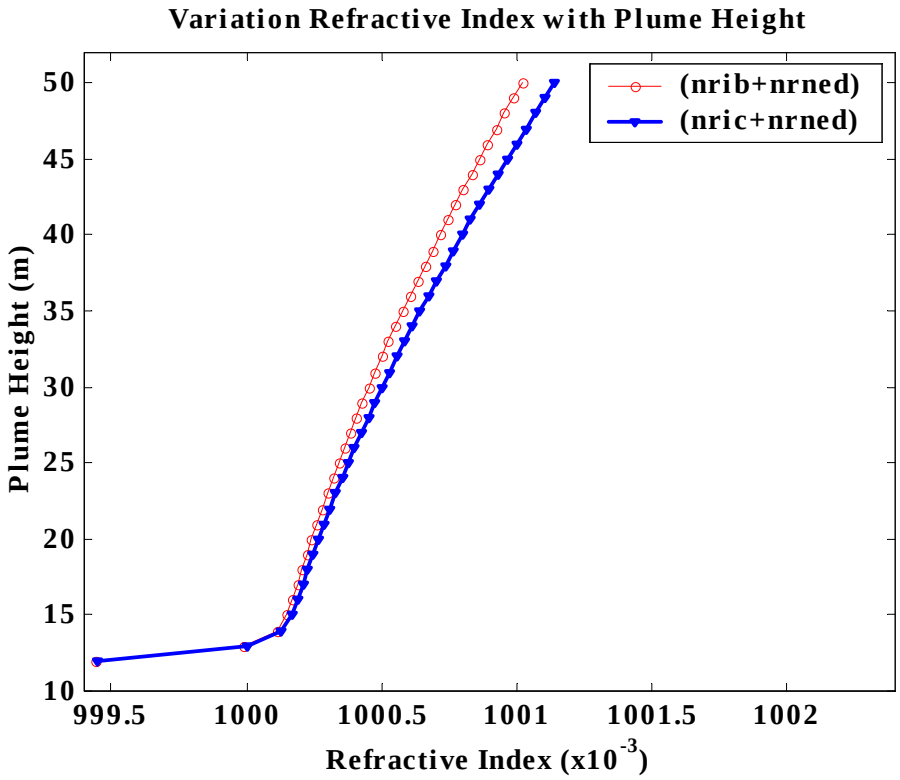

Figure 7.24. *Influence of plume gases on the radio refractivity at 2.0%K and nric*

7.4.3. Ray refraction in the bushfire plume

7.4.3.1. A weakly ionized plasma model

Disregarding the constituent particles in the plume, radio rays were observed to be refracted upwards. The refraction is higher in the lower part of the flame than at its tip. Over a distance of 48.25 m, a collimated beam 10cm wide incident at 13.8 m above ground is deviated 14.69 mm (for bottom ray (*br*)) to 12.44mm (for top ray (*tr*)) from their original path. The flame height is about 30m. The extent of ionization does not go beyond 16m; therefore at the tip of the flame radio rays are not refracted. Figures 7.25 and 7.26 show the radio wave refraction at 13.8 and 20.8 m for different densities of potassium.

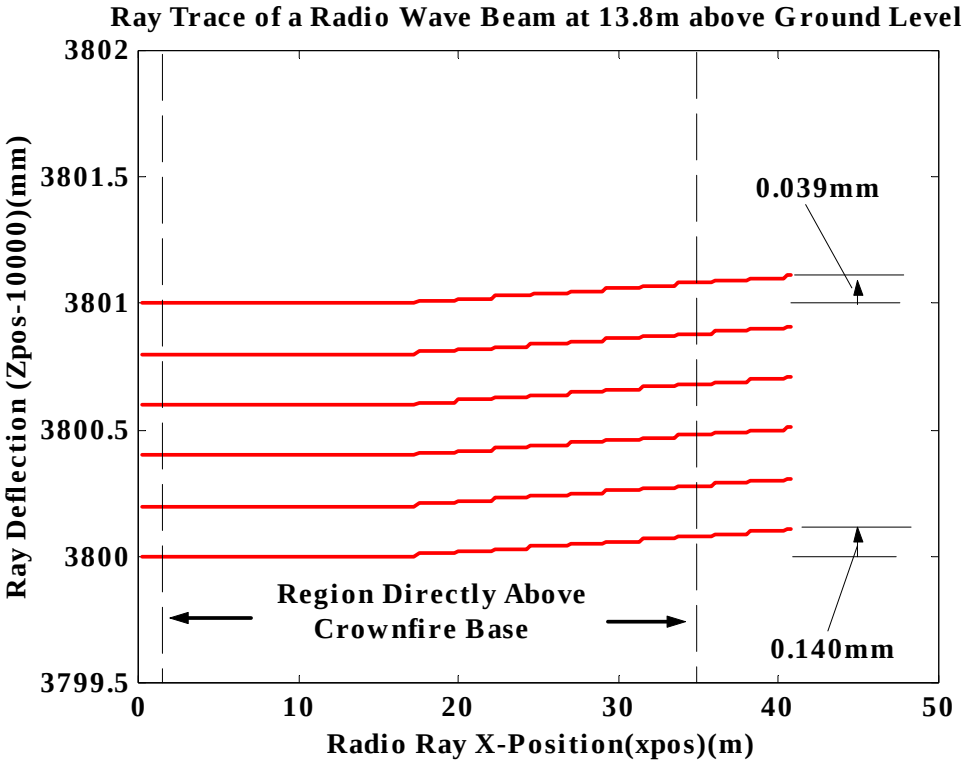

Figure 7.25(a). *Radio ray deflection at 13.8 due to ionization at 0.1%K*

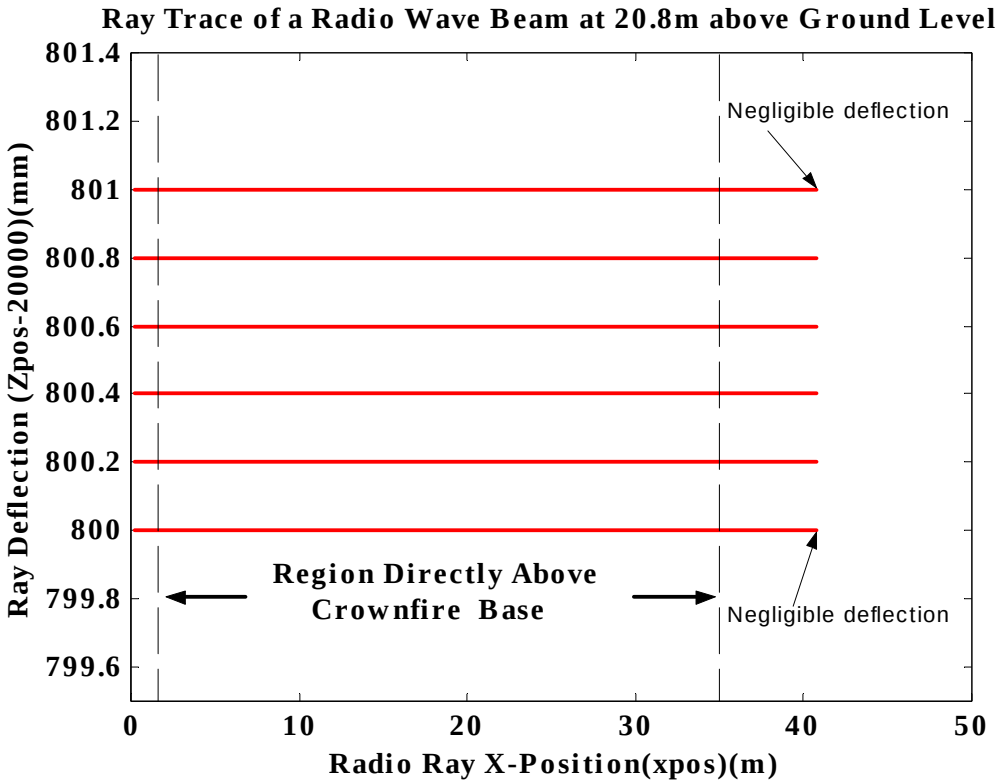

Figure 7.25(b). *Radio ray deflection at 20.8 due to ionization at 0.1%K*

7.4.3.2. Ray refraction due to nria and altitude correction term

A correction term (0.157 x *h* (altitude)) is often added to the refractivity equation to account for the curvature of the earth (Brooks *et al.* 1999). The factor has been added to the refractivity equation in the experiment.

Radio refraction of a collimated beam incident at 13.8 m above ground level show a deviation of 66.65 mm (for *tr*) to 66.42 mm (for *br*) over a distance of 48.25 m. This is more than five times that produced by ionization only (Figure 7.26). The deflection at 19.8 m height is significant and ranges from 34.11 mm (*br*) to 34.83 mm (*tr*). The deflection continues to fall with height to 16.23 mm (*tr*) to 16.25 mm (*br*) at 29.8 m above ground (Figure 7.27 and 7.28). Deflection in the thermal plume at 49.8 m is around 10.74 mm (tr)-10.76 mm (br) (Figure 7.29). This explained by the fact that the temperatures are low at this region.

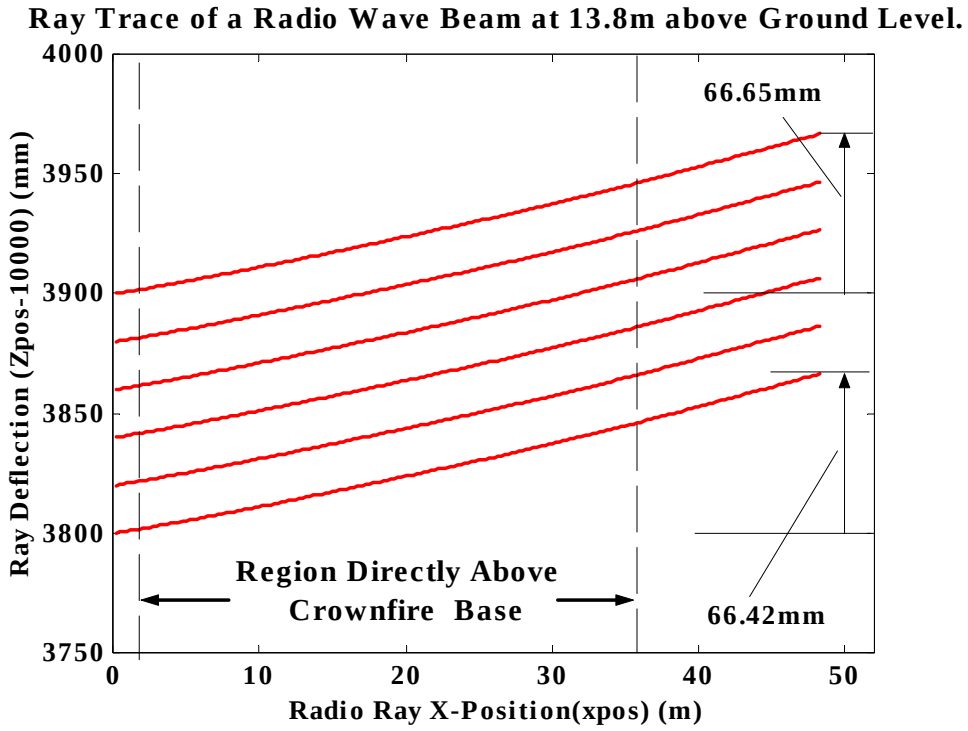

Figure 7.26. *Radio ray deflection at 13.8 due to(nria+ alti. correction)*

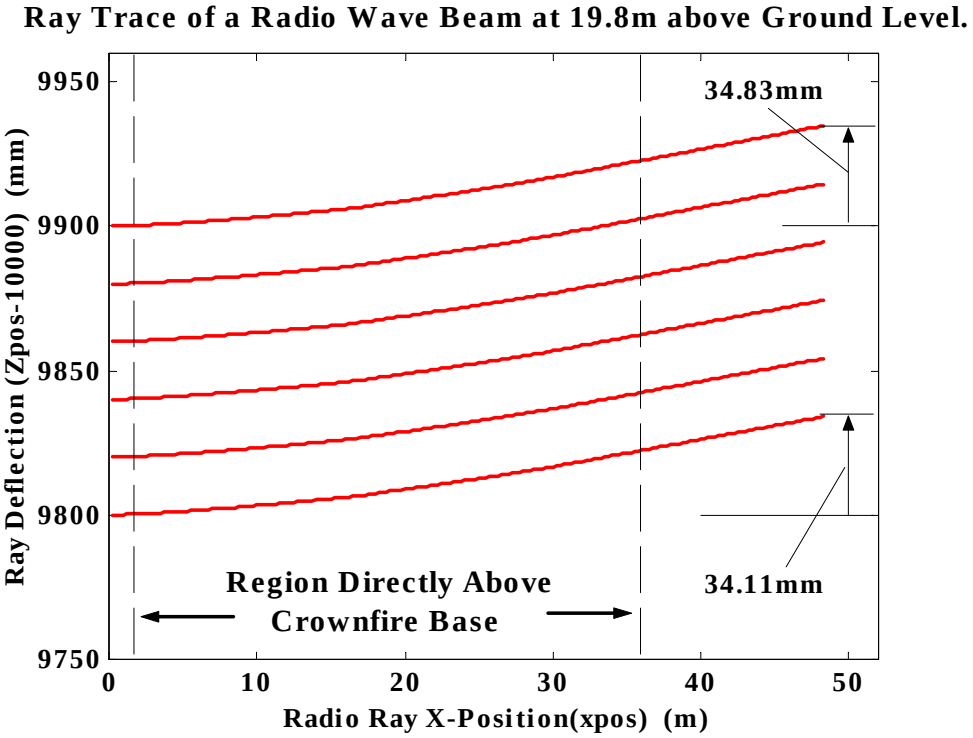

Figure 7.27. *Radio ray deflection at 19.8 due to (nria+ alti. correction)*

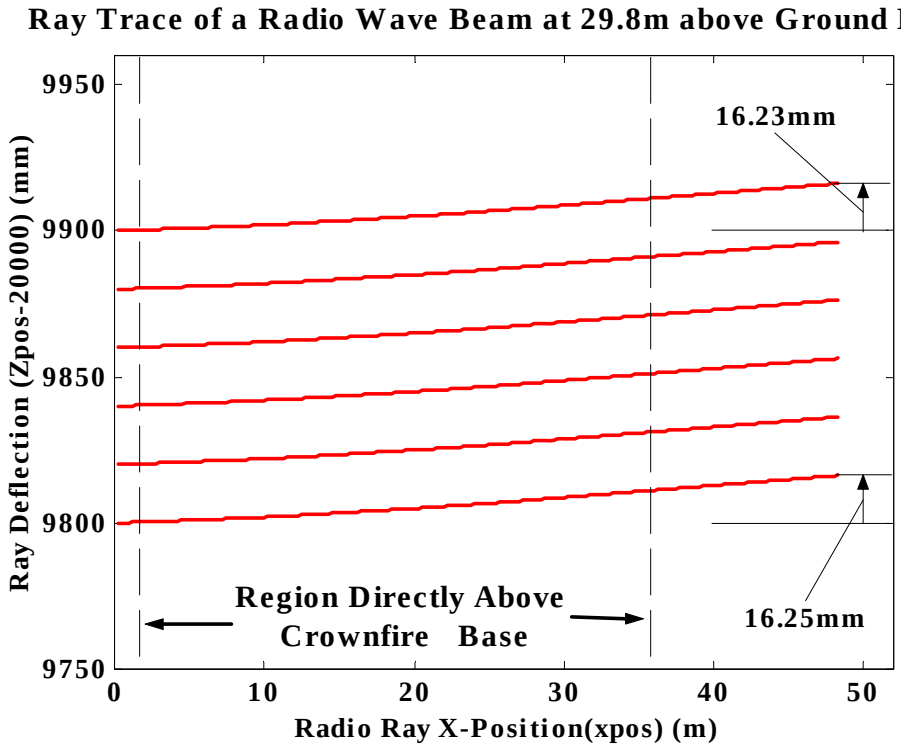

Figure 7.28 Radio ray deflection at 29.8 due to (nria+ alti. Correction)

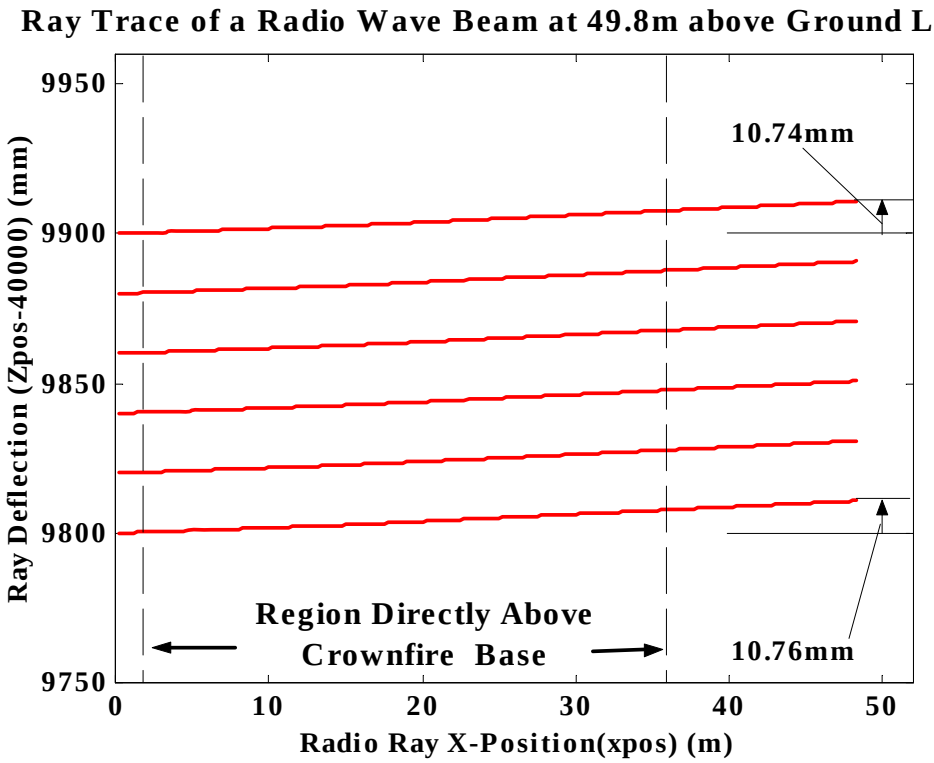

Figure 7.29. *Radio ray deflection at 49.8 due to (nria+ alti. Correction)*

7.4.3.3. Ray refraction due to the nria and ionization combined.

The combined effect of ionization and polarization produce a higher deflection than either one of them alone. The model predicts that a collimated beam incident at 13.8m above ground experiences a deviation of 81.46 mm (for *tr*) to 88.84 mm (Figure 7.30) over a distance of 48.25 m. This is more than six times than that produce by electrons and almost 1.3 times that produced by the gaseous constituents (H_2O, CO and CO_2) alone. At 19.8 m the deviations are predicted to be in the range that produced by the *nria* and altitude correction term because the of lack of influence due to ionization at this height. However, there are some differences in the refractivities. The deflection at 19.8 m height ranges from 34.11 mm (for *br*) to 34.83 mm (for *tr*) (Figure 7.31). The deflections at 29.8 m are to 16.23 mm (for *tr*) -16.2 mm (for *br*) (Figure 7.32). Deflection in the thermal plume at 49.8 m is around 10.74 mm (for *tr*)-10.76 mm (for *br*) (Figure 7.33).

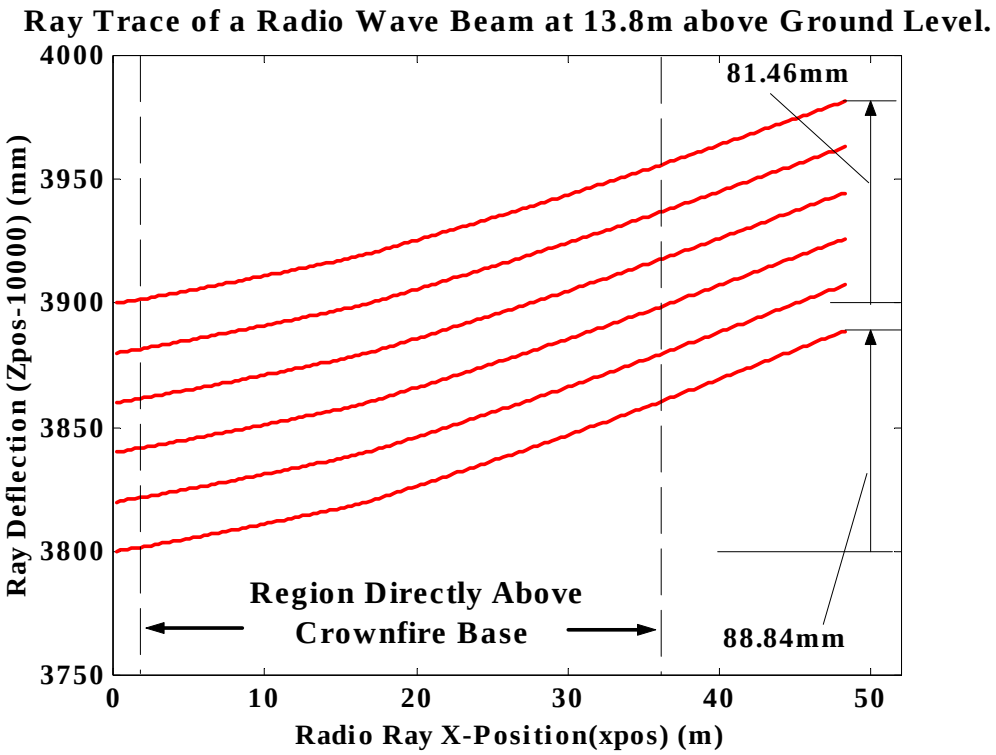

Figure 7.30. *Radio ray deflection at 13.8m due to (nria+ alti. Correction) and 0.1%K*

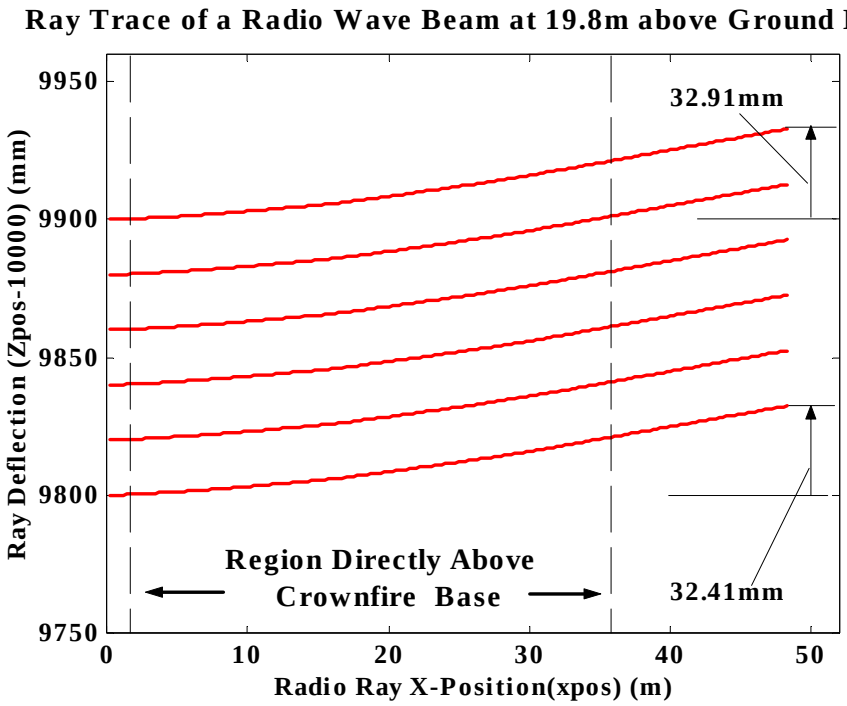

Figure 7.31. *Radio ray deflection at 19.8m due to (nria+ alti. Correction) and 0.1%K*

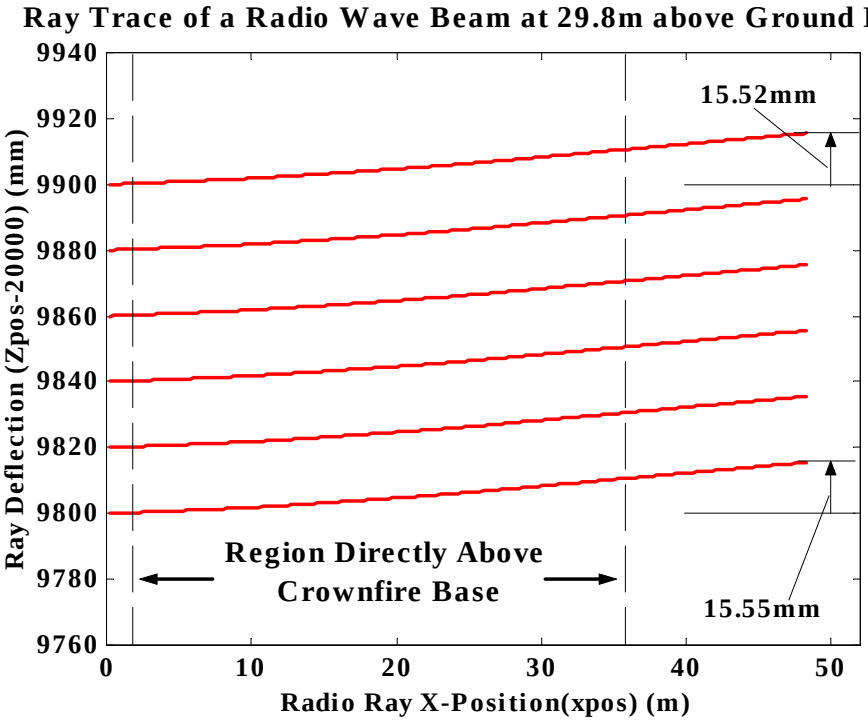

Figure 7.32. *Radio ray deflection at 29.8m due to (nria+ alti. Correction) and 0.1%K*

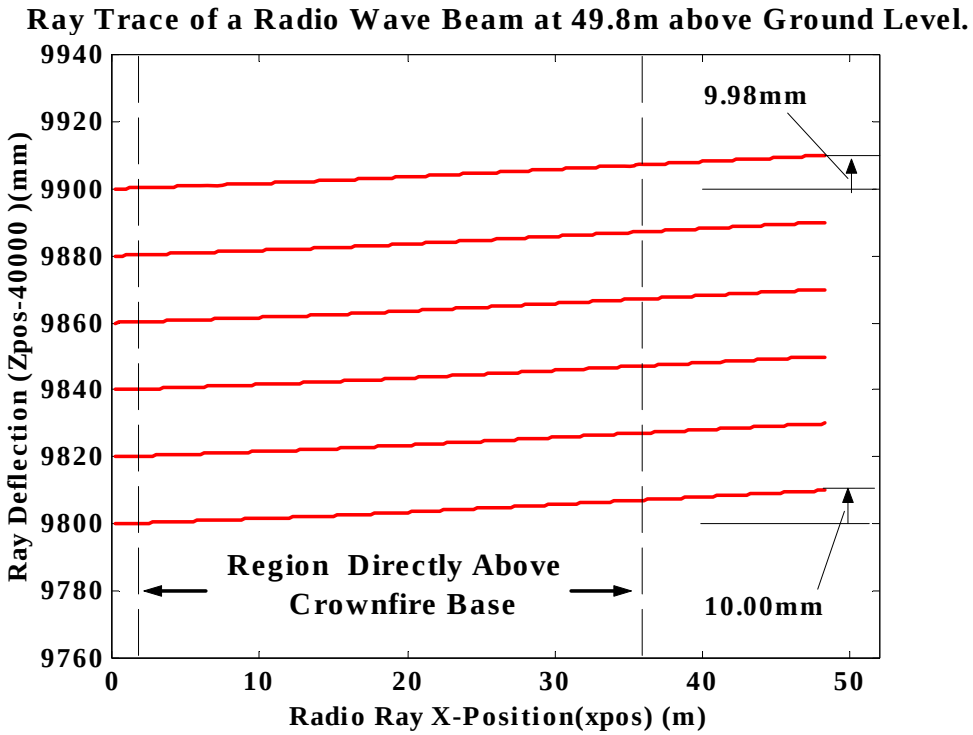

Figure 7.33. *Radio ray deflection at 49.8m due to (nria+ alti. Correction) and 0.1%K*

7.4.3.4. Attenuation due to refraction

Deflection of radio rays from their original path causes focusing and de-focussing in signal intensity at the targeted area. As equi-spaced rays are representative of amplitude at the source, therefore the number radio rays reaching the target area (N_r) is directly proportion to signal amplitude (E_r) at the area, thus:

$$E_r = \zeta N_r \qquad \text{(Equation 7.61)}$$

If N_t is the total number of rays targeted at the area (also proportional to intensity E_t), then attention due to deflection is given by:

$$dB = 20\log\left(\frac{N_t}{N_r}\right) \qquad \text{(Equation 7.62)}$$

The number of rays falling on the targeted area (N_r) is obtained by running the 2-D ray tracer model with rays spaced by a millimeter, shot at the same level as the target area. Rays falling on the area are identified and counted.

At 13.8 m above ground level, it was observed a plume that contains 0% K attenuate a radio wave by 9.78 dB. This is doubled if the potassium concentration is raised to 0.1%. The attenuation rises steeply after 0.1 % to reach 42.66 dB at potassium concentration of 0.18 %. Figure 7.34 shows the attenuation variation at this height.

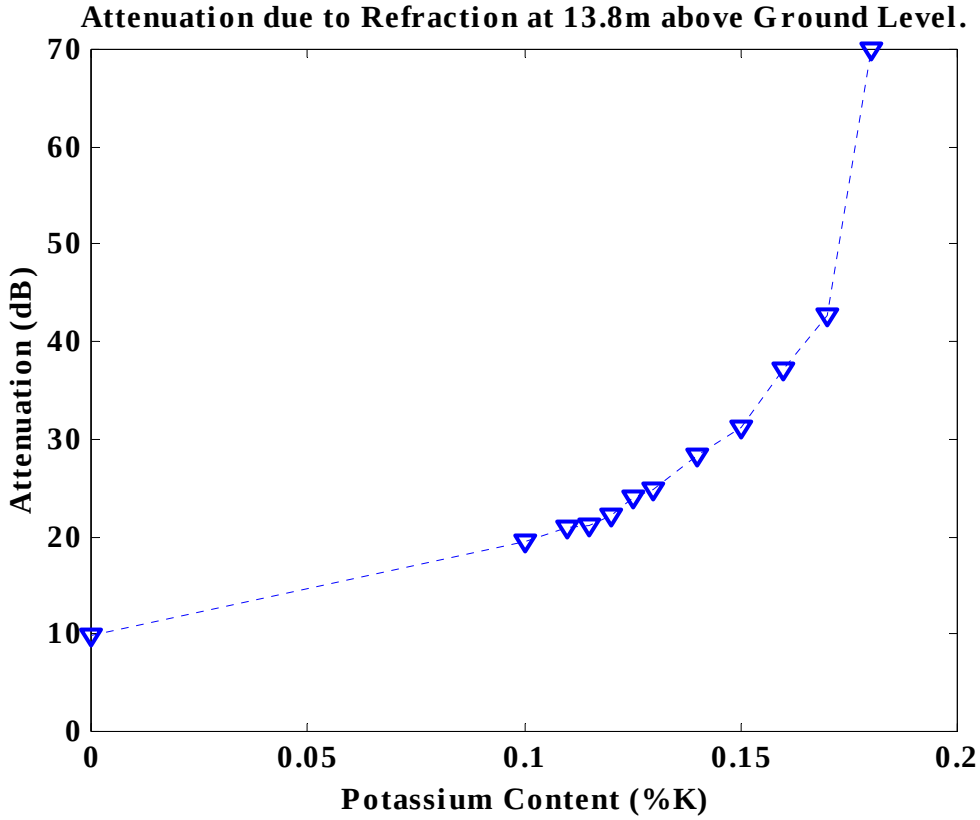

Figure 7.34. *Radio ray attenuation at 13.8m Versus Potassium Concentration.*

Attenuation was observed to decrease with height above ground. At 19.8 m attenuation maintained a constant value of 3.4 dB even if the potassium content is increased up to 2.0%. For 29.8 and 49.8 m, attenuation maintained values of 1.66 dB and 0.92 dB respectively. Figure 7.35 shows the variations.

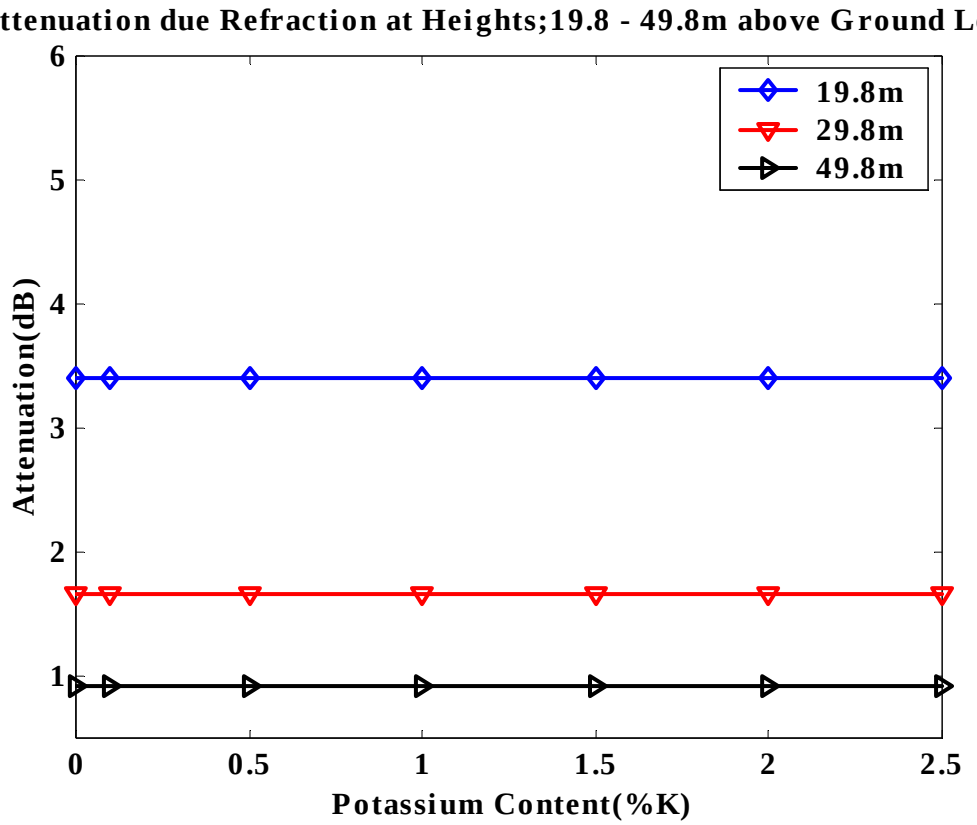

Figure 7.35. *Radio ray attenuation versus potassium content at heights: 19.8-49.8m*

7.5. A case study:

7.5.1. Euroka Operation and Flambeau Project

Between 1962 and 1979, fire and communication scientists from Australia, United Kingdom and United States carried out a multinational project to study the behavior of large bushfires and their effect on radio communication. This involved burning a large amount of vegetation matter (fuel) arranged in 30 windrows (Williams *et al.,* 1970). The fuel was piled in an square area of 15 x15 m with an average mass of 50 tonnes. 7.5 m aisles separated the fuel piles (see Figure 7.36). The project in Australia was called Operation Euroka while in the United States it was called the Flambeau Project. Australian project fuel material was brigalow (*accacia harpophylla*). Pinyon pine-juniper fuel was used in the United States. The mass fire in Australia burned under dry adiabatic lapse rate atmosphere. Fuel consumption rate at 25 mins after the fire started was 225 kg/s and average inflow of 4.5 m/s. Maximum temperature for the Flambeau project was about 1600 K. The rest of fire behavior is described in Williams *et al.,* 1970 and Palmer (1980).

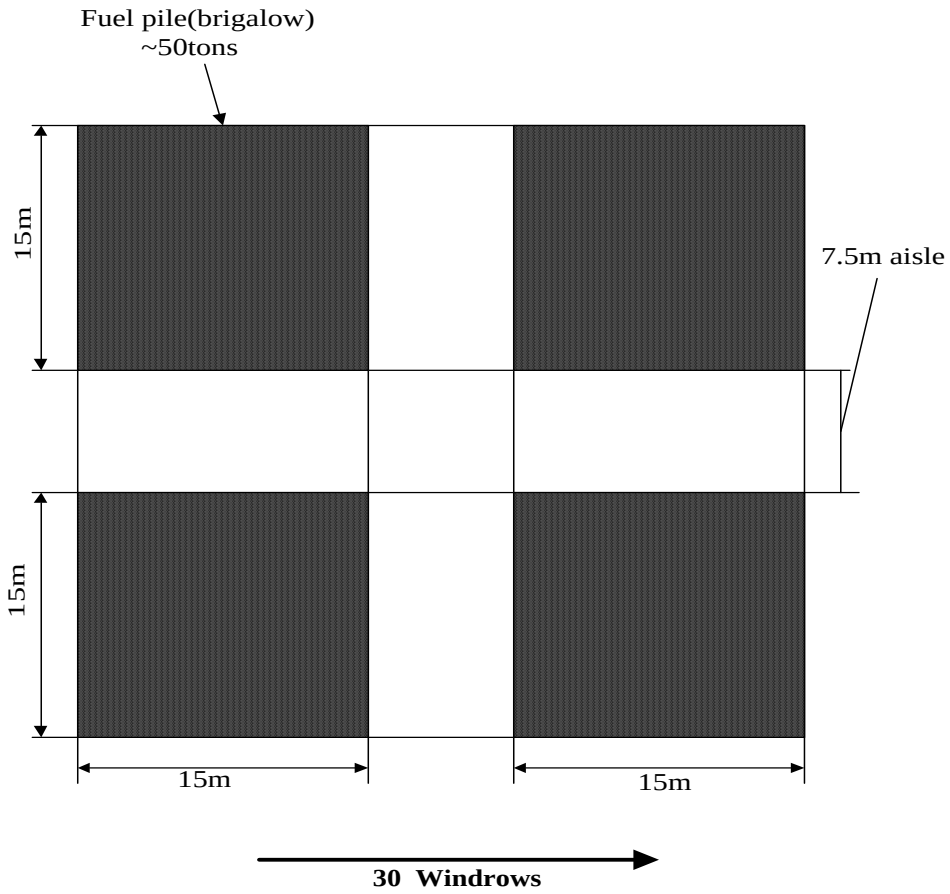

Figure 7.36. *Fuel arrangement in the Operation Euroka Mass fire*

Communication equipment was set up during mass fire experiments to measure radio wave refraction. The refraction measurements were carried out at 1.5 to 2.5m above the fuel pile. Ray bending of 3 to 9mins was report in the mass fires.

The ray deflections were investigated using the constructed 2-D ray-tracing model. Assuming that temperature above the fuel pile varies as given by Weber *et al.*, then its variation with height is as given in Figure 7.37.

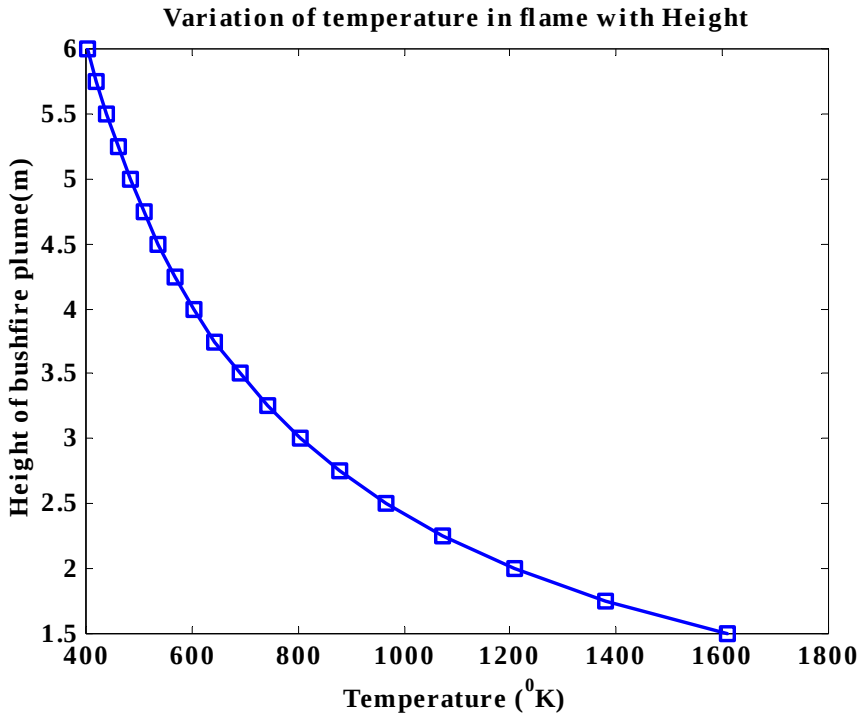

Figure 7.37. *Estimated variation of temperature with height over a brigalow fuel pile*

Temperature at 2.5 meters above the fuel is expected to vary as in Figure 7.38 below. The 2-D ray tracing code was run on the assumption that the fuel piles behave as arrays of discrete "potholes" separated by aisles 7.5 m wide with refractive index of determined by air temperature variations only. 30 of the windrows make a propagation distance of 668 m. For potassium content of 0.1 to 2.0%, deflection ranged from 0.084 to 0.086 arcmins at 2.5 m. At 2.0 m deflections were observed to be 0.37 to 1.42 arcmins while at 1.8 m they ranged from 2.1 to 7.6 arcmins. At grazing angles deflections 19.81 to 39.35 arcmins were predicted (see Figure 7.39). This consistent with the measured deflections (reference) in Operation Euroka (3 to 9 arcmins) and indicates that refractive deflection is significant contributor to signal fluctuations.

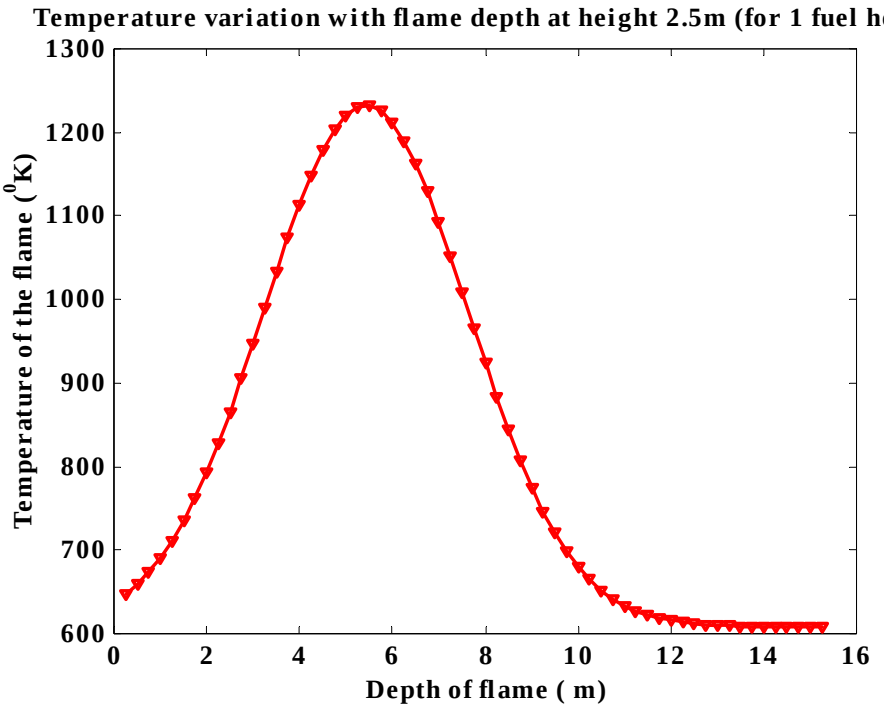

Figure 7.38. *Variation of temperature with height flame depth at 2.5m*

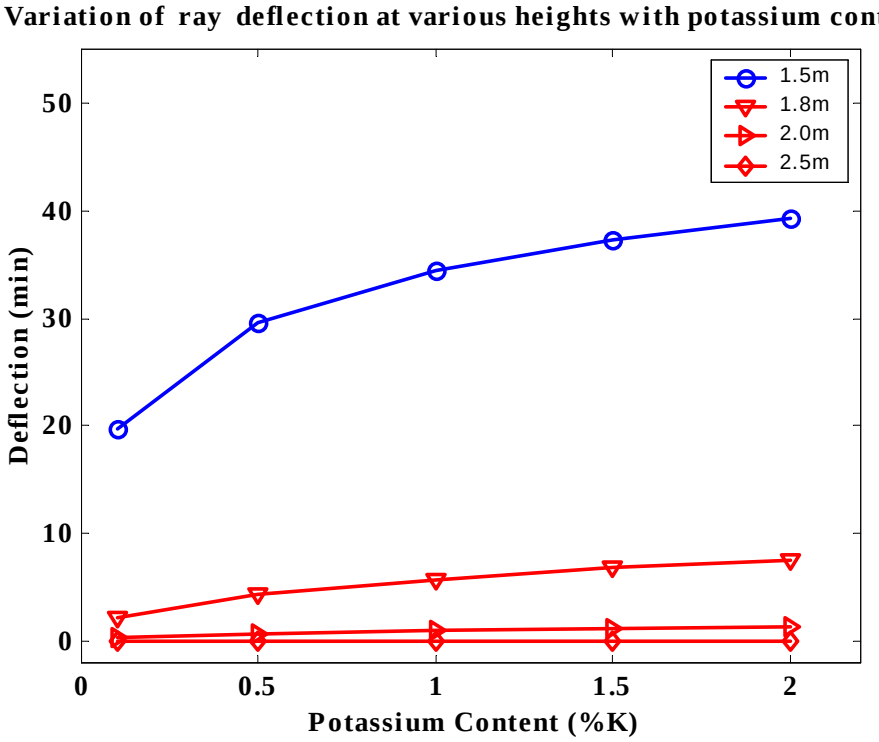

Figure 7.39. *Deflection versus potassium content at different heights above the flame*

7.6. Conclusions

Deflection of collimated radio wave beam as determined from the thermal biconcave lens model for a bushfire is dependent on the size of the fire and its intensity. Size of the fire relates to the radius of the curvature of the lens (R_c). Intensity of the fire determines the refractive index of the lens dielectric material. Alkali content also plays a significant effect of the refractive index of the lens. A bushfire of approximate depth of 40m ($2R_c$) and potassium content of 0.1% had maximum deviations of about 1.12 arcmin near the hottest part of the flame that reduced to zero at the center and edges of the thermal lens. A similar behavior was observed at potassium content of 2.0% where the deflections rose to a maximum of 1.66 arcmin near the lens center and dropped to zero at the edges.

The 2-D ray trace model predicted a deflection of 6.6 arcmin for a plume that contained *nria* constituent composition and 0.1% K near the hottest part of the flame. The major contribution for this deflection was from plume constituents and not from the ionization. The deflection from the ionization was 1.04 arcmin, which is about 16% of the total deflection. In the plume where ionization is expected not to contribute the deflection was measured to be 0.7 arcmin. The deflection is however lower than that produced by the neutral gas without ionization (0.76 arcmin). It appears the combined refractivity is not an algebraic sum of individual gas refractivity.

In the simulation of refraction in Operation Euroka mass fire the 2-D predicted values that are within range. Thus for 1.8 m above the fuel pile deflections predicted were 2 to 7.6 arcmin compared to those reported 3 to 9 arcmin.

Attenuation was observed to decrease with height for the 35 m-depth bushfire. At the hottest part of the fire it was observed to increase exponentially with the increase of potassium content. At 13.8 m, attenuation was observed to increase from 10 dB when there was potassium content was zero to maximum of 42.66 dB at 0.18% K. Then it rose to infinity beyond 0.18% K. At 19.8 m attenuation had constant valve of 3.4 dB for a potassium content of 0.1-2.0%. At 29.8 m, attenuation was 1.6 dB and at 49.8 m it was 1.0 dB for the same range potassium content.

CHAPTER 8

General Discussions and Conclusions

Alkali and alkaline earth metals (AAEMs) exist in substantial quantities in vegetation. Potassium is the most abundant of the omnipresent AAEMs followed by calcium, magnesium and sodium respectively. The metals exist in different forms; as inorganic salts in plant cells and voids, and attached to oxygen containing functional groups such as carboxylates and formates. Potassium content in Australian vegetation ranges from 0.05 to 2.71% of plant's dry weight. The potassium content varies from one region of Australia to another, as it is a factor of soil contamination. Vegetation in southwest Western Australia has potassium content up to 2.0% while that in southeastern Australia has content reaching up to 2.71%. In northern Australia, potassium content in eucalyptus and sorghum grass species can be up to 1.8%.

Bushfires are most intense in southeastern and Western Australia with peak intensity and temperatures reaching about 100 MWm^{-1} and 1600ºC respectively. Theoretically, bushfire temperatures could be up to 2000ºC. During a bushfire, the high temperature environment volatilises AAEM species from a thermally crumbling organic structure of vegetation into the fire plume. The volatiles are dominated by potassium species, for example KCl, K atoms and KOH. Several factors such as the quantity of water vapour in the fire plume, flame temperature and presence of reducing agents, such as radicals in air that flows in the fuel, determine dominant potassium species during the emision. High quantities of water vapour in a low temperature combustion environment favour the emission of KOH as dominant volatiles. The presence of H radicals in a wood charcoal matrix leads to a reduction reaction, which displaces K atoms from oxygen-associated functional groups that could then be emitted as dominant K species. High chlorine content in vegetation promotes the release of potassium as KCl as dominant K species in dry combustion environment. KOH is unstable at very high temperatures. It dissociates into K atoms and other species at a temperature of about 1100 K. Conversely, KCl is a very stable salt. It persists to temperatures around 1600ºC, the temperature at which it is significantly dissociated into its respective atoms.

For vegetation combustion, global chemical equilibrium calculations using MINGTSYS and CHEMSAGE 3.0 software programs, predict the formation of gaseous K and Na atoms at temperatures above 800ºC. The concentration of the atoms increases rapidly with the increase in temperature. However, the chemical equilibrium software programs do not account for the K atoms from the H radical reduction reaction. The MINGTSYS and CHEMSAGE 3.0 programs predict very low concentration of magnesium and calcium atoms at temperatures less than 1600ºC. Calcium and magnesium species require high temperature to be volatilised. For example, calcium is volatised at temperatures in the range of about 1434ºC. Green to near infrared spectrometry of bushfires confirms the predictions made by the chemical equilibrium softwares on the existence of sodium and potassium atoms in vegetation combustion. Doublet line emissions of potassium and sodium are observed in the spectrometer. The most prominent of the line emissions in the spectrometer are those of potassium as it is the more abundant than sodium in vegetation and has the lowest ionisation energy of 4.34 eV.

The thermodynamic calculations and spectrometry suggest that in thermal ionisation, potassium is the most important of the AAEM species present in vegetation. Most of the thermal ionisation that occurs in bushfires burning in vegetation with high potassium comes from the element, at least for fires with temperatures below 1600ºC. Of the amount of potassium present in plant matter, about 10 to 20% is ionised in the combustion zone of the fire.

Grassfires produce a weakly ionised medium with electron density in the range of 10^{14}-10^{17} m^{-3}. Through collisions, electrons absorb electromagnetic wave energy and dissipate it into the grassfire plume. Grassfires burn under atmospheric pressure. By nature, weakly ionised gases at atmospheric pressure are highly collisional with collision frequencies up to one terahertz (1×10^{12} s^{-1}). However, a high temperature combustion environment could lower the collision frequency to about 10^{11} s^{-1}. Considering that grassfire temperatures are generally less than 1000°C, and assuming collision frequency of 10^{11} s^{-1}, attenuations in the range of up to 11.4 dB/m were predicted for flames with a maximum temperature of 1200 K in a numerical experiment carried out in Chapter 3. The maximum attenuation rate predicted in the experiment is high enough to cause radio wave communication failure, as flame depths of more than 50m are possible in large grassfires. Phase shift can also cause signal strength loss through interference of out of phase radio waves. The numerical simulation predicts phase shift as high as 1036º at 1200 K for collision frequency for collision frequencies of about 1×10^{11} s^{-1}. Both attenuation and phase shift

in the signals are dependent on the collision frequency and the fire temperature, therefore very high intensity grassfires are more likely to cause HF/VHF communication blackout.

Field measurements of attenuation and phase shift of radio waves were carried out in a moderate intensity controlled grassfire of intensity of 554 kWm^{-1}. The grass fuel characteristics just before ignition were determined. It was observed that the grass was 9.9% cure. The grassfire depth was determined to be around 0.89 m. Maximum flame temperature was measured to be 899 K at 75 cm above the ground inside the grass fuel stratum. Inductively coupled plasma-atomic emission spectrometer (ICP-AES) analysis for alkalis (K and Ca) of the grass revealed that they were 1.2 and 0.7% w/w respectively. As potassium and other AAEMs were emitted during grassfire, they were emitted in different forms. Since the grass in this experiment was partly cured, the most likely forms of potassium emissions are potassium hydroxide (KOH), K atoms and potassium carbonate (K_2CO_3) or sulphate (K_2SO_4). Water vapor from the partially cured fuel promoted the release of potassium as a hydroxide than chloride. Theoretical calculations of electron density in the grassfire, using local thermal equilibrium theory assuming KOH, K and K_2CO_3 to be 20% of K salts in the flame, predicted ionization at the maximum temperature to be 5.35×10^{15} m^{-3}.

Electron density in the grassfire was determined experimentally by comparing the signal strength of a radio wave before and after traversing the fire. This was carried out using an instrument specifically built for the purpose, thus the Radio Wave Interferometer (RWI). The instrument was built with two transmitting limbs; one at 30 MHz and another at 150 MHz. During the experiment, the 150 MHz limb become unstable and was therefore abandoned. Signal strength loss and phase change for the 30 MHz signal from RWI after traversing the grassfire were then used to calculate the electron density in the flame (Chapter 4). From the experiment, the 30 MHz signal suffered an attenuation rate of 0.029 dBm^{-1} when the flame intercepted the propagation path. The hot ground also slightly affected the 30MHz signal as it attenuated the signal at the rate of 0.0072 dBm^{-1}.The phase shift induced on the 30MHz signal was significant. A phase shift of 3.08º was observed as the signal path was intercepted by the grassfire. With this amount of phase shift and from the geometry of the experimental set up, it estimated that the electron density in the grassfire was around 5.29×10^{15} m^{-3}.

RADIOMETRIX® 151.3 MHz radio wave transmitter and receiver modules were set beside the RWI to transmit through the grassfire. The attenuation rate of the 151.3 MHz signal due to the grassfire flame was observed to be 0.052 dBm^{-1}. The hot ground after the fire refracted the radio

waves and induced a 0.013 dB signal loss.

Another propagation experiment was carried out in a moderate intensity prescribed cane fire at 151.3 MHz frequency. Cane fires are normally set when weather conditions do not favour the development of a very high intensity fire. This is for the safety reasons; thus if perhaps the fire gets out of control, it should be contained easily with minimum economical costs. In the cane fire experiment, maximum flame temperature observed was 904K (Chapter 5). The 151.3MHz signal was attenuated by $0.04 dBm^{-1}$ while the carbon-coated stocks, which were left after the burning, attenuated the signal by $0.03 dBm^{-1}$. As sugar cane was not 100% cure, the most likely forms of AAEM emissions were potassium hydroxide (KOH), K atoms and potassium carbonate (K_2CO_3).

Laboratory experiments were performed on forest litter flames to determine electron density and collision frequency in the moderate intensity fire (Chapter 6). The electron density of forest fuel flames with radiant heat up to about 57k Wm^{-2} was observed to range from 0.32 - 1.64 $x10^{16}$ m^{-3}. The collision frequency in the flames ranged from 1.1 - 4.0 x 10^{10} s^{-1}. The range is lower than electron-neutral collision frequency at normal air temperature. It must be observed that the flames were enclosed and therefore had a limited supply of neutral particles. The collision frequency is directly related to the neutral gas density and medium temperature. For the forest fuel flames, attenuation is however related in a complex way to both electron density and collision frequency, which are both related to alkali content and flame temperature. From the experiment, X-band microwaves experienced relative attenuation coefficient in the range of 1.0 - 4.5 dB/m when propagating in a line-of-sight mode through flame of radiant heat up to 57 kWm^{-2}. A phase shift coefficient of 29.3-6.3 degrees was imposed on the microwaves.

In studies of refraction (Chapter 7), deflection of collimated radio wave beam as determined from the thermal biconcave lens model has been observed to be dependent on the size of the bushfire and its intensity. Size of the fire influences the radius of the curvature of the thermal lens and the number of roll vortices that could be formed in the fire. Large fires may promote the development of a series of roll vortices. Fire intensity has an effect on radio refractive index of the lens' dielectric material. Alkali content also plays a significant role in the refractive index of the lens. A bushfire of approximate depth of 40m and potassium content of 0.1% had maximum deviations of about 1.12 arcmins near the hottest part of the flame that reduced to zero at the edges of the thermal lens. A similar behavior was observed at potassium content of 2.0% where the deflections rose to a maximum of 1.66 arcmins near the lens center and dropped to zero at the edges.

A two dimensional (2-D) ray-tracing scheme predicted a deflection of 6.6 arcmins for a plume that contained *nria* (Chapter 7) constituent composition and 0.1% K near the hottest part of the flame. The major contribution for this deflection was from plume constituents and not from the ionization. The deflection from the ionization was 1.04 arcmins. This is about 16% of the total deflection. In the smoke plume where ionization is expected not to contribute the deflection was measured to be 0.7 arcmins. The deflection is however lower than that produced by the neutral gas without ionization (0.76 arcmins). It appears the combined refractivity is not an algebraic sum of individual gas refractivity.

On simulating the refraction determined during the Operation Euroka mass fire experiment using the 2-D ray-tracing scheme, the values predicted by the scheme were within range obtained from the experiment. At 1.8m above the fuel pile deflections of 2 to 7.6 arcmins were predicted. The values compare well with those reported, thus 3 to 9 arcmins.

When a 35m-depth high intensity bushfire burning in 12 m crowns is simulated to determined attenuation due to refraction, it was observed that attenuation decreased with increase in height above the vegetation canopy. At about 2 m above the canopy, attenuation rate was observed to increase exponentially with the increase of potassium content. At 13.8 m, attenuation rate was observed to increase from 0.21 dBm^{-1} when the potassium content was zero (0%) in the combusting vegetation, to value of 1.45 dBm^{-1} at 0.19% K. Attenuation rate at 13.8 m above ground increases to high attenuation rate values when potassium content is increased beyond 0.19%. At 19.8 m above ground, attenuation rate had constant value of 0.07dBm^{-1} for a potassium content of 0.1 - 2.0%. At 29.8 m, attenuation rate was 0.03 dBm^{-1} and was 0.02 dBm^{-1} at 49.8 m for the same range of potassium content.

This study has revealed that electron-neutral momentum transfer collision frequency is a factor of both neutral gas density and flame temperature. Atmospheric air nitrogen is a major component of the neutral gas that supports of fuel combustion in bushfires. Flames produced in a combustion environment where high concentrations of neutral gas could easily reach the combusting fuel have high collision frequencies, e.g., up to $3 \times 10^{11}\ s^{-1}$. In the network analyzer experiment carried out in Chapter 6, collision frequencies were measured to be up to $4.0 \times 10^{10}\ s^{-1}$, thus lower than those in open flames. A limited amount of atmospheric air could reach the combusting forest fuel

material in the burner in the network analyzer experiment. Generally, flames produced from hot and enclosed combustion environment will have lower collision frequencies than those produced from hot and open combustion environment. Comparisons can also be made from experiments performed by Belcher *et al.* 1950 and Adler, 1954, where collision frequencies of hydrocarbon flames of comparable temperatures were determined to be 8.8×10^{10} and 6.5×10^{8} s^{-1} respectively. The difference in the flames was the combustion environment. Flames studied by Belcher *et al.* were in an open environment while those of Adler were enclosed.

Electron density in bushfires is a factor of both flame temperature and potassium content in vegetation. Very hot flames with high ionisable potassium produced high electron densities. The size or the physical structure of the combusting fuel material has also been observed to affect the flame electron density. It could be that ionisable potassium species are more easily given out from thin fuel such as grass and pine needle than from eucalyptus twigs (Chapter 6). There are also possibilities of secondary reactions at the surface of a thick fuel material before the potassium species could be released into the flame.

Generally, high radio wave frequencies are the most affected in bushfire environments. Propagation experiments in moderate intensity fires show that X-band frequencies were the most affected with maximum attenuation rate of 4.5 dBm^{-1}. The 151.3 MHz signals suffered a maximum attenuation rate of 0.05 dBm^{-1} while the 30 MHz signals suffered at most an attenuation of 0.03 dBm^{-1}. The attenuation rates could be higher for very high intensity bushfires as predicted by numerical simulations.

Bushfire behaviour information is very important for fire suppression authorities for fire spread model validation. There has been a proposal to employ Autonomous Fire Detectors (AFDs) in projected fire paths to gather information on fire behaviour. AFDs are devices designed to transmit and receive data at very high frequency. In bushfire environments, the highly collisional and ionized flames may incapacitate the devices. Flames with an average electron density of about 1.82×10^{16} m^{-3} as in eucalyptus leaves fires (Chapter 6) and collision frequencies of about 1×10^{11} s^{-1}, are predicted to attenuate a signal from an AFD, when engulfed, at the rate of 5.2 dB/m. This may lead to communication blackout in large bushfires.

Electromagnetic constitutive parameters of a bushfire are very important for channel characterization in bushfire environments. Numerical experiments employed in the study were

based on the assumption that flame electrons are in thermal equilibrium with neutral gases in the fire plume, thus the electron energy distribution function is assumed to be Maxwellian. There is no doubt that the assumption is good enough for bushfires as the predicted attenuation rate were very close to the measured values. In order to maintain the Maxwellian distribution, the requirement was that a weak electric field should be used. Research needs to be carried out to determine the minimum required field to perturb the electron distribution function in the fire from Maxwellian. Also, in this study, effective collision frequencies were used. The effective collision frequency concept disregards the range of possible types of electron-neutral interactions in a Maxwellian energy distribution. Theoretical studies need to be carried out on the effect of assuming a different particle interaction mechanism, which then leads to a different collision frequency term than the effective collision frequency. This study has also shown that the classical electron gas model for a bushfire is sufficient in predicting of radio wave absorption. The electron gas model is too ideal in explaining the charging mechanism in a bushfire. A weakly charged dusty plasma model may also be sufficient in explaining electrophysical behaviour of a bushfire.

The laboratory experiments in the study employ very expensive and sensitive instruments to determine electron densities and collision frequencies. Though known for perturbation problems, Langmuir probes which are less expensive than the vector network analyzer, may be adapted for electron density and distribution function determination in a fire. Research may be directed to adapting the Langmuir probe for the task.

APPENDIX

Table A1. *nria, nrib, nric composition of plume gases*

Gas:	**H_2O**	**CO**	**CO_2**	**N_2**
nria:				
(% /v)	0.056	0.0024	0.025	0.703
nrib				
(%/v)	0.226	0.0024	0.025	0.703
nric				
(%/v)	0.256	0.0143	0.149	0.602

BIBLIOGRAPHY

Adler, F.P. 1954. Measurement of conductivity of a jet flame. *Journal of Applied Physics* **25**, 903-908.

Akhtar, K., E.J. Scharer, S.M. Tysk, and E. Kho, 2003. Plasma interferometry at high pressures. *Review of Scientic Instruments* **74**, 996-1001.

Albini, F.A., and R.G. Jahn, 1961. Reflection and transmission of electromagnetic waves at electron density gradients. *Journal of Applied Physics* **32**, 75-82.

Alkemade, M.A. 1979. *Fundamentals of analytical flame spectroscopy*. Bristol: Hilger.

Allan, R., J. Lindesay, and D.E. Parker, 1996. *El Nino-Southern Oscillation and climatic variability*. Melbourne: CSIRO.

Andre, P. 1995. Partition functions for plasma out of thermal equilibrium. *IEEE Trans. Plasma Science* **23**, 453- 458.

Andersen A.N., G.D. Cook, L.K. Corbett, M.M. Douglas, R.W. Eager, J. Russell-Smith, S.A. Setterfield, R.J. Williams and J.C.Z. Woinarski, 2005. Fire frequency and biodiversity conservation in Australian tropical savanna: implications from the Kapalga fire experiment. *Austral Ecology* **30**, 155-167.

Arblaster J.M., G.A. Meehl, and A.M. Moore, 2002. Interdecadal modulation of Australian rainfall. *Climate Dynamics* **18**, 519-531.

Asfaw, A., and G.Wibetoe, 2005. Direct Analysis of Beer by ICP-AES: A very simple method for determination of CU, Mn and Fe. *Microchim Acta* **152**, 61- 68.

Ashton D.H., and H.J. Chinner, 1999. Problems of regeneration of the mature Eucalyptus regnans F. Muell, (The Big Ash) forest, in the absence of fire at Wallaby Creek, Victoria, Australia. *Australian Forestry* **64**, 265-280.

Attiwill, P.M. 1981. Energy, Nutrition Flow and Biomass. In "*Proceeding of Australian Forest Nutrition workshop; Productivity in Perpetuity*". pp 131-144.

Attiwill, P.M., P.J. Polglase, C.J., Weston, and M.A. Adams, 1996. Nutrient cycling in forests of south-eastern Australia. *In:* P.M.Attiwill and M.A. Adams, (eds). *Nutrition of Eucalypts*, Melbourne: CSIRO Publishing, pp.155-187.

Ayers, G.P. 2005. Air pollution and climate change: has air pollution suppressed rainfall over Australia. *Clean Air and Environmental Quality* **39**, 51-57.

Balbi, J.H., P.A. Santoni, J.L. Dupuy, 1999. Dynamic modelling of fire spread across a fuel bed. *International Journal Wildland Fire* **9**, 275–284.

Baird, D.C.1988. *Experimentation: An introduction to measurement theory and experimental design*, 2nd Edition. Prentice Hall, Englewood NJ 07632, pp 137 -150.

Bean B.R., and J.E. Dutton, 1966. Radio meteorology. *NBS Monogr*. 92, Washington D.C: US G.P.O, 435pp

Belcher, H., and T.M. Sudden, 1950b. Studies on ionisation produced by metallic salts in flames I. Determination of collision frequency of electrons in coal gas-air flame. *Proc. Roy. Soc.* A **201**, 480-488.

Bennett, W.F, 1996. (ed). Nutrient deficiencies and toxicities in crop plants. St. Paul: APS Press.

Bjorkmann E., and B. Stromberg, 1997. Release of chlorine from biomass at pyrolysis and gasification conditions. *Energy and Fuels* **11**, 1026 – 1032.

Braithwaite R.W.1995. A healthy savanna, endangered mammals and aboriginal burning *In:* D.B. Rose, (ed). *Country in flames*, Canberra: Biodiversity Unit, pp 91-102.

Bridge, R.G. 2004. Fine fuel in dry sclerophyll forest of south-eastern New South Wales. Australian Forestry **67** (2), 88-100.

Britton, N.R. 1982. The Bushfires in Tasmania, February 1982-how the disaster relevant organizations responded- Disaster Investigation Report No.6, Townsville: JCU.

Brown L.A., D.C. Dayton, and J.W. Daily, 2001.A study of Cellulose Pyrolysis Chemistry and Global Kinetics at High Heating Rates, *Energy and Fuels*,**15**, 1286 - 1294.

Burrows, W. G. 1984. Distortion of a narrow radio beam in a convective medium," *AGARD Characteristics of the Lower Atmosphere Influencing Radio Wave Propagation* **21**(N84–24943), 15 - 32.

Burrows, N. D. 2001. Flame residence times and rates of weight loss of eucalypt forest fuel particles. *International Journal of Wildland Fire* **10**, 137 - 143.

Burrows W.G. 1968. *V.H.F. Radio Wave Propagation in the troposphere*. London: Intertex.

Butler, C.J., and A.N. Hayhurst, 1998. Kinetics of gas-phase ionization of an alkali metal, A, by the electron and proton transfer reactions: $A + H_3O^+ \longrightarrow A + .H_20 + H$; $AOH + AOH2+ + H20$ in fuel-rich flames at 1800-2250K. *Jour. Chem. Soc. Faraday Trans.* 98, 2729-2734.

Butler, B.W., J. Cohen, D.J. Latham, R.D. Schuette, P. Sopko, K.S. Shannan, D. Jimenet, L.S.Bradshaw, 2004. Measurements of radiant emission power and temperature in crown fires, *Can. J. For. Res.* **34**, 1577-1587.

Cabannes, F., and J. Chapelle, 1972. Spectroscopic plasma diagnostics. *In*: M.Venugopalan, (ed). *Reaction under plasma conditions*, New York: Willey-Interscience, pp 367-469.

Cai, Y., J. Su, and L.Q. Ma, 2004. Low molecular weight thiols in arsenic hyperaccumulator *Pteris vttata* upon exposure to arsenic and other trace elements. *Environmental Pollution* **129**, 69- 78.

Caron, P. R. 1968. Techniques of measuring the Electron density of Dense, Thick, Steady State Plasmas. *IEEE Antennas and Propagation Magazine* **1**, 611-612.

Catchpole, W. 2000. The international Scene and Impact on Australia In: Fire-The Australian experience seminar held on 30 Sep-1 October 1999. National Academies Forum Australia.

Catchpole, W.R., E.A. Catchpole, A.G. Tate, B. Butler, and R.C. Rothermel, 2002. A model for the steady spread of fire through a homogeneous fuel bed. *In*: D.X. Viegas (ed). *Forest Fire Research and Wildland Fire Safety*, Rotterdam: Millpress, pp1-11.

Chafer C., M. Noonan, and E. Macnaught, 2004. The Post-Fire Measurement of fire Severity and Intensity in the Christmas 2001 Sydney Wildfires. *International Journal of Wildland Fire* **12**, 227-240.

Chandler, C.P., P. Cheney, P. Thomas, L. Trabaud, and D. Williams, 1983. *Fire in forestry Vol II*, New York: John Wiley and Sons, pp 231-48.

Chang, C.H. Hsieh C.H., Wang H.T., Jeng J.Y., Leou K.C. and C. Lin, 2007. A transmission-line microwave interferometer for plasma electron density measurement. *Plasma Sources Sci and Technology* **16**, 67-71.

Chippendale G.M. and W. Ludek, 1981. The natural distribution of Eucalyptus in Australia. Australian national parks and wildlife Service Special Publication No 6. Canberra.

Charlesworth, P.B., C. Chinn, K.L. Bristow, and G.J. Ham, 2002. Healthy crop and health groundwater-sugarcane in the Burdekin delta. *In: IAA National Conference-Conserve or Conflict, 22-24 May 2002, Sydney.*

Chase, M.W., C.A. Davies, J.R. Downey, D.J. Frurip, R.A. McDonald, A.N. Syverud, 1985. JANAF Thermochemical Tables. *Journal of Physical Chemistry*. Ref. Data, Vol **14**, 1.

Chen, X., and P. Han, 1999. On the thermodynamic derivation of Saha equation modified to a two-temperature plasma. *Journal of Physics D: Applied Physics* **32**, 1711-1718.

Cheney N.P. and J.S. Gould, 1995. Fire growth to a quasi-steady rate of forward spread. *International Journal of Wildland Fire* **5**(4), 237 -247.

Cheney, N.P. 1994. The effectiveness of fuel reduction by burning for fire management. *In: Proceedings of fire and biodiversity conference, 8-9 October 1994, Melbourne.* Canberra: the Biodiversity Unit, pp 9-16.

Cheney, N.P., J.S. Gould, and L. McCaw, 2001. Dead-Man Zone-A neglected area of fire fighter safety. Australian Forestry **64** (1), 45-50.

Chu, P., W. Yan, and F. Fujioka, 2002. Fire-Climate relationships and long-lead seasonal and wildfire prediction for Hawaii. *International Journal of Wildland Fire* **11,** 25-31.

Church, C. R., J. T. Snow, and J. Dessens, 1980. Intense atmospheric vortices associated with 1000MW fire. *Bulletin of the American Meteorological Society* **61**, 682-694.

Clark, T.L., M. Griffiths, M.J.Reeder, and D. Latham, 2003. Numerical simulations of grassland fires in the Northern Territory, Australia: A new subgrid-scale fire parameterization. *Journal of Geophysical Research,* **108** D18, Pages 4589 ACL 14-1 – 14-15.

Collett, N.G. 1999. Effects of three short rotation prescribed fires in spring on surface-active arthropods in dry sclerophyll eucalypt forest of west-central Victoria. *Australian Forestry* **62**, 295-306.

Collett, N.G. 2000. Catastrophic wildfire and its short term effects on the families of *Order Coleoptera* (beetles) in *Eucalyptus regnans* forest in central highlands of Victoria, *Australian Forestry* **63** (1), 1-7.

Collett, N.G. 2003. Short and long-term effects of prescribed fires in autumn and spring on surface-active arthropods in dry sclerophyll eucalypt forests of Victoria. *Forest Ecology and Management* **182**, 117-138.

Cook, G.D., and M.H. Andrew, 1991. The nutrient capital of indegeneous Sorghum species and other understorey components of Savannas in north-western Australia. *Australian Journal of Ecology* **16**, 375-384.

Cook, G.D. 1994. The fate of nutrients during fires in tropical savanna. *Australian Journal of Ecology* **19**, 359-365.

Cook, G.D. 2003. Fuel dynamics, nutrients, and atmospheric chemistry. *In:* A.N. Andersen, G.D. Cook and R.J. Williams, (eds.). *Fire in tropical savanna, the Kapalga Experiment*, New York: Springer, pp 47-58.

Crompton, R.W., D.K. Gibson, and A.I. McIntosh, 1969. Mechanisms of element transfer to the atmosphere during vegetation burning, *Australian Journal of Physics* **22**, pp 715.

Crutzen, P.J., and M.O. Andreae, 1990. Biomass Burning in the Tropics: Impact on the Atmospheric Chemistry and Biogeochemical Cycles. *Science* **250**, 1669-1677.

Daniels G.E. 1968. Measurement of gas temperature and the radiation compensating thermocouple. *Journal of Applied Meteorology* **7,** 1026 - 1035.

Darr B. 1996. Tree fertilization, a world of options *Arbor Age* **16**, 14 - 17.

Dayton D.C and D. Belle-Oudry (1999).Effect of coal minerals on chlorine and alkali metals released during biomass/coal cofiring. *Energy and Fuels* **13**, 1203-1211

Dayton D.C., B.M. Jenkins, S.Q. Turn, R.R. Bakker, R.B.Williams, D. Belle-Oudry, and L.M.Hill, 2000. Release of inorganic constituents from leached biomass during thermal conversion *Energy and Fuels* **13,** 860-870.

Davidsson, K.O., J.G. Korsgren, J.B.C Pettersson and U., Jaglid, (2002) The effect of

fuel washing techniques on alkali release. *Fuel* **81**, 137-142.

de Groot W.J., P.M. Bothwell, S.W.Taylor, B.M. Wotton, B.J. Stocks, M.E. Alexander, 2004. Jack pine regeration and crownfire. *Can. J. For. Res.* 34, 1634-1641.

Deschamps G.A. 1972. Ray techniques in electromagnetics. *IEEE Proceedings* **60**, 1022- 1035.

Dickinson M.B. and E.A. Johnson, 2001. Fire Effects on Trees, *In :* E.A. Johnson and K Miyanishi, (eds), *Forest Fires: Behaviour and ecological effects*, Sydney: Academic press, pp. 477-525.

Dowden R.L, C.J. Rodger, and D. Nuan, 2001. Minimun sprite plasma density as determined by VLF Scattering. *IEEE Antennas and Propagation Magazine* **43** (2), 12-24.

Drawin H.W. 1971. Thermodynamic properties of the equilibrium and nonequilibrium state of plasma. *In*: M.Venugupalan, (ed). *Reactions under plasma conditions*, New York: Wiley-Interscience, pp 53-238.

Duesing B. 1985. *Calcium Cycle.* New Heaven: Yale teacher institute publication

Dupuy J.L., and M. Larini, 1999. Fire spread through a porous fuel bed: a radiative and convective model including fire-induced flow effects. *International Journal of Wildland Fire* **9**, 155-172.

Dupuy, J.L., J.Marechal, and D. Morvan, 2003. Fires from acylindrical forest fuel burner: combustion dynamics and flame properties. *Combustion and Flame* **135**, 65-76.

Edwards D.H., G. Hooper and A.A., Collyer. 1971. Ionisation measurement in reactive shock and detonation waves using microwave techniques. *J. Phys. D. Appl. Phys.***25**, 854-869.

Engstrom, J.D., J.K.Butler, L.L. Baxter, T.H. Fletcher, and D.R. Weise, 2004. Ignition behavior of live Chaparral leaves. *Combustion Science and Technology* **176**, 1577-1591.

Epstein, M. 1962. Electromagnetic-Wave propagation with plasma with nonlinear electrical conductivity. *Physics of Fluids* **5**, 492-496.

Fauchereau, N., S.Trzaska, M. Rouault, and Y. Richard, 2003. Rainfall variability and changes in Southern Africa during the 20th century in global Warming Context. *Natural Hazard* **9**, 139-154

Feller, M.C. 1980. Biomass and nutrient distribution in two-eucalyptus forest ecosystem *Australian Journal of Ecology* **5**, 309-333.

Fendell, F.E., and M.F. Wolff, 2001. Wind-aided fire spread. In: E.A. Johnson and K. Miyanishi, (eds.). *Forest Fires: Behaviour and Ecological Effects*, Sydney:Academic press pp 171-223.

Fensham, R.J., and M.J.S. Bowman, 1995. A comparison of foliar nutrient concentration in trees from monsoon rainforest and savanna in northern Australia. *Australian Journal of Ecology* **20**, 335-339.

Fernandes, P.M., and H.S. Botelho, 2003. A review of prescribed burning effectiveness in fire hazard reduction. *International Journal of Wildland Fire* **12**, 117 -128.

Fleming G.A. 1973. Mineral composition of herbage. *In:* G.W. Butler and B. Bailey (eds). *Chemistry and Biochemistry of Herbage Vol. I,* London: Academic Press , pp 529 - 563.

Foster T. 1976. *Bushfire: history, prevention and control*. Sydney: A. H. and A.W. Reed.

Frost, L.S., 1961. Conductivity of seeded atmospheric pressure plasmas. *Journal of Applied Physics* **32**, 2029 - 2036.

Gaydon, A.G. and H.G. Wolfhard, 1978. *Flames: Their structure, radiation and temperature.* London: Chapman and Hall.

Gibbins C. J. and R. Chadha. 1987. Millimeter- wave propagation through a hydrocarbon flame. *IEE proceedings 134(.Pt.H*)**2**, 169 - 173.

Gilchrist B.E., S.G. Ohler, and A.D. Gallimore, 1997. Flexible microwave system to measure the electron number density and quantify the communications impact of electric thruster plasma plumes. *Rev. Sci.Instrum.* **68**, 1189-1194.

Giles, BD and C. Balafoutis, 1990. The Greek heatwaves of 1987 and 1988. *International Journal of Climatology* **10**, 505-17

Gill, A. M., P.H.R. Moore, and R.J. Williams, 1996. Fire Weather in the wet-dry tropics of the World Heritage Kakadu National Park, Australia., *Australian Journal of Ecology* **22**, 302-308.

Gossard, E. E., 1977. Refractive index variance and its height distribution in different air masses. *Radio Science* **12**, 89 - 105.

Grant, C.D., W.A. Loneragan, J.M. Koch, and D.T. Bell, 1997. Fuel characteristics, vegetation structure and fire behaviour of 11-15 year old rehabilitated bauxite mine in Western Australia. *Australian Forestry* **52**, 321-326.

Grønli, G.M., and M.C. Melaaen, 2000. Mathematical Model for Wood Pyrolysis- Comparision of Experimental Measurements with Model Predictions. *Energy and Fuel* **14,** 791-800.

Grove, T.S., B.D. Thompson, and N. Malajczuk,1996. Nutritional physiology of the eucalypts: distribution and utilisation. *In:* P.M.Attiwill and M.A. Adams, (eds). *Nutrition of Eucalypts,* Melbourne: CSIRO Publishing, pp.77-108.

Guo, B., and X., Wang, 2005. Power absorption of high frequency electromagnetic waves in a partially ionized plasma layer in atmosphere conditions. *Plasma Sci. Technol.* **7,** 2645-2648

Hagge, M., and K.M. Bryden, 2002. Modeling the impact of shrinkage on the pyrolysis of dry biomass. *Chemical Engineering Science* **57**, 2811-2823.

Haines, D. A. 1982. Horizontal roll vortices and crown fires," *Journal of Applied Meteorology* **21**, 751-763.

Haines, D. A. and M. C. Smith, 1987. Three types of horizontal vortices observed in wildland mass and crown fires. *Journal of Applied Meteorology* **26**, 1624-1637.

Hajat, S., R.S. Kovats, R.W. Atkinson, and A. Haines, 2002. Impact of hot temperatures on death in London: a time series approach, *J. Epidemiol. Community Health* **56**, 367- 372.

Hake, R.D and A.V. Phelps, 1967. Momentum-Transfer and Inelastic-Collision Cross Sections for Electrons in O_2, CO, and CO_2. *Phys. Rev.* **158**, 70-84.

Hata, M., and D. Shigeyuki, 1983. Propagation tests for 23GHz and 40GHz, *IEEE Journal on selected areas in Communications* **1**, 658-673.

Heil, A. 1998. Air Pollution caused by Large Scale Forest Fires in Indonesia in 1997, *In*: South- East Asian land /forest fires: science and policy workshop, 30 April – 2 May 1998 Singapore.

Heron, M.L. and K., Mphale, 2004. Radio wave attenuation in bushfires, tropical cyclones and other severe atmospheric conditions, Final Report on EMA Project 60/2001, James Cook University.

Heskestad, G. 1998. Dynamics of fire plume. *Phil. Trans. R. Soc. London A* **356**, 2815-2833.

Koseki, H., and T. Yumoto, 1988. Air entrainment and thermal radiation from heptane pool fires. Fire Technol. 24, 33-47.

Hingston F.J. and Galbraith .J.H. (1989) Nutrients in Ash Fall-Out during Forest Fires in the south west of Western Australia., *Australian Forestry* **52** (4), 321-326.

Hinnant, R.T., and M.M. Kothmann, 1982. Potassium Content of three Grass Species During Winter, Journal of Range Management, *Forest Ecology and Management* **35**, 211-213.

Hu, W., S.A. Harding, J. Lung, J.L. Popko, J. Ralph, D.D. Stokke, C. Tsai , and V.L.Chiang, 1999. Repression of lignin biosynthesis promotes cellulose accumulation and growth in transgenic trees. *Nature Biotechnol.***17**, 808-812

Incoll R. (1994) Asset protection in a fire prone environment. . *In: Proceedings of fire and biodiversity conference, 8-9 October 1994, Melbourne.* Canberra: the Biodiversity Unit, pp 213-217.

Isaacs I., (ed.) 2000. *A dictionary of Physics*. New York: Oxford university press.

Itikawa, Y.1973. Effective collision frequency of electrons in gases, *Physics of fluids* **16**, 831-835.

Jensen, A.P., F.J. Frandsen, K. Dam-Johansen, and B.Sander, 2000. Experimental investigation of the transformation and release to gas phase of potassium and chlorine during straw pyrolysis conditions. *Energy and Fuels* **11**, 1026-1032

Jiang, Z., Hu X., Liu M., Zhang, S., He, Y. and Y. Pan, 2007. Attenuation and propagation of a scattered electromagnetic wave in two dimensional atmospheric pressure plasma, *Plasma Sources and Technology* **16**, 97 - 103.

Jones C. and J. Jacobsen, 2001. *Plant Nutrition and Soil Fertility Module* . Madison: American Society of Agronomy.

Judd T.S., P.M. Attiwill, and M.A. Adams, 1996. Nutrient Concentrations in Eucalyptus: A synthesis in relation to difference between taxa, sites and components, *In*: P.M. Attiwill and M.A., (eds). *Nutrition of Eucalypts*, Melbourne: CSIRO Publishing, pp.123-153.

Kasel, S. 1991. Soil nutrient availability: Its effect on the distribution and productivity of East Gippsland Forests. B Sc(Hons) thesis, University of Melbourne.

Keith, D.A., J.E. Williams, and J.C.Z. Woinarski, 2002. Fire management and biodiversity conservation: key approaches and principles. *In*: R.Bradstock, J.E.Williams, and A.M.Gill, (eds). *Flammable Australia: The fire regimes and biodiversity of a continent* pp 401- 425

Kitzberger, T. 2002. ENSO as a forewarning tool of regional fire occurrence in northern Pantagonia, Argentiana, *International Journal of Wildland Fire* **11**, 33-39.

Knudsen, J.N., A. Peter, P.A. Jensen, and K. Dam-Johansen, 2004.Transformation and release to the gas phase of Cl, K,and S during combustion of annual biomass. *Energy and Fuels* **18**, 1385-1399.

Koalaga, Z. 2001. Determination of equilibrium composition of CxHyOzNt plasmas out of thermodynamic equilibrium. *Eur. Phys.Journal D* **17**, 235-247.

Koalaga, Z., and F. Zougmore, 2003. Composition of C/sub x/H/sub y/O/sub z/N/sub t/ plasmas out of thermal equilibrium using quite different modified forms of Saha and Guldberg-Waage equations. *IEEE Transaction on Plasma Science* **31**, 82-93.

Korb, N., C. Jones, and J. Jacobsen, 2002. *Nutrition Management Module N0.5 (4449-5)* Montana: MSU extension publication

Koretzsky, E., and S.P. Kuo. 1998. Characterization of atmospheric pressure plasma generated by a plasma torch array. *Physics of Plasmas* **5**, 3774-3780.

Kremens, R., J. Faulring, A. Gallagher, A. Seema , and A. Vodacek, 2003. Autonomous field-deployable wildland fire, *International Journal of Wildland Fire* **12**, 237-244.

Krishna, P.K., E. Sangen, and P. Visser, 1985. Wood burning stove. *Advances in heat transfer* **17**, 215-223.

Kuhlbusch,T.A.J, M.O. Andreae, H. Cachier, J.G. Goldammer, J.P. Lacaux, R. Shea, and P.J. Crutzen, 1996. Black carbon formation by Savanna fires: measurements and implications for global carbon cycle, *Journal of Geophysical research* **101** (D19), 23,651-23,665.

Kuhnel, I. and L. Coates, 2000. El niño-Southern Oscillation: Related Probabilities of Fatalities from Natural Perils in Australia. *Natural Hazards* **22**, 117-138.

Kulemin G. P. and V.B. Razskazovsky, 1997. Radar reflections from explosions and gas wake of operting engine. *IEEE Transactions on Antennas and Propagation* **45**, 731-739.

Kuei-Chaio, 1970. Theory of Raman intensities of Diatomic molecule. *Chinese Journal of Physics* **8**, 58-63.

Lambert, M.J. 1981. Inorganic constituents in wood and bark of New South Wales forest tree species. *For. Comm. N.S.W. Research Notes* **45**, 43pp.

Lamont, B.A., R. Wittkuhn and D. Korczynskyj, 2004. Turner Review No. 8. Ecology and ecophysiology of grasstrees. *Australian Journal of Botany* **52,** 562-582.

Laroussi, M. and J.R. Roth, 1993. Numerical calculation of the reflection, absorption, and transmission of microwave by a nonuniform plasma slab, *IEEE Transaction on Plasma Science* **21**, 366 -372.

Laroussi, M.1995. Interaction of microwaves with atmospheric pressure plasmas. *Int. J. Infrared Millimeter Waves* **16**. 2069-83

Latham, D. 1998. Near-infrared spectral lines in natural. *In: Proceedings of the III International Conference on Forest Fire Research/14th Conference on Fire and Forest Meteorology, 16–20 November 1998, Coimbra*. Coimbra: ADAI , pp. 513–515.

Latham, D. 1999. Space charge generated by wind tunnel fires. *Atmospheric Research* **51**, 267-278.

LeVan, S.L. 1989. *In*: Schniewind, Arno P. (ed). *Concise Encyclopedia of Wood and wood – based Material 1st edition* , NewYork: Pergamon, pp. 271-273.

Ling, H., H.Kim, G.A.Hallock, B.W. Birkner, A.J.M. Zaman, 1991. Effect of Arcjet plume on satellite reflector performance. *IEEE trans. Ant. and Prop.* **39,** 1412-1419.

Liu, S., L.M. Leslie, M. Speer, R. Bunker, X. Mo, 2004. The effect of bushfires on the hydrological process using a paired-catchment analysis. *Meteorol. Atoms. Phys* **86**, 31- 44.

Ljung, A and A. Nordin, 1997. Theoretical Feasibility for Ecological Biomass Ash Recirculation: Chemical Equilibrium Behaviour of nutrients Elements and Heavy Metals during Combustion. *Environmental Science and Technology* **31**, 2499-2504.

Lobert, J.M. and J. Warnatz, 1993. Emissions from the Combustion Process in Vegetation. In Crutzen P. J.and Goldammer J.G.eds., *Fire in the Environment: The Ecological, Atmospheric and Climatic Importance of Vegetation Fires.* New York: John Willey and Sons Inc., pp 15-37.

Lokker, C. 2000. Draft revegetation strategy for the Townsville City Council. Townsville City Council, Townsville.

Luke, R. H. and A.G. McAuthur, 1978. *Bushfires in Australia*. Canberra: Australsan Government Publishing Service.

Mackey, B., D.B. Lindenmayer, A.M. Gill, M.A. McCarthy, and J. Lindesay, 2002. *Wildlife, Fire and Future Climates.* Melbourne: CSIRO Publishing.

Maczek, A. 1998. *Statistical Thermodynamics*. New York: Oxford University Press..

Machand, E.W. 1972. Ray tracing in cylindrical gradient-index media. *Applied Optics***11**, 1104 – 1106

Maenhaunt W., I.Salma, J. Cafmeyer, H.J. Annegarn, and O. Andreae, 1996. Regional Atmospheric aerosol composition and sources in eastern transvaal, South Africa and biomass burning. *Journal of Geophysical Research*, **101** (D15), 23 631 - 23 650.

Mannetje L.T., S.J.Cook, and J.H. Wildin, 1983. The effect of fire on buffel grass and siratro pasture. *Tropical grasslands* **17**, 30-39.

Maouhoub, E., H. Coitout, and M.J. Parizet, 1999. Excitation Temperature Measurements in an Argon – CO2 Thermal Plasma, *IEEE Transaction on Plasma Science* **27**, 1469-1475.

Margenau, H. 1946. Conduction and dispersion of ionised at high frequencies. *Phys. Rev.* **69**, 508 -513.

Marcelli, T., P. A. Santoni, A. Simeoni, E. Leoni, and B. Porterie, 2004. Fire spread across pine needle fuel beds: characterization of temperature and velocity distribution within the fire plume. *International Journal of Wildland Fire* **13**, 37- 48.

Martins, C. A., A.P. Pimenta, J.A. Carvalho, M.A. Ferreira, A.A. Caldeira-Pires, 2005. Ch and C_2 radicals characterization in natural gas turbulent diffusion flames. *J. Braz. Soc. Mech. Sci. & Eng*. **27**, 110-118

Maser P. Gierth M. and Schroeder J.I., (2002) Molecular mechanisms of potassium and sodium uptake in plants., *plant and soil* **247**, 43-54.

Matsukata, T., T. Fujikawa T.,Kikuchi E., and Y. Morita (1989). Quantitative behavior of potassium species on an amorphous carbon under steam gasification conditions. *Energy and Fuels* **3**, 336-341

McMahon C.K. 1983. Characteristics of forest fuels, fires and emissions. *In: 76th Annual meeting of the air pollution control association. 19-24 June 1983. Atlanta, Georgia* . Atlanta: APAC annual meeting. 24p.

Meyer, G., S. Godfrey, A. Gordon, P. Hacker, J. Mark, B. Lau, S. Shetye, T. Sribimawati , and T. Yamagate , 2001. A Southern hemisphere perspective: Monsoon, Seasonal and interannual application of an Indian Ocean Observing System. *In :* C.J. Koblinsky and N.R. Smith (eds). O*bserving the Oceans in the 21st Century*, Melbourne: International GODAE Office and Bureau of Meteorology, pp. 48-65.

Mecer, G.N., and R.O. Weber, 1994. Plumes above line fires in cross wind. *International Journal of Wildland Fire* **4**, 201-207.

Miyanishi, K. 2001. Duff Consumption. *In*: E.A. Johnson and K. Miyanishi K, (eds). *Forest fires: Behaviour and ecological effects*. San Diego: Academic Press, pp 437- 476.

Mohr, H, and P. Schopfer, 1994. *Plant physiology*. New York: Springer-Verlag.

Molmud, P. 1959. Langevin Equation and the ac conductivity of non Maxwellian plasmas, *Phys. Rev.* 114, 29 - 32.

Morandini, F., P.A. Santoni, J.H. Balbi, 2001. The contribution of radiant heat transfer to laboratory-scale fire spread under the influence of wind and slope, *Fire Safety Journal* **36**, 519-543.

Morrision, D.A. 2002. Effect of fire intensity on plant species composition of sandstone communities in Sydney region. *Austral Ecology* **27,** 433-441

Mphale, K.M., and M.L. Heron, 2007. Plant alkali content and radio wave communication efficiency in high intensity savanna wildfires. *Journal of Atmospheric and Solar-Terrestrial Physics* **69**, 471- 484.

Neda, Z.,and S.Vilakan-Kacso, 2002. Flatness of the setting sun. *American Journal of Physics* **71,** 379 - 385.

Nelson R.M. 2002. An effective wind speed for models of fire spread, *International Journal of Wildland Fire* **11**, 153 –161.

Nelson R.M. 2003. Power of the fire- a thermodynamic analysis, *International Journal of Wildland Fire* **12**, 51 - 65.

Neyland, M. G. and M.J. Brown, 1994. Disturbance of cool temperate rainforest patches in eastern Tasmania. *Australian Forestry* **57**, 1-10

Nicholls, N. 1997. Developments in the prediction of climate variability and implication for insurance, *In:* N.R. Britton and J.Oliver, (eds.). *Finacial Risk Management for Natural Catastrophe.* Griffith University, pp 85-104.

Nikolaenko, A., and G. Ahlers, 2003. Nusselt number measurements for turbulent rayleigh-bernard convection. *Physical Review Letters* **9**, 1- 4.

Noble, I. R., G.A.V. Bary, and A.M. Gill, 1980. McArthur's fire danger meters expressed as equations. *Australian Journal of Ecology* **5**, 201-203.

Nussbaumer, T. 2003. Combustion and co-combustion of biomass: fundamentals, technologies, and primary measures for emission reduction. *Energy and Fuels* **17**, 1510-1521

Obernbeger, I., F. Biedermann, W. Widmann, and R. Riedl, 1997. Concentration of inorganic elements in biomass fuels and recovery in different ash fractions. *Biomass and Bioenergy* **12**, 211-224.

O'Connell, A.M. and T.S. Grove, 1996. Biomass production, nutrient uptake and nutrient cycling in Jarrah (Eucalyptus marginata) and Karri (Eucalyptus Diversicolor) forests of south-western Australia. *In:* P.M.Attiwill and M.A. Adams, (eds). *Nutrition of Eucalypts,* Melbourne: CSIRO Publishing, pp.155-150

Øgaard, A.F., T. Krogstad, and A.K. Løes, 2001. Potassium up take by grass from clay and silt soil in relation to soil tests. *Acta Agric Scand. Sect. B Soil and Plant Sci*. **51**, 97-105.

Okuno, T., N. Sonoyama, J. Hayashi, C. Li, C. Sathe, and T. Chiba, 2005. Primary release of alkali and alkaline earth metallic species during pyrolysis of pulverized biomass. *Energy and Fuels* **19**, 2164-2171.

Oliveira, L.A., D.X. Veigas, V. Vareli, and A.M. Raimudo, 1994. On the soil thermal effect under the surface fire conditions Proc. 2nd Int. Conf. Forest Fire Research Coimbra Vol III D03, 833-847.

Olson, J.S. 1963. Energy storage and balance of producers and decomposers in ecological systems. *Ecology* **44,** 322-331.

Olsson, J.G., U. Jäglid, and J.B.C. Pettersson, 1997. Alkali metal emission during pyrolysis of biomass *Energy and Fuels* **11**, 779-784.

Pack, J., R.E.Voshal, and A.V. Phelps, 1962. Drift Velocities of Slow Electrons in Krypton, Xenon, Deuterium, Carbon Monoxide, Carbon Dioxide, Water Vapor, Nitrous Oxide, and Ammonia .*Phys. Rev.* **127**, 2084-2089.

Pal, Y., R.J. Gilkes, and M.T.F. Wong, 2002. Mineral source of potassium to plants for seven soils from south-western Australia. *Aust. J. Soil. Res*. **40**, 1357-1369.

Palmer, T.Y. 1981. Visible, Infrared (IR) and microwave propagation in and near large fires. *SPIE Vol.35 Atmospheric Effects on System Performance* .

Peixoto, J. P. and A.H.Oort, 1992. *Physics of climate*. New York: American Institute of Physics.

Porterie B.,J.C. Loraud, D. Morvan, and M. Larini, 1999. A numerical study of buoyant plumes in cross–flow conditions. *International Journal of Wildland Fire* **10**, 137-143.

Power, S., T. Casey, C. K. Folland, A. Colman, and V. Mehta, 1999. Inter-decadal modulation of the impact of ENSO on Australia, *Climate Dynamics* **15**, 319-323.

Pozar, D.M. 1993. *Microwave Engineering*. New York: Addison-Wesley.

Potter, B. E. 2002. A dynamics based view of Atmospheric-fire interactions. *International Journal of Wildland Fire* **11**, 247–255.

Price, O., J. Russell-Smith, and A. Edwards, 2003. Fine-scale patchiness of different fire intensities in sandstone heath vegetation in Northern Australia. *International Journal of Wildland Fire* **12**, 227 – 236.

Qureshi M.E., P.B. Charlesworth, K.L.Bristow, and M.K. Wegener 2002. Profitability of growing sugarcane under alternative irrigation systems in the Burdekin delta. In *Proceedings of the Australian Society of Sugar Cane Technologists* **24**, 107-112.

Raison, R.J., P.K. Khaina, and P.Woods, 1985. Mechanisms of element transfer to the atmosphere during vegetation burning. *Canad. Journal of Forest Res.* **15**, 132-140.

Radojevic, M. 2003. Chemistry of Forest Fires and Regional Haze with Emphasis on Southeast Asia. *Pure and Applied Geophysics* **12**, 157-187.

Rawson, R. and B. Rees, 1982. A summary of forest fire statistics, 1972-73 to 1980-81, *Forests Commission of Victoria Fire Research Branch Report* 12.

Richerzhagen, B. 1996. Finite element ray tracing: a new method for ray tracing in gradient-index media. *Applied Optics* **35**, 6186 - 6188.

Machand, E.W. 1972. Ray tracing in cylindrical gradient-index media. *Applied Optics* **11**, 1104 -1106.

Santoni P.A, T. Marcelli, and E. Leoni, 2002. measurenet of fluctuating temperature in continuous flame spreading across a fuel bed using a double thermocouple probe. *Combustion and flame* **131**, 47-58.

Salisbury, F.B., and C. Ross, 1992. *Plant physiology*. Belmont: Wadsworth Publishing Company.

Schneider, J., and F.W. Hofmann, 1959. Absorption and dispersion of microwaves in flames. *Physical Review* **116**, 244 - 249.

Schulte, E.E., and K.A. Kelling, 2002. *Understanding Plants Nutrients: Soil and Applied potassium* A2521. Madison: University of Wisconsin.

Seeger, J.A. 1986. *Microwave theory, components and devices*. New Jersey: Prentice-Hall, Englewood Cliff.

Simeoni A., P.A. Santoni, M. Larini, and J.H. Balbi, 2001. Proposal for theoretical improvement of semi-physical forest fire spread models thanks to a multiphase approach: Application to a fire spread model across a fuel bed. *Combust. Sci. Technol.***162**, 59–84.

Setterfield, S.A. 2002. Seedling establishment in an Australian tropical savanna: effects of seed supply, soil disturbance and fire. *Journal of Applied Ecology* **39**, 949-959.

Simoneit, B.R.T. 2002. Biomass burning—a review of organic tracers for smoke from incomplete combustion, *Applied Geochemistry* **17**, 129-162.

Solheim, F.S., J. Vivekanandan, R.H. Ware, and C.Rocken, 1999. Propagation delays induced in GPS signals by dry air, water vapour, hydrometeors and other particulates. *Journal of Geophysical Research* **104** (D8), 9663 -9670.

Sorokin, A, X. Vancassel, and P. Mirabel, 2002. Emission of ions and charged soot particle by aircraft engines. *Atmos. Chem. Phys*.**2**, 2045-2074.

Steward, H.T.L, D.W. Flinn, and J.M. James, 1981. Biomass and nutrient distribution in radiata pine. In: *Proceeding of Australian Forest Nutrition workshop; Productivity in Perpetuity*". Canberra: CSIRO Division of Forest Research, pp 173-185

Streifer, W., and K.B. Paxton, 1971. Analytical sollution of ray equation in cylindrical inhomogeneous guiding medium. I. Meridonial rays. *Applied Optics* **10**, 769 -775.

Stott, P. 2000. Combustion in tropical biomass fires: a critical review. *Progress in Physical Geography* **24**, 355 -377.

Sullivan, A. 2004. *Nature of severe Fire Events* Client report (No.1470) for Fire Management Unit. Dept. Urban Services. Canberra: CSIRO

Tarbuck, E.J. and F.K. Lutgens, 2002. *Earth: an introduction to physical geology*. New Jersey: Prentice Hall.

Tendero, C., C. Tixier, P. Tristant, J. Desmaison, and P., Leprince, 2006. Atmospheric pressure plasmas: A review. *Spectrochimica Acta. Part B: Atomic spectroscopy* **61**, 2-30.

Thayer, G. 1974. An improved equation for radio refractive index of air. *Radio Science* **9**, 803 – 807.

Thomas, B., A. Thompson, V.A. Oyenuga, and R.H. Armstrong, 1952. The ash constituents of some herbage plants at different stages of maturity. *Emp. J. Exp. Agric.* **20**,10-22.

Turner, J., and M. Singer, 1976. Nutrient distribution and cycling in sub-alpine coniferous forest ecosystem. *Journal of Applied Ecology* **13**, 295-301.

Turner, J., and M. Lambert, 1996. Nutrient cycling and forest management. *In:* P.M.Attiwill and M.A. Adams, (eds). *Nutrition of Eucalypts*, Melbourne: CSIRO Publishing, pp.229-248

Turner, J. and M. Lambert, 2002. Litterfall and forest floor dynamics in *Eucalyptus pilularis*

Turvey, N.D., and P.J. Smethurst, 1994. Soil types as classes for managing the nutrient status of planted *Pinus radiata* in Victoria, Australia. *Australian Forestry* **57**, 148-156.

Underwood, R.J. and P.E.Christensen, 1981. *Forest Fire management in western Australia*. Perth: Government printing Office.

Vandrey, J. F. 1963. Elementary solutions for the normal transmission of electromagnetic signals through nonuniform plasma layers, *IEEE Antennas and Propagation Magazine* **11**, 709-711.

Varadan, V. V., K.A. Jose, and V.K. Varadan, 2000. *In situ* microwave characterization of nonplanar dielectric objects. *IEEE Trans. Microw. Theory Tech.* **48**, 388–94

Ventura, M.P., J.M.C. Mendes-Lopes, F.M.C. Rego, and H.S. Botelho, 1994. Temperature-time curves in forest fires. 2nd International Conference on Forest Fire Research, Proceedings, Vol. I, 335-342.

Viegas, D. X. 1993. Fire Behaviour and Fireline Safety., *Ann. Medit. Burns Clu.* **6**(3), 1-7.

Viegas, D.X. 1998. Forest fire propagation. *Phil. Trans. R. .Soc. Lond.* A **356**, 2907 - 2928.

Vodacek, A., R.L. Kremens, S.C. Fordham, S.C.VanGorden, D. Luisi, J.R.Schott, and D.J. Latham, 2002. Remote optical detection of biomass burning using potassium emission signature. *Int. Journal of Remote Sensing* **23,** 2721-2726.

Wade, H.D. 1965. A wave equation for electromagnetic wave propagation in a linear, lossy, compressible magneto-ionic medium, *IEEE Antenna and Propagation Magazine* **13**(4), 650 -651.

Ward D.E. 2001. Combustion chemistry and smoke. *In*: E.A. Johnson and K. Miyanishi K, (eds). *Forest fires: Behaviour and ecological effects.* San Diego: Academic Press, pp 55-75.

Webber R.O., A.M. Gill, P.R.A. Lyons, P.H.R. Moore, R.A.Bradstock, and G.N.Mercer, 1995. Modelling Wildland Fire Temperatures. CALMScience Supplement **4**, 23-26

Welch, S., A. Jowsey, S. Deeny, A. Morgan and J.L. Torero, 2007. BRE large compartment fire tests- Characterising post-flashover fires for model validation. *Journal. Fire Safety* **42**, 548-567.

Westberg, H.M., M. Bystrom, and B. Lecker, 2003. Distribution of potassium, chlorine and sulphur between solid and vapour phases during combustion of wood and coal. *Energy and Fuels* **17**, 18-28.

Williams, D.W., J.S. Adams, J.J. Batten, G.F.Whitty, and G.T.Richardson, ., "Operation Euroka: An Australian Mass Fire Experiment." Report 386, Maribyrnor, Victoria, Australia, Defense Standards Laboratory, 1970.

Williams, R.J., G.D. Cook, A.M. Gill, and P.H.R. Moore, 1999. Fire Regimes, fire intensity and tree survival in a tropical savanna in northern Australia. *Australian Journal of Ecology* **24**, 50-59

Williams, R.J., A.D. Griffiths, and G.E. Allan, 2002. Fire Regimes and biodiversity in the savannas of Northern Australia. *In*: A.M. Gill, R.A. Bradstock and J.E. Williams, (eds.). *Flammable Australia—The Fire Regimes and Biodiversity of a Continent*, Cambridge: Cambridge University Press, pp. 281–304.

Williams D., and G. Cook, 2001. Savanna fire regimes. *In*: R. Dryer, P. Jackyln, I. Partridge, J. Russel-Smith and D. Williams, (eds.). *Savanna Burning: Understanding and Using Fire in Northern Australia*, Darwin: Tropical Savanna CRC, pp 15 –28.

Williams, P.R., R.A. Congdon, and P. Clarke, 2003. Effect of fire regimes on plant abundance in tropical eucalyptus savanna of north-eastern Australia. *Austral Ecology* **28**, 324-338

White, R. H., and M. A. Dietenberger. 2001. Wood products: Thermal degradation and fire. *In:* K. H. J. Buschow, R. W. Cahn, M. C. Flemings, B. Ilschner, E. J. Kramer, and S.

Mahajan. (eds.). Encyclopedia of materials: Science and technology. New York: Elsevier Science Ltd, pp 9712 –9716.

Whiting, D., C. Wilson, and C. Card, 2004. *Plant Nutrition CMG No.S31*. Fort Collins: CSU Cooperative Extension.

Whitmer, R.F. 1956. Microwave studies of electron loss processes in gaseous discharges. *Physical review* **104** , 572-575

Xu, B., Shi J. and Yuan. Z, 2006. The interaction of the collisional plasma with Microwave *Plasma Science and Technology* **8**, 535 – 538

Yokelson, J.T., W.T. Griffith, and E.Ward, 1996. Fourier transform infrared studies of large-scale laboratory biomass fires, *Journal of Geophysical research* **101**(D15), 21067 -21080.

Yuan, Z., Shi J. and Y. Pan, 2007. Experimental studies of microwave reflection and attenuation by plasmas produced by burning chemicals in atmosphere, *Plasma Science and Technology* **9**, 158 -161.

Zhou, X.Y., and J.C.F. Pereira, 2000. A multidimensional model for simulating vegetation fire spread using a porous media sub-model. *Journal of Fire and Material* **24**, 37- 43.

Zivanovic, S.V., H.M. Musal, and I.R. Primich, 1964. Determination of plasma layer Properties form the measured Electromagnetic Transmission Coefficient. *IEEE Transaction on Antennas and Propagation* **1**, 618 – 624.